AN ENGINEERING CONTROL SYSTEM PARADIGM FOR QUANTITATIVE UNDERSTANDING OF HEMOSTASIS

by

Chia-Hung Tsai

A dissertation submitted to the Faculty of the University of Delaware in partial fulfillment of the requirements for the degree of Doctor of Philosophy in Chemical Engineering

Summer 2016

© 2016 Chia-Hung Tsai
All Rights Reserved

ProQuest Number: 10192146

All rights reserved

INFORMATION TO ALL USERS
The quality of this reproduction is dependent upon the quality of the copy submitted.

In the unlikely event that the author did not send a complete manuscript
and there are missing pages, these will be noted. Also, if material had to be removed,
a note will indicate the deletion.

ProQuest 10192146

Published by ProQuest LLC (2016). Copyright of the Dissertation is held by the Author.

All rights reserved.
This work is protected against unauthorized copying under Title 17, United States Code
Microform Edition © ProQuest LLC.

ProQuest LLC.
789 East Eisenhower Parkway
P.O. Box 1346
Ann Arbor, MI 48106 - 1346

AN ENGINEERING CONTROL SYSTEM PARADIGM FOR

QUANTITATIVE UNDERSTANDING OF HEMOSTASIS

by

Chia-Hung Tsai

Approved: _____

Abraham M. Lenhoff, Ph.D.
Chair of the Department of Chemical and Biomolecular Engineering

Approved: _____

Babatunde A. Ogunnaike, Ph.D.
Dean of the College of Engineering

Approved: _____

Ann L. Ardis, Ph.D.
Senior Vice Provost for Graduate and Professional Education

I certify that I have read this dissertation and that in my opinion it meets the academic and professional standard required by the University as a dissertation for the degree of Doctor of Philosophy.

Signed: _____

Babatunde A. Ogunnaike, Ph.D.
Professor in charge of dissertation

I certify that I have read this dissertation and that in my opinion it meets the academic and professional standard required by the University as a dissertation for the degree of Doctor of Philosophy.

Signed: _____

Ulhas P. Naik, Ph.D.
Professor in charge of dissertation

I certify that I have read this dissertation and that in my opinion it meets the academic and professional standard required by the University as a dissertation for the degree of Doctor of Philosophy.

Signed: _____

Antony N. Beris, Ph.D.
Member of dissertation committee

I certify that I have read this dissertation and that in my opinion it meets the academic and professional standard required by the University as a dissertation for the degree of Doctor of Philosophy.

Signed: _____

Abraham M. Lenhoff, Ph.D.
Member of dissertation committee

I certify that I have read this dissertation and that in my opinion it meets the academic and professional standard required by the University as a dissertation for the degree of Doctor of Philosophy.

Signed: _____

Peter J.T. Verheijen, Ph.D.
Member of dissertation committee

ACKNOWLEDGMENTS

First and foremost, I thank Mother Nature for creating this complex yet interesting process of hemostasis that sustains many forms of lives on earth since some 450 million years ago. Without such process, I would not even exist.

I thank my advisors, Prof. Ogunnaike and Prof. Naik. Thank you, Prof. Ogunnaike for taking me in as student when I had no background in biology and not much experience with computer simulation, and for the patience you had for me when I was sluggishly learning about the project and making progress. Thank you, Prof. Naik, for lending me, on the first day we met, the biology textbook that opened a door to a new field of knowledge for me, and for the numerous lively examples during our meetings that connect the macroscopic perception with the tiny little things that happen in biology. In addition, I thank my committee members, Prof. Lenhoff, Prof. Beris, and Prof. Verheijen for their valuable technical discussions and input throughout my research. It has been an invaluable experience to get comments from different perspectives. In particular, I thank Prof. Verheijen for letting me know of the Law of Conservation of Trouble, which I think is probably a law that exists in every possible universe out there.

I thank all members, both past and present, in the Ogunnaike and Naik research groups. I thank Dr. Seung-Wook Chung, Dr. Melissa St. Amand, Dr. Jacob McGill for their constant encouragement and mentorship in my first few years in the group. I thank Dr. Zachary Whiteman, Devesh Radharkrishnan, James Park, Dr. Robert Lovelett, and Daniel Cook for their company, support, and the fun moments they

make. In particular, I thank Robert for allowing me to crash the sever countless times without any complaints (or without letting me know of the complaints). I thank James for letting me occupy the server for a long time, and for the many motivation talks in the office. I thank Devesh, whom I shared the office most of the time with, for troubling me all the time, for not actually stealing my lunch, for making the days in the office much more fun, and of course for the delicious foods he generously shared with me.

I thank Meghna Naik, whose continuous encouragement and kindness are the light in the dark shadow of failed experiments. I thank Dr. Ramya Turaga and Arjit Nigam, who showed me how the experiments were done in a biology lab when I first joined the group. I thank Dr. Xi Chen for teaching me everything, including those minor but important tips, in the microfluidic experiments. I thank Dr. Kalyan Golla for the warm greetings every time I met you, whether it was at UD or at TJU, and for the technical discussions we had in the lab. I thank Pravin Patel, for giving me a Biolab 101 tutorial on my first day at TJU. That was a really heart-warming welcome. I thank Randall Derstine for providing me with the blood I needed for the experiments, and for the numerous scientific discussions in the lab. I thank Brandon Bachman for also providing me with the blood I needed, and for tying the record of getting my blood at the third poke. I thank Drew Kilker for the company and for the interesting discussions we had about your research.

I thank my friends who have given me moral support and encouraged me over the years, in the form of kindly spoken words either over the phone or in person, in the form of heart-warming writings, in the form of delicately prepared foods and desserts, and in the form of the time we spent together. In particular, I thank Dr. Ming-Feng

Hsieh, whose numerous phone calls made sure that I was not alone and whose inspiring stories always lifted my spirit. I also thank Dr. Li-Chiang Lin and Dr. Szu-Chia Chien, whose kind encouragement walked me through the dark times throughout the years.

Most importantly, I thank my family for their unending love and encouragement. I thank my parents, for setting examples of positive attitude and perseverance, and for the occasional snack packages they sent me from home. I thank my sister for those postcards, some personalized, with delightful stories and kind prayers for me. I thank my brother-in-law, for trying to help me with my research from a different perspective. Finally, I thank my 20-month-old niece, who always reminds me how fun it is to scream when you are happy and how wonderful life can be.

TABLE OF CONTENTS

LIST OF TABLES xiv
LIST OF FIGURES xvi
ABSTRACT xxvii

Chapter

1 INTRODUCTION 1

1.1 Motivation: Hemostasis and Diseases 1
1.2 Hemostasis: a Physiological System and an Automatic Control System . 3
1.3 Integrative Modeling: an Engineering Control System Paradigm for Hemostasis 7
1.4 Dissertation Overview 10

2 MODELING AND ANALYSIS OF THE SINGLE PLATELET 11

2.1 Introduction 11
2.2 Model Development and Validation 12

2.2.1 ADP-Mediated Signaling Overview 12

2.2.1.1 $P2Y_1$ Signaling Overview 13
2.2.1.2 $P2Y_{12}$ Signaling Overview 14
2.2.1.3 Positive Feedback: Outside-In Signaling, Granule Secretion and TxA2 Synthesis 15
2.2.1.4 Inherent Inhibitory Signaling Pathways 15
2.2.1.5 Platelet aggregation 15

2.2.2 Model Development: Single Platelet Model 16
2.2.3 Model Validation 21

2.2.3.1 Platelet Dense Granule Secretion 21
2.2.3.2 Platelet Aggregation 22

2.2.4 Parametric Sensitivity Analysis 23

2.3 Summary 27

3 A NOVEL MATHEMATICAL REPRESENTATION OF PRIMARY HEMOSTASIS 29

3.1 Introduction 29

3.1.1 Mechanistic Basis of Primary Hemostasis 29
3.1.2 Previous Work on Modeling Primary Hemostasis 30

3.2 Model Development: Primary Hemostasis 31

3.2.1 Controlled Process: Area of Exposed Sub-Endothelium 32
3.2.2 Primary Hemostasis Sensor and Controller 33

3.2.2.1 Number of Available Collagen Fibers 33
3.2.2.2 ADP and TxA2 Release from Collagen-Induced Platelet Activation 33

3.2.3 Primary Hemostasis Actuator: Platelet Aggregation 35

3.3 Results and Discussion 45
3.4 Effect of Protein Inhibition on Collagen-Induced Platelet Aggregation: Experiments and Model Prediction 54

3.4.1 Microfluidic Experiments: Methodology 55

3.4.1.1 Fabrication of Microfluidid Devices 55

3.4.1.1.1 Casting and Device Preparation 55
3.4.1.1.2 Surface Functionalization 55
3.4.1.1.3 Blood Collection and Perfusion 56
3.4.1.1.4 Imaging and Quantitation 57

3.4.2 Effect of Protein Inhibition on Platelet Aggregation 57

3.4.2.1 PI3K Inhibition 57
3.4.2.2 PKC Inhibition 60

3.5 Summary 62

4 A HOLISTIC MATHEMATICAL REPRESENTATION OF HEMOSTASIS 63

4.1 Introduction 63
4.2 Physiological Description of Secondary Hemostasis 64

4.2.1 The Extrinsic Pathway 65
4.2.2 The Intrinsic Pathway 66
4.2.3 The Common Pathway 67
4.2.4 Inhibitory Reactions 67
4.2.5 Platelet-Derived Pro-Coagulant Molecules 68

4.3 Secondary Hemostasis Model 69

4.3.1 Previous Modeling Efforts 69
4.3.2 Model Adaptation 71

4.3.2.1 Fibrin Production Reactions 71
4.3.2.2 Additional Inhibitory Mechanisms in the Secondary Hemostasis Model 72
4.3.2.3 Additional Activation Mechanisms Between Heterogeneous Phases 73
4.3.2.4 Addition of the Intrinsic Pathway: Factor XI 73
4.3.2.5 Platelet Granule Content: Polyphosphate 74

4.3.3 Model Parameters and Initial Conditions 74

4.4 Integration of Primary and Secondary Hemostasis Model 80

4.4.1 Number of Activated Platelets for Sites for Coagulation 80
4.4.2 FV Release from Platelets 80
4.4.3 Polyphosphates Released by the Platelets 82
4.4.4 Thrombin-Induced Platelet Activation 83
4.4.5 Interaction Strength 84
4.4.6 Change in Porosity of Platelet Aggregate 84

4.5 Simulation Results 85

4.5.1 Nominal Conditions 85
4.5.2 Disease Conditions and Interventions 87

4.5.2.1 Hemophilia A and B 87
4.5.2.2 Immune Thrombocytopenic Purpura 89
4.5.2.3 Differential Inhibition of ADP Receptors on Platelets 91
4.5.2.4 Inhibition of TxA2 Synthesis 92

4.6 Model Analyses 93

4.6.1 Modular Sensitivity Analysis 93

4.6.1.1 Controlled Process 94
4.6.1.2 Primary Hemostasis Sensor 96
4.6.1.3 Primary Hemostasis Controller 98
4.6.1.4 Primary Hemostasis Actuator 99
4.6.1.5 Secondary Hemostasis Sensor 101
4.6.1.6 Secondary Hemostsasis Controller 103
4.6.1.7 Secondary Hemostasis Actuator 105

4.6.2 Effect of Interaction Strength between Primary and Secondary Hemostasis 106

4.7 Summary 110

5 RATIONAL IDENTIFICATION OF TREATMENT TARGETS FOR HEMOSTATIC DISORDERS 112

5.1 Model-based Treatment Target Identification 112
5.2 Methodology 113
5.3 Thrombophilic Diseases 115

5.3.1 Hyperactive Primary Hemostasis: Hyperactive Platelets 115
5.3.2 Hyperactive Secondary Hemostasis: Antithrombin Deficiency 120

5.4 Hemophilic Diseases 124

5.4.1 Deficient Secondary Hemostasis: Hemophilia A 124
5.4.2 Deficient Secondary Hemostasis: Hemophilia B 129
5.4.3 Deficient Primary Hemostasis: Immune Thrombocytopenic Purpura 134

5.5 Summary 136

6 PLATELET COUNT CONTROL IN PATIENT WITH IMMUNE THROMBOCYTOPENIC PURPURA 138

6.1 Introduction 138
6.2 ITP and Current Treatments 140

6.2.1 Mechanism of Platelet Production Regulation 140
6.2.2 Pathology and Treatment of ITP 141

6.3 Development and Validation of Patient-Specific Physiological Model 145

6.3.1 A Pharmacokinetic-Pharmacodynamic Model of ITP patient ... 145
6.3.2 Model Parameter Estimation and Validation 150

6.3.2.1 Clinical Data Collection 150
6.3.2.2 Parameter Estimation and Model Validation 150

6.4 Model Analysis 153

6.4.1 Parameter Values 153
6.4.2 Theoretical Dose Responses 153

6.5 Platelet Count Control in ITP Patient 156

6.5.1 Motivation of Engineering Control Systems Approach to the Development of Treatment Protocols 156
6.5.2 Control System Design 157

6.5.2.1 Open-loop Control 157
6.5.2.2 Discrete PI Controller without Zero-Order Hold 157
6.5.2.3 Model-based Open-Loop Optimal Control 158

6.5.3 Implementation of Control Strategie 159

6.5.3.1 Open-Loop Control 159
6.5.3.2 Discrete PI Controller without Zero-Order Hold 160
6.5.3.3 Model-based open-loop optimal control 162

6.6 Discussion and Conclusions 163

7 CONCLUSIONS AND FUTURE DIRECTIONS 166

7.1 Conclusions 166
7.2 Future Directions 168

7.2.1 Comprehensive Hemostasis Model 168

7.2.1.1 Incorporating Effect of Shear Rate 168
7.2.1.2 Incorporating Additional Proteins of Significance in the Single Platelet Model 169
7.2.1.3 Investigating Effect of Model Structure and Model Parameters in Secondary Hemostasis 170
7.2.1.4 Investigating Various Geometries of the Wound 170
7.2.1.5 Validating the Comprehensive Model 171

7.2.2 Platelet Count Control in ITP Patients 171

REFERENCES 172

Appendix

A LIST OF PARAMETERS IN THE SINGLE PLATELET MODEL 183
B EQUATIONS AND PARAMETER VALUES IN THE SECONDARY HEMOSTASIS MODEL 189

B.1 List of Equations in the Updated Secondary Hemostasis Model. 189
B.2 Parameter Values Used in the Secondary Hemostasis Model.....204

C A PHARMACOKINETIC–PHARMACODYNAMIC MODEL OF ROMIPLOSTIM-INDUCED PLATELET PRODUCTION 208

C.1 Equations for the Pharmacokinetic/Pharmacodynamic (PKPD) Model208

C.1.1 The Pharmacokinetic Model 208
C.1.2 The Pharmacodynamic Model 210

C.2 Initial Conditions and Original Clinical Data for Parameter Estimation212

D EFFECT OF SHEAR RATE ON PLATELET ADHESION AND AGGREGATION 214

LIST OF TABLES

Table 2.1 Reactions and parameters governing ADP-induced platelet activation, granule secretion, and platelet aggregation 18

Table 2.2. Initial non-zero metabolite concentrations used in the simulation of an ADP-stimulated human platelet..... 20

Table 2.3. List of most significant parameters in platelet dense granule secretion . 26

Table 3.1. List of parameters and their values in the primary hemostasis model. The parameter index corresponds to the x-axis in the figure for sensitivity coefficients..... 44

Table 3.2. Outputs of parametric sensitivity analysis. 53

Table 4.1. Notations of the rate constants used in the secondary hemostasis model. The notations are used in the equations listed in Appendix A and their corresponding values are listed in Table A.1. k1 is the reaction constant for the forward reaction, k-1 for the reverse reaction, kcat for first-order catalytic reaction, kscat for second-order catalytic reaction. 76

Table 4.2. List of non-zero initial conditions used for variables in secondary hemostasis. 79

Table 4.3. List of new parameters involved in augmenting the primary hemostasis model for incorporating the effect of secondary hemostasis 84

Table 5.1. List of parameters in the comprehensive model that are used for parametric sensitivity analysis and for treatment target identification. .113

Table 5.2. List of potential treatment targets for hyperactive Gq activation. 118

Table 5.3. List of potential treatment targets for ATIII deficiency.....123

Table 5.4. List of potential treatment targets for hemophilia A.....127

Table 5.5. List of potential treatment targets for hemophilia B.....132

Table 6.1. Physiological implications of platelet count 139

Table 6.2. List of parameters in the PKPD model. 149

Table 6.3. Parameter values for healthy individuals and the ITP patient. 152

Table 6.4. Parameter values for optimally tuned discrete PI controller. 160

Table A.1. List of parameters used for sensitivity analysis of the single platelet model.....183

Table B.1. Parameter values of the rate constants used in the updated secondary hemostasis model.....204

Table C.1. Initial conditions of the PKPD model. 212

Table C.2. Original data of romiplostim dose and platelet count. 213

LIST OF FIGURES

Figure 1.1. Schematic of hemostasis in response to vascular injury. 5

Figure 1.2. A high-level control system block diagram of hemostasis. Biological events in hemostasis are divided into distinguishable modules in this diagram. See main text for explanation. The arrows represent flow of information into and out of the subsystem blocks. 8

Figure 2.1 Platelet activation pathways. Solid lines: essential signals; dashed lines: auxiliary signals; arrows: stimulatory effect; dots: inhibitory effect..... 14

Figure 2.2. Control system block diagram of single platelet. 17

Figure 2.3. ATP release with different stimulating ADP concentrations: (a) simulation; (b) experimental data by Dawood et al. 22

Figure 2.4 Platelet aggregation in response to stimulation with different ADP concentrations: (a) simulation; (b) experimental data by Dawood et al. 24

Figure 2.5. Sensitivity of amount of ATP release to a 10% increase in parameters: normalized sensitivity coefficients for all parameters. 25

Figure 2.6. Sensitivity of platelet dense granule secretion to a 10% increase in parameters: absolute normalized sensitivity coefficients of the most significant parameters. 26

Figure 3.1. Nominal profiles of (a) numbers of platelet attached to collagen (PLT_{col}) and in the aggregate (PLT_{agg}), (b) ADP concentrations resulted from collagen-bound platelet (ADP_{col}) and the entire aggregate (ADP_{agg}), and (c) TxA2 concentrations resulted from collagen-bound ($TxA2_{col}$) platelet and the entire aggregate ($TxA2_{agg}$)... 46

Figure 3.2. Effect of integrin $\alpha_{IIb}\beta_3$ activation rate on (a) platelet aggregation, (b) ADP secretion and (c) TxA2 synthesis. The rate constant for integrin activation is reduced from its nominal value (blue solid line) to 50% (green dash-dot line), 5% (magenta dotted line), and 0% (cyan dashed line) of the nominal value. Reduced integrin activation rate not only results in reduced platelet aggregation but also reduced ADP and TxA2 levels. 47

Figure 3.3. Effect of JAM-A deficiency on platelet aggregation. (a) non-zero JAM-A level; (b) complete removal of JAM-A. JAM-A level is reduced from 45 (blue solid line) to 30 (green dash-dot line), 15 (magenta dotted line), and 0 (red dashed line in (b)). Platelet aggregation becomes out-of-bound when the effect of JAM-A is completely removed from the model. 48

Figure 3.4. Platelet aggregation in response to various wound sizes ranging from 20 to 400 μm^2. (a-e) Wound area coverage with respect to time; (f) Percentage of wound area coverage. Increasing wound size corresponds to decreasing wound coverage. 50

Figure 3.5. (a) Estimated bleeding rate and (b) blood loss in response to various wound sizes. The wound sizes correspond to the wound sizes used in Figure 6. Blood loss does not completely stop as fibrin production is not considered in the model. The bleeding rate reaches a steady state once the platelet aggregate stabilizes. 51

Figure 3.6. Hemostatic phenotypes as a result of the dysfunction of signaling proteins that leads to integrin activation. The rate constants for the activation of proteins (19 in total) are reduced to 5% of the baseline value one at a time. 52

Figure 3.7. Parameter sensitivity analysis. The relative changes in multiple outputs were calculated based on a simulation with a 10% decrease in a given parameter value. The percentage change to the baseline output values were normalized by the sign and magnitude of the change to the parameter value as described in main text. (a) time to reach the maximum in platelet aggregation; (b) average platelet number during the first 3 minutes; (c) average platelet number during the simulation time of 5 minutes; (d) bleeding time; and (e) total blood loss..... 54

Figure 3.8. Microfluidic device used in the microfluidic experiments. Patterned PDMS strip is firmly press against the glass slide to form the microfluidic device. Four bigger ports are the inlets of the microfluidic channels with lengths of 12 mm. Four small ports are the outputs that are to be connected to a syringe pump. 56

Figure 3.9. Effect of Wortmannin (60 nM) on platelet aggregation over collagen-coated surface at t = 180 seconds. Upper panel: phase contrast images; bottom panel: fluorescence images. Left: untreated group (control); right: treated group (Wortmannin). 58

Figure 3.10. Quantitation of the fluorescence intensity for collagen-induced platelet aggregation with or without Wortmannin at 180 seconds. Error bars represent standard error of the mean (n=3). 59

Figure 3.11. Platelet aggregation profiles from the primary hemostasis model. A 92% reduction of $k_{5\text{-}1}$ and $k_{5\text{-}2}$ was shown to be corresponding to a Wortmannin concentration of 60 nM. 59

Figure 3.12. Effect of Bis on platelet aggregation over collagen-coated surface. Upper panel: phase contrast images; bottom panel: fluorescence images. Left: untreated group (control); right: treated group (Bis). 60

Figure 3.13. Quantitation of the fluorescence intensity for collagen-induced platelet aggregation with or without Bis at 180 seconds.. Error bars represent standard error of the mean (n=3). 61

Figure 3.14. Platelet aggregation profiles from the primary hemostasis model. A 75% reduction of $k_{9\text{-}1}$ and $k_{9\text{-}2}$ was shown to be corresponding to a Bis concentration of 10 μM. 61

Figure 4.1. Schematic of the coagulation cascade. 65

Figure 4.2. Thrombin concentration profiles from the reproduced KF model (blue solid line) and the reproduced KF model with additional fibrin formation reactions (green dashed lines) on (a) log scale and (b) linear scale. 72

Figure 4.3. Schematic of reactions considered in the updated secondary hemostasis model. 75

Figure 4.4. Profile of (a) number of activated platelet in the aggregate, (b) ADP concentration, (c) TxA2 concentration, and (d) thrombin concentration under the nominal condition in response to an initial wound size of 100 μm^2 at a shear rate of 400 s^{-1}. 86

Figure 4.5. Wound coverage profiles in response to various wound intensities, or wound sizes: (a) 20 μm^2, (b) 50 μm^2, (c) 100 μm^2, (d) 200 μm^2, (e) 400 μm^2. (f) Relative percentage of wound coverage to the corresponding wound intensity. 88

Figure 4.6. A comparison of (a) the aggregation profile and (b) the thrombin concentration profile from the nominal condition, hemophilia A and hemophila B in response to a wound size of 100 μm^2 at a shear rate of 400 s^{-1}. Hemophilia A and hemophilia B are simulated using a plasma FVIII level 0.1% of the nominal condition and a plasma FIX level 0.1% of the nominal condition, respectively. 89

Figure 4.7. System response to a wound size of 100 μm^2 at a shear rate of 400 s^{-1} with various levels of platelet count. (a) platelet aggregation; (b) thrombin concentration profile; (c) percentage ratio of covered wound area to the initial wound size. 90

Figure 4.8. Differential effect of inhibition of ADP receptors on the system response to a wound size of 100 μm^2 and a shear rate of 400 s^{-1}. (a) platelet aggregation; (b) thrombin concentration profile; (c) percentage ratio of covered wound area to the initial wound size. 92

Figure 4.9. Effect of inhibition of TxA2 synthesis in response to a wound size of 100 μm^2 and a shear rate of 400 s^{-1}. (a) platelet aggregation; (b) thrombin concentration profile; (c) percentage ratio of covered wound area to the initial wound size. 93

Figure 4.10. Dynamic system responses to ±10% of the controlled process. (a) number of activated platelets, (b) [thrombin], (c) [ADP_{col}], (d) [ADP_{sec}], (e) [$TxA2_{col}$], (f) [$TxA2_{sec}$], (g) bleeding rate, (h) fibrin dimer 95

Figure 4.11. Focused dynamic system responses to ±10% of the controlled process. (a) number of activated platelets, (b) [thrombin], (c) [ADP_{col}], (d) [ADP_{sec}], (e) [$TxA2_{col}$], (f) [$TxA2_{sec}$], (g) bleeding rate, (h) fibrin dimer concentration. 96

Figure 4.12. Dynamic system responses to ±10% of the primary hemostasis sensor. (a) number of activated platelets, (b) [thrombin], (c) [ADP_{col}], (d) [ADP_{sec}], (e) [$TxA2_{col}$], (f) [$TxA2_{sec}$], (g) bleeding rate, (h) fibrin dimer concentration. 97

Figure 4.13. Focused dynamic system responses to ±10% of the primary hemostasis sensor. (a) number of activated platelets, (b) [thrombin], (c) [ADP_{col}], (d) [ADP_{sec}], (e) [$TxA2_{col}$], (f) [$TxA2_{sec}$], (g) bleeding rate, (h) fibrin dimer concentration. 97

Figure 4.14. Dynamic system responses to ±10% of the primary hemostasis controller output (1) ADP_{col} and output (2) $TxA2_{col}$. (a) number of activated platelets, (b) [thrombin], (c) [ADP_{col}], (d) [ADP_{sec}], (e) [$TxA2_{col}$], (f) [$TxA2_{sec}$], (g) bleeding rate, (h) fibrin dimer concentration. 98

Figure 4.15. Focused dynamic system responses to ±10% of the primary hemostasis controller output (1) ADP_{col} and output (2) $TxA2_{col}$. (a) number of activated platelets, (b) [thrombin], (c) [ADP_{col}], (d) [ADP_{sec}], (e) [$TxA2_{col}$], (f) [$TxA2_{sec}$], (g) bleeding rate, (h) fibrin dimer concentration. 99

Figure 4.16. Dynamic system responses to ±10% of the primary hemostasis actuator. (a) number of activated platelets, (b) [thrombin], (c) [ADP_{col}], (d) [ADP_{sec}], (e) [$TxA2_{col}$], (f) [$TxA2_{sec}$], (g) bleeding rate, (h) fibrin dimer concentration.....100

Figure 4.17. Focused dynamic system responses to ±10% of the primary hemostasis actuator. (a) number of activated platelets, (b) [thrombin], (c) [ADP_{col}], (d) [ADP_{sec}], (e) [$TxA2_{col}$], (f) [$TxA2_{sec}$], (g) bleeding rate, (h) fibrin dimer concentration. 101

Figure 4.18. Dynamic system responses to ±10% of the secondary hemostasis sensor. (a) number of activated platelets, (b) [thrombin], (c) [ADP_{col}], (d) [ADP_{sec}], (e) [$TxA2_{col}$], (f) [$TxA2_{sec}$], (g) bleeding rate, (h) fibrin dimer concentration. 102

Figure 4.19. Focused dynamic system responses to ±10% of the secondary hemostasis sensor. (a) number of activated platelets, (b) [thrombin], (c) [ADP_{col}], (d) [ADP_{sec}], (e) [$TxA2_{col}$], (f) [$TxA2_{sec}$], (g) bleeding rate, (h) fibrin dimer concentration. 103

Figure 4.20. Dynamic system responses to ±10% of the secondary hemostasis controller. (a) number of activated platelets, (b) [thrombin], (c) [ADP_{col}], (d) [ADP_{sec}], (e) [$TxA2_{col}$], (f) [$TxA2_{sec}$], (g) bleeding rate, (h) fibrin dimer concentration.....104

Figure 4.21. Focused dynamic system responses to ±10% of the secondary hemostasis controller. (a) number of activated platelets, (b) [thrombin], (c) [ADP_{col}], (d) [ADP_{sec}], (e) [$TxA2_{col}$], (f) [$TxA2_{sec}$], (g) bleeding rate, (h) fibrin dimer concentration.....104

Figure 4.22. Dynamic system responses to ±10% of the secondary hemostasis actuator. (a) number of activated platelets, (b) [thrombin], (c) [ADP_{col}], (d) [ADP_{sec}], (e) [$TxA2_{col}$], (f) [$TxA2_{sec}$], (g) bleeding rate, (h) fibrin dimer concentration.....105

Figure 4.23. Focused dynamic system responses to ±10% of the secondary hemostasis actuator. (a) number of activated platelets, (b) [thrombin], (c) [ADP_{col}], (d) [ADP_{sec}], (e) [$TxA2_{col}$], (f) [$TxA2_{sec}$], (g) bleeding rate, (h) fibrin dimer concentration.....106

Figure 4.24. Effect of interaction gains on thrombin production. Group 1: high and sustained thrombin concentration. 107

Figure 4.25. Effect of interaction gains on thrombin production. Group 2: high and sustained thrombin concentration with a peak. 108

Figure 4.26. Effect of interaction gains on thrombin production. Group 3: medium and sustained thrombin concentration.....109

Figure 4.27. Effect of interaction gains on thrombin production. Group 4: medium thrombin concentration with a peak.....109

Figure 4.28. Effect of interaction gains on thrombin production. Group 5: minimum thrombin concentration. 110

Figure 5.1. Platelet aggregation profiles in response to wound sizes of (a) 50 μm^2, (b) 100 μm^2, and (c) 200 μm^2 with various degrees of hyperactive Gq activation at a shear rate of 400 s^{-1}. 117

Figure 5.2. Sensitivity coefficients from local sensitivity analysis for the hyperactive Gq activation case with 1.5X $k_{nominal}$, and a wound size of 100 μm^2. A 10% decrease in the parameter values of the disease condition is applied. 117

Figure 5.3. Ratio of parameter values used for treating hyperactive Gq activation to corresponding original values. The figure number (a-r) corresponds to the pair index used in Table 5.2 and the number of each bar corresponds to the parameter index in Table 5.1. 119

Figure 5.4. Platelet aggregation profiles of the nominal case, the hyperactive Gq activation case, and the treated cases. 120

Figure 5.5. Platelet aggregation profiles in response to wound sizes of (a) 50 μm^2, (b) 100 μm^2, and (c) 200 μm^2 with various degrees of ATIII deficiency at a shear rate of 400 s^{-1} 121

Figure 5.6. Sensitivity coefficients from local sensitivity analysis for ATIII deficiency with an initial ATIII level 10% of the nominal level, and a wound size of 100 μm^2 122

Figure 5.7. Ratio of parameter values used for treating ATIII deficiency to corresponding original values. The figure number (a-i) corresponds to the pair index used in Table 5.3 and the number of each bar corresponds to the parameter index in Table 5.1. 123

Figure 5.8. Platelet aggregation profiles of the nominal case, the ATIII deficiency case in question, and the treated cases. 124

Figure 5.9. Total blood loss in response to wound sizes of (a) 50 μm^2, (b) 100 μm^2, and (c) 200 μm^2 with various degrees of hemophilia A at a shear rate of 400 s^{-1}. 125

Figure 5.10. Sensitivity coefficients from local sensitivity analysis for hemophilia A with a FVIII level 1% of the nominal case and a wound size of 200 μm^2 at a shear rate of 400 s^{-1}. 126

Figure 5.11. Ratio of parameter values used for treating hemophilia A to corresponding original values. The figure number (a-o) corresponds to the pair index used in Table 5.4 and the number of each bar corresponds to the parameter index in Table 5.1. 128

Figure 5.12. Profiles of bleeding rate for the nominal case, the hemophilia A case in question, and the treated cases using the identified targets. 129

Figure 5.13. Total blood loss in response to wound sizes of (a) 50 μm^2, (b) 100 μm^2, and (c) 200 μm^2 with various degrees of hemophilia B at a shear rate of 400 s^{-1}. 131

Figure 5.14. Sensitivity coefficients from local sensitivity analysis for hemophilia B with a FIX level 1% of the nominal case and a wound size of 200 μm^2 at a shear rate of 400 s^{-1}. 131

Figure 5.15. Ratio of parameter values used for treating hemophilia B to corresponding original values. The figure number (a-t) corresponds to the pair index used in Table 5.5 and the number of each bar corresponds to the parameter index in Table 5.1. 133

Figure 5.16. Profiles of bleeding rate for the nominal case, the hemophilia B case in question, and the treated cases. 134

Figure 5.17. Total blood loss in response to wound sizes of (a) 50 μm^2, (b) 100 μm^2, and (c) 200 μm^2 with various degrees of ITP at a shear rate of 400 s^{-1}. 135

Figure 5.18. Sensitivity coefficients from local sensitivity analysis for ITP with a platelet count of 50×10^9/L and a wound size of 100 μm^2 at a shear rate of 400 s^{-1}. 136

Figure 6.1. Schematic of platelet production regulation. TPO: thrombopoietin; P: precursor (megakaryocyte); PLT: platelet....141

Figure 6.2. Schematic representation of the pharmacokinetic/pharmacodynamic (PKPD) model illustrating mechanisms of romiplostim-induced platelet production. Subcutaneous injection of romiplostim is described by rate constant k_{SC} and bioavailability F, with the dose implemented as a rectangular pulse. Romiplostim at the subcutaneous site, whose amount is represented by A_{SC}, is absorbed into the blood stream, represented by rate constant k_a. Free romiplostim is distributed between the serum and the peripheral part with rate constants k_{PC} and k_{CP}. The specific serum volume is denoted as V_c. The amount of romiplostim in the serum and the peripheral part are denoted as A_C and A_P, respectively. Romiplostim can also bind to platelets in the blood stream and form a drug-receptor complex. Formation of such complex, whose amount is represented by DR, is described with rate constant k_{on}. A proportionality constant ξ representing the average number of receptor on each platelet is defined to determine the total amount of receptor on platelets. Dissociation of romiplostim from the drug-receptor complex is described by rate constant k_{off}. Two mechanisms are responsible for romiplostim clearance: receptor internalization, represented by rate constant k_{int}; and metabolic clearance of romiplostim, represented by k_{eli}. The total amount of romiplostim in circulation, A_{tot}, is the summation of Ac and DR. Free romiplostim, with concentration denoted as C, exerts a stimulatory effect on megakaryocyte maturation through a process described by a Hill function, with S_{max} as the maximal effect, SC_{50} as the concentration required to reach half the maximal effect, and n as the Hill coefficient. P_1, P_2, …, P_{NP} are the number of megakaryocytes in different stages, where N_P is the number of stages of megakaryocyte. Similarly, PLT_1, PLT_2, …, P_{NPLT} are the number of platelets in different stages, where N_{PLT} is the number of stages of platelet. Megakaryocytes and platelets move into the next stage at a rate inversely proportional to their respective lifespans, T_P and $T_{PLT.}$ The intrinsic megakaryocyte maturation rate, denoted as k_{in}, maintains the homeostasis of platelet production when romiplostim is absent. 147

Figure 6.3. Clinical treatment data and platelet count profile with the PKPD model. Upper panel: romiplostim injection profile. Lower panel: platelet count data collected at the clinic and corresponding model prediction. Data in red circles are used to obtain patient-specific parameters for the PKPD model. 151

Figure 6.4. Model response to single romiplostim injection of 1 μg/kg for various initial platelet counts. Higher initial platelet count leads to attenuated platelet count response, a result that is consistent with the fundamental mechanism of platelet count regulation. 154

Figure 6.5. Model response to a single romiplostim injection of various doses. Each dose response consists of three phases: an initial induction period of approximately 5 days (regardless of dosage) with no noticeable change in platelet count; a gradual increase in platelet count culminating in a peak response occurring around 14-16 days, with the peak occurring progressively later with increasing doses; a final declining phase with platelet count gradually returning to the original starting value after 25-30 days.....155

Figure 6.6. Performance under open-loop control. (a) 2 μg/kg every 7 days; (b) 2 μg/kg every 14 days; (c) 1 μg/kg every 7 days; (d) 1 μg/kg every 14 days; (e) 0.5 μg/kg every 7 days; (f) 0.5 μg/kg every 14 days. The results show that the open-loop strategy is ineffective in maintaining a stable platelet count.....159

Figure 6.7. Platelet count control: weekly treatments with optimally-tuned discrete PI controller. Stable platelet count is achieved with this control strategy within 50 days, with steady-state romiplostim doses of approximately 1 μg/kg. 161

Figure 6.8. Platelet count control: bi-weekly treatments with optimally-tuned discrete PI controller. Platelet count continues to oscillate even after a long period of time has elapsed. Although measurements taken from 70 days onward show values close to the target value, the complete platelet count profile remains mostly, below the target—an indication of the inadequacy of this measurement and treatment frequency.....162

Figure 6.9. Platelet count control: weekly and bi-weekly treatments under optimal open-loop control. (a) With weekly injections, platelet count is stable after approximately 50 days. (b) With bi-weekly injections, beyond 80 days, the platelet count profile shows sustained oscillations with a period of approximately two weeks. This coincides almost perfectly with the natural period of the response to a single injection, with the implication that treatment regimen of single injections administered bi-weekly will always result in sustained oscillations. 163

Figure D.1. Representative pictures of the effect of shear rate on platelet adhesion and aggregation over collagen-coated surface. Upper panel: phase contrast images. Lower panel: fluorescence images. Anti-coagulated human blood was perfused through collagen-coated channel for 3 minutes at designated shear rate. 215

Figure D.2. Surface coverage in microfluidic experiments of collagen-induced platelet adhesion and aggregation under various shear rates. Error bar indicates standard error of the mean. 215

Figure D.3. Fluorescence intensity in microfluidic experiments of collagen-induced platelet adhesion and aggregation under various shear rates. Fluorescence intensity is proportional to number of activated platelets. Error bar indicates standard error of the mean. 216

ABSTRACT

Hemostasis is an essential physiological process whose proper function relies on the rapid formation of a blood clot in order to minimize blood loss after a vascular injury. To that end, effective hemostasis is a result of the regulation of a delicate balance between two opposite pathological conditions: hemophilia and thrombophilia. When the hemostatic response is too weak, as in the case of hemophilia, blood clot formation is delayed, causing excessive bleeding; while overactive hemostasis could lead to thrombosis where a blood vessel is completely occluded by a blood clot, a common manifestation of thrombophilia. Understanding the hemostatic process is of significant importance because of the acute danger associated with hemostatic disorders. In particular, they can lead to heart attack and stroke, two major causes of death in the world.

The complete process of hemostasis consists of numerous components organized into two mutually interacting sub-processes known as *primary* and *secondary* hemostasis. To date, quantitative modeling studies of hemostasis have been restricted to a few individual components in isolation. Since in actuality these components never function in isolation, such studies provide only limited understanding of the individual components in question, not of the entire complex process. Obtaining a useful, holistic and high fidelity representation of the complete system requires a more comprehensive approach that adequately captures the full characteristics of all components and their interactions. However, because of intrinsic

system complexity, a traditional modeling approach will generate an overly complex, computationally intractable, and hard-to-validate model.

In this dissertation, in recognition of the defining characteristic of hemostasis as an automatic physiological control system, an engineering control system framework was used to provide a modular structure for organizing the overwhelming amount of information in hemostasis. In the case of primary hemostasis, mathematical expressions, specifically algebraic equations and ordinary differential equations, were developed to represent the biological events associated with each primary hemostasis module: biological equivalents of a sensor, controller, and actuator. These modules were then connected to form a mathematical model of primary hemostasis.

An existing ordinary differential equation model of secondary hemostasis was updated and adapted to include additional recent biological findings on secondary hemostasis. The primary and secondary hemostasis models were modified to incorporate the interactions between the two subsystems before they were connected to form a comprehensive mathematical representation of hemostasis. This comprehensive model was used to simulate various physiological and pathological test cases, generating results consistent with experimental observations and known characteristics. We subsequently used the comprehensive model to study select disease conditions representative of one of the four categories of hemostatic disorders: hyperactive primary hemostasis, deficient primary hemostasis, hyperactive secondary hemostasis, and deficient secondary hemostasis. This exercise enabled us to identify new potential treatment targets that we recommend for future experimental investigations, but which include targets that are already being used as the basis for

current clinical treatment strategies for hemophilia A and hemophilia B, demonstrating the effectiveness and predictive power of the comprehensive model.

Finally, we carried out an experimental and simulation case study involving an actual patient with low platelet count due to immune thrombocytopenic purpura, a pathology that represents a deficiency in the primary hemostasis controller and the actuator. Using an existing model customized to describe the drug dose-response relationship in the patient, a weekly treatment frequency was found to be capable of achieving a stable platelet count, while biweekly treatment regimen always resulted in oscillations due to the pharmacological properties of the drug.

Chapter 1

INTRODUCTION

1.1 Motivation: Hemostasis and Diseases

Hemostasis is the physiological process that responds to a vascular injury to a blood vessel and stops bleeding by restoring the integrity of the blood vessel wall. As blood vessels run through our entire body, such process will have to respond to vascular damages everywhere, in blood vessels as thin as capillaries, and as thick as arteries. When hemostasis does not function properly, pathological conditions could lead to undesired results. On the one hand, when the hemostatic response is too weak or too slow, excessive bleeding occurs, which is the case in hemophilia A and hemophilia B. On the other hand, when the hemostatic response is too strong, the blood vessel could be completely occluded as a result of overly produced clot, a pathological process called thrombosis, as in the case of heart attack and stroke.

Cardiovascular diseases (CVDs) are currently the leading cause of death in the world [1]. An estimated 17.5 million people died from CVDs in 2012, accounting for 31% of total deaths. Of the 17.5 million deaths, an estimated 7.4 million were caused by coronary heart disease, which is a disease of blood vessels supplying the heart muscle, and 6.7 million were due to stroke. Both conditions are closely related to thrombosis. Although not as prevalent as thrombosis, bleeding disorders can arise from a broad range of causes, since a wide variety of cells, proteins and lipids (on the order of thousands for proteins alone) are involved in this entire process and malfunctions of some of them, sometimes just one, could lead to dire consequences.

Despite many efforts in treating an enormous number of hemophilic and thrombotic diseases, the intrinsic characteristics of hemostasis make the treatment of related pathological conditions a challenging task. When a patient is treated for hemophilic conditions by enhancing the function of hemostasis, the risk of thrombosis in the patient is enhanced at the same time. By the same token, when a patient is treated for thrombophilic conditions by suppressing the function of hemostasis to a certain degree, the risk of excessive bleeding is increased as well. Therefore, a better understanding of the hemostatic process and new ways of assessing treatment effects are highly desired.

Even though the hemostatic process has been studied for decades and the understanding of the process has been greatly advanced, the process is still not completely understood. In addition, the huge amount of information generated demonstrates the enormous degree of complexity of the process. As more and more information is being generated on the process, the complexity of hemostasis as we perceive could only be increasing. Take, for example, the proteomic data that have been recently reported on platelet, a tiny cell that plays a key role in the process. It has been estimated that platelets express more than 5000 different proteins [2], and many of them have not yet been studied. The complexity of the system is not just because of the wide variety of molecules that are involved in the process, the reaction network resulted from the many molecules adds another layer of complexity to the process. Such complexity makes it hard to pinpoint the fundamental cause of pathological conditions because of the intertwined nature of the sub-processes. Traditional experimental approach only concerns about a handful of players in hemostasis at a

time. To understand the process with a full picture, a different approach is needed for the task.

Mathematical modeling has been established as an efficient tool in organizing the information contained in complex biological systems for summarizing and quantifying known information about complex biological systems, and via appropriate model analysis, obtaining useful insight into such systems. Hence, the main goal of this dissertation is to develop a comprehensive model of hemostasis that incorporates up-to-date, essential information in order to gain system-level understandings of the entire process of hemostasis.

1.2 Hemostasis: a Physiological System and an Automatic Control System

In the normal, undisturbed state, the mammalian blood vessel wall is lined with a single sheet of endothelial cells that maintains the integrity of the wall. The integrity of the endothelial lining also prevents platelets in the blood stream from becoming activated by releasing platelet inhibitors such as prostacyclin (PGI2) and nitric oxide (NO). When an injury to the vessel wall compromises this integrity, causing undesirable hemorrhage, the first step in repairing the damaged blood vessel is to arrest the bleeding as soon as possible. This is the responsibility of hemostasis, a process consisting of two major sub-processes: primary and secondary hemostasis. Primary hemostasis, responsible for platelet aggregation, is initiated when the injury to the blood vessel wall exposes the sub-endothelium outside the endothelial lining and collagen in the exposed sub-endothelium comes in contact with and binds to the platelets circulating in the blood stream. The binding of collagen to its receptors on the platelet membrane stimulates signaling pathways downstream of the receptors, causing the platelets to become activated, change their morphology, release their

granule contents, and synthesize a variety of bioactive molecules. Of the numerous biomolecules released from activated platelets, the most important for primary hemostasis are adenosine diphosphate (ADP) and thromboxane A2 (TxA2) because both are platelet agonists capable of activating platelets in their own right. ADP and TxA2 molecules released into the blood stream bind to their respective receptors on nearby platelet membranes, activating those platelets, and recruiting them to the wound site. The newly recruited platelets undergo the same processes of shape change, granule content release, and biomolecule synthesis, leading to the activation of yet more platelets, which in turn recruit even more platelets, in a classic positive feedback loop, resulting in a rapidly escalating accumulation of platelets at the wound site. The result is a platelet plug, which, while porous, yet provides partial blockage of the vessel breach, slowing down blood loss. The process is schematically demonstrated in Figure 1.1 [3].

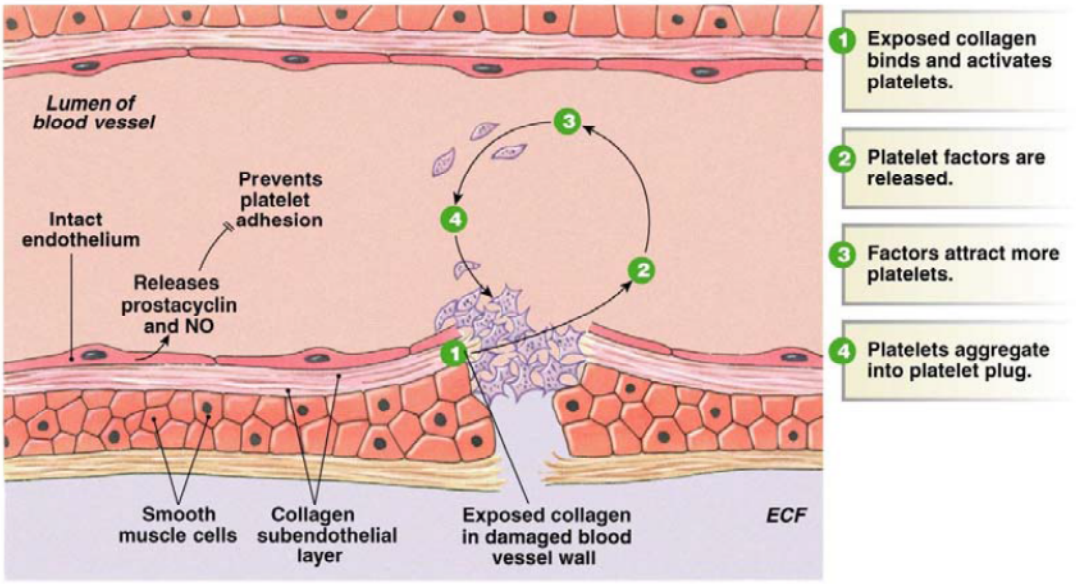

Figure 1.1. Schematic of hemostasis in response to vascular injury.

Concurrent with the just-described platelet aggregation process, the smooth muscle cells in the exposed sub-endothelium express tissue factor (TF), which, upon contact with the circulating blood, initiates secondary hemostasis, responsible for blood coagulation. Mechanistically, TF initiates the "coagulation cascade", which is a sequence of enzyme reactions culminating in the production of thrombin, a serine protease that mediates multiple functions, including production of fibrin and activation of coagulation factors in the same coagulation cascade. Such thrombin-mediated activation of coagulation factors ultimately leads to additional thrombin production, which feeds back for more coagulation factor activation and even more thrombin production, constituting a second positive feedback loop in the coagulation cascade, resulting in rapid and efficient production of thrombin, and fibrin, similar to what obtains in primary hemostasis with platelet aggregation. Fibrin produced at the end of

the coagulation cascade plays a crucial role in the entire hemostatic process: it crosslinks and forms a mesh that reinforces the porous platelet plug, turning it into a solid, impermeable clot that is able to arrest blood loss. Thus, primary hemostasis produces a porous platelet plug; secondary hemostasis reinforces it and turns it into a solid impermeable clot.

In addition to the positive feedback loops in primary and secondary hemostasis, the two sub-processes also interact mutually. The interaction mechanisms further enhance the individual sub-process positive feedback loops, whereby a strong response in one sub-process promotes and boosts the complementary response in the other, and vice versa, further amplifying response signals and thus promoting a truly ultra-rapid response to vascular injury. As is the case with engineering control systems, such positive feedback loops and amplifying interactions are potentially destabilizing if not regulated appropriately. Nevertheless, under normal conditions, hemostasis is stable and effective. This implies that there are additional stabilizing mechanisms involved in this biological control system.

At the heart, hemostasis is an automatic control system adopted by nature with the purpose to maintain the integrity of the blood vessel and minimize the total blood loss resulted from an injury to the blood vessel wall, through highly collaborative effort between numerous participants, positive feedback loops, as well as regulatory mechanisms. The thousands of proteins expressed in platelets [2] and the numerous biochemical reactions in the coagulation cascade, confounded by the interactions between them as well as the effect of flow, however, have made the balance between normal hemostasis and pathological thrombosis multi-factorial by its nature [4]. For this reason, how the various components work together to implement fast, effective

and stable responses to vascular injury has been difficult to understand using traditional methods alone—quantitative methods are required.

1.3 Integrative Modeling: an Engineering Control System Paradigm for Hemostasis

The approach proposed in this dissertation is based on the premise that from a process engineering perspective, hemostasis is mediated by an automatic biological control system. An engineering control system representation will therefore provide a structure for organizing the massive information efficiently in terms of the control system components as "functional modules," thereby facilitating systematic analysis of the complete hemostatic process as a combination of the component modules.

The hemostatic process is divided into the 4 major components of a generic control system: (i) controlled process: the process of interest in which a control objective is to be fulfilled by control actions; (ii) sensor: receives information about the current state of the controlled process and generates appropriate signals that are conveyed to the regulatory component; (iii) controller: produces appropriate corrective action signal in response to the sensor signal; and (iv) actuator: implements desired corrective action based on controller signals. The corresponding high-level engineering control system block diagram of hemostasis, shown in Figure 1.2, is used as the foundational basis of the holistic model of hemostasis. A physical injury of intensity d (a "process disturbance" in control engineering language) produces a wound of area S_8 through which blood will leak at a rate of S_9. The injury also exposes an area S_{10} in the sub-endothelium. The signal is converted by the injury sensors to the amount of exposed collagen fibers (S_1) and the thickness of the tissue factor-

containing layer (S_2), thereby initiating primary and secondary hemostasis, respectively.

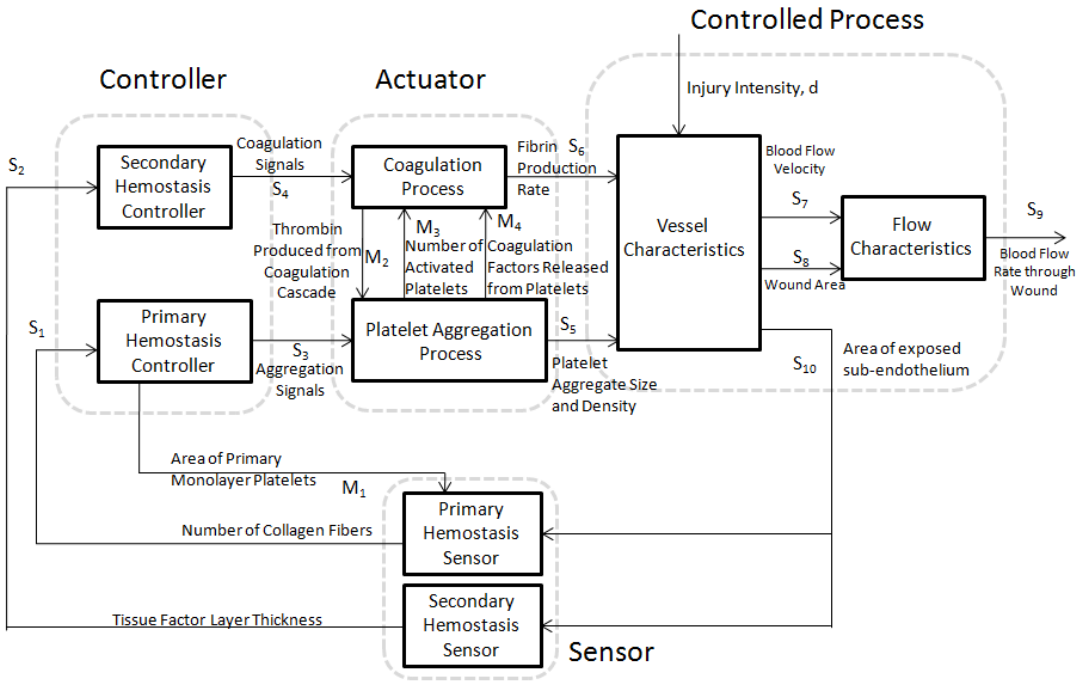

Figure 1.2. A high-level control system block diagram of hemostasis. Biological events in hemostasis are divided into distinguishable modules in this diagram. See main text for explanation. The arrows represent flow of information into and out of the subsystem blocks.

The controller also consists of two components: (i) primary hemostasis controller: responsible for regulating the platelet aggregation process; (ii) secondary hemostasis controller: responsible for regulating the coagulation process. The stimulus to the primary controller is the amount of exposed collagen fibers S1, which mediate collagen-induced platelet adhesion and activation; the primary response is platelet adhesion, resulting in M1 (the area of exposed sub-endothelium covered by platelets), and the release of agonists, signal S_3 being the concentrations of the released pro-aggregation ADP and TxA2. The secondary hemostasis controller is stimulated by the tissue factor in the exposed smooth muscle cell layer, whose thickness, signal S2, determines the rate of formation of the TF:FVIIa complex whose concentration is signal S_4.

The platelet aggregation process and the coagulation process constitute the actuator. The desired control actions, signal S_3 in primary hemostasis, and signal S_4 in secondary hemostasis, produce the final desired corrective action: a platelet aggregate of size S_5, which is reinforced and stabilized by the polymerized fibrin mesh of concentration S_6. Note the interactions between the two actuator components through M_2, M_3, and M_4. Thrombin produced by the coagulation cascade, M_2, is a potent platelet agonist, thereby influencing S_5; multiple coagulation reactions take place on the surface of aggregated platelets, so that S_6 is affected by M_3, the number of activated platelets; coagulations factor V and polyphosphate released from platelets, M_4, assist in the coagulation cascade, thus promoting S_6., The two actuator output signals combine in the vessel characteristics block to produce the blood clot whose size grows and whose porosity decreases progressively, eventually bringing the actual controlled variable, the rate of blood loss through the wound, S_9,to zero. Since there is

no physiological sensor for blood loss, S_9 is not measured directly. However, the exposed sub-endothelium area serves as the initial measure of blood loss; and when this exposed sub-endothelium is completely covered, the initiation signals stop but the propagation signals within the controller and actuator continue. The rate of blood loss is determined by injury intensity, the blood flow velocity, the porosity of the platelet plug, and the platelet plug area covering the wound created by the injury.

1.4 Dissertation Overview

The overall goal of this dissertation is to develop a comprehensive mathematical model of hemostasis based on the engineering control system structure proposed in the preceding section in order to obtain quantitative insight into the process of hemostasis. After completion of developing and validating the comprehensive model, the model can be further used for identifying potential treatment targets for hemophilic and thrombotic disorders.

Chapter 2 presents a mathematical description of the process of platelet activation. Chapter 3 is devoted to the development of a mathematical model of primary hemostasis. Chapter 4 consists of the development of the comprehensive model and model analyses. Chapter 5 presents how the comprehensive model developed in Chapter 4 can be used for identifying potential treatment targets for a number of disease states of hemostatic disorders. Chapter 6 is devoted to model-based solutions for maintaining a constant platelet count profile in a specific patient with low platelet count. Chapter 7 concludes the work of the dissertation and discusses future directions.

Chapter 2

MODELING AND ANALYSIS OF THE SINGLE PLATELET

2.1 Introduction

Platelet is the most important element in primary hemostasis. A detailed mathematical representation that can capture the characteristics of a single platelet is therefore required in order to develop a comprehensive model of hemostasis. As platelets have to respond quickly to vascular injuries, multiple mechanisms are used to sense and interact with its surrounding environment. In the next few sections, we introduce the physiological mechanisms of platelet response and how we use such information to develop a mathematical model of a single platelet.

Compared to other cell types, the modeling of the signaling pathways in the platelets is largely lacking. Purvis et al. presented a mathematical model on the $P2Y_1$ signaling pathway activated by ADP [5]. Their model used a system of ordinary differential equations (ODEs) to describe the reactions happening in different compartments in platelets. They were able to identify a handful of steady states that describe the resting condition of a single platelet. The stochastic nature due to the small volume of a platelet was also demonstrated with stochastic counterpart of their model. Lenoci et al. developed a mathematical model for the PAR1 signaling pathway activated by thrombin [6]. The positive feedback loops resulted from the release of ADP and synthesis of TxA2 were considered.

Other than the two studies mentioned above, there is no specific effort dedicated to simulating the complex signaling network in the platelet. One of the main

challenges is that there are multiple receptors on the platelet, hence multiple signaling pathways. As the signaling pathways crosstalk, which also occur in many other cell types, the result is a complex signaling network, and the behavior we see in a single platelet is the synergistic effect of multiple signaling pathways. In addition, as platelets release platelet agonists such as ADP and TxA2, they enhance their own activation and form positive feedback loops. Such process indicates that even with a single given stimulus to a platelet, additional stimuli will be generated and become in contact with the platelet. Therefore, a single platelet model that is able to capture the synergistic effect seen in platelet is crucial for predicting the behavior of the platelet.

2.2 Model Development and Validation

Platelets activated by collagen in the extracellular matrix respond by releasing platelet agonists adenosine diphosphate (ADP) and thromboxane A2 (TxA2), which together constitute the aggregation signal S_3 in Figure 1.2. The release of agonists leads to the activation of more platelets which subsequently aggregate to form a platelet plug, the size and porosity of which constitute signal S_5 in Figure 1.2, the output of the aggregation process. Our mathematical model of single platelet therefore began with quantifying the roles of ADP and TxA2 during the activation of a single platelet.

2.2.1 ADP-Mediated Signaling Overview

Two types of ADP receptors are expressed on the plasma membrane of platelets: $P2Y_1$ and $P2Y_{12}$, both G-protein coupled receptors (GPCRs). Figure 2.1 shows a schematic diagram of the major signaling transduction pathways induced by

ADP and TxA2, as well as the signaling pathways induced by platelet inhibitors PGI2 and NO, which are secreted by intact endothelial cells.

2.2.1.1 $P2Y_1$ Signaling Overview

Upon ADP stimulation, $P2Y_1$ is activated and quickly activates heterotrimeric G_q protein, whose α subunit then activates phospholipase C β (PLCβ) [7]. PLCβ then converts the phosphatidylinositols (PIs) on the plasma membrane into diacylglycerol (DAG) and inositol phosphates [8]. Of the various inositol phosphates, inositol 1,4,5-triphosphate (IP_3) is the most important in triggering calcium release from platelet dense tubular system (DTS); it achieves this by binding to the inositol triphosphate receptors (IP_3R) on DTS, leading to rapid intracellular calcium increase [9]. Both DAG and the rise in intracellular Ca^{2+} concentration modulate the activity of protein kinase C (PKC) [10, 11]. Ca^{2+} and DAG-regulated guanine nucleotide exchange factor (CalDAGGEF) has been found to be crucial in integrating Ca^{2+} and DAG signals, leading to activation of the small GTPase Ras-related protein 1 (Rap1), which then works with activated PKC and results in integrin $\alpha_{IIb}\beta_3$ activation required for platelet aggregation [12, 13].

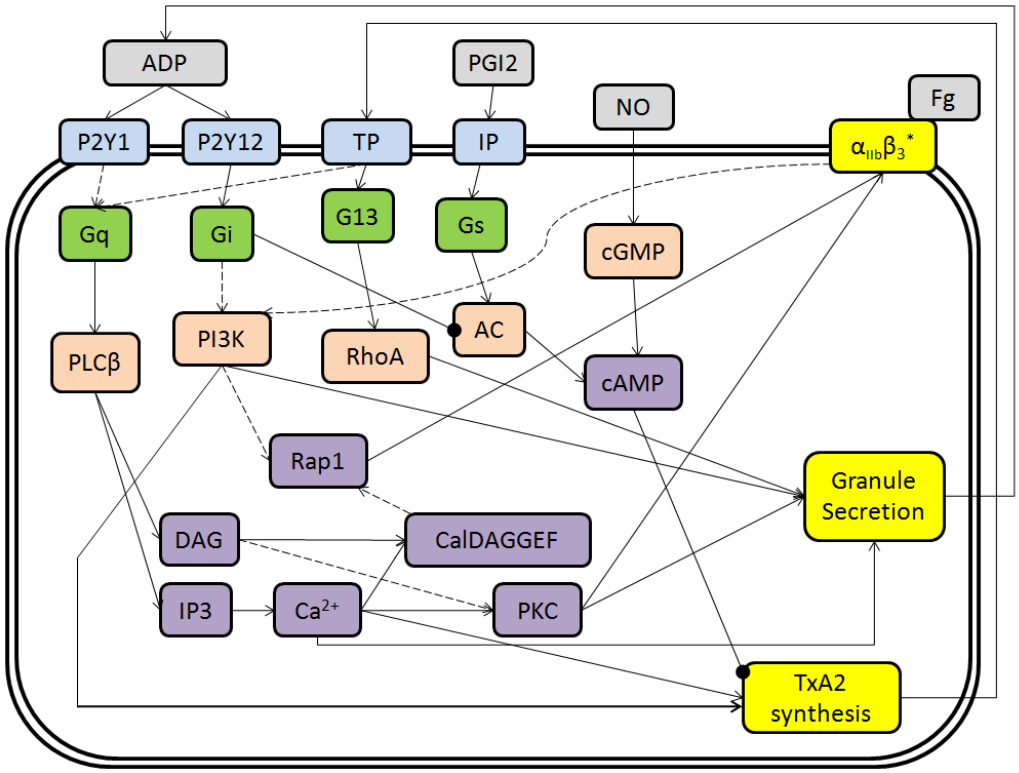

Figure 2.1 Platelet activation pathways. Solid lines: essential signals; dashed lines: auxiliary signals; arrows: stimulatory effect; dots: inhibitory effect.

2.2.1.2 $P2Y_{12}$ Signaling Overview

$P2Y_{12}$ is a GPCR that couples with heterotrimeric G_i protein. After activation by ADP, $P2Y_{12}$ quickly transforms G_i into its GTP-bound form, triggering two major pathways. G_i activates phosphoinositides 3-kinases (PI3K), which plays a role in the activation of Rap1 [14], granule secretion [15], and TxA2 synthesis [16]. As Rap1 is required in activating integrin $\alpha_{IIb}\beta_3$, $P2Y_{12}$ signaling is also crucial in platelet aggregation. Another major function of G_i is that G_i inhibits adenylyl cyclase (AC), leading to a decrease in the cAMP level which when high prevents platelet activation [17] and TxA2 synthesis [18].

2.2.1.3 Positive Feedback: Outside-In Signaling, Granule Secretion and TxA2 Synthesis

Once activated, $\alpha_{IIb}\beta_3$ binds to fibrinogen in the blood stream and triggers outside-in signaling to activate PLCγ and PI3K [19] and reinforce platelet activation. Outside-in signaling also activates phospholipase A2 (PLA2) to help with TxA2 synthesis. When TxA2 is released from platelets, it activates nearby TxA2 receptors, (TP) on the plasma membrane of platelets. Signaling events downstream of TP lead to activation of RhoA, which is required for the release of platelet dense granules, resulting in the release of ADP, which further activates more platelets, thereby forming a positive feedback loop.

2.2.1.4 Inherent Inhibitory Signaling Pathways

As mentioned in Chapter 1, endothelial cells secrets platelet inhibitors such as prostacyclin (PGI2) and nitric oxide (NO) to prevent platelets from activating when the blood vessel is under the normal state. PGI2 binds to its receptor IP on platelet membranes to stimulate the activation of Gs protein, which stimulates AC activation, eventually leading to an elevated cAMP level that inhibits TxA2 production. NO, on the other hand, directly enters the cells and increase the level of cGMP, resulting in an increase in cAMP, further reducing synthesis of TxA2. Note that these two inhibitory pathways should cease to work once an injury occurs to a blood vessel and the endothelial lining is discontinued.

2.2.1.5 Platelet aggregation

Platelet aggregation occurs when two platelets are joined together by fibrinogen, whose two ends can bind to active integrins $\alpha_{IIb}\beta_3$ on two different platelets, thereby forming the connection between platelets and causing aggregation.

2.2.2 Model Development: Single Platelet Model

Based on the signaling pathways and mechanisms summarized in the preceding sections, the information of the reactions involved in ADP-induced platelet activation is divided into a more detailed block diagram shown in Figure 2.2, which will be used as the structure to develop the single platelet model to simulate the behavior of a single platelet in the presence of agonists. The blocks and connections are based on known reactions and mechanisms. Mathematical expressions will be developed to link the input to the output of the blocks in order to represent the biological events occurring in those blocks. Reaction schemes employed in the mathematical expressions are based on (i) existing computational models, or (ii) our postulates that aim to match known biological characteristics of the reactions in question. The reactions and their corresponding kinetic rate constants used in the single platelet model are summarized in Table 2.1. In principle, the parameters β, a, and n in Table 2.1 are parameters of the Hill function commonly used to represent the dynamics of biological reactions. For example, the rate equation for reaction A → B is written as:

$$\frac{d[B]}{dt} = \beta \frac{[A]^n}{a^n + [A]^n} \tag{2.1}$$

where β is the rate constant for the production of B induced by A, a is the affinity constant that represents the concentration of A needed to achieve 50% of the maximum production rate of B, and n is the Hill coefficient. Parameter k in Table 2.1 is the rate constant for describing elementary reactions of the formation or degradation of a protein or a signaling molecule.

The parameter values in Table 2.1 and the non-zero initial concentrations of the signaling molecules in Table 2.2 were obtained either from the literature [5, 6] or

estimated to fit the theoretical or experimental data available in the literature [5, 6, 20]. The single platelet model is an ODE model built in MATLAB/Simulink (R2008a, The Mathworks, Natick, MA). The resulting system of ODEs is solved over a time period of 250 seconds using the ODE15s solver.

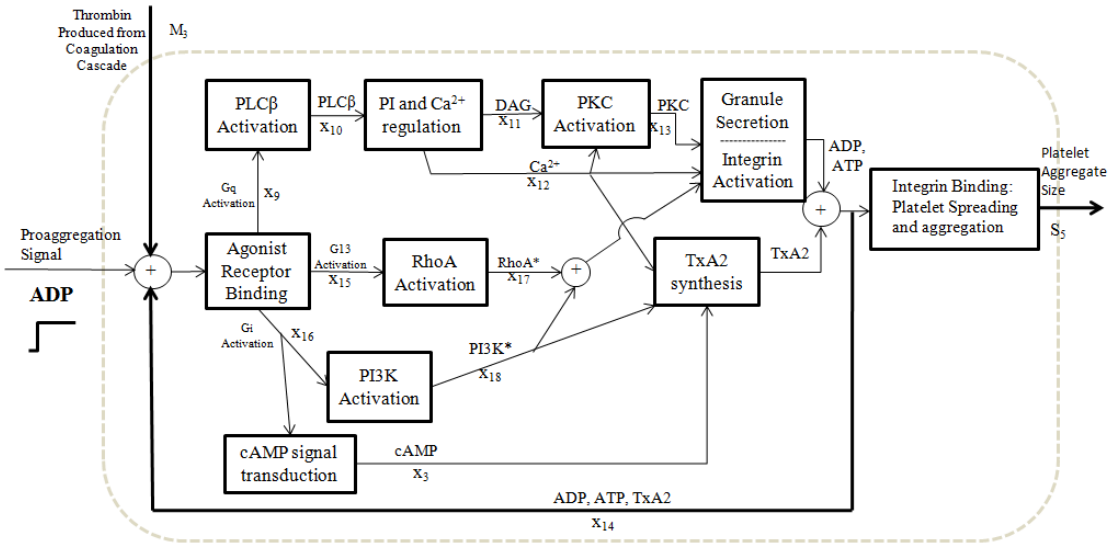

Figure 2.2. Control system block diagram of single platelet.

Table 2.1 Reactions and parameters governing ADP-induced platelet activation, granule secretion, and platelet aggregation

Symbolic reactions	Constants	References
Reactions governing Gq activation downstream of $P2Y_1$		
ADP → GqGTP	β=0.0205 $\mu M\ s^{-1}$, a=2 μM, n=1.5	
GqGTP→ null	k=0.1005 s^{-1}	
Reactions governing Gi activation downstream of $P2Y_{12}$		
ADP → GiGTP	β=0.0205 $\mu M\ s^{-1}$, a=5 μM, n=1.16	
GiGTP→ null	k=0.1005 s^{-1}	
Reactions governing Gq and G13 activation downstream of TxA2 receptor		
TxA2 → GqGTP	β=0.015 $\mu M\ s^{-1}$, a=0.003 μM, n=5	
GqGTP→ null	k=0.1005 s^{-1}	
TxA2 → G13GTP	β=0.0205 $\mu M\ s^{-1}$, a=0.003 μM, n=5	
G13GTP→ null	k=0.1 s^{-1}	
Reactions governing Gs activation downstream of PGI2 receptor		
PGI2 + GsGDP → GsGTP	k=1 $\mu M\ s^{-1}$	
GsGTP→ null	k=0.00136 s^{-1}	
Reactions governing PLCβ activation		
GqGTP+PLCβ ↔ PLCβ*GqGTP	k_1=1.2 $\mu M^{-1}s^{-1}$, k_{-1}=0.06 s^{-1}	
PLCβ*GqGTP→ PLCβGqGDP	k=25 s^{-1}	
PLCβGqGDP ↔ PLCβ + GqGDP	k_1=0.5 s^{-1}, k_{-1}=5 $\mu M^{-1}s^{-1}$	
Reactions governing PI3K activation		
GiGTP→ PI3K*	β=5 $\mu M\ s^{-1}$, a=0.05 μM, n=3	
G13GTP → PI3K*	β=1.5 $\mu M\ s^{-1}$, a=0.1 μM, n=3	
PI3K* → null	k=0.5 s^{-1}	
Reactions governing RhoA activation		
G13GTP + RhoA → RhoA*	β=100 $\mu M\ s^{-1}$, a=0.15 μM, n=1.5	
RhoA* → null	k=0.003 s^{-1}	
Reactions governing AC regulation		
GsGTP + AC → AC*	k=0.02 $\mu M^{-1}s^{-1}$	
GiGTP + AC* → AC	β=5 s^{-1}, a=0.12 μM, n=7	
AC* → AC	k=0.00375 s^{-1}	
Reactions governing cGMP regulation		
NO → cGMP	k=0.000181 s^{-1}	
cGMP→ null	k=0.136 s^{-1}	
Reactions governing IP3 and DAG production		
PLCβ* + PI ↔ PLCβ*-PI	k_1=100 $\mu M^{-1}s^{-1}$, k_{-1}=70499 s^{-1},	
→ PIP + DAG	k_{cat}=1.43 s^{-1}	[5]
PLCβ* + PIP ↔ PLCβ*-PIP	k_1=100 $\mu M^{-1}s^{-1}$, k_{-1}=19000 s^{-1},	
→ PIP2 + IP3 + DAG	k_{cat}=0.35 s^{-1}	[5]
PLCβ* + PIP2 ↔ PLCβ*-PIP2	k_1=100 $\mu M^{-1}s^{-1}$, k_{-1}=49990 s^{-1},	
→ PIP3 + DAG	k_{cat}=9.8505 s^{-1}	[5]

Table 2.1 continued

Symbolic reactions	Constants	References
IP3 → null	$k = 0.15\ s^{-1}$	
DAG + DGK → null	$k_{cat}=0.26\ s^{-1}$, $K_M=250\ \mu M$	[5]
DAG → null	$k=0.01\ s^{-1}$	
Reactions governing cAMP regulation		
AC* →cAMP	$\beta=3.25\ \mu M\ s^{-1}$, $a=0.08\ \mu M$, $n=3$	
cGMP → cAMP	$k=0.1674\ s^{-1}$	
cAMP→ null	$k=1\ s^{-1}$	
Reactions governing intracellular Ca^{2+} increase		
IP3 → Ca^{2+}	$\beta=11000\ \mu M\ s^{-1}$, $a=0.02\ \mu M$, $n=1.1$	
Ca^{2+}→ null	$k=20000\ s^{-1}$	
Reactions governing PKC and CalDAGGEF activation		
PKC + Ca^{2+} ↔ PKC*	$k_1=10\ \mu M^{-1}s^{-1}$, $k_{-1}=1\ s^{-1}$	
PKC + DAG + Ca^{2+} ↔ PKC*	$k_1=1\ \mu M^{-2}s^{-1}$, $k_{-1}=0.01\ s^{-1}$	
DAG + Ca2+ →CalDAGGEF	$\beta=10^7\ s^{-1}$, $a_{Ca2+}=0.01\ \mu M$, $n_{Ca2+}=1.2$	
CalDAGGEF→ null	$k=10^4\ s^{-1}$	
Reactions governing dense granule secretion		
ATP_{inplt}+ Ca^{2+} + PKC* + PI3K + RhoA→ ATP	$k=2.7\ \mu M^{-3}s^{-1}$, $a_{RhoA}=5\ \mu M$, $n_{RhoA}=5$	
ATP → null	$k=0.008\ s^{-1}$	
Reactions governing Rap1 activation		
Rap1GDP + PI3K → Rap1GTP	$\beta=10^7\ s^{-1}$, $a_{PI3K}=12\ \mu M$, $n_{PI3K}=6$	
Rap1GDP + CalDAGGEF → Rap1GTP	$k=10^7\ s^{-1}$	
Rap1GTP → Rap1GDP	$k=5\times10^7\mu M^{-1}s^{-1}$	
Reactions governing $\alpha_{IIb}\beta_3$ activation		
PKC* + Rap1GTP + $\alpha_{IIb}\beta_3$ ↔ $\alpha_{IIb}\beta_3$*	$k=10^8\ \mu M^{-1}s^{-1}$, $a_{Rap1}=3\ \mu M$, $n_{Rap1}=6$, $k_{-1}=0.1\ s^{-1}$	
Reactions governing platelet aggregation		
PLT + Fg + $\alpha_{IIb}\beta_3$* ↔ PLT aggregate	$k_1=10^{-11}\ \mu M^{-2}s^{-1}$, $k_{-1}=0.15\ s^{-1}$	
Reactions governing outside-in signaling		
Fg + $\alpha_{IIb}\beta_3$* →Fg-$\alpha_{IIb}\beta_3$*	$k=0.01\ \mu M^{-1}s^{-1}$	
Fg-$\alpha_{IIb}\beta_3$* → null	$k=0.005\ s^{-1}$	
(outside-in signal)=(Fg-$\alpha_{IIb}\beta_3$*)÷8×10^4		
Reactions governing outside-in signaling-mediated PLCγ activation		
outside-in signal + PLCγ→PLCγ*	$\beta=5\times10^{-5}\ s^{-1}$, $a_{OI}=2\times10^5$, $n_{OI}=3$	
PLCγ* → null	$k=0.1\ s^{-1}$	
Reactions governing outside-in signaling-mediated PI3K activation		
outside-in signal → $PI3K_o$*	$\beta=1\ s^{-1}$, $a_{OI}=2\times10^5$, $n_{OI}=3$	
$PI3K_o$* → null	$k=1\ s^{-1}$	

Table 2.1 continued

Symbolic reactions	Constants	References
Reactions governing outside-in signaling-mediated PLA2 activation		
outside-in signal → PLA2*	$\beta=5\ s^{-1}$, $a_{OI}=4\times10^{5}$, $n_{OI}=5$	
PLA2* → null	$k=0.5\ s^{-1}$	
Reactions governing TxA2 synthesis		
Ca^{2+} + AA + PLA2* + $cAMP^{-1}$ → TxA2	$\beta=10^{1}\mu M^{-2}s^{-1}$, $a_{PLA2}=0.7\ \mu M$, $n_{PLA2}=3$	
Ca^{2+} + AA + PLA2* + $cAMP^{-1}$ + PI3K → TxA2	$\beta=10^{2}\mu M^{-3}s^{-1}$, $a_{cAMP}=100\ \mu M^{-1}$, $n_{cAMP}=5$	
TxA2 → TxB2	$k=0.0217\ s^{-1}$	[21]

Table 2.2. Initial non-zero metabolite concentrations used in the simulation of an ADP-stimulated human platelet

Species	Initial Condition	Unit	Referece
PLCβ	1	μM	[5]
PLCβGqGDP	1×10^{-6}	μM	[5]
GqGDP	0.01	μM	[5]
RhoA	3×10^{-3}	μM	[6]
AC*	0.08	μM	
AC	0.1	μM	
PI	0.1	μM	[5]
PIP	0.1	μM	[5]
GsGTP	0.15	μM	
PIP2	0.02	μM	[5]
DGK	0.5	μM	[5]
cAMP	1.65	μM	[22]
cGMP	0.181	μM	[22]
PKC	0.05	μM	[5]
PLCγ	1	μM	
AA	10^{5}	mlc/plt	[23]
ATP	2×10^{7}	mlc/plt	[24]
Fg	2.1	mg/mL	[25]

2.2.3 Model Validation

The single platelet model is tested under various conditions to see whether its prediction is consistent with experimental observations. In the following sections, the single platelet model is used to simulate platelet activation, dense granule secretion, and platelet aggregation in response to varying ADP concentrations. The resulting profiles of dense granule secretion and platelet aggregation are compared with experimental data in [20]

2.2.3.1 Platelet Dense Granule Secretion

Granule secretion is an important step in forming a positive feedback loop in which the rapid release of ADP results in additional activation of new platelets. As ADP itself is not easily measured, ATP, which is stored in platelet dense granules along with ADP, is usually used as an indicator of dense granule secretion. The model simulation result in Figure 2.3a shows that stimulation with 1 μM ADP is insufficient to cause dense granule secretion; stimulation with 3 μM and 10 μM ADP causes granule secretion as indicated by the ATP release profile shown. The general trend as well as the amount of ATP released predicted from our model are consistent with the experimental results found in [20], as shown in Figure 2.3b.

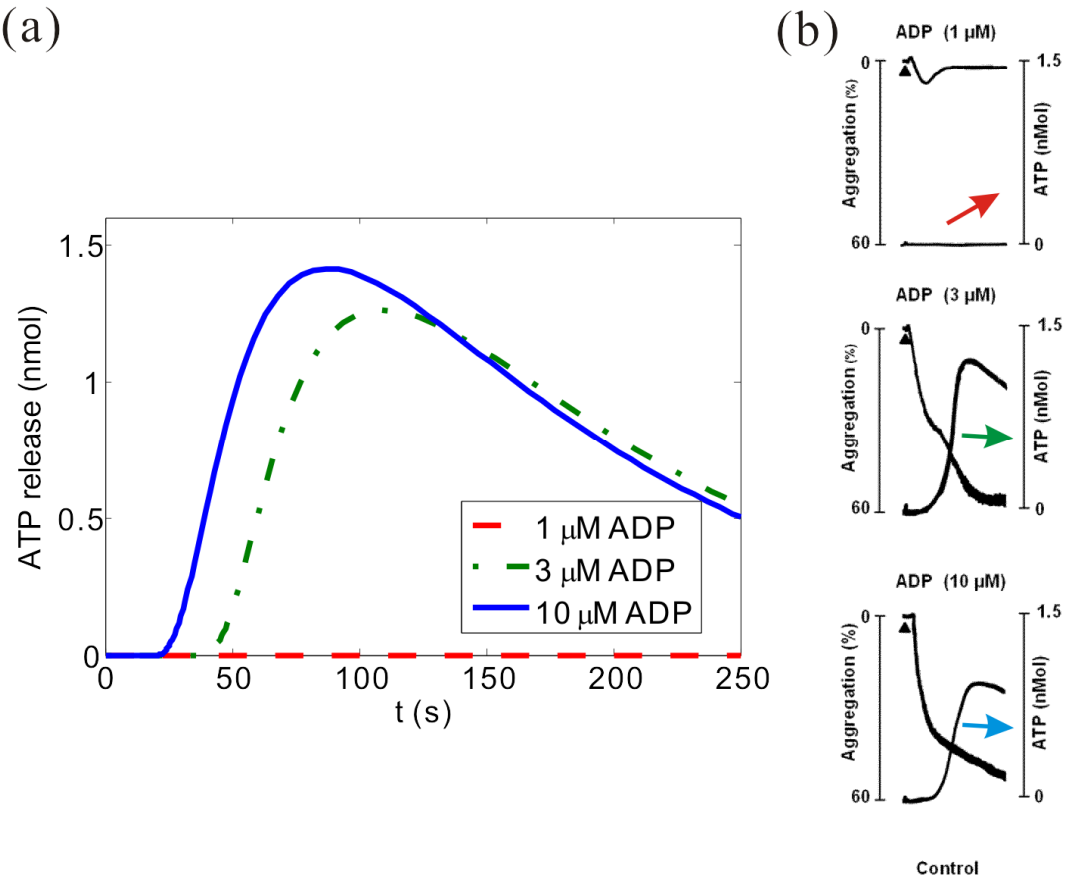

Figure 2.3. ATP release with different stimulating ADP concentrations: (a) simulation; (b) experimental data by Dawood et al.[20]

2.2.3.2 Platelet Aggregation

As Figure 2.4a shows, upon stimulation with 1 μM ADP, only a small number of platelets aggregate initially, which then disaggregate soon thereafter. This simulation result is consistent with experimental data shown in the top panel of Figure 2.4b. With 3 μM ADP stimulation, experimental data in the middle panel of Figure 2.4b show two waves of aggregation. Comparing the platelet aggregation profile with the ATP secretion profile, it is obvious that the second wave of platelet aggregation is resulted from dense granule secretion, indicating the importance of the granule content

in supporting platelet aggregation. Our model also shows similar characteristics. Although the aggregation rate in the first wave is not as fast as observed in the experiment, the two waves of aggregation are clear.

In the experiment with 10 μM ADP, the resulting aggregation rate is so fast that the second wave is no longer as clear (bottom panel of Figure 2.4b). The same characteristic is observed in our corresponding simulation result. Our simulation of the system in response to 10 μM ADP shows subsequent disaggregation, a phenomenon not seen in the corresponding experiment data, possibly because the duration of the experiment is shorter than the simulation.

2.2.4 Parametric Sensitivity Analysis

To identify which model parameters are the most significant and therefore gain insight into the dominant components in a platelet, we performed sensitivity analysis on our model. The computations are based on the following expression for normalized sensitivity coefficients (NSC):

$$NSC_i = \frac{\partial y_i(p)/y_0}{\partial p_i / p_{i,0}} \tag{2.2}$$

The model was first run with the nominal parameter set p_0 to obtain the nominal primary response, y_0, which in this specific case is the amount of ATP released. The value of one parameter (p_i) was then increased by 10% and the model was run to obtain the amount of ATP released under the changed condition (y_i). The NSC was then calculated according to the above equation. The same procedure was repeated for every parameter listed in Table A.1 in Appendix A and the resulting NSCs are presented in Figure 2.5.

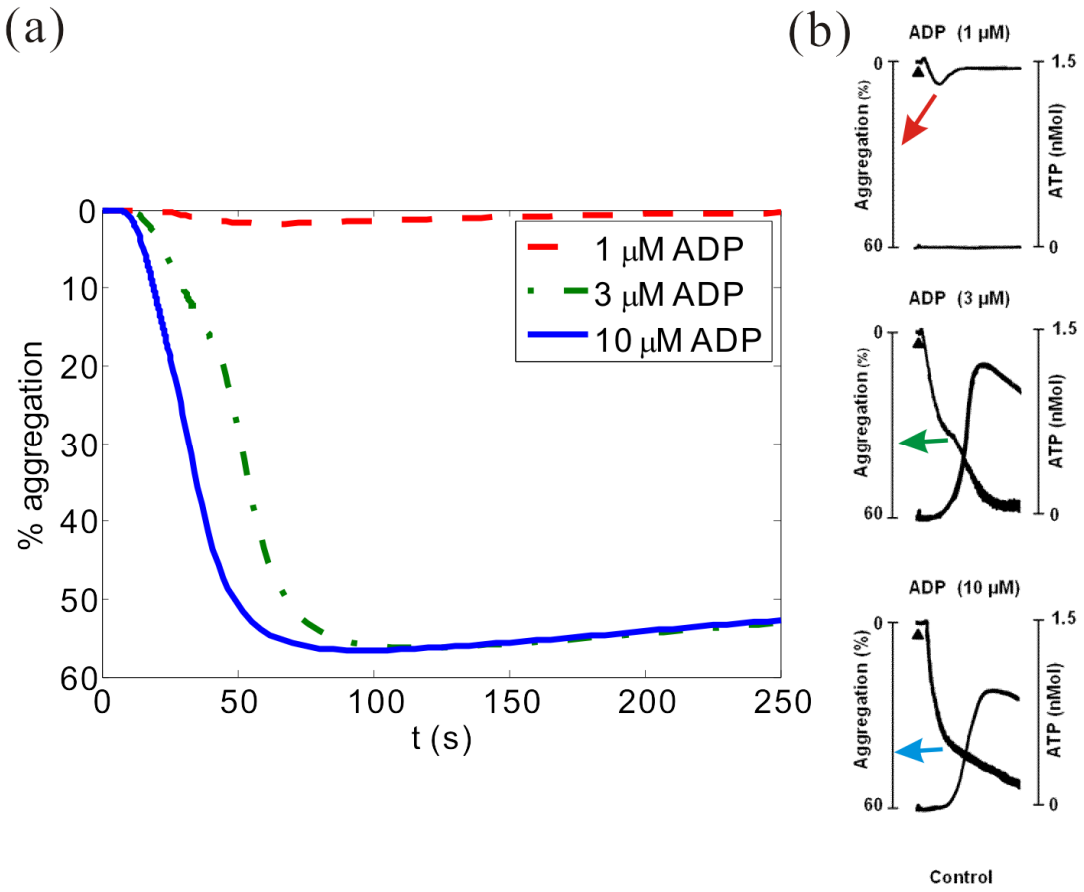

Figure 2.4 Platelet aggregation in response to stimulation with different ADP concentrations: (a) simulation; (b) experimental data by Dawood et al.[20]

The most significant parameters (parameters with the largest absolute normalized sensitivity coefficients) in dense granule secretion are shown in Figure 2.6 and their physiological meanings are summarized in Table 2.3. These results indicate that the parameters associated with RhoA for granule secretion have the most significant effect on dense granule secretion, thereby indicating the importance of TxA2 signaling and emphasizing the importance of the positive feedback loop (the implementation of which depends on TxA2). The parameters associated with Ca^{2+}

increase are also shown to be significant, as expected, since Ca^{2+} is involved in many biological phenomena in cells. In addition, the parameters associated with the production of IP3 play a major role in granule secretion. As IP3 is the molecule for triggering Ca^{2+} increase, this again signifies the importance of Ca^{2+} increase in the process of dense granule secretion.

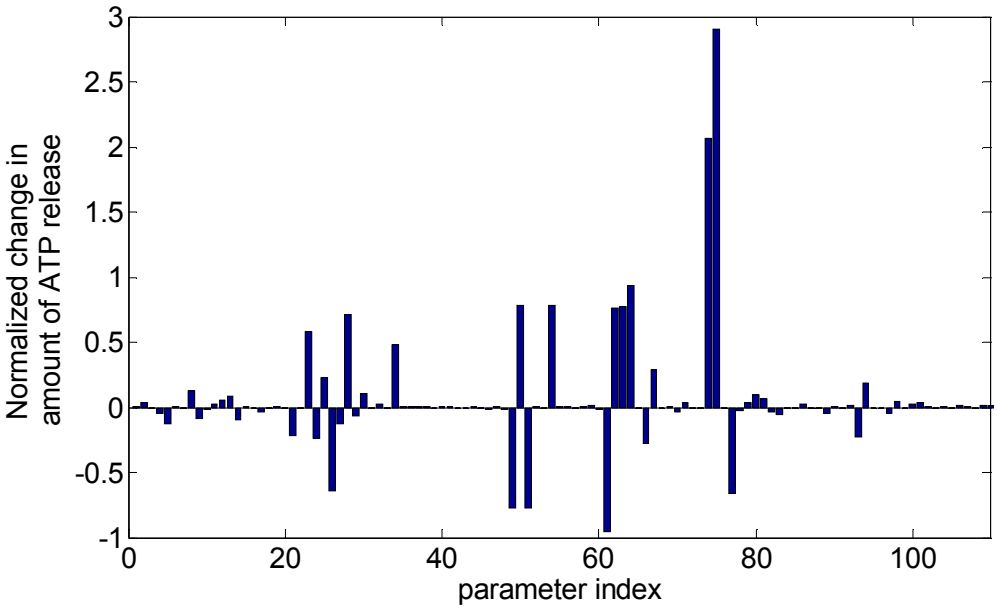

Figure 2.5. Sensitivity of amount of ATP release to a 10% increase in parameters: normalized sensitivity coefficients for all parameters.

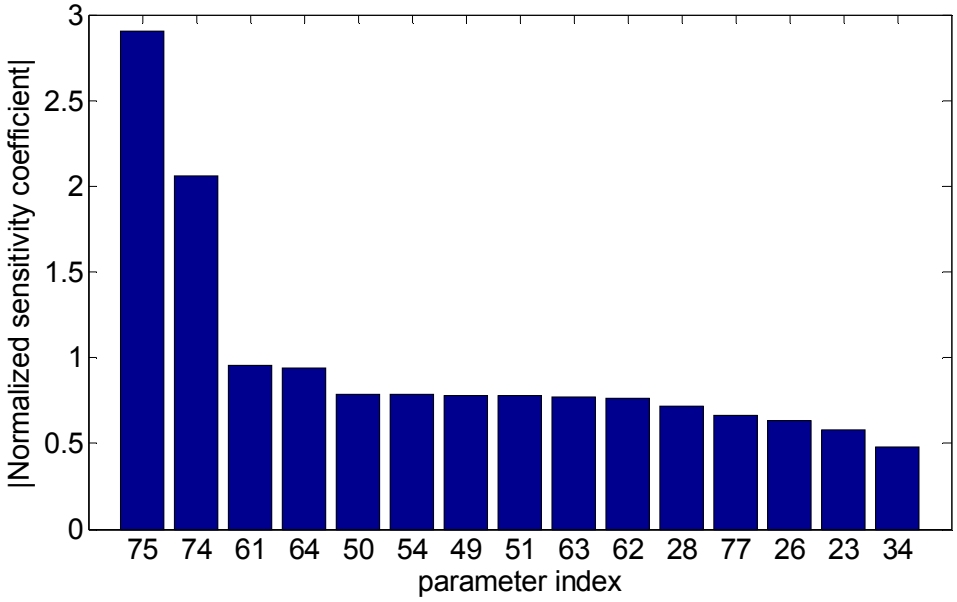

Figure 2.6. Sensitivity of platelet dense granule secretion to a 10% increase in parameters: absolute normalized sensitivity coefficients of the most significant parameters.

Table 2.3. List of most significant parameters in platelet dense granule secretion

Parameter index	Related regulatory event	Notation	Description
75	dense granule secretion	a	affinity constant for the effect of RhoA on dense granule secretion
74	dense granule secretion	n	Hill coefficient for the effect of RhoA on dense granule secretion
61	calcium release	β	rate constant of calcium increase induced by IP3
64	calcium release	k	rate constant of calcium consumption
50	DAG production and IP3 formation	k_{-1}	dissociation of PLCβ*PIP2
54	DAG production and IP3 formation	k	rate constant of degradation of IP3
49	DAG production and IP3 formation	k_1	binding of PLCβ* to PIP2

Table 2.3. continued

51	DAG production and IP3 formation	k_{cat}	rate constant of production of PIP3 and DAG
63	calcium release	a	affinity constant for calcium increase induced by IP3
62	calcium release	n	Hill coefficient for calcium increase induced by IP3
28	PI3K activation by inside-out signaling	k	rate constant of degradation of PI3K
77	dense granule secretion	k	rate constant for the release of dense granules
26	PI3K activation by inside-out signaling	β	rate constant of PI3K activation induced by GiGTP
23	PLCβ activation	k_{cat}	deactivation of PLCβ*GqGTP
34	RhoA activation	k	rate constant of degradation of RhoA

2.3 Summary

In this chapter, in order to mathematically describe the platelet aggregation process in *in vivo* hemostasis, we first developed a single platelet model that was intended for quantitatively describing platelet activation induced by important platelet agonists. Using a hybrid approach, where part of the model was based on known detailed reaction mechanisms and part of the model was based on our postulated mechanisms, we were able to develop a model capable of describing ADP-induced platelet activation. The major molecules in the signaling pathways downstream of ADP receptors, as well as the signaling pathways induced by TxA2 and inhibitors such as PGI2 and NO, were included, enabling the model to describe platelet dense granule secretion, integrin outside-in signaling, TxA2 synthesis, and *in vitro* platelet aggregation in a test tube.

The resulting profiles from the single platelet model in response to ADP stimulation were shown to be consistent with *in vitro* experiments of ATP release and platelet aggregation. Local parametric sensitivity analysis was performed on the single platelet model. It was shown that signaling pathways downstream of TxA2 receptor and reactions related to calcium release significantly affect ADP secretion, highlighting the important roles of these events in the positive feedback loop in primary hemostasis.

Chapter 3

A NOVEL MATHEMATICAL REPRESENTATION OF PRIMARY HEMOSTASIS

3.1 Introduction

3.1.1 Mechanistic Basis of Primary Hemostasis

As briefly introduced in Chapter 1, primary hemostasis is initiated when an injury compromises the integrity of the endothelial lining of a blood vessel, consequently exposing the sub-endothelial layer. Such exposure presents collagen in the sub-endothelium to the blood stream. Platelets in the blood stream therefore come into contact with collagen, a strong agonist to platelet, and become activated. Collagen-induced platelet activation results in the secretion of platelet dense granule content such as ADP, and the synthesis of TxA2. As ADP and TxA2 are both platelet agonists, they can activate and recruit nearby platelets upon release. ADP and TxA2 bind to their respective receptors on platelets and activate the pathways downstream of the receptors, as introduced in Chapter 2. These platelets release their own ADP and TxA2 that will further activate even more platelets, forming a positive feedback loop. The end product of such positive feedback loop is a platelet aggregate that partially blocks blood loss. With the help of fibrin from secondary hemostasis, the platelet plug turns into a clot and conceals the wound. In addition to fibrin, thrombin, another product of secondary hemostasis, also plays an important role in primary hemostasis for being a strong platelet agonist that promotes the platelet aggregation process.

3.1.2 Previous Work on Modeling Primary Hemostasis

Even though quite a few mathematical models of hemostasis have been developed, the models either majorly focus on secondary hemostasis [26], or they do not consider the complex signaling pathways occurring in the platelets and use much simplified equations to represent the complex dynamics of platelet activation, aggregation, granule secretion, and disaggregation [27-29]. Sorensen et al. [27, 28], Kuharsky et al. [26], and Storti et al. [29] developed mathematical models that use simple mechanisms to describe the process of primary hemostasis. However, the first step of primary hemostasis is the activation of platelets through the multiple signaling pathways that occur within the platelets. Therefore, previous models are not able to predict or consider the cases when a certain protein is dysfunctional and the platelet function becomes defective or hyperactive. The inclusion of the signaling network in the platelet into a primary hemostasis model is important because that is ultimately how one can interfere with the process of platelet aggregation, through the function of a certain molecule that binds and affect the downstream signaling in platelets.

As introduced in the previous chapter, Purvis and colleagues developed a mathematical model on ADP-induced $P2Y_1$ activation up to the release of calcium. Lenocci et al. focused on the thrombin-induced PAR1 receptor signaling pathway [6] and validated their mathematical model against *in vitro* experiments. Sorensen et al. [27, 28] used convection-diffusion-reaction equations to describe platelet deposition, agonist release, and thrombin production with simplified and hypothesized mechanisms. Xu et al. developed multi-scale models that use a cellular Potts model to account for platelet aggregation and incorporate partially the coagulation pathways [30, 31]. Flamm and colleagues [32] developed a multi-scale model that describes various contributors to primary hemostasis, including a neural network for

representing the platelet phenotype of an individual in order to simulate individual-specific platelet deposition under flow Storti et al. [29] developed a continuum model of primary hemostasis where they used a moving boundary to describe the spatial profile of the occurrence of platelet aggregation.

In spite of all previous effort, no model on primary hemostasis has described how, from platelet activation, platelet aggregation occurs through fibrinogen binding and how the activation of new platelets is driven by the agonists secreted by aggregating platelets. As the signaling events and the platelet secretion process are crucial in the normal functioning of primary hemostasis, incorporating such information in the model will enable us to gain further insight into the dynamics of the process. In this chapter, we present a mathematical model of ordinary differential equations (ODEs) that incorporates the physiological events in primary hemostasis without thrombin. The mathematical model is developed using the structure of a classical engineering control system proposed in Chapter 1, where the biological events occurring in primary hemostasis are divided into its components: biological equivalents of a sensor, controller, and actuator.

3.2 Model Development: Primary Hemostasis

Using the physiological details introduced in section 3.1.1, we develop a model of primary hemostasis based on the engineering control system framework proposed in Chapter 1. In the following sections, each block regarding primary hemostasis in Figure 1.2 is investigated and represented with mathematical expressions.

3.2.1 Controlled Process: Area of Exposed Sub-Endothelium

The effect of an injury intensity d in Figure 1.2 is an initial wound area of A_{wound}, or S_8(t = 0). The area is considered to be circular for deducing the perimeter of the wound. Assuming a sub-endothelium thickness of T_{sub}, the area of exposed sub-endothelium A_{sub}, or S_{10} in Figure 1.2, is therefore

$$A_{sub} = 2T_{sub}\sqrt{\pi d} \tag{3.1}$$

The rate of bleeding following wound occurrence, Q_{blood} (S_9 in Figure 1.2) is estimated using the following equation:

$$\begin{aligned} Q_{blood} &= v_{blood} A_{uncovered} \\ &= v_{blood}(A_{wound} - A_{covered}\phi_p) \end{aligned} \tag{3.2}$$

where v_{blood} (S_7 in Figure 1.2) is the linear velocity of the blood flow, $A_{uncovered}$ (S_8 in Figure 1.2) is the area of the wound that has not been covered by the aggregate, $A_{covered}$ is the wounded area covered by the aggregate, and ϕ_p is the porosity of the aggregate. The porosity of the aggregate is set at a constant of 0.5 in the primary hemostasis model, since fibrin, the medium of decreasing the porosity of the platelet aggregate, is not considered in the primary hemostasis model.

The total volume of blood loss is estimated by

$$V_{loss} = \int_0^t Q_{blood} dt \tag{3.3}$$

3.2.2 Primary Hemostasis Sensor and Controller

3.2.2.1 Number of Available Collagen Fibers

Exposure of the sub-endothelium leads to the exposure of collagen. However, only a fraction, F, of the exposed sub-endothelium contains collagen. The collagen-containing area capable of activating platelets is thus $A_{sub} \times F$. In addition, the number of collagen fibers is affected by the density of collagen, ρ_{col}, expressed in the sub-endothelium. Hence the number of collagen fibers that determines the intensity of the stimulus is expressed as $A_{sub} \times F \times \rho_{col}$.

As platelets bind to the collagen-abundant area, they cover the area and form a physical barrier between collagen and other platelets. Eventually only a monolayer of platelets will be bound to collagen. The number of available collagen fibers is thus dynamically changing with the area covered by collagen-bound platelet A_{mono}, or M_1 in Figure 1.2. The number of available collagen fibers, N_{col} in Eq. (3.4) or S_1 in Figure 1.2, is therefore:

$$N_{col} = \left(A_{sub} \times F - A_{mono} \right) \rho_{col} \tag{3.4}$$

3.2.2.2 ADP and TxA2 Release from Collagen-Induced Platelet Activation

The rate of platelet adhesion to collagen fibers is assumed to be proportional to the number of available collagen fibers. A Hill function is used to incorporate the effect of platelet count in the blood stream, since a much reduced platelet count will lead to defect in thrombus formation, a phenomenon seen in patients with Immune Thrombocytopenic Purpura. As collagen is a strong activator, platelet detachment from collagen fibers is considered negligible. The process is described by the following equation:

$$\frac{d\left(PLT_{col}\right)}{dt} = R_{PLT_{col}} = k_{16} N_{col} \frac{[PLT]^{n_{16}}}{a^{n_{16}} + [PLT]^{n_{16}}} \tag{3.5}$$

where PLT_{col} refers to the number of collagen-bound platelets.

Each single platelet is capable of releasing only a limited amount of ADP and TxA2, denoted by Q_{ADP} and Q_{TxA2}, respectively. Hence the total amount of ADP and TxA2 that can be released by collagen-bound platelet is dynamically changing with the expressions $PLT_{col} \times Q_{ADP}$ and $PLT_{col} \times Q_{TxA2}$, respectively. The rate of ADP secretion and TxA2 activation are assumed to be proportional to both the remaining amount of the agonists within the platelets and the number of collagen-bound platelet. The equations used are as follows:

$$\frac{d\left(ADP_{col,released}\right)}{dt} = R_{ADP,col,rel} = k_{17} PLT_{col} \left(PLT_{col} Q_{ADP} - ADP_{col,released}\right) \tag{3.6}$$

$$\frac{d\left(TxA2_{col,released}\right)}{dt} = R_{TxA2,col,rel} = k_{18} PLT_{col} \left(PLT_{col} Q_{TxA2} - TxA2_{col,released}\right) \tag{3.7}$$

As blood stream keeps carrying these agonists away, the effect of advection is described by a first order term. The resulting equations for the amount of agonist molecules are therefore:

$$\frac{d\left(ADP_{col}\right)}{dt} = R_{ADP,col} = \frac{d\left(ADP_{col,released}\right)}{dt} - k_{cflow} ADP_{col} \tag{3.8}$$

$$\frac{d\left(TxA2_{col}\right)}{dt} = R_{TxA2,col} = \frac{d\left(TxA2_{col,released}\right)}{dt} - k_{cflow} TxA2_{col} \tag{3.9}$$

As the concentration of molecules is the quantity that is physiologically meaningful, as opposed to the amount of molecules, the amount of agonist molecules is converted to molar concentrations with a volume of interest. To define such volume, a boundary layer within which the agonists are assumed to be well-mixed is required. The boundary layer thickness is calculated with the following equation [26]::

$$\bar{h} = \frac{3}{4}\left(\frac{R \cdot L \cdot D}{V}\right)^{1/3} = \frac{3}{4}\left(2\frac{L \cdot D}{\dot{\gamma}}\right)^{1/3} \tag{3.10}$$

where L is the thickness of the collagen-abundant layer, D is the diffusivity of platelet, and $\dot{\gamma}$ is the shear rate. The volume of interest is therefore:

$$V_{col} = \frac{1}{2} A_{sub} \bar{h} \tag{3.11}$$

and the agonist concentrations that constitute the pro-aggregation signal S_3 in Fig. 1.1, are then:

$$[ADP_{col}] = \frac{ADP_{col}}{V_{col}} \tag{3.12}$$

$$[TxA2_{col}] = \frac{TxA2_{col}}{V_{col}} \tag{3.13}$$

3.2.3 Primary Hemostasis Actuator: Platelet Aggregation

After collagen-bound platelets start releasing platelet agonists, platelets in the blood stream become activated. One of the consequences is the activation of integrin $\alpha_{IIb}\beta_3$. The activation of $\alpha_{IIb}\beta_3$ is key in the aggregation process because two platelets

are joined together through the integrins on both platelets with fibrinogen being the ligand. In order to describe integrin activation of new platelets induced by ADP and TxA2, we selected widely studied pathways that occur in the platelets and simulate the pathways with simplified mechanisms. Two ADP receptors are expressed on the plasma membrane of platelet: $P2Y_1$ and $P2Y_{12}$, both G protein-coupled receptors (GPCRs). $P2Y_1$ is coupled with a Gq subunit while $P2Y_{12}$ is coupled with a Gi subunit. The signaling pathways that follow the activation of the two receptors are different. Gq protein activation leads to the activation of phospholipase C-β (PLC-β), followed by the conversion of phosphoinositide (PI) to diacylglycerol (DAG) and inositol trisphosphate (IP3). IP3 then releases the calcium ions stored in the dense tubular system of the platelet. Released calcium works either alone or with DAG to activate protein kinase C (PKC). DAG also works with calcium to activate CalDAGGEF, which activates Rap1, a small GTPase. Rap1 can also be activated by phosphoinositide 3-kinases (PI3K), which is downstream of the Gi signaling pathway. Additional PI3K can be activated by the G13 subunit, which is coupled to TxA2 receptor. Activation of $\alpha_{IIb}\beta_3$ is eventually achieved through the collaboration between PKC and Rap1. The equations used to describe these processes are given below

$$\frac{d[GqGTP]}{dt} = \eta V_{eff} \left(\begin{array}{l} k_{1-1} \dfrac{[ADP]^{n_{1-1}}}{a_{1-1}{}^{n_{1-1}} + [ADP]^{n_{1-1}}} \\ +k_{1-2} \dfrac{[TxA2]^{n_{1-2}}}{a_{1-2}{}^{n_{1-2}} + [TxA2]^{n_{1-2}}} \end{array} \right) \frac{[PLT]^{n_{1-3}}}{a_{1-3}{}^{n_{1-3}} + [PLT]^{n_{1-3}}} \\ - k_{1-4}[GqGTP] \tag{3.14}$$

$$\frac{d[GiGTP]}{dt} = \eta V_{eff} k_{2-1} \frac{[ADP]^{n_{2-1}}}{a_{2-1}{}^{n_{2-1}} + [ADP]^{n_{2-1}}} \frac{[PLT]^{n_{2-2}}}{a_{2-2}{}^{n_{2-2}} + [PLT]^{n_{2-2}}} - k_{2-3}[GiGTP] \tag{3.15}$$

$$\frac{d[G13GTP]}{dt} = \eta V_{eff} k_{3-1} \frac{[ADP]^{n_{3-1}}}{a_{3-1}{}^{n_{3-1}} + [ADP]^{n_{3-1}}} \frac{[PLT]^{n_{3-2}}}{a_{3-2}{}^{n_{3-2}} + [PLT]^{n_{3-2}}} - k_{3-3}[G13GTP] \tag{3.16}$$

$$\frac{d[PLC\beta^*]}{dt} = k_{4-1}[GqGTP] - k_{4-2}[PLC\beta^*] \tag{3.17}$$

$$\frac{d[PI3K]}{dt} = k_{5-1}[GiGTP] + k_{5-2}[G13GTP] - k_{5-3}[PI3K] \tag{3.18}$$

$$\frac{d[DAG]}{dt} = k_{6-1}[PLC\beta^*] - k_{6-2}[DAG] \tag{3.19}$$

$$\frac{d[IP3]}{dt} = k_{7-1}[DAG] - k_{7-2}[IP3] \tag{3.20}$$

$$\frac{d[Ca^{2+}]}{dt} = k_{8-1}[IP3] - k_{8-2}[Ca^{2+}] \tag{3.21}$$

$$\frac{d[PKC^*]}{dt} = k_{9-1}[Ca^{2+}] + k_{9-2}[Ca^{2+}][DAG] - k_{9-3}[PKC^*] \tag{3.22}$$

$$\frac{d[CalDAGGEF]}{dt} = k_{10-1}[DAG]\frac{[Ca^{2+}]^{n_{10-1}}}{a^{n_{10-1}} + [Ca^{2+}]^{n_{10-1}}} - k_{10-2}[CalDAGGEF] \tag{3.23}$$

$$\frac{d[Rap1^*]}{dt} = k_{11-1}[PI3K] + k_{11-2}[CalDAGGEF] - k_{11-3}[Rap1^*] \tag{3.24}$$

$$\frac{d\left(\alpha_{IIb}\beta^*_{3\,new}\right)}{dt} = k_{12-1}[PKC^*][Rap1^*] - k_{12-2}\left(\alpha_{IIb}\beta^*_{3\,new}\right) \tag{3.25}$$

The growth rate of the platelet aggregate is assumed to be proportional to the product of active integrins on newly activated platelets and on the platelet aggregate. As fibrinogen is the most impotant ligand for integrin $\alpha_{IIb}\beta_3$, the concentration of fibrinogen in the blood stream is another key factor affecting the rate of aggregation. In addition, it has been shown with *in vivo* experiments using mice that JAM-A is negatively associated with thrombus growth, and the effect of JAM-A is only apparent when a thrombus becomes large [33]. Thus, the aggregation rate is assumed to be inversely proportional to the term $1+[JAM\text{-}A](PLT_{agg})^n$.

After a platelet joins the platelet aggregate, there is still a possibility that the platelet will be carried away by the blood stream, a process called disaggregation. Since the blood stream is only in contact with the surface of the platelet aggregate, whose surface area is proportional to the number of activated platelets, disaggregation caused by flow is assumed to be proportional to the 2/3 power of the number of activated platelets in the aggregate. When the agonist concentration is high, platelets should be in a highly activated state, and less disaggregation occurs. On the contrary, when the agonist concentration is low, disaggregation rate should be more related to the effect of flow, and should be proportional to the surface area of the platelet aggregate. Hence, an extra term dependent on the concentration of agonists is included. In addition, the platelets that join the aggregate in the beginning should be less prone to disaggregate since a longer stay in the aggregate should keep the platelets in a highly activated state. This is considered in the last component of the disaggregation term. The rate of platelet aggregation growth is therefore described by:

$$\frac{d(PLT_{agg})}{dt} = \frac{k_{13-1}(\alpha_{IIb}\beta_3^*{}_{agg})(\alpha_{IIb}\beta_3^*{}_{new})[Fg]}{\left(1+[JAM-A](PLT_{agg})^{n_{13-1}}\right)}$$
$$-k_{13-2}(PLT_{agg})^{2/3}\left(1-\frac{\left(\frac{[ADP]}{ADP_{50}}+\frac{[TxA2]}{TxA2_{50}}+\frac{[Thr]}{Thr_{50}}\right)^{n_{13-2}}}{3^{n_{13-2}}+\left(\frac{[ADP]}{ADP_{50}}+\frac{[TxA2]}{TxA2_{50}}+\frac{[Thr]}{Thr_{50}}\right)^{n_{13-2}}}\right) \quad (3.26)$$
$$\times\frac{\left(\frac{[ADP]}{ADP_{50}}+\frac{[TxA2]}{TxA2_{50}}+\frac{[Thr]}{Thr_{50}}\right)^{n_{13-2}}}{3^{n_{13-2}}+\left(\frac{[ADP]}{ADP_{50}}+\frac{[TxA2]}{TxA2_{50}}+\frac{[Thr]}{Thr_{50}}\right)^{n_{13-2}}}$$

In order to make the number of available integrin $\alpha_{IIb}\beta_3$ physiologically reasonable, we performed mass balance on the integrins in the platelet aggregate. The equations are separated into two parts: (i) number of integrin from platelets bound to collagen fibers $\alpha_{IIb}\beta_{3}{}^*_{col}$ and (ii) number of integrin from platelets that are activated by agonists other than collagen $\alpha_{IIb}\beta_{3}{}^*_{sec}$. The activation rate for $\alpha_{IIb}\beta_{3}{}^*_{col}$ is assumed to be proportional to the rate of platelet adhesion to collagen multiplied with the average number of integrin on each platelet. ϕ_{col} is a fraction of the integrin on the plasma membrane facing the side of the blood flow. Integrin on the side of collagen fiber is not available for binding and therefore should not be counted here. As a new platelet joins the platelet aggregate with collagen bound-platelets, a fraction of integrin, ϕ_1, will be used to form the bound with new platelets and no longer available to other platelets. Once a platelet binds to collagen-bound platelets, a fraction of its integrins will then be used for binding new platelets that are activated by agonists other than collagen. When a new platelet activated by agonists other than collagen joins the platelet aggregate by attaching to collagen-bound platelets, a fraction of their integrin, ϕ_2, then becomes available to bind other new platelets. In the other scenario,

when newly activated platelets attach to platelets that are bound to platelets that are not bound to collagen, or "secondary platelets", they cover a fraction of the integrin on the platelets they attach to (ϕ_3) while part of their integrin will be used for binding other new platelets (ϕ_4). As disaggregation occurs, the reverse process will occur accordingly. A fraction of platelet integrins (ϕ_5) will be carried away by the blood stream while a fraction of the integrins on the remaining platelets (ϕ_6) will be exposed to the blood stream after the removal of the platelets that originally occupy or cover the integrins. Same mechanism applies to the effect of JAM-A-induced inhibition on platelet aggregation. Previous studies have shown that during thrombus growth, there is a core-and-shell structure, where the platelets in the core (closer to the wound site) are in a highly active state and the platelets in the shell (farther from the wound site) are in a less active state [34]. Hence, the activation of integrins in newly activated platelets is expected to be less and less as the thrombus grows. Therefore, the fraction of integrins in the aggregate consumed during the binding with new platelets is expected to be more than the fraction of integrins obtained after new platelets join the aggregate. The fractions ϕ_1, ϕ_3, and ϕ_5 are thus chosen to be 0.5, while the fractions ϕ_{col}, ϕ_2, ϕ_4, and ϕ_6 are set as 0.4.

$$\frac{d(\alpha_{IIb}\beta_3{}^*{}_{col})}{dt} = \frac{d(PLT_{col})}{dt} Q_{IIbIIIa}\phi_{col} - \frac{k_{13-1}(\alpha_{IIb}\beta_3{}^*{}_{agg})(\alpha_{IIb}\beta_3{}^*{}_{new})[Fg]}{\left(1+[JAM-A](PLT_{agg})^{n_{13-1}}\right)} Q_{IIbIIIa}\phi_1 \tag{3.27}$$

$$\frac{d(\alpha_{IIb}\beta_3{}^*{}_{\sec})}{dt} = \frac{k_{13-1}(\alpha_{IIb}\beta_3{}^*{}_{agg})(\alpha_{IIb}\beta_3{}^*{}_{new})[Fg]}{\left(1+[JAM-A](PLT_{agg})^{n_{13-1}}\right)} Q_{IIbIIIa}\phi_2$$
$$+\frac{k_{13-1}(\alpha_{IIb}\beta_3{}^*{}_{agg})(\alpha_{IIb}\beta_3{}^*{}_{new})[Fg]}{\left(1+[JAM-A](PLT_{agg})^{n_{13-1}}\right)} Q_{IIbIIIa}(\phi_3-\phi_4)$$
$$-k_{13-2}(PLT_{agg})^{2/3}\left(1-\frac{\left(\frac{[ADP]}{ADP_{50}}+\frac{[TxA2]}{TxA2_{50}}+\frac{[Thr]}{Thr_{50}}\right)^{n_{13-2}}}{3^{n_{13-2}}+\left(\frac{[ADP]}{ADP_{50}}+\frac{[TxA2]}{TxA2_{50}}+\frac{[Thr]}{Thr_{50}}\right)^{n_{13-2}}}\right) \tag{3.28}$$
$$\times\frac{\left(\frac{[ADP]}{ADP_{50}}+\frac{[TxA2]}{TxA2_{50}}+\frac{[Thr]}{Thr_{50}}\right)^{n_{13-2}}}{3^{n_{13-2}}+\left(\frac{[ADP]}{ADP_{50}}+\frac{[TxA2]}{TxA2_{50}}+\frac{[Thr]}{Thr_{50}}\right)^{n_{13-2}}} Q_{IIbIIIa}(\phi_5-\phi_6)$$

$$(\alpha_{IIb}\beta_3{}^*{}_{agg}) = (\alpha_{IIb}\beta_3{}^*{}_{col}) + (\alpha_{IIb}\beta_3{}^*{}_{\sec}) \tag{3.29}$$

After platelets join the platelet aggregate, the agonists (ADP and TxA2) inside them become sources of agonists for activating and recruiting more platelets. Therefore, we define two variables ADP_{res} and $TxA2_{res}$ as reservoirs to describe such phenomenon. The rate of increase in the amount of agonist is proportional to the rate at which new platelets join the platelet aggregate. When platelets are carried away by the blood stream, agonists that are still within platelets will be carried along and are no longer capable of recruiting new platelets. As each platelet in the platelet aggregate joins the aggregate at different times, the remaining amount of agonists is heterogeneously distributed within the platelet aggregate, with the platelets in the outer layers carrying a larger amount and the platelets at the core carrying the least.

Hence parameters ϕ_{ADP} and ϕ_{TxA2} are used to incorporate this effect. The equations used are as follows:

$$\frac{d(ADP_{res})}{dt} = \frac{k_{13-1}(\alpha_{IIb}\beta_3^{*}{}_{agg})(\alpha_{IIb}\beta_3^{*}{}_{new})[Fg]}{\left(1+[JAM-A](PLT_{agg})^{n_{13-1}}\right)} \times Q_{ADP}$$
$$- k_{13-2}(PLT_{agg})^{2/3}\left(1 - \frac{\left(\frac{[ADP]}{ADP_{50}} + \frac{[TxA2]}{TxA2_{50}} + \frac{[Thr]}{Thr_{50}}\right)^{n_{13-2}}}{3^{n_{13-2}} + \left(\frac{[ADP]}{ADP_{50}} + \frac{[TxA2]}{TxA2_{50}} + \frac{[Thr]}{Thr_{50}}\right)^{n_{13-2}}}\right) \tag{3.30}$$
$$\times \frac{\left(\frac{[ADP]}{ADP_{50}} + \frac{[TxA2]}{TxA2_{50}} + \frac{[Thr]}{Thr_{50}}\right)^{n_{13-2}}}{3^{n_{13-2}} + \left(\frac{[ADP]}{ADP_{50}} + \frac{[TxA2]}{TxA2_{50}} + \frac{[Thr]}{Thr_{50}}\right)^{n_{13-2}}} \frac{ADP_{res}}{(PLT_{agg}+1)\cdot\phi_{ADP}}$$
$$- k_{14}ADP_{res}$$

$$\frac{d(ADP_{\sec})}{dt} = k_{14}ADP_{res} - k_{cflow}ADP_{\sec} \tag{3.31}$$

$$\frac{d(TxA2_{res})}{dt} = \frac{k_{13-1}(\alpha_{IIb}\beta_3{}^*{}_{agg})(\alpha_{IIb}\beta_3{}^*{}_{new})[Fg]}{\left(1+[JAM-A](PLT_{agg})^{n_{13-1}}\right)} \times Q_{TxA2}$$
$$- k_{13-2}(PLT_{agg})^{2/3}\left(1 - \frac{\left(\frac{[ADP]}{ADP_{50}} + \frac{[TxA2]}{TxA2_{50}} + \frac{[Thr]}{Thr_{50}}\right)^{n_{13-2}}}{3^{n_{13-2}} + \left(\frac{[ADP]}{ADP_{50}} + \frac{[TxA2]}{TxA2_{50}} + \frac{[Thr]}{Thr_{50}}\right)^{n_{13-2}}}\right) \quad (3.32)$$
$$\times \frac{\left(\frac{[ADP]}{ADP_{50}} + \frac{[TxA2]}{TxA2_{50}} + \frac{[Thr]}{Thr_{50}}\right)^{n_{13-2}}}{3^{n_{13-2}} + \left(\frac{[ADP]}{ADP_{50}} + \frac{[TxA2]}{TxA2_{50}} + \frac{[Thr]}{Thr_{50}}\right)^{n_{13-2}}} \frac{TxA2_{res}}{(PLT_{agg}+1)\cdot\phi_{TxA2}}$$
$$- k_{15}TxA2_{res}$$

$$\frac{d(TxA2_{\sec})}{dt} = k_{15}TxA2_{res} - k_{cflow}TxA2_{\sec} \quad (3.33)$$

By the same reasoning as the case in agonists released by collagen-bound platelets, the amount of agonists secreted by secondary platelets needs to be converted into concentration to obtain a physiologically meaningful quantity. To do so, we need to define an effective volume within which new platelets are prone to be activated. Intuitively, such volume should be related to the surface area of platelet aggregate since new platelets will be activated and attached to the outer surface of the aggregate. We estimated the surface area of the aggregate by assuming a semispherical shape for the aggregate. The surface area can thus be expressed as

$$A_{agg} = \left(\frac{PLT_{agg}\cdot V_{plt}}{\phi_p}\sqrt{18\pi}\right)^{2/3} \quad (3.34)$$

where V_{plt} is the volume of a single platelet and ϕ_p is the porosity of the platelet aggregate.

As for the third dimension of the volume of interest, the thickness is assumed to be $\bar{h} = 2$ μm. Platelets activated more than 2 μm away from the surface of the aggregate are very unlikely to join the aggregate, since the binding between two integrins through fibrinogen is merely 0.2 μm. The volume of interest is therefore:

$$V_{eff} = A_{agg} \cdot \bar{h} \tag{3.35}$$

The parameter values of the parameters that are later used for sensitivity analysis are listed in Table 3.1.

Table 3.1. List of parameters and their values in the primary hemostasis model. The parameter index corresponds to the x-axis in the figure for sensitivity coefficients.

parameter index	parameter name	parameter value used	unit	parameter index	parameter name	parameter value used	unit
Block: Gq activation				Block: Cytosolic Ca2+ increase			
1	k_{1-1}	1	1/s	31	k_{8-1}	9.35×10^{4}	1/s
2	n_{1-1}	1.62	-	32	k_{8-2}	1.24×10^{4}	1/s
3	a_{1-1}	1.88	μM	Block: PKC and CalDAGGEF activation			
4	k_{1-4}	8.59×10^{-2}	1/s	33	k_{9-1}	8.6	1/s
5	k_{1-2}	1	1/s	34	k_{9-2}	1	1/s
6	n_{1-2}	1.96	-	35	k_{9-3}	1	1/s
7	a_{1-2}	0.1	μM	36	k_{10-1}	9.97×10^{-1}	1/s
8	a_{1-3}	6.59×10^{1}	μM	37	k_{10-2}	8.39×10^{1}	1/s
9	n_{1-3}	5.22	-	38	n_{10-1}	1.24	-

Table 3.2 continued

Block: Gi activation				39	a_{10-1}	5.77×10^{-3}	μM
10	k_{2-1}	1	1/s	Block: integrin activation			
11	n_{2-1}	2.06	-	40	k_{11-1}	4.98×10^{-1}	1/s
12	a_{2-1}	2	μM	41	k_{11-2}	1	1/s
13	k_{2-3}	5.6×10^{-2}	1/s	42	k_{11-3}	1	1/s
14	n_{2-2}	2	-	43	k_{12-1}	6.65×10^{8}	1/s-μM
15	a_{2-2}	2.78×10^{1}	μM	44	k_{12-2}	7.34×10^{1}	1/s
Block: G13 activation				Block: aggregation			
16	k_{3-1}	7	1/s	45	k_{13-1}	1.88×10^{-5}	1/s
17	n_{3-1}	1.87	-	46	k_{13-2}	1.99	1/s
18	a_{3-1}	8.63×10^{-2}	μM	47	n_{13-1}	1	-
19	k_{3-3}	2.35×10^{-1}	1/s	48	n_{13-2}	2.07	-
20	a_{3-2}	2.72×10^{1}	μM	49	k_{14}	5.36×10^{-3}	1/s
21	n_{3-2}	5.68	-	50	ϕ_{ADP}	2.72×10^{-1}	-
Block: PLCβ activation				51	k_{15}	9.27×10^{-2}	1/s
22	k_{4-1}	1.21	1/s	52	ϕ_{TxA2}	3.19×10^{-1}	-
23	k_{4-2}	2.45×10^{1}	1/s	Block: Primary hemostasis controller			
Block: PI3Ki activation				53	k_{16}	5.00×10^{-9}	1/s
24	k_{5-1}	1	1/s	54	a_{16}	4.64×10^{1}	$10^5/mm^3$
25	k_{5-2}	1.47	1/s	55	n_{16}	3.84	-
26	k_{5-3}	4.82×10^{-1}	1/s	56	k_{17}	3.51×10^{-3}	1/s
Block: DAG and IP3 formation				57	k_{18}	1.07×10^{-1}	1/s
27	k_{6-1}	1.51×10^{1}	1/s				
28	k_{6-2}	9.52	1/s				
29	k_{7-1}	2.01×10^{1}	1/s				
30	k_{7-2}	8.51×10^{1}	1/s				

3.3 Results and Discussion

Figure 3.1 shows the platelet aggregate profile and the resulting ADP and TxA2 concentrations in response to a vascular injury of 100 μm^2 at a shear rate of 400 s^{-1} (this shear rate is used throughout the entire study). The blue solid lines are resulted

from collagen-bound platelets. The most prominent feature in collagen-induced ADP and TxA2 release (solid lines in Figures 3.1b and 3.1c) is that even though the release mechanisms are considered mathematically the same in the model, the profiles differ significantly, where the profile of ADP is more similar to a step function while the profile of TxA2 looks closer to a pulse function. This indicates that TxA2 has an important role in activating new platelets in the very beginning of the hemostatic process, while ADP has a more lasting effect on recruiting new platelets.

Compared with the profiles of ADP and TxA2 from the platelet aggregate (green dashed lines in Figures 3.1b and 3.1c), it can be seen that the platelet aggregate profile (green dashed lines in Figure 2(a)) closely follows the profile of ADP and TxA2, demonstrating that the positive feedback loops involving ADP and TxA2 release are important in the process.

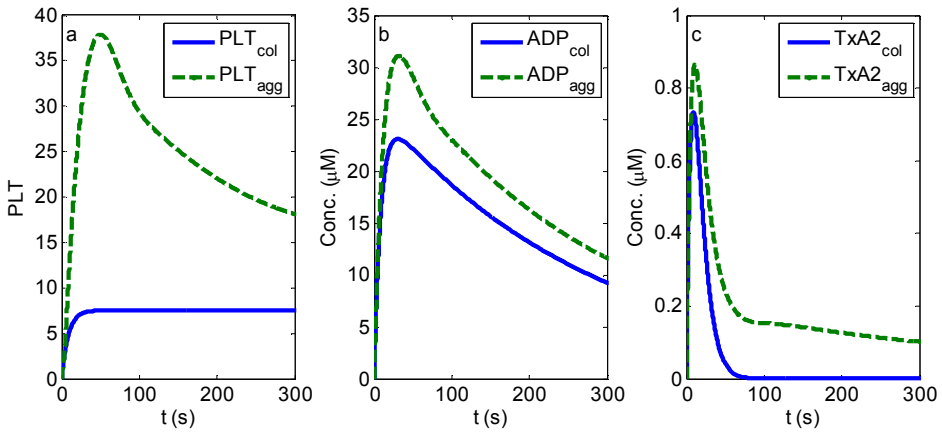

Figure 3.1. Nominal profiles of (a) numbers of platelet attached to collagen (PLT_{col}) and in the aggregate (PLT_{agg}), (b) ADP concentrations resulted from collagen-bound platelet (ADP_{col}) and the entire aggregate (ADP_{agg}), and (c) TxA2 concentrations resulted from collagen-bound ($TxA2_{col}$) platelet and the entire aggregate ($TxA2_{agg}$).

As $\alpha_{IIb}\beta_3$ is the most abundant integrin in platelets and thus an important receptor for fibrinogen, through which the platelets are joined together and form an aggregate, we investigated how the extent of $\alpha_{IIb}\beta_3$ activation affects the process of platelet aggregation. In Figure 3.2, the rate constant for $\alpha_{IIb}\beta_3$ activation is decreased to various percentages of the baseline rate constant, leading to a decreased number of active integrin. Reduced integrin activation then results in reduced platelet aggregation, which in turn reduced the level of ADP and TxA2 near the aggregate.

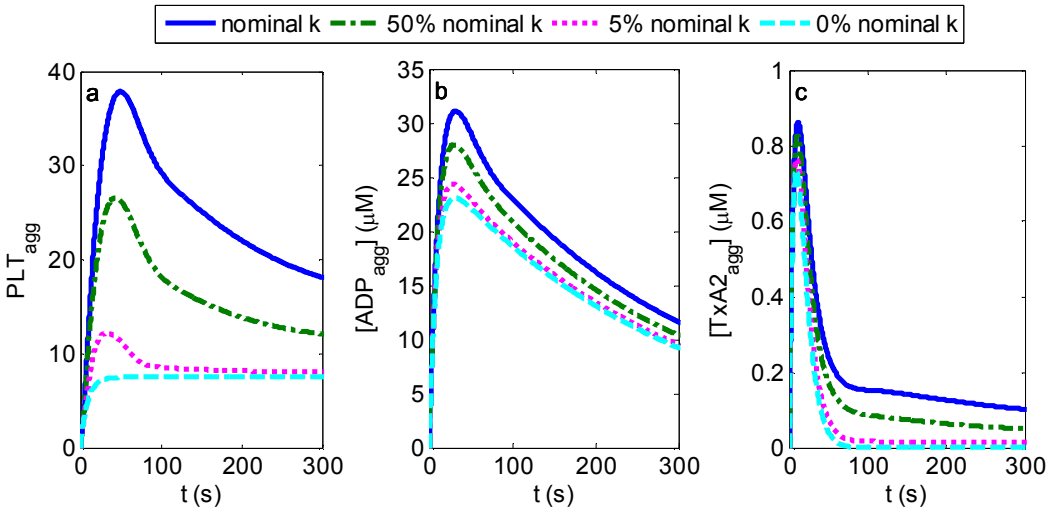

Figure 3.2. Effect of integrin $\alpha_{IIb}\beta_3$ activation rate on (a) platelet aggregation, (b) ADP secretion and (c) TxA2 synthesis. The rate constant for integrin activation is reduced from its nominal value (blue solid line) to 50% (green dash-dot line), 5% (magenta dotted line), and 0% (cyan dashed line) of the nominal value. Reduced integrin activation rate not only results in reduced platelet aggregation but also reduced ADP and TxA2 levels.

As shown previously with *in vivo* experiments, junctional adhesion molecule A (JAM-A) plays a significant role in hemostasis [33]. JAM-A$^{-/-}$ mice exhibit larger thrombi after laser-induced wound. In Figure 3.3, we gradually decreased the amount of JAM-A in the model. As expected, the thrombus grows larger as the effect of JAM-A on limiting platelet aggregation diminishes. Interestingly, when JAM-A level goes to zero, the thrombus growth becomes out-of-bound, even in the presence of flow. This suggests that an inhibitory signal from within the platelet aggregate is necessary in limiting the aggregate size, even in the presence of flow that takes away platelets from the aggregate.

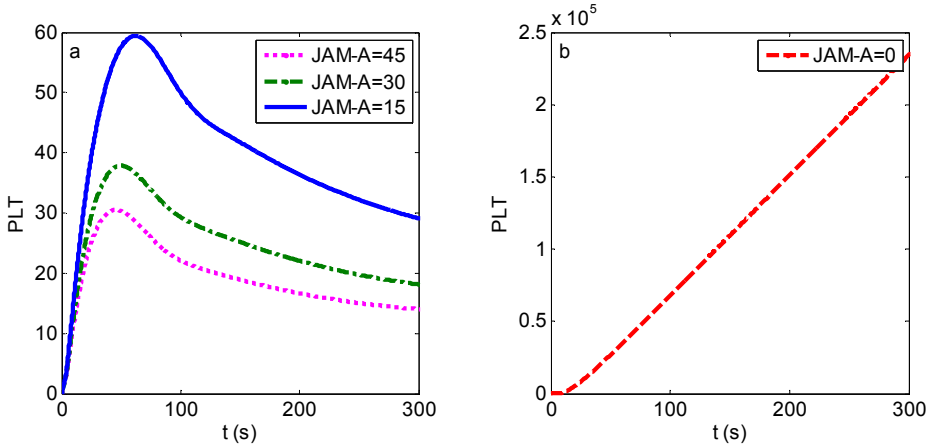

Figure 3.3. Effect of JAM-A deficiency on platelet aggregation. (a) non-zero JAM-A level; (b) complete removal of JAM-A. JAM-A level is reduced from 45 (blue solid line) to 30 (green dash-dot line), 15 (magenta dotted line), and 0 (red dashed line in (b)). Platelet aggregation becomes out-of-bound when the effect of JAM-A is completely removed from the model.

With the primary hemostasis model developed, we then subjected our primary hemostasis model to different intensities of disturbance, which are representative of different wound sizes in physiology. The first thing to note in Figure 3.4a is the overshoot of the platelet aggregate profile compared to the wound size. This shows that with a small wound, the aggregate produced solely by primary hemostasis will be larger than what is needed for covering the entire wound. Such behavior is expected since the aim of hemostasis is to respond to the wound occurrence quickly and seal the wound as soon as possible in order to minimize blood loss. Even though an overshoot comes along with the fast response, the overshoot will not do any harm as long as the thrombus does not entirely occlude the vessel. Comparing Figures 3.4a-e, it can be seen that as the wound size increases, less and less wound area is being covered by the platelet aggregate. This indicates that primary hemostasis itself can only achieve a limited extent of platelet aggregation and additional measures are required for larger wounds. Hence secondary hemostasis is not only important in producing fibrin and reinforcing the platelet aggregate. Secondary hemostasis is also an additional driving force for thrombus growth, and this function is even more prominent in the case of larger wounds.

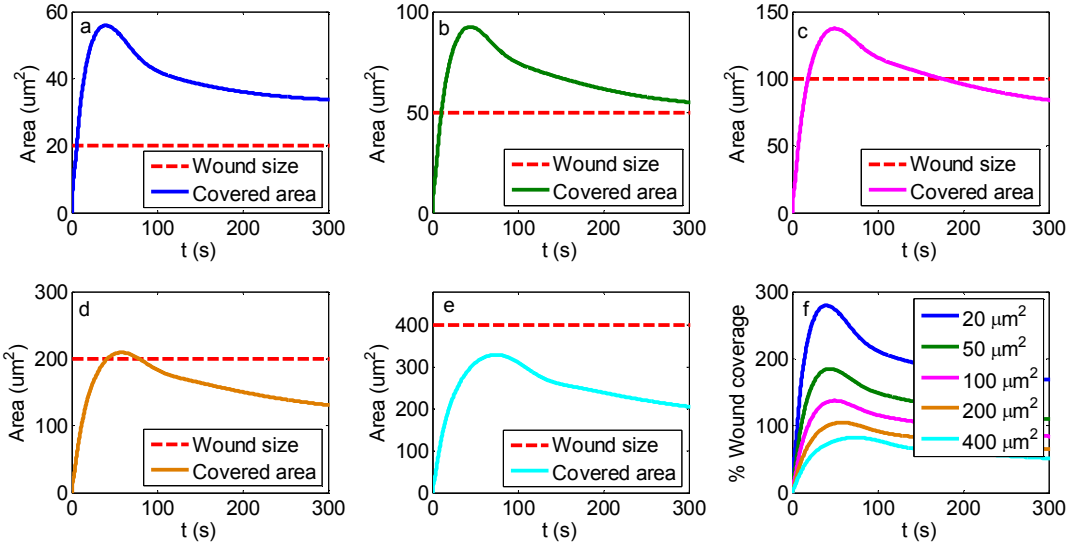

Figure 3.4. Platelet aggregation in response to various wound sizes ranging from 20 to 400 μm^2. (a-e) Wound area coverage with respect to time; (f) Percentage of wound area coverage. Increasing wound size corresponds to decreasing wound coverage.

Figure 3.5 shows the bleeding rate and total blood loss from the beginning of wound occurrence to the end of simulation. Because the primary hemostasis model does not consider thrombin, platelet aggregate is unable to be converted into an impermeable clot due to lack of fibrin production. Blood loss thus does not stop. It can be seen in Figure 3.5b that the blood loss is not proportional to the wound size. For example, a wound size of 100 μm^2 leads to a blood loss of approximately 0.18×10^{-5} cm^3 while a wound size of 400 μm^2 results in a blood loss of 0.82×10^{-5} cm^3. This is a result of the nonlinear process of platelet aggregation in primary hemostasis.

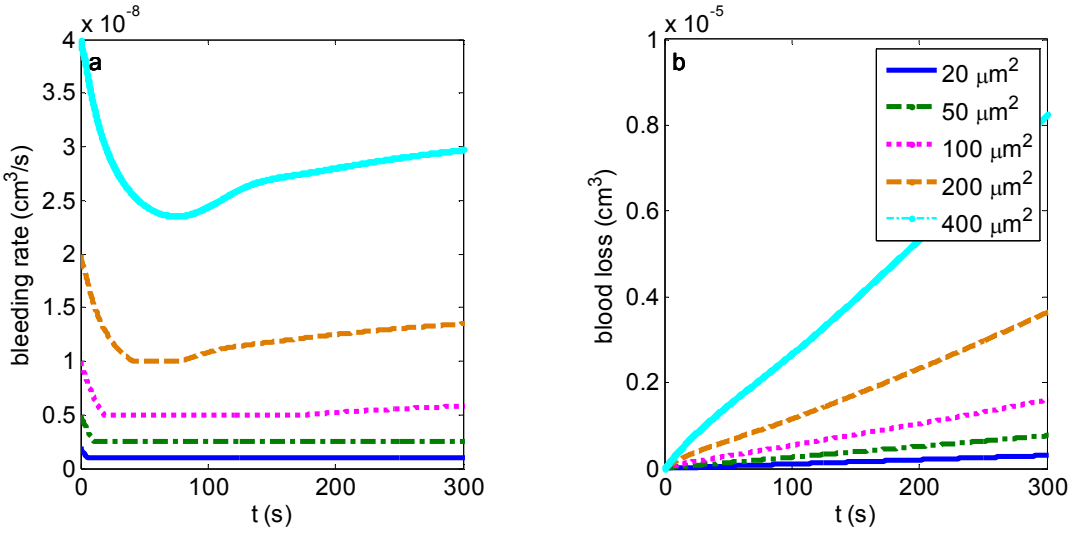

Figure 3.5. (a) Estimated bleeding rate and (b) blood loss in response to various wound sizes. The wound sizes correspond to the wound sizes used in Figure 6. Blood loss does not completely stop as fibrin production is not considered in the model. The bleeding rate reaches a steady state once the platelet aggregate stabilizes.

How the activation of individual proteins affects platelet function and eventually hemostasis has been a major focus for biologists in the past few decades. We investigated this same question by changing the rate constants in the equations for the activation of new platelets. With a certain model topology, the network of platelet signaling affects integrin activation and thereby platelet aggregate formation. We reduced, one at a time, the rate constants in the equations related to new platelet activation to represent the dysfunction of proteins and observe the resulting platelet aggregate size and the positive feedback signals. It can be seen in Figure 3.6 that there are 6 phenotypes of the platelet aggregate profile among the 19 rate constants changed. This demonstrates the redundancies in the biological pathways commonly seen in biological systems.

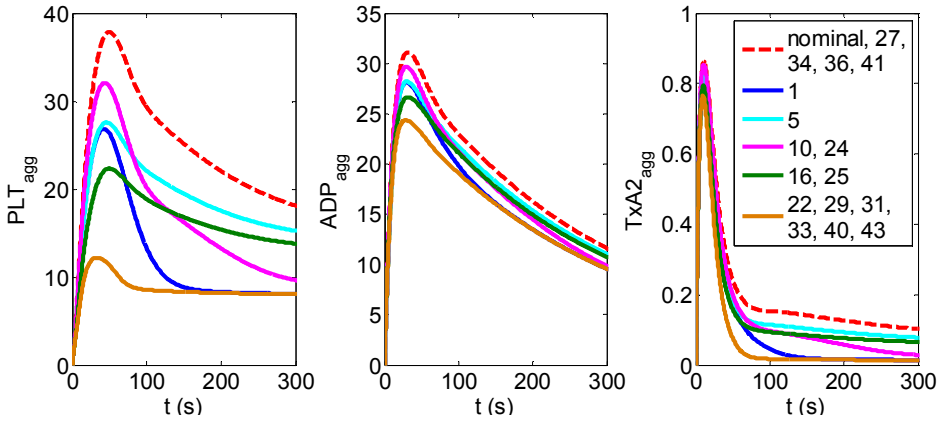

Figure 3.6. Hemostatic phenotypes as a result of the dysfunction of signaling proteins that leads to integrin activation. The rate constants for the activation of proteins (19 in total) are reduced to 5% of the baseline value one at a time.

To identify the most significant parameter in the hemostatic process, we performed sensitivity analysis to address this issue. As there are many aspects of the hemostatic process, we looked at five metrics in hemostasis that are considered important in achieving the task of primary hemostasis, which is to produce a platelet plug quickly and efficiently. The five metrics are, as listed in Table 2: (1) time to reach maximum platelet number in the aggregate, (2) average platelet number in the first 3 minutes after wound occurrence, (3) average platelet number during the entire simulation time of 5 minutes, (4) final bleeding rate, and (5) total blood loss. Figure 3.7 shows the results of the parametric sensitivity analysis for the primary hemostasis model. In the case of time to peak platelet number (Figure 3.7a), the metric is most sensitive to the exponent for the effect of agonists on disaggregation. The average number of platelets in the first 3 minutes is also most sensitive to the same parameter (Figure 3.7b). When the calculation of the average number of platelets is extended to 5

minutes (Figure 3.7c), the results are very similar to Figure 3.7b, indicating that the response of primary hemostasis is mostly determined in the first 3 minutes. In the case of bleeding rate at the end of simulation and total blood loss, both metrics are most sensitive to the exponent in the effect of JAM-A. As previously mentioned, with only primary hemostasis, bleeding cannot be stopped due to lack of fibrin. Hence the bleeding rate and total blood loss will be determined by the size of the platelet aggregate, which is sensitive to the inhibitory effect of JAM-A.

Table 3.2. Outputs of parametric sensitivity analysis.

Output Index	Description
1	time to reach maximum platelet number in the aggregate
2	average platelet number in the first 3 minutes after wound occurrence
3	average platelet number during the entire simulation time of 5 minutes
4	final bleeding rate
5	total blood loss

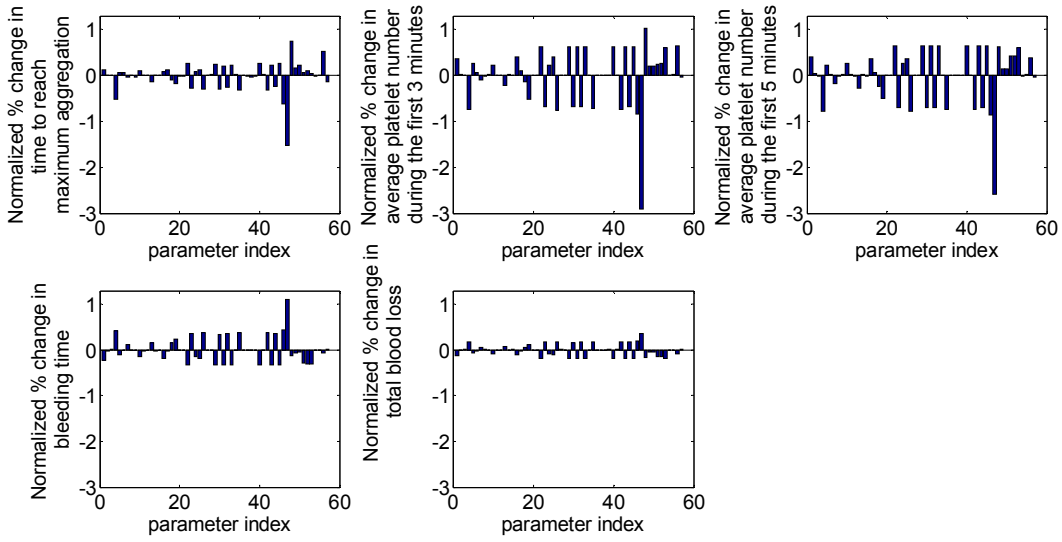

Figure 3.7. Parameter sensitivity analysis. The relative changes in multiple outputs were calculated based on a simulation with a 10% decrease in a given parameter value. The percentage change to the baseline output values were normalized by the sign and magnitude of the change to the parameter value as described in main text. (a) time to reach the maximum in platelet aggregation; (b) average platelet number during the first 3 minutes; (c) average platelet number during the simulation time of 5 minutes; (d) bleeding time; and (e) total blood loss.

3.4 Effect of Protein Inhibition on Collagen-Induced Platelet Aggregation: Experiments and Model Prediction

In this section, in order to investigate how the inhibition of signaling proteins in the primary hemostasis model can be linked to an experimental setting, microfluidic experiments of collagen-induced platelet aggregation were performed. Although the primary hemostasis model does not include the roles of protein inhibitors directly, protein inhibitors are considered to be acting on the reaction rate constants for the activation of the proteins they target. Two important signaling proteins, PI3K and PKC, were studied in the experiments.

3.4.1 Microfluidic Experiments: Methodology

3.4.1.1 Fabrication of Microfluidid Devices

A silicon wafer with designed patterns of 4 micro-channels (dimension: 500 μm × 100 μm × 12 mm) was used as the mold for making the microfluidic devices used in the experiments. Fabrication of microfluidic devices with the wafer generally follows protocols reported in [35].

3.4.1.1.1 Casting and Device Preparation

Before casting microfluidic devices, patterned silicon wafer was cleaned with double-distilled (DI) water and taped to a petridish. Polydimethylsiloxane (PDMS) pre-polymer and curing agent (Sylgard 184, Dow Corning, Midland, MI) were mixed at a ratio of 10:1 and degassed under vacuum. The mixture was then poured over the silicon wafer and allowed to sit at 65ºC for 3 hours in an oven. After cooling, the molded devices were peeled from the wafer and cut to size. Input and output ports were punctured with sharpened 21 and 16 gauge needles, respectively. Prior to use, the devices were cleaned with (i) DI water and (ii) 100% ethanol for 10 minutes.

Glass slides for the bottom of the devices were cleaned with 1 M HCl and 100% ethanol for 1 hour on a shaker. The slides were then cleaned with DI water and were stored in DI water for later use.

3.4.1.1.2 Surface Functionalization

Glass slides prepared in section 3.4.1.1 were dried and the PDMS devices were pressed firmly against the glass slides to form the complete microfluidic devices. The resulting microfluidic device is shown in Figure 3.8. Fibrillar type I collagen (Chrono-log Corp, Havertown, PA) was diluted to 250 μg/mL using Tyrode buffer.

Microfluidic devices were perfused with collagen for at least 1 hour. Afterwards, the channels were perfused with Tyrode buffer to wash away unbound collagen, and were perfused with 3% BSA for at least 30 minutes to block the surfaces not covered by collagen.

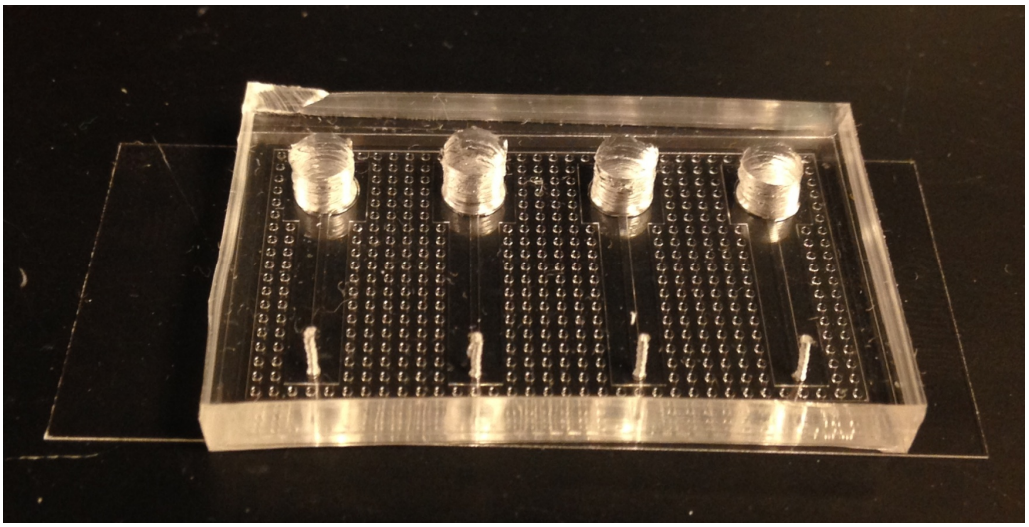

Figure 3.8. Microfluidic device used in the microfluidic experiments. Patterned PDMS strip is firmly press against the glass slide to form the microfluidic device. Four bigger ports are the inlets of the microfluidic channels with lengths of 12 mm. Four small ports are the outputs that are to be connected to a syringe pump.

3.4.1.1.3 Blood Collection and Perfusion

Healthy individuals who self-reported as not taking medication that would affect blood function were recruited. Whole blood was collected via venipuncture into tubes containing sodium citrate (final concentration 3.8 vol%). Blood was incubated with DiOC6 (final concentration1 μg/mL) for fluorescence imaging for at least 10 minutes at 37.5ºC. If an inhibitor was used, the inhibitor was incubated along with the

DiOC6 dye. After incubation, blood was perfused through the collagen-coated channels over a desired time period using a syringe pump connected to the outputs of the channels. The channels were then perfused with Tyrode buffer for 3 minutes, followed by 5% paraformaldehyde (PFA) for 3 minutes to fix the platelets.

3.4.1.1.4 Imaging and Quantitation

PDMS strip was carefully removed from the glass slide and the bottom surface of the channels on the glass slides was exposed. The channels were then placed under a microscope for imaging. Pictures were taken under (i) phase contrast mode and (ii) fluorescence mode. The picturess were quantified using ImageJ for obtaining (i) surface coverage that estimates how much collagen-coated area is occupied by platelets and (ii) fluorescence intensity that indicates the number of platelets in the platelet aggregate.

3.4.2 Effect of Protein Inhibition on Platelet Aggregation

The objective of the experiments was to find the parameter value that corresponds to the effect of a protein inhibitor at a certain concentration.

3.4.2.1 PI3K Inhibition

The inhibitor used for PI3K inhibition in the microfluidic experiments was Wortmannin. A final Wortmannin concentration of 60 nM was used in all three biological triplicates. The representative pictures of the effect of Wortmannin on platelet aggregation were shown in Figure 3.9. Fluorescence intensity of the pictures were quantified and shown in Figure 3.10. A Wortmannin concentration of 60 nM caused a 63% reduction in platelet aggregation. A corresponding change in the parameters for PI3K activation ($k_{5\text{-}1}$ and $k_{5\text{-}2}$) was shown to be a 92% reduction of the

original values. The resulting platelet aggregation profiles from the primary hemostasis model were shown in Figure 3.11.

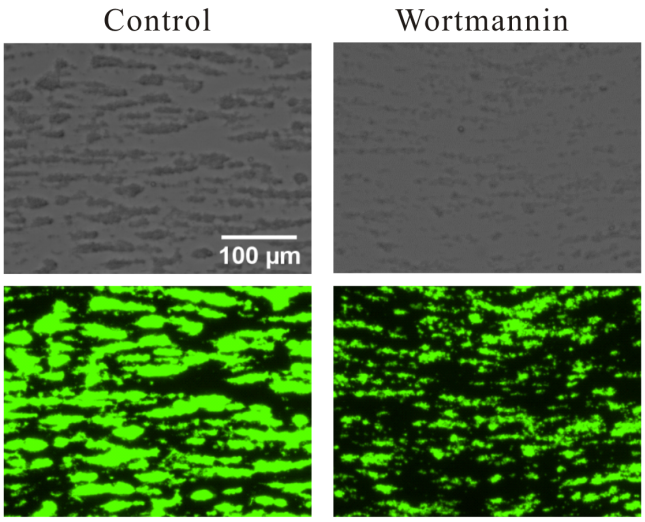

Figure 3.9. Effect of Wortmannin (60 nM) on platelet aggregation over collagen-coated surface at t = 180 seconds. Upper panel: phase contrast images; bottom panel: fluorescence images. Left: untreated group (control); right: treated group (Wortmannin).

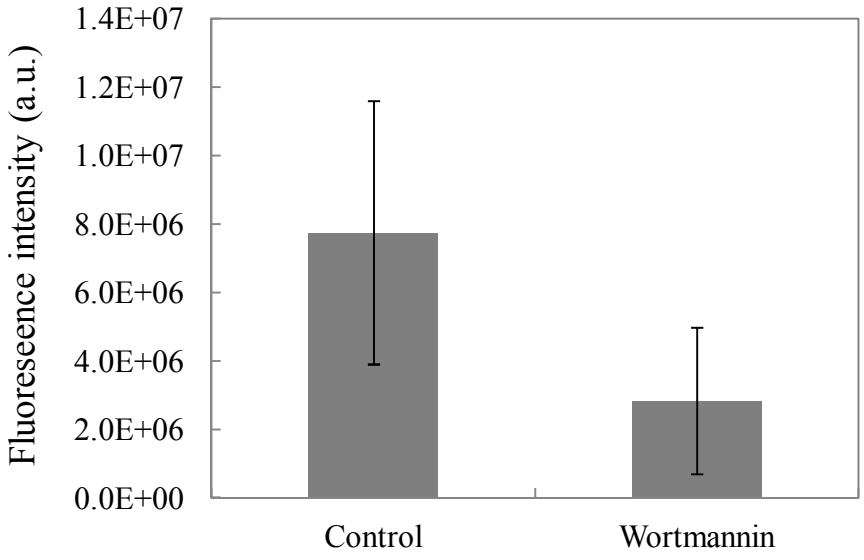

Figure 3.10. Quantitation of the fluorescence intensity for collagen-induced platelet aggregation with or without Wortmannin at 180 seconds. Error bars represent standard error of the mean (n=3).

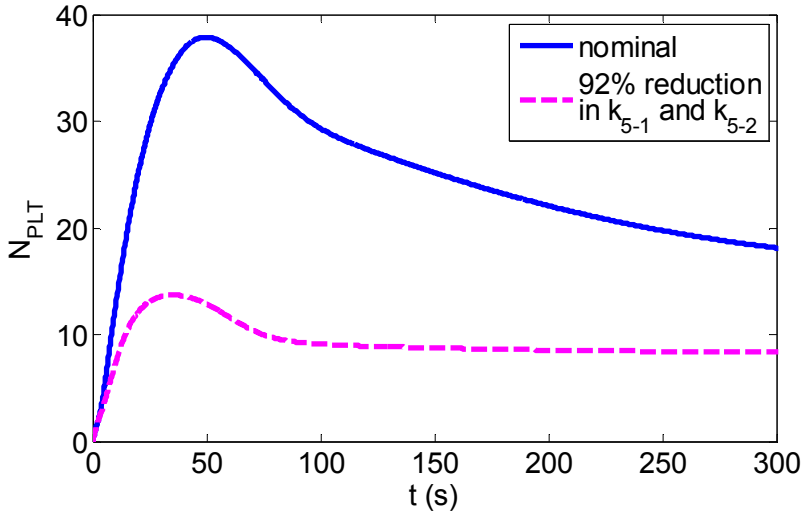

Figure 3.11. Platelet aggregation profiles from the primary hemostasis model. A 92% reduction of k_{5-1} and k_{5-2} was shown to be corresponding to a Wortmannin concentration of 60 nM.

3.4.2.2 PKC Inhibition

Inhibition of PKC was achieved with the use of 10 μM of Bis. Three biological replicates the same as those used in the PI3K inhibition experiments were used for this set of experiments. The representative pictures were shown in Figure 3.12 and the quantification was shown in Figure 3.13. It was found that a Bis concentration of 10 μM resulted in a 54% reduction in platelet aggregation. The change in the parameters for PKC activation was found to be a reduced 75%, as shown in Figure. 3.14.

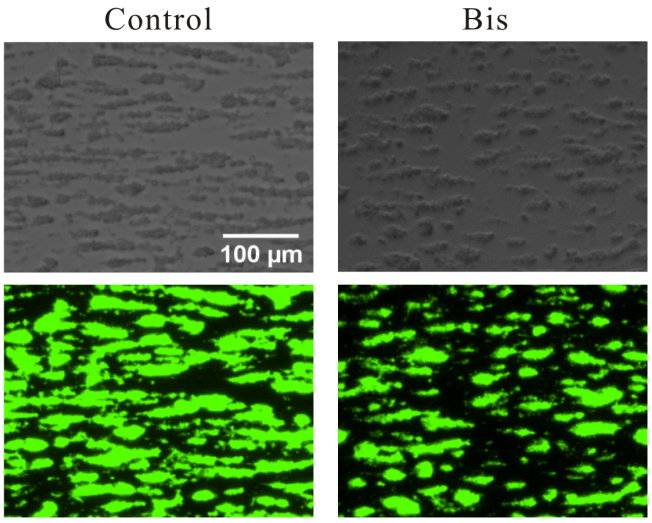

Figure 3.12. Effect of Bis on platelet aggregation over collagen-coated surface. Upper panel: phase contrast images; bottom panel: fluorescence images. Left: untreated group (control); right: treated group (Bis).

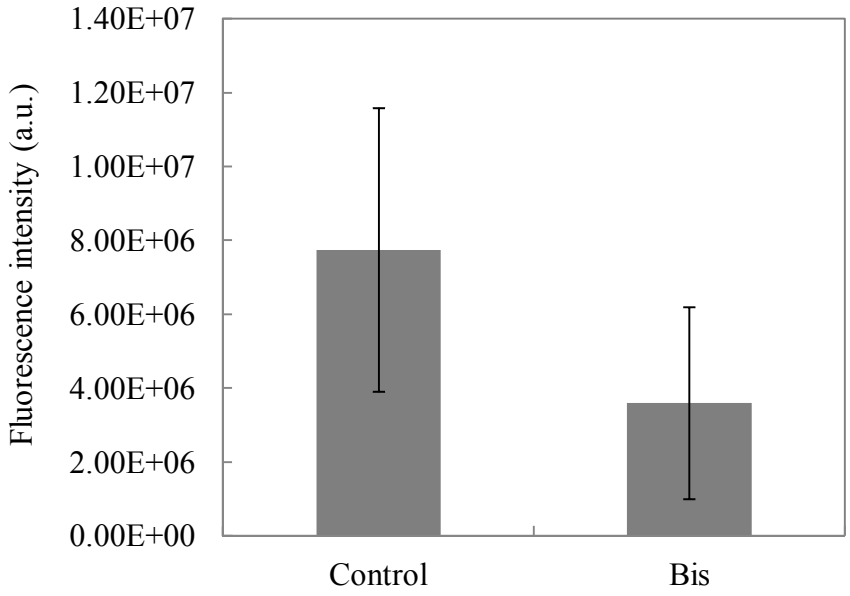

Figure 3.13. Quantitation of the fluorescence intensity for collagen-induced platelet aggregation with or without Bis at 180 seconds.. Error bars represent standard error of the mean (n=3).

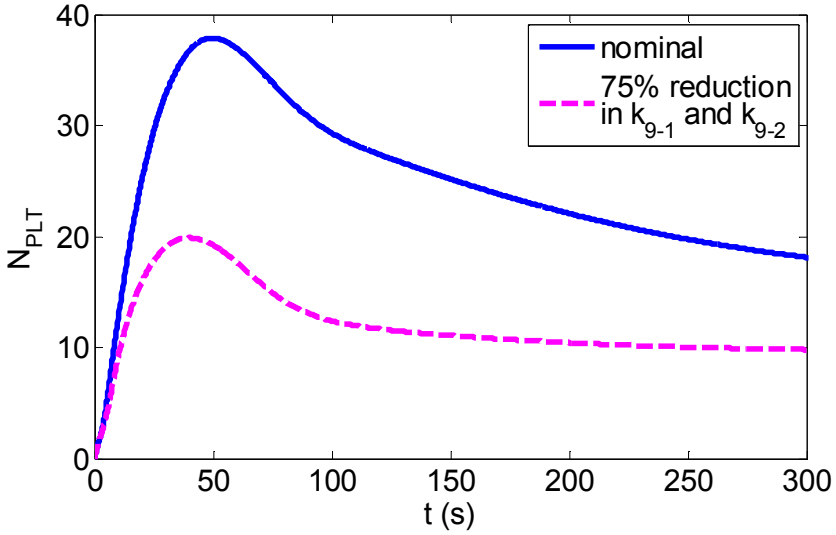

Figure 3.14. Platelet aggregation profiles from the primary hemostasis model. A 75% reduction of $k_{9\text{-}1}$ and $k_{9\text{-}2}$ was shown to be corresponding to a Bis concentration of 10 μM.

3.5 Summary

In this chapter, we developed a mathematical model of primary hemostasis based on the engineering control system framework proposed in Chapter 1. The primary hemostais model shows, among other things, how, as wound size increases, additional mechanisms are required in order to completely cover the injured blood vessel wall. We performed microfluidic experiments and showed that model parameter values can be used to represent the effect of a protein inhibitor at a certain concentration.

Chapter 4

A HOLISTIC MATHEMATICAL REPRESENTATION OF HEMOSTASIS

4.1 Introduction

As introduced in the Chapter 1, the two main sub-processes in hemostasis, which are primary and secondary hemostasis, interact and promote the final output of each other, forming a clot that contains products from both sub-processes in order to stop bleeding. It is therefore necessary to consider the two sub-processes together to obtain the mechanistic insight into how the various components in hemostasis work collaboratively to achieve fast and effective response to vascular injury. The entire process is very complicated as thousands of participants are involved. This is a major challenge. Computational modeling provides an advantage in organizing relevant information and a means of understanding the entire system as a whole.

In this chapter, as part of the development of a comprehensive mathematical representation of hemostasis proposed in Chapter 1, a mathematical model of secondary hemostasis is developed. The physiological processes in the coagulation cascade upon which the model is built are first introduced. An ODE model representing the coagulation cascade is then developed to be integrated with the primary hemostasis model introduced in the previous chapter. The combined, comprehensive model of hemostasis is then used for further analysis to gain insight into the entire process. Five *in silico* disease scenarios that have real-life counterparts are created and the comprehensive model is used for identifying potential treatment strategies for the diseases.

4.2 Physiological Description of Secondary Hemostasis

The high-level mechanisms involved in secondary hemostasis are schematically represented in Figure 4.1. Traditionally, secondary hemostasis is divided into three parts: the extrinsic pathway, the intrinsic pathway, and the common pathway. As can be seen in Figure 4.1, in both the extrinsic and intrinsic pathways, the ultimate event is the activation of factor X (FX) to factor Xa (FXa). The events after FX activation are categorized into the common pathway. Two prominent features are widely recognized in secondary hemostasis: (i) A coagulation factor is converted from an inactive form (a zymogen) into its active form (enzyme) sequentially, in many cases, by an active coagulation factor activated in the preceding catalytic reaction, leading to a chain of reactions—thus a cascade; (ii) The activation of the inactive coagulation factors will eventually, through the chain of reactions, lead to additional production of the original active coagulation factors that activate those inactive coagulation factors, forming multiple positive feedback loops. In the following sections, more detailed description of the mechanistic processes will be provided.

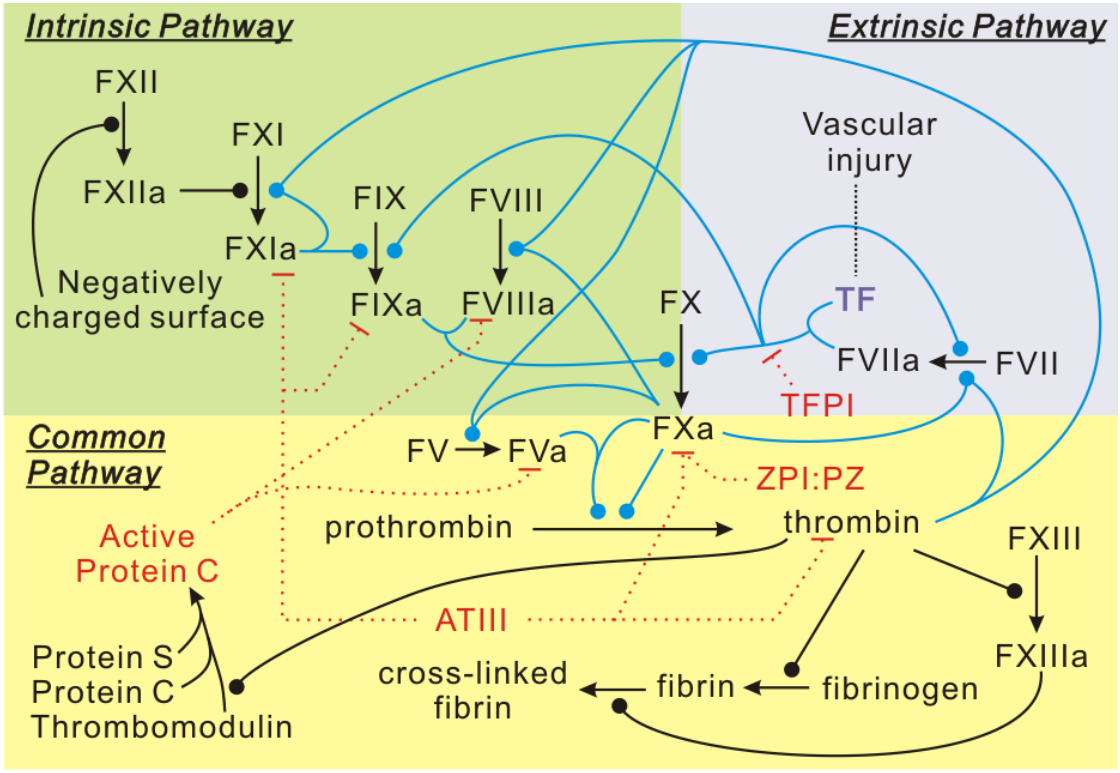

Figure 4.1. Schematic of the coagulation cascade.

4.2.1 The Extrinsic Pathway

Also known as the tissue factor pathway, the extrinsic pathway is considered the *in vivo* initiator of secondary hemostasis in response to vascular injury [36]. After vascular injury, the exposed tissue factor (TF) expressed on the cells embedded in the vessel wall forms a complex with coagulation factor VIIa (FVIIa), the active form of factor VII (FVII) that naturally exists in the blood stream. Although the exact mechanism of the activation of FVII to FVIIa in the absence of external stimuli is still unknown, it is generally accepted that FVIIa exists in the plasma at 1% of total FVII [37]. The enzyme complex TF:FVIIa activates a small amount of factor X (FX) to factor Xa (FXa) [38], eventually producing a small amount of thrombin. As one of its

multiple functions, thrombin then activates FVII to FVIIa [39], forming a positive feedback loop. The TF:FVIIa complex also activates FVII [39], forming another positive feedback loop that would further enhance thrombin production. In addition, TF:FVIIa is also capable of activating factor IX (FIX) [38], thereby partially activating the intrinsic pathway. An additional mechanism of FVII activation is executed by FXa [39], forming another positive feedback loop. In sum, the extrinsic pathway contains multiple positive feedback loops that amplify thrombin production. Together with thrombin, which activates factors V (FV), VIII (FVIII), and XI (FXI) [40-44], the extrinsic pathway initiates the intrinsic pathway and common pathway.

4.2.2 The Intrinsic Pathway

In addition to the numerous activation mechanisms by the extrinsic pathway mentioned in the previous section, the intrinsic pathway can also be activated by hydrophobic surfaces as well as negatively charged surfaces such as glass, leading to the activation of factor XII (FXII) to factor XIIa (FXIIa) [45]. The intrinsic pathway is therefore often referred to as the contact pathway. Once FXII is activated, FXIIa activates FXI to factor XIa (FXIa). FXIa undergoes autocatalytic reactions and promotes its own production [43, 46], forming a positive feedback loop. FXIa also activates FIX to factor IXa (FIXa) [47]. The minute amount of FXa and thrombin produced from the extrinsic pathway activates FVIII to FVIIIa, which forms tenase with FIXa on platelet membranes. The resulting tenase activates FX with a much faster rate (almost 20 times faster) compared to the TF:VIIa complex, eventually leading to much more production of FXa. As FXa activates FVIII, another positive feedback loop is thus formed.

4.2.3 The Common Pathway

The activation events that occur after FX activation are known as the common pathway. FXa is a serine protease with multiple functions. In addition to its role in amplifying the reactions in the extrinsic and the intrinsic pathways introduced in the previous sections, FXa also plays an important role in the common pathway. FXa activates FV to factor Va (FVa), which works as a cofactor and forms a complex known as the prothrombinase with FXa. The catalytic activity of the prothrombinase on the activation of prothrombin to thrombin is more than 10^5-fold higher than FXa alone [48]. Since thrombin activates FV, FVIII and FXI, multiple positive feedback loops are formed as a result of direct and indirect activation of multiple coagulation factors, and eventually thrombin production is significantly amplified through theses entangled positive feedback loops.

The utmost task of thrombin is to help turn the porous platelet plug into a solid impermeable clot. To achieve this, two reactions have to be carried out: (i) convert fibrinogen into fibrin and (ii) activate factor XIII (FXIII) to factor XIIIa (FXIIIa). Fibrinogen is an abundant plasma protein, and its cleaved product, fibrin, serves as a monomer to be polymerized, by FXIIIa, into a fibrin mesh, filling the space in between the platelet aggregate and enhances the mechanical properties of the entire blood clot.

4.2.4 Inhibitory Reactions

Since the coagulation cascade contains multiple positive feedback loops that make it strongly self-amplifying, regulatory mechanisms are necessary to limit the production of its bioactive products. One natural *in vivo* mechanism for eliminating the effectors in the positive feedback loops is the blood flow, whose continuous

transport carries the active effectors away from the site of injury and thus prevents the effectors from further participating in the positive feedback loops.

In addition to the blood flow, a number of inhibitors that nullify the effects of active coagulation factors are involved in the secondary hemostasis process. The most abundant inhibitor in the plasma is antithrombin III (ATIII), or simply antithrombin. ATIII inhibits irreversably multiple enzymes in the coagulation cascade, including thrombin, FIXa, FXa and FXIa [49-51]. Tissue factor pathway inhibitor is a regulator specifically for the extrinsic pathway. The inhibition starts with a reversible binding to FXa. The resulting complex can then reversibly bind with the TF:FVIIa complex, thereby preventing TF:VIIa from further activating FX and FIX [52]. Protein Z-related protease inhibitor (ZPI) and protein Z (PZ) are plasma proteins, and they exist in the plasma in two forms: ZPI alone, or the ZPI:PZ complex. Although their affinity to their substrates is not high, studies have shown that people with ZPI or PZ deficiency has increased thrombotic risks [53, 54]. Although thrombin is where all the positive feedback loops converge to, thrombin also initiates its own regulation. Thrombin first complexes with thrombomodulin (TM) on intact endothelial cells, and then activate protein C in the plasma to Active protein C (APC), which works with Protein S and catalytically degrades FVIIIa and FVa on platelet membranes [55].

4.2.5 Platelet-Derived Pro-Coagulant Molecules

Not only do platelets provide a surface for the coagulation cascade to occur, but the content of the platelets plays a significant role in secondary hemostasis. Hence the interactions between primary and secondary hemostasis are mediated through the release of platelet granule content, as briefly explained in Chapter 1. The most intuitive pro-coagulant molecule in platelets is FV, which is stored in the α-granules

[56]. Recently, studies have shown that platelet derived polyphosphates—inorganic phosphates polymerized into chains of various length—are also pro-coagulant, which makes them a potential target of anti-thrombotic treatment [57].

4.3 Secondary Hemostasis Model

4.3.1 Previous Modeling Efforts

Previous modeling effort involving secondary hemostasis can generally be divided into two categories: (1) models of the *in vitro* scenario, where the models are simulating the behavior of the coagulation cascade in a test tube and the effect of flow is not present [58-62]; (2) models of the *in vivo* scenario, where the effect of blood flow is considered [26, 31, 63-65].

To understand quantitatively the coagulation cascade in the test tube, individual enzyme activity was first studied [66]. The model was then expanded to study thrombin production by the extrinsic pathway and FVIII and FIX in the intrinsic pathway without considering the effect of inhibitory mechanisms [67]. The Hockin and Mann model later included two inhibitors, TFPI and ATIII, into their mathematical representation of the *in vitro* coagulation system [58]. These models assume an excess of phospholipids so that the potential regulatory roles of limited binding sites on platelets are not investigated. The protein C pathway and FXI were later incorporated for studying the spatial effect in regulating the coagulation cascade [61]. Chatterjee et al. included the fibrin production reactions in their mathematical model and studied how blood treated with inhibitors of the intrinsic pathway can still produce thrombin without external stimulation of the TF pathway [59].

For the flow-based models, the Kuharsky and Fogelson model (hereafter referred to as the KF model), is one of the first studies to introduce both the flow effect and the role of platelet membranes into a mathematical model of secondary hemostasis [26]. The KF model is an ODE model that assumes a well-mixed control volume whose size is dependent on the flow rate. The model considers the extrinsic pathway, FVIIII and FIX in the intrinsic pathway, along with three inhibitors, ATIII, APC, and TFPI. The model is later augmented by a more detailed description on protein C activation [64] and the incorporation of FXI [65]. A multiscale model developed by Xu et al. uses a stochastic discrete cellular Potts model for [31] describing platelet aggregation. The model is combined with (i) Navier-Stokes equations that consider the diffusion and the advection effects in the system, and (ii) static thrombin generation profile for each activated platelet.

However, the mathematical models that study the *in vivo* scenario either do not have detailed description of the primary hemostasis part and the activation of platelets is much simplified or the kinetics of the network of secondary hemostasis is largely neglected. Even more, the role of the bioactivity of the platelet membrane is seldom considered. As noted in previous sections, secondary hemostasis cannot function without primary hemostasis, a representative model of secondary hemostasis should also have appropriate description for primary hemostasis in order to obtain physiologically-relevant information. Also, as more and more new details on hemostasis are discovered, an update on secondary hemostasis model is necessary.

In the following sections, we present an updated and adapted secondary hemostasis model and combine the secondary hemostasis model with our primary hemostasis model, forming a comprehensive representation of the hemostatic proces.

Subsequently, this comprehensive model is subjected to multiple conditions in order to obtain insight into the complete hemostatic process.

4.3.2 Model Adaptation

The KF model serves as the foundation of the secondary hemostasis model. The equations regarding primary hemostasis in the original model will later be replaced with the primary hemostasis model developed in the previous chapter. In addition, reaction mechanisms deem necessary are included into the KF model to have an up-to-date, state-of-the-art knowledge on secondary hemostasis. The details of the addition of new mechanisms are introduced in the following sections.

4.3.2.1 Fibrin Production Reactions

Since fibrin is the ultimate product of secondary hemostasis that enhances the mechanical strength of the platelet aggregate, the inclusion of its production in the secondary hemostasis model is essential for describing the complete process of hemostasis. However, the KF model does not cover this aspect. Therefore, related reaction mechanisms are added to the KF model according to the work done by Chatterjee and colleagues [59]. The resulting thrombin concentration profile with respect to time is significantly lowered compared to the reproduced profile of the original KF model, as shown in Figure 4.2. The final concentration of thrombin with fibrin production reactions is reduced by more than half of the original concentration. Such significant reduction in thrombin concentration is consistent with experimental observation that a large portion of thrombin appears to be inhibited as a result of non-substrate binding to fibrin, an activity termed antithrombin I (AT-I) [68].

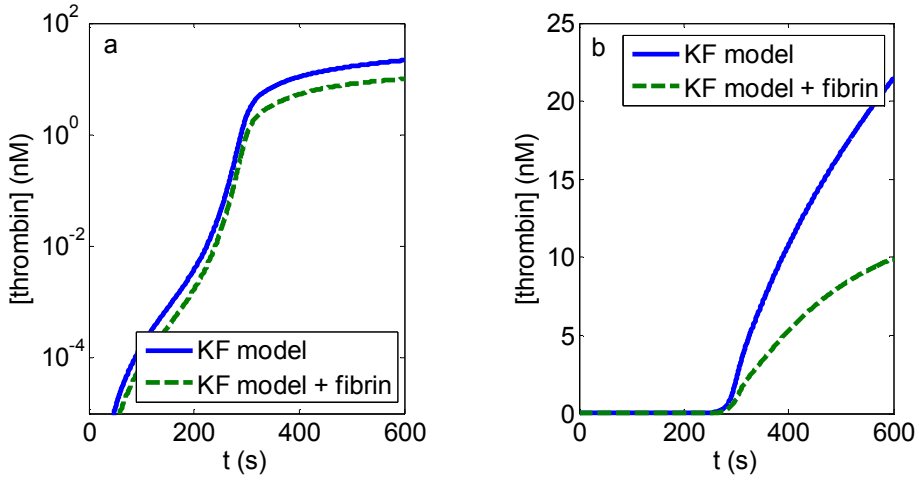

Figure 4.2. Thrombin concentration profiles from the reproduced KF model (blue solid line) and the reproduced KF model with additional fibrin formation reactions (green dashed lines) on (a) log scale and (b) linear scale.

4.3.2.2 Additional Inhibitory Mechanisms in the Secondary Hemostasis Model

As antithrombin is the most abundant inhibitory molecule in the plasma, we look into the literature to see whether there are additional inhibitory mechanisms that are not considered in the KF model. It has been shown that in the presence of phospholipids, ATIII can still yield a significant inhibitory effects on thrombin, FXa, and prothrombinase [50], suggesting that ATIII in the solution phase still react with membrane bound enzymes. Three additional terms describing these events are therefore added to the equation of ATIII and the equation of membrane-bound thrombin, FXa and prothrombinase.

As mentioned in the previous section, Protein Z-dependent protease inhibitor and its cofactor Protein Z have been shown to inhibit FXa, especially towards the membrane-bound species [69], the effect of Protein Z-related reactions are added to membrane-bound FXa with the kinetic rate constants obtained in [53].

4.3.2.3 Additional Activation Mechanisms Between Heterogeneous Phases

One of the major considerations in the KF model is that reactions take place in two different phases: the plasma phase and the membrane-bound phase. Catalytic reactions in the KF model mainly occur within the same phase, with the exception of the reaction between the TF:FVIIa complex and plasma FX. Recent studies, however, have shown a high collision frequency (9000 collision/s) between the plasma phase proteins and the channel walls of the porous structure formed by the platelet aggregate [70]. Not only does the confined space between platelets increases the probability of the collision between the plasma phase molecules and the membrane bound species, the elongated intrathrombus transport time for the molecules as a result of reduced flow velocity should also increase the total number of successful reactions between a protein and its substrates or ligand. Therefore, the reactions between the plasma phase molecule and the membrane-bound species seem very likely.

The modeling work carried out by Burghaus et al. appears to substantiate such possibility [63]. In their model, they consider both the extrinsic and the intrinsic pathways. The interactions between membrane-bound species and the solution species are also applied in the model. As a result, the prothrombin time, a clinical measurement of the function of the extrinsic pathway, is lower than 12.5 seconds, which is very comparable with the clinical standard of 12-13 seconds.

4.3.2.4 Addition of the Intrinsic Pathway: Factor XI

The role of the intrinsic pathway is not addressed in the KF model. Although the intrinsic pathway starts from the activation of FXII, it has been shown that deficiency in FXII might be asymptomatic. Deficiency in FXI, however, could lead to serious hemophilia. It is therefore desirable to include FXI into the secondary

hemostasis model. The relevant reaction mechanisms of FXI in the plasma phase are derived from [59] and the plasma level of FXI is used as reported in [71].

Similar to other coagulation factors, FXI binds to platelet membranes. Since the reactions of FXI used in [59] do not differentiate the membrane-bound FXI from solution FXI, we use the strategies applied in the KF model. FXI and FXIa in the solution bind to or dissociate from the limited binding sites on platelet membranes. Those membrane-bound FXI and FXIa on the platelet membranes can then undergo membrane-related reactions including FXI activation by thrombin and auto-activation by FXIa and FIX activation by FXIa.

4.3.2.5 Platelet Granule Content: Polyphosphate

The reactions that polyphosphates are involved in are [57, 72, 73]: (i) activation of plasma FXI by thrombin; (ii) activation of membrane-bound FXI by membrane-bound thrombin; (iii) activation of plasma FV by thrombin; (iv) activation of membrane-bound FV by membrane-bound FXa; (v) activation of membrane bound FV by membrane-bound thrombin; (vi) activation of membrane-bound FV by plasma FXa; (vii) activation of plasma FV by plasma FXa; (viii) activation of plasma FV by membrane-bound FXa. Due to lack of quantitative understanding of the effect of polyphosphate, the effect is assumed to be proportional to the concentration of polyphosphates in μM in addition to the original reaction rate in the absence of polyphosphates.

4.3.3 Model Parameters and Initial Conditions

The reaction network of the updated secondary hemostasis model is schematically shown in Figure 4.3, and the model equations are summarized in

Appendix A. The complete list of reactions and the notations for the corresponding reaction rate constants are shown in Table 4.1, with the parameters values provided in Table A.1. The non-zero initial conditions of the variables are listed in Table 4.2.

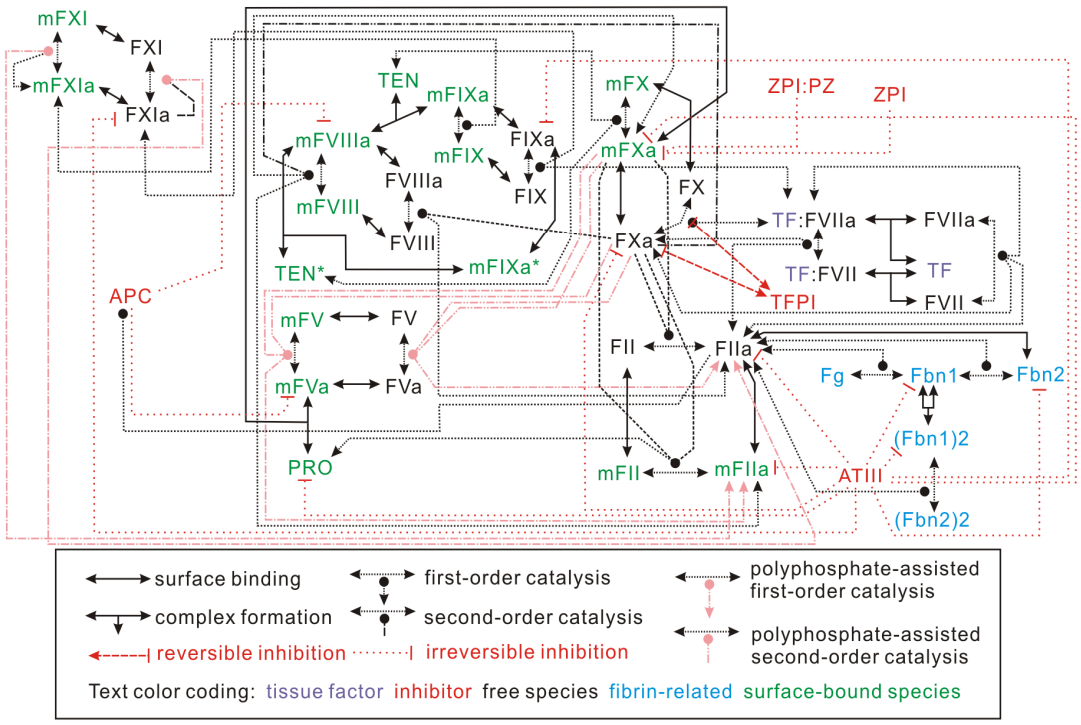

Figure 4.3. Schematic of reactions considered in the updated secondary hemostasis model.

Table 4.1. Notations of the rate constants used in the secondary hemostasis model. The notations are used in the equations listed in Appendix A and their corresponding values are listed in Table A.1. k1 is the reaction constant for the forward reaction, k-1 for the reverse reaction, kcat for first-order catalytic reaction, kscat for second-order catalytic reaction.

Rxn	Model Expressions	k_1 ($nM^{-1}s^{-1}$)	k_{-1} (s^{-1})	k_{cat} (s^{-1})	k_{scat} ($nM^{-1}s^{-1}$)	ref.
1	$Z_7 + TF \leftrightarrow Z_7^m$	k_{7z}^{on}	k_7^{off}			[26, 58]
2	$E_7 + TF \leftrightarrow E_7^m$	k_7^{on}	k_7^{off}			[26]
3	$Z_7^m + E_{10} \leftrightarrow Z_7^m : E_{10} \rightarrow E_7^m + E_{10}$	k_2^+	k_2^-	k_2^{cat}		[26]
4	$Z_7^m + E_2 \leftrightarrow Z_7^m : E_2 \rightarrow E_7^m + E_2$	k_3^+	k_3^-	k_3^{cat}		[26]
5	$Z_{10} + E_7^m \leftrightarrow Z_{10} : E_7^m \rightarrow E_7^m + E_{10}$	k_8^+	k_8^-	k_8^{cat}		[26, 38]
6	$Z_9 + E_7^m \leftrightarrow Z_9 : E_7^m \rightarrow E_7^m + E_9$	k_9^+	k_9^-	k_9^{cat}		[26, 38]
7	$Z_7 + E_{10} \leftrightarrow Z_7 : E_{10} \rightarrow E_7 + E_{10}$	k_1^+	k_1^-	k_1^{cat}		[26]
8	$Z_7 + E_2 \leftrightarrow Z_7 : E_2 \rightarrow E_7 + E_2$	k_{18}^+	k_{18}^-	k_{18}^{cat}		[26]
9	$Z_5 + E_2 \leftrightarrow Z_5 : E_2 \rightarrow E_5 + E_2$	k_{12}^+	k_{12}^-	k_{12}^{cat}		[26]
10	$Z_8 + E_2 \leftrightarrow Z_8 : E_2 \rightarrow E_8 + E_2$	k_{14}^+	k_{14}^-	k_{14}^{cat}		[26]
11	$Z_9 + P_9 \leftrightarrow Z_9^m$	k_9^{on}	k_9^{off}			[26]
12	$E_9 + P_9 \leftrightarrow E_9^m$	k_9^{on}	k_9^{off}			[26]
13	$E_9 + P_9^* \leftrightarrow E_9^{m*}$	k_9^{on}	k_9^{off}			[26]
14	$Z_{10} + P_{10} \leftrightarrow Z_{10}^m$	k_{10}^{on}	k_{10}^{off}			[26]
15	$E_{10} + P_{10} \leftrightarrow E_{10}^m$	k_{10}^{on}	k_{10}^{off}			[26]
16	$Z_5 + P_5 \leftrightarrow Z_5^m$	k_5^{on}	k_5^{off}			[26]
17	$E_5 + P_5 \leftrightarrow E_5^m$	k_5^{on}	k_5^{off}			[26]
18	$Z_8 + P_8 \leftrightarrow Z_8^m$	k_8^{on}	k_8^{off}			[26]
19	$E_8 + P_8 \leftrightarrow E_8^m$	k_8^{on}	k_8^{off}			[26]
20	$Z_2 + P_2 \leftrightarrow Z_2^m$	k_2^{on}	k_2^{off}			[26]
21	$E_2 + P_2 \leftrightarrow E_2^m$	k_2^{on}	k_{2e}^{off}			[26]
22	$Z_5^m + E_{10}^m \leftrightarrow Z_5^m : E_{10}^m \rightarrow E_5^m + E_{10}^m$	k_5^+	k_5^-	k_5^{cat}		[26]
23	$Z_5^m + E_2^m \leftrightarrow Z_5^m : E_2^m \rightarrow E_5^m + E_2^m$	k_{13}^+	k_{13}^-	k_{13}^{cat}		[26]
24	$Z_8^m + E_{10}^m \leftrightarrow Z_8^m : E_{10}^m \rightarrow E_8^m + E_{10}^m$	k_6^+	k_6^-	k_6^{cat}		[26]
25	$Z_8^m + E_2^m \leftrightarrow Z_8^m : E_2^m \rightarrow E_8^m + E_2^m$	k_{15}^+	k_{15}^-	k_{15}^{cat}		[26, 41, 42]
26	$E_8^m + E_9^m \leftrightarrow TEN$	k_{ten}^b	k_{ten}^{ub}			[26]
27	$E_8^m + E_9^{m*} \leftrightarrow TEN*$	k_{ten}^b	k_{ten}^{ub}			[26]
28	$E_5^m + E_{10}^m \leftrightarrow PRO$	k_{pro}^b	k_{pro}^{ub}			[26]
29	$Z_{10}^m + TEN \leftrightarrow Z_{10}^m : TEN \rightarrow E_{10}^m + TEN$	k_4^+	k_4^-	k_4^{cat}		[26]

Table 4.1 continued.

30	Z_{10}^{m} + TEN* ↔ Z_{10}^{m}:TEN* → E_{10}^{m} + TEN*	k_4^+	k_4^-	k_4^{cat}		[26]
31	Z_2^m + PRO ↔ Z_2^m:PRO → E_2^m + PRO	k_7^+	k_7^-	k_7^{cat}		[26]
32	APC + E_8^m ↔ APC: E_8^m → $E_8^{m,in}$	k_{17}^+	k_{17}^-	k_{17}^{cat}		[26]
33	APC + E_5^m ↔ APC: E_5^m → $E_5^{m,in}$	k_{16}^+	k_{16}^-	k_{16}^{cat}		[26]
34	TFPI + E_{10} ↔ TFPI: E_{10}	k_1^b	k_1^{ub}			[26]
35	TFPI: E_{10} + E_7^m ↔ TFPI: E_{10}:E_7^m	k_2^b	k_2^{ub}			[26]
36	ATIII + E_9 → E_9^{in}				k_1^{in}	[26]
37	ATIII + E_{10} → E_{10}^{in}				k_3^{in}	[26]
38	ATIII + E_2 → E_2^{in}				k_2^{in}	[26]
39	Fg + E_2 ↔ Fg: E_2 → Fbn_1 + E_2 + FPA	k_{10}^+	k_{10}^-	k_{10}^{cat}		[59]
40	Fbn_1 + E_2 ↔ Fbn_1 : E_2 → Fbn_2 + E_2 + FPB	k_{11}^+	k_{11}^-	k_{11}^{cat}		[59]
41	2 Fbn_1 ↔ $(Fbn_1)_2$	k_4^b	k_4^{ub}			[59]
42	$(Fbn_1)_2$ + E_2 ↔ $(Fbn_1)_2$: E_2 → $(Fbn_2)_2$ + E_2 + 2 FPB	k_{19}^+	k_{19}^-	k_{19}^{cat}		[59]
43	Fbn2 + E_2 ↔ Fbn2: E_2	k_5^b	k_5^{ub}			[59]
44	$(Fbn_1)_2$: E_2 + ATIII → $(Fbn_1)_2$2:E2:ATIII				k_9^{in}	[59]
45	Fbn_1 : E_2 + ATIII → Fbn_1 : E_2 :ATIII				k_{10}^{in}	[59]
46	Fbn_2 : E_2 + ATIII → Fbn_2 : E_2 :ATIII				k_{11}^{in}	[59]
47	TFPI + E10m ↔ TFPI:E10m	k_3^b	k_3^{ub}			[74]
48	PRO + ATIII → PRO:ATIII				k_5^{in}	[50]
49	E_2^m + ATIII → E_2^m:ATIII				k_6^{in}	[50]
50	E_{10}^m + ATIII → E_{10}^m:ATIII				k_4^{in}	[50]
51	ZPI + E_{10}^m ↔ ZPI: E_{10}^m				k_7^{in}	[54]
52	ZPI:PZ + E_{10}^m ↔ ZPI:PZ: E_{10}^m				k_8^{in}	[54]
53	Z_2 + E_{10} → E_2 + E_{10}				k_2^{scat}	[63]
54	Z_2 + E_{10}^m → E_2 + E_{10}^m				k_2^{scat}	[63]
55	Z_2^m + E_{10} → E_2^m + E_{10}				k_2^{scat}	[63]
56	Z_2^m + E_{10}^m → E_2^m + E_{10}^m				k_2^{scat}	[63]
57	Z_5 + E_{10} → E_5 + E_{10}				k_3^{scat}	[63]
58	Z_5 + E_{10}^m → E_5 + E_{10}^m				k_3^{scat}	[63]
59	Z_5^m + E_{10} → E_5^m + E_{10}				k_3^{scat}	[63]
60	Z_8 + E_{10} →E_8 + E_{10}				k_4^{scat}	[63]
61	Z_8 + E_{10}^m → E_8 + E_{10}^m				k_4^{scat}	[63]

Table 4.1 continued.

62	$Z_8^m + E_{10} \rightarrow E_8^m + E_{10}$				k_4^{scat}	[63]
63	$Z_7 + E_{10}^m \rightarrow E_7 + E_{10}^m$				k_5^{scat}	[63]
64	$Z_7 + E_7^m \rightarrow E_7 + E_7^m$				k_6^{scat}	[63]
65	$Z_{11} + P_{11} \leftrightarrow Z_{11}^m$	k_{11}^{on}	k_{11}^{off}			[63]
66	$E_{11} + P_{11} \leftrightarrow E_{11}^m$	k_{11e}^{on}	k_{11e}^{off}			[63]
67	$Z_{11} + E_2 \leftrightarrow Z_{11}: E_2 \rightarrow E11 + E_2$	k_{20}^{+}	k_{20}^{-}	k_{20}^{cat}		[59]
68	$Z_{11} + E_{11} \leftrightarrow Z_{11}: E_{11} \rightarrow 2\,E_{11}$				k_1^{scat}	[59]
69	E_{11} + ATIII $\rightarrow$ E11:ATIII				k_{12}^{in}	[59]
70	$Z_9 + E_{11} \leftrightarrow Z_9 : E_{11} \rightarrow E_9 + E_{11}$	k_{21}^{+}	k_{21}^{-}	k_{21}^{cat}		[59]
71	$Z_{11}^m + E_{11}^m \leftrightarrow Z_{11}^m: E_{11}^m \rightarrow 2\,E_{11}^m$	k_{22}^{+}	k_{22}^{-}	k_{22}^{cat}		[59, 75]
72	$Z_9^m + E_{11}^m \leftrightarrow Z_9^m: E_{11}^m \rightarrow E_9^m + E_{11}^m$	k_{24}^{+}	k_{24}^{-}	k_{24}^{cat}		[59]
73	$Z_{11}^m + E_2^m \leftrightarrow Z_{11}^m: E_2^m \rightarrow E_{11} + E_2^m$	k_{23}^{+}	k_{23}^{-}	k_{23}^{cat}		[59]
74	$Z_{11}^m: E_2^m$ + polyP $\rightarrow E_{11} + E_2^m +$ polyP			k_{23}^{cat}		[59, 72]
75	$Z_{11}: E_2$ + polyp $\rightarrow E_{11} + E_2 +$ polyP			k_{20}^{cat}		[59, 72]
76	$Z_5 : E_2$ + polyP $\rightarrow E_5 + E_2 +$ polyP			k_{12}^{cat}		[26, 72]
77	$Z_5^m: E_2^m$ + polyP $\rightarrow E_5^m + E_2^m +$ polyP			k_{13}^{cat}		[26, 72]
78	$Z_5^m: E_{10}^m$ + polyP $\rightarrow E_5^m + E_{10}^m +$ polyP			k_5^{cat}		[26, 72]
79	$Z_5^m + E_{10}$ + polyP $\rightarrow E_5^m + E_{10} +$ polyP				k_3^{scat}	[63, 72]
80	$Z_5 + E_{10}$ + polyP $\rightarrow E_5 + E_{10} +$ polyP				k_3^{scat}	[63, 72]
81	$Z_5 + E_{10}^m$ + polyP $\rightarrow E_5 + E_{10}^m +$ polyP				k_3^{scat}	[63, 72]
82	E_2 + PC $\rightarrow$ APC				k_{APC}	[26]

Table 4.2. List of non-zero initial conditions used for variables in secondary hemostasis.

Variable	I.C.	Unit	Reference
$\boldsymbol{Z_2}$	1400	nM	[26]
$\boldsymbol{Z_5}$	10	nM	[26]
$\boldsymbol{Z_7}$	10	nM	[26]
$\boldsymbol{E_7}$	0.1	nM	[26]
$\boldsymbol{Z_8}$	1	nM	[26]
$\boldsymbol{Z_9}$	90	nM	[26]
$\boldsymbol{Z_{10}}$	170	nM	[26]
$\boldsymbol{Z_{11}}$	25	nM	[71]
$\boldsymbol{N_2^{pl}}$	2000	-	[26]
$\boldsymbol{N_5^{pl}}$	3000	-	[26]
$\boldsymbol{N_8^{pl}}$	450	-	[26]
$\boldsymbol{N_9^{pl}}$	250	-	[26]
$\boldsymbol{N_{9^*}^{pl}}$	250	-	[26]
$\boldsymbol{N_{10}^{pl}}$	2700	-	[26]
$\boldsymbol{N_{11}^{pl}}$	250	-	[76]
TFPI	2.5	nM	[26]
ATIII	3400	nM	[59]
ZPI:PZ	34.4	nM	[77]
ZPI	23.6	nM	[77]
fibrinogen	9000	nM	[59]

Most parameter values used in the secondary hemostasis model are directly taken from the studies listed in Table 4.1 and Table A.1, with the exception of the parameters of the autocatalytic reactions of FXI. The autocatalytic activity of FXIa has long been speculated [43, 46] but few kinetic studies have been carried out. Kramoroff and Nigretto [75] estimated the secondary reaction rate constant for the reaction to be 3.19×10^{-3} $s^{-1}nM^{-1}$. As the rate constant is speculated to be overestimated [59], for the membrane-bound autocatalytic reaction (reaction 71 in Table 4.1), we use a quarter of the literature value following the assumption made in [59] and assumed (i) a forward

reaction rate constant of 0.1 $s^{-1}nM^{-1}$ (diffusion-limited reaction), and (ii) a turnover number k_{cat} 13-fold lower than the action of thrombin on FXI activation, to determine the reverse reaction rate constant.

4.4 Integration of Primary and Secondary Hemostasis Model

In order to connect the updated secondary hemostasis model to our previously introduced model of primary hemostasis, a few modifications are required. The following sections introduce the modifications applied for the three interactions between primary and secondary hemostasis shown in Figure 1.2.

4.4.1 Number of Activated Platelets for Sites for Coagulation

The binding sites on platelet membranes for coagulation factors in the updated secondary hemostasis model are used as concentrations. Therefore, the number of activated platelets in the aggregate from the primary hemostasis model first needs to be converted into concentration using the volumes of interest introduced in the primary hemostasis model:

$$\left[PLT_{col}\right] = \frac{PLT_{col}}{V_{col}} \tag{4.1}$$

$$\left[PLT_{\text{sec}}\right] = \frac{PLT_{\text{sec}}}{V_{eff}} \tag{4.2}$$

4.4.2 FV Release from Platelets

FV is stored by platelet alpha granules and will be released by platelets upon activation. The process of FV release is therefore described by an equation similar to those used for ADP and TxA2:

$$\frac{d\left(FV_{col,released}\right)}{dt} = R_{FV,col,rel} = k_{19} PLT_{col}\left(PLT_{col} Q_{FV} - FV_{col,released}\right) \tag{4.3}$$

$$\begin{aligned}\frac{d(FV_{res})}{dt} &= \frac{k_{13-1}(\alpha_{IIb}\beta_3^{*}{}_{agg})(\alpha_{IIb}\beta_3^{*}{}_{new})[Fg]}{\left(1+[JAM-A](PLT_{agg})^{n_{13-1}}\right)} \times Q_{FV} \\ &- k_{13-2}(PLT_{agg})^{2/3}\left(1-\frac{\left(\frac{[ADP]}{ADP_{50}}+\frac{[TxA2]}{TxA2_{50}}+\frac{[Thr]}{Thr_{50}}\right)^{n_{13-2}}}{3^{n_{13-2}}+\left(\frac{[ADP]}{ADP_{50}}+\frac{[TxA2]}{TxA2_{50}}+\frac{[Thr]}{Thr_{50}}\right)^{n_{13-2}}}\right) \\ &\times \frac{\left(\frac{[ADP]}{ADP_{50}}+\frac{[TxA2]}{TxA2_{50}}+\frac{[Thr]}{Thr_{50}}\right)^{n_{13-2}}}{3^{n_{13-2}}+\left(\frac{[ADP]}{ADP_{50}}+\frac{[TxA2]}{TxA2_{50}}+\frac{[Thr]}{Thr_{50}}\right)^{n_{13-2}}} \frac{FV_{res}}{(PLT_{agg}+1)\cdot\phi_{FV}} \\ &- k_{20} FV_{res}\end{aligned} \tag{4.4}$$

$$\frac{d(FV_{plt})}{dt} = k_{20} FV_{res} \tag{4.5}$$

The rate of release is calculated and becomes an input to the secondary hemostaisis model, where the rate of release of FV from platelets is considered in the differential equation of FV in the updated secondary hemostasis model. The parameters involved in the process are estimated such that the resulting profile of FV release rate is comparable to other terms in the differential equation of FV

4.4.3 Polyphosphates Released by the Platelets

Since polyphosphates are stored in the dense granules along with ADP and ATP in platelets, the release of polyphosphates from platelets is described by the same equations for ADP release with the same parameters except for the total amount of polyphosphates each single platelet carries, Q_{polyP}. The equations regarding the release of polyphosphate, or polyP, from collagen-bound platelets and secondary platelets are expressed as follows:

$$\frac{d\left(polyP_{col,released}\right)}{dt} = R_{polyP,col,rel} = k_{17} PLT_{col}\left(PLT_{col} Q_{polyP} - polyP_{col,released}\right) \tag{4.6}$$

$$\frac{d\left(polyP_{col}\right)}{dt} = R_{polyP,col} = \frac{d\left(polyP_{col,released}\right)}{dt} - k_{cflow} polyP_{col} \tag{4.7}$$

$$\begin{aligned}
\frac{d(polyP_{res})}{dt} = {} & \frac{k_{13-1}(\alpha_{IIb}\beta_3{}^{*}{}_{agg})(\alpha_{IIb}\beta_3{}^{*}{}_{new})[Fg]}{\left(1+[JAM-A](PLT_{agg})^{n_{13-1}}\right)} \times Q_{polyP} \\
& - k_{13-2}(PLT_{agg})^{2/3}\left(1 - \frac{\left(\frac{[ADP]}{ADP_{50}} + \frac{[TxA2]}{TxA2_{50}} + \frac{[Thr]}{Thr_{50}}\right)^{n_{13-2}}}{3^{n_{13-2}} + \left(\frac{[ADP]}{ADP_{50}} + \frac{[TxA2]}{TxA2_{50}} + \frac{[Thr]}{Thr_{50}}\right)^{n_{13-2}}}\right) \\
& \times \frac{\left(\frac{[ADP]}{ADP_{50}} + \frac{[TxA2]}{TxA2_{50}} + \frac{[Thr]}{Thr_{50}}\right)^{n_{13-2}}}{3^{n_{13-2}} + \left(\frac{[ADP]}{ADP_{50}} + \frac{[TxA2]}{TxA2_{50}} + \frac{[Thr]}{Thr_{50}}\right)^{n_{13-2}}} \frac{polyP_{res}}{(PLT_{agg}+1)\cdot\phi_{ADP}} \\
& - k_{14} polyP_{res}
\end{aligned} \tag{4.8}$$

$$\frac{d(polyP_{\text{sec}})}{dt} = k_{14} polyP_{res} - k_{cflow} polyP_{\text{sec}} \tag{4.9}$$

4.4.4 Thrombin-Induced Platelet Activation

The effect of platelet activation by thrombin is added to the single platelet model in the primary hemostasis actuator. As thrombin receptors are also G protein coupled receptors, the effects of thrombin are described by Hill functions similar to the effects of ADP and TxA2 on G protein activation. The original equations for G protein activation therefore become:

$$\frac{d[GqGTP]}{dt} = \eta V_{eff} \left(\begin{array}{l} k_{1-1} \dfrac{[ADP]^{n_{1-1}}}{a_{1-1}{}^{n_{1-1}} + [ADP]^{n_{1-1}}} \\ +k_{1-2} \dfrac{[TxA2]^{n_{1-2}}}{a_{1-2}{}^{n_{1-2}} + [TxA2]^{n_{1-2}}} \\ +k_{1-5} \dfrac{[Thr]^{n_{1-5}}}{a_{1-5}{}^{n_{1-5}} + [Thr]^{n_{1-5}}} \end{array} \right) \frac{[PLT]^{n_{1-3}}}{a_{1-3}{}^{n_{1-3}} + [PLT]^{n_{1-3}}} - k_{1-4}[GqGTP] \tag{4.10}$$

$$\frac{d[GiGTP]}{dt} = \eta V_{eff} \left(\begin{array}{l} k_{2-1} \dfrac{[ADP]^{n_{2-1}}}{a_{2-1}{}^{n_{2-1}} + [ADP]^{n_{2-1}}} \\ +k_{2-4} \dfrac{[Thr]^{n_{2-4}}}{a_{2-4}{}^{n_{2-4}} + [Thr]^{n_{2-4}}} \end{array} \right) \frac{[PLT]^{n_{2-2}}}{a_{2-2}{}^{n_{2-2}} + [PLT]^{n_{2-2}}} - k_{2-3}[GiGTP] \tag{4.11}$$

$$\frac{d[G13GTP]}{dt} = \eta V_{eff} \left(\begin{array}{l} k_{3-1} \dfrac{[ADP]^{n_{3-1}}}{a_{3-1}{}^{n_{3-1}} + [ADP]^{n_{3-1}}} \\ +k_{3-4} \dfrac{[Thr]^{n_{3-4}}}{a_{3-4}{}^{n_{3-4}} + [Thr]^{n_{3-4}}} \end{array} \right) \frac{[PLT]^{n_{3-2}}}{a_{3-2}{}^{n_{3-2}} + [PLT]^{n_{3-2}}} - k_{3-3}[G13GTP] \tag{4.12}$$

The parameters involved in the reactions describing the effect of thrombin on primary hemostasis are listed in Table 4.3.

Table 4.3. List of new parameters involved in augmenting the primary hemostasis model for incorporating the effect of secondary hemostasis

parameter name	parameter value	unit
$k_{1\text{-}5}$	2.15×10^{-1}	1/s
$n_{1\text{-}5}$	9.06×10^{-1}	-
$a_{1\text{-}5}$	8.48	μM
$k_{2\text{-}4}$	1.39×10^{-2}	1/s
$n_{2\text{-}4}$	1.93	-
$a_{2\text{-}4}$	7.85	μM
$k_{3\text{-}4}$	2.35×10^{-2}	1/s
$n_{3\text{-}4}$	5.77	-
$a_{3\text{-}4}$	20.1	μM
k_{20}	7×10^{-4}	1/s
ϕ_{FV}	2.78×10^{-1}	-
k_{19}	4.10×10^{-7}	1/s
Q_{polyP}	5.94×10^{4}	-

4.4.5 Interaction Strength

As it has been shown in murine experiments that the micro-environment within a thrombus is heterogeneous [34], the interactions between primary and secondary hemostasis are not universal. For example, thrombin is shown to be produced only near the vessel wall, making thrombin unavailable to the secondary platelets farther away from the vessel wall. To address this issue, a gain block is imposed on each of the interactions, and a gain of 0.5 used as the nominal condition.

4.4.6 Change in Porosity of Platelet Aggregate

The initial porosity of the platelet aggregation is assumed to be 0.5. The change in porosity of the aggregate is carried out by the following equation:

$$\phi_{agg} = 0.5 + [(fbn_2)_2] \times 6.02 \times 10^{-10} \times 23^2 \times 90 \quad (4.13)$$

with a constraint of $\phi_{agg} \leq 1$.

4.5 Simulation Results

4.5.1 Nominal Conditions

Because currently there is no way of validating our mathematical model of *in vivo* hemostasis in humans, we use the model under various conditions to evaluate the performance of the model. The time profiles of the platelet aggregate and the three major positive feedback signaling molecules, i.e. ADP, TxA2, and thrombin, under nominal conditions are shown in Figure 4.4. The profiles are a result of a wound intensity of 100 μm^2 and a shear rate of 400 s^{-1}. Compared with the results from the primary hemostasis model, it can be seen in the platelet aggregation profile (Fig. 4.4 (a)) that thrombin from secondary hemostasis (Fig. 4.4d) gives platelet aggregation a boost. As a result of additional platelet activation, ADP and TxA2 (Fig. 4.4b-c) release also have a boost, with an effect more profound in ADP than TxA2. Note in this nominal case of the comprehensive model, the thrombin production initiation time (t_{thr}), or the time to reach a thrombin level of 2 nM, is significantly reduced compared to the KF model. Such reduced t_{thr} is believed to be closer to the physiological scenario, since fibrin production in *in vivo* murine experiments [34] is quickly observed after wound occurrence. In addition, clinical indices for coagulation function, prothrombin time (PT) and activated partial thromboplastin time (aPTT), have standard ranges of 12-13 seconds and 30-40 seconds, respectively, suggesting normal production of thrombin should occur within 1 minute.

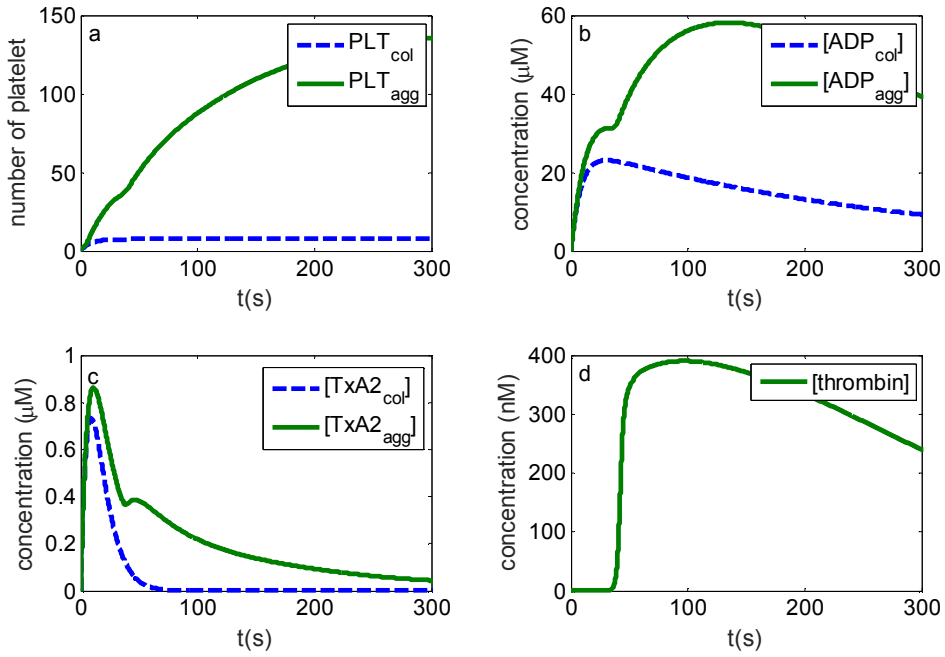

Figure 4.4. Profile of (a) number of activated platelet in the aggregate, (b) ADP concentration, (c) TxA2 concentration, and (d) thrombin concentration under the nominal condition in response to an initial wound size of 100 μm^2 at a shear rate of 400 s^{-1}.

To compare with the primary hemostasis only case, the comprehensive model is subjected to various wound intensities, or wound sizes, under nominal conditions. The results, shown in Figure 4.5, demonstrate a trend similar to the primary hemostasis only case. At a wound size of 20 μm^2 (Figure 4.5 a), a thrombus with a size larger than the wound size is produced. As the wound size gradually increases from 20 μm^2 to 400 μm^2 (Figure 4.5b-e), an oversized thrombus is still produced, but the thrombus size relative to the wound size becomes smaller and smaller, as shown in (Fig. 4.5f). Therefore, one could expect that when the wound size is large enough, the

hemostatic process will not be able to completely seal the wound, and additional external force, e.g., pressure, is required to help close the wound.

4.5.2 Disease Conditions and Interventions

In order to evaluate how the comprehensive model behaves, we subject the model to a number of disease conditions and a number of scenarios where interventions to hemostatic functions are applied.

4.5.2.1 Hemophilia A and B

Hemophilia A and B are resulted from deficiency in plasma FVIII and FIX, respectively. Because FVIIIa and FIXa are essential components in the tenase complex, which activates FX to FXa that eventually activates prothrombin, deficiency in FVIII or FIX translates to a reduced level of tenase level, leading to a reduced thrombin level and a bleeding diathesis. Figure 4.6 shows the platelet aggregation profiles and the thrombin concentration profiles of the nominal condition, hemophilia A, and hemophilia B in response to a wound size of 100 μm^2 at a shear rate of 400 s^{-1}. The deficiency levels of hemophilia A and B are set at 0.1% of the nominal FVIII and FIX level, respectively. Compared with the nominal case, platelet aggregation (Figure 4.6a) with hemophilic conditions is much delayed as a result of the delayed production of thrombin (Figure 4.6b). With a plasma level reduced to 1% of the nominal level in both hemophilia A and B, it appears that despite a delayed thrombin production in both cases, hemophilia B is slightly better than hemophilia A. Although hemophilia A and B are said to be clinically indifferentiable, recent studies have shown hemophilia A patients appear to have more serious symptoms [78, 79].

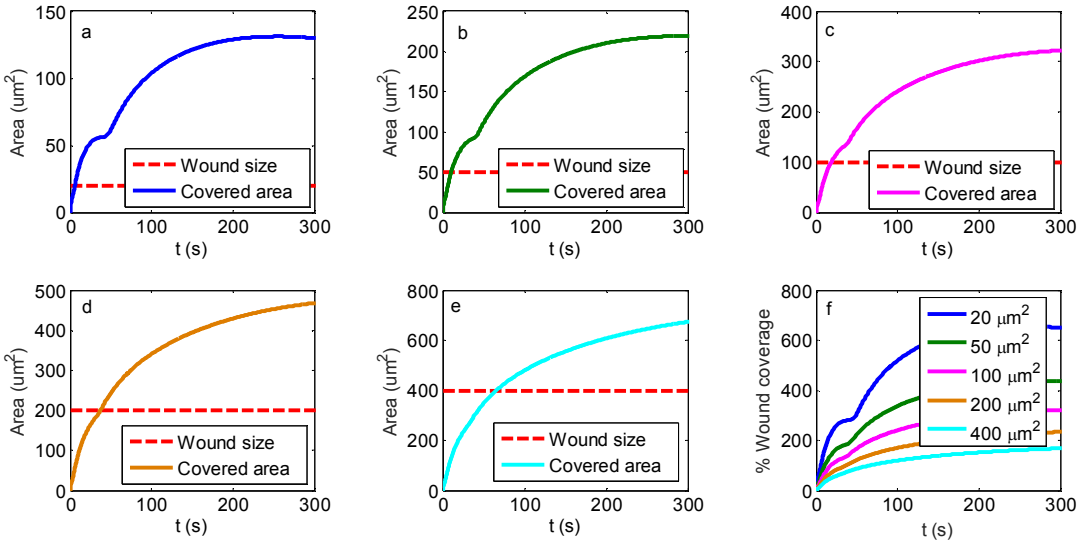

Figure 4.5. Wound coverage profiles in response to various wound intensities, or wound sizes: (a) 20 μm^2, (b) 50 μm^2, (c) 100 μm^2, (d) 200 μm^2, (e) 400 μm^2. (f) Relative percentage of wound coverage to the corresponding wound intensity.

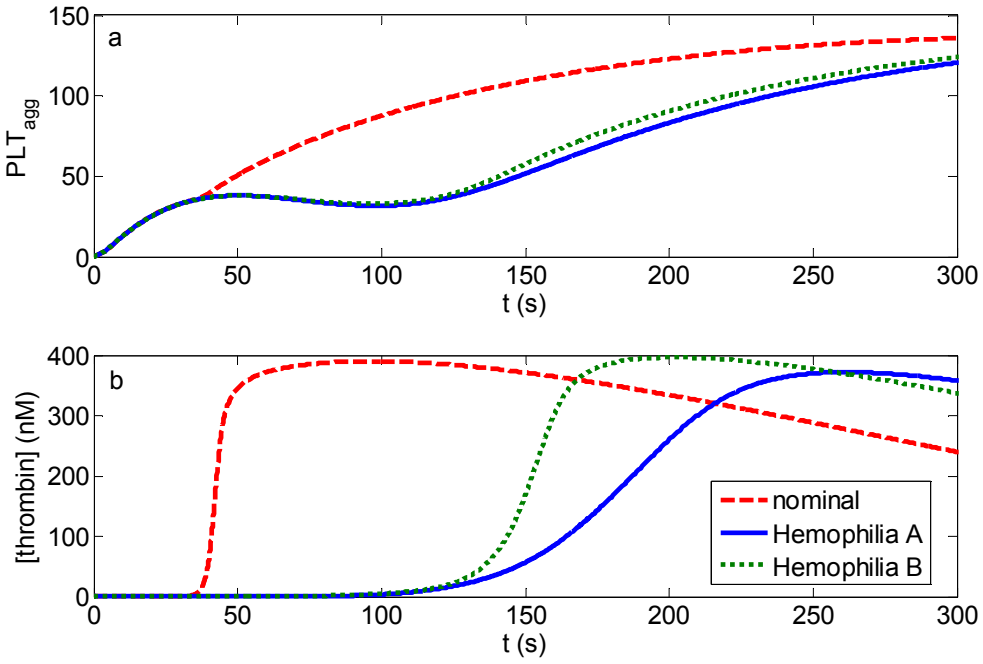

Figure 4.6. A comparison of (a) the aggregation profile and (b) the thrombin concentration profile from the nominal condition, hemophilia A and hemophila B in response to a wound size of 100 μm^2 at a shear rate of 400 s^{-1}. Hemophilia A and hemophilia B are simulated using a plasma FVIII level 0.1% of the nominal condition and a plasma FIX level 0.1% of the nominal condition, respectively.

4.5.2.2 Immune Thrombocytopenic Purpura

Immune thrombocytopenic purpura, or ITP, is characterized by an abnormally low platelet count in an individual. Traditionally, a platelet count of between 150×10^9/L and 400×10^9/L is considered to be the healthy range. ITP is therefore diagnosed when platelet count is lower than 150×10^9/L. Here we use the comprehensive heomostasis model to investigate how the platelet count affects the system response.

Four platelet count values are used for investigation: 200, 50, 30, and 10×10^9/L, where 200×10^9/L is the nominal case and the other three scenarios represent different severities of ITP. As expected, as platelet count decreases, both the platelet aggregation and thrombin level (Figure 4.7a-b) are reduced, and the wound coverage (Figure 4.7c) is gradually reduced to a level where the wound cannot be completely covered. Note that with a platelet count of 30×10^9/L, even though thrombin production eventually rises (magenta curve in Figure 4.7b), platelet aggregation still does not benefit from that event, as not enough platelets are in place to be activated, leading to an undersized thrombus.

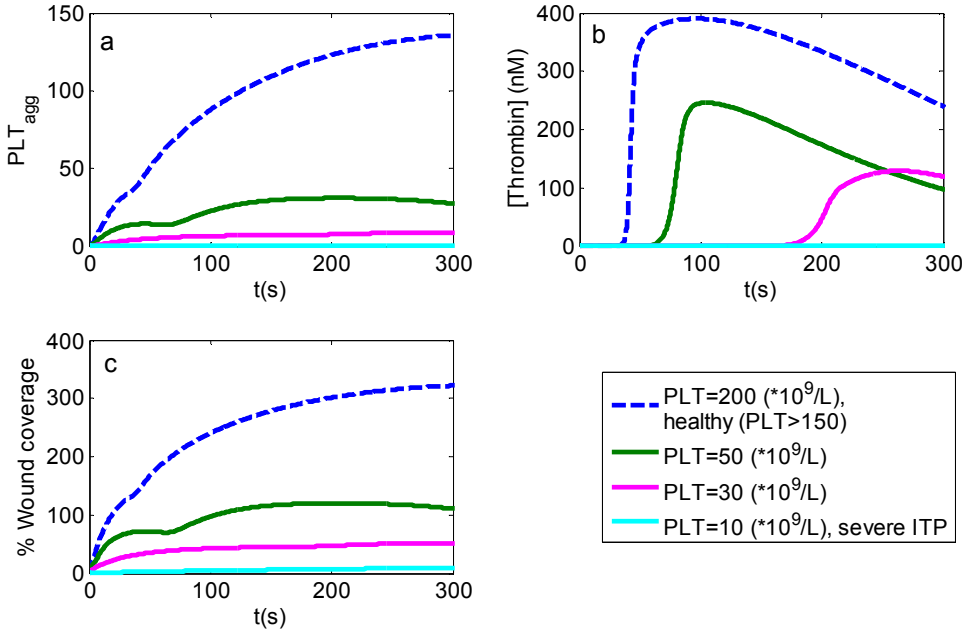

Figure 4.7. System response to a wound size of 100 μm^2 at a shear rate of 400 s^{-1} with various levels of platelet count. (a) platelet aggregation; (b) thrombin concentration profile; (c) percentage ratio of covered wound area to the initial wound size.

4.5.2.3 Differential Inhibition of ADP Receptors on Platelets

ADP receptors on platelets, $P2Y_1$ and $P2Y_{12}$, have long been of interest for the pharmaceutical industry because they are potential therapeutic targets for reducing thrombotic risks in individuals. Currently, three $P2Y_{12}$ inhibitors have been approved for clinical use: clopidogrel, prasugrel, and ticagrelor [80], and $P2Y_1$ inhibitor is still under development. Here we use the comprehensive model to investigate the differential effect of inhibition of $P2Y_1$- and $P2Y_{12}$-induced platelet activation. The inhibition is achieved by reducing the corresponding activation rate constant to 10% of the nominal value. In Figure 4.8, it is seen that a 90% reduction in the activation rate constant for $P2Y_1$ leads to a greater degree of inhibition in platelet aggregation, thrombin production, and the wound coverage.

However, this does not necessarily mean that $P2Y_1$ inhibitors will be more effective in reducing thrombotic risk. As shown by Li et al. with microfluidic experiments using human whole blood [81], different donors respond differently to the same inhibitor. It has been observed that in some donors, $P2Y_1$ inhibitors work more effectively in reducing platelet aggregation, while in other donors, $P2Y_{12}$ inhibitors are more powerful. Therefore, the properties demonstrated by our comprehensive model only represent certain phenotypes.

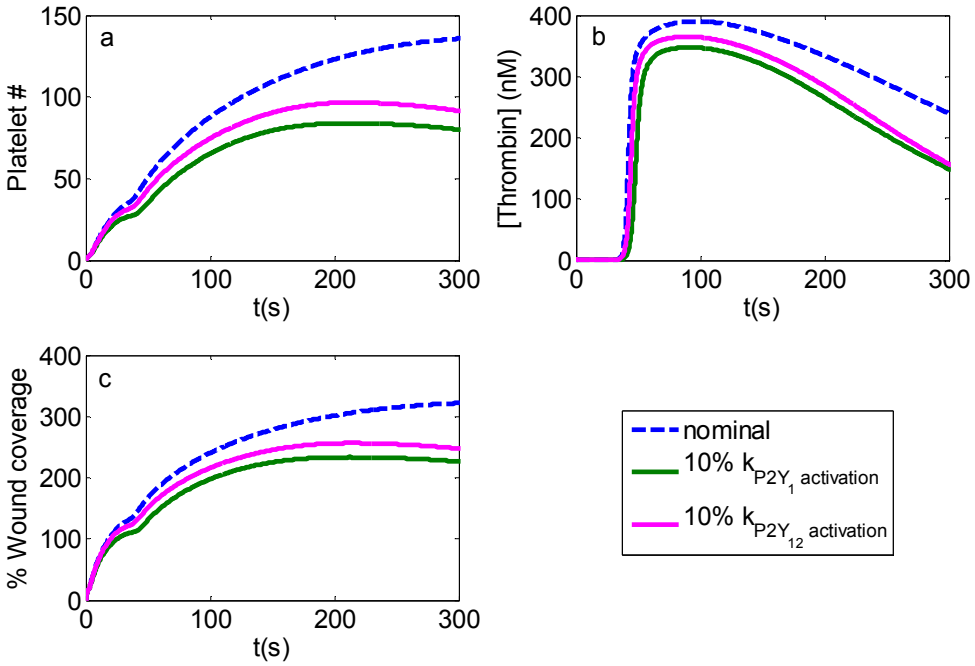

Figure 4.8. Differential effect of inhibition of ADP receptors on the system response to a wound size of 100 μm^2 and a shear rate of 400 s^{-1}. (a) platelet aggregation; (b) thrombin concentration profile; (c) percentage ratio of covered wound area to the initial wound size.

4.5.2.4 Inhibition of TxA2 Synthesis

The most commonly prescribed medicine for reducing thrombotic risk is aspirin, which works by inhibiting TxA2 synthesis. We simulate the effect of aspirin by reducing the total amount of TxA2 each platelet can produce, Q_{TxA2}, to 10% of the nominal value, while keeping the wound size at 100 μm^2 and the shear rate at 400 s^{-1}. The resulting profiles are shown in Figure 4.9. It can be seen that TxA2 effectively reduces platelet aggregation and thrombin production, as well as wound coverage.

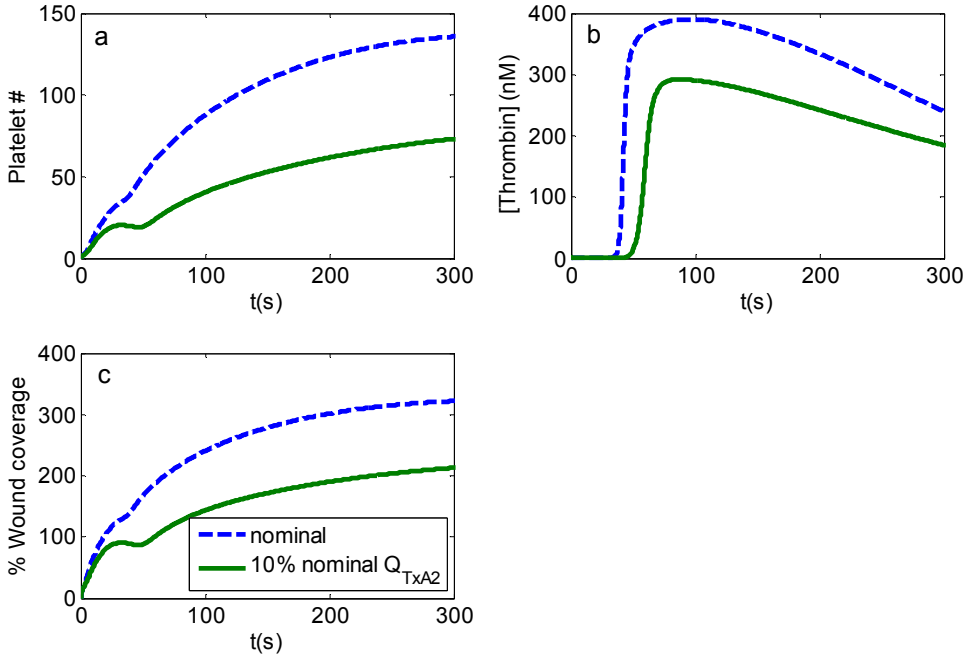

Figure 4.9. Effect of inhibition of TxA2 synthesis in response to a wound size of 100 μm^2 and a shear rate of 400 s^{-1}. (a) platelet aggregation; (b) thrombin concentration profile; (c) percentage ratio of covered wound area to the initial wound size.

4.6 Model Analyses

We perform systematic analyses on the comprehensive model for gaining insight into the complete process of hemostasis. Modular sensitivity analysis is performed to understand how sensitive the system is to changes in the modules that our comprehensive model is built on. We then investigate the effect of interaction strength to see which interaction is the most important in thrombin production.

4.6.1 Modular Sensitivity Analysis

In the following sections, we investigate the system using the engineering control system structure the model is based on, and study how a change, whether

positive or negative, in a particular control system component would affect the overall system response. For example, what happens if the sensor is overresponsive? In an engineering setting, this would mean that the sensor is giving a signal that is stronger than it should actually be, thereby making the controller generating an action stronger than it should have. In the physiological setting, this would be translated to a pathological condition associated with the components in the overresponsive sensor. In the case of primary hemostasis sensor, this would mean that the amount of collagen fiber per unit volume, or the collagen density, is higher than the normal healthy state, or an abnormal generation of collagen fibers from additional sources. Such event might lead to a hyperactive controller that generates a response much larger than it should. Using this approach, we will be able to understand, and possibly identify, the most significant component in the entire system.

4.6.1.1 Controlled Process

The first component we look into is the controlled process, which is composed of vessel characteristics, the flow condition, and an output being the thickness of the exposed subendothelium that triggers primary and secondary hemostasis. The thickness of the exposed subendothelium is either increased or decreased by 10% using a gain block in the Simulink model and eight dynamic profiles, shown in Fig. 4.10, are examined: (a) number of activated platelet in the platelet aggregate, (b) thrombin concentration [thrombin], (c) ADP concentration from collogen-bound platelets [ADP_{col}], (d) ADP concentration from secondary platelets [ADP_{sec}], (e) TxA2 concentration from collagen-bound platelets [$TxA2_{col}$], (f) TxA2 concentration from secondary platelets [$TxA2_{sec}$], (g) bleeding rate, (h) fibrin dimer concentration [$(fbn_2)_2$].

It can be readily seen in Figure 4.10a that the number of activated platelets is affected the most, which is expected. A thicker subendothelium translates into a thicker collagen-containing layer that is capable of activating more platelets and eventually leads to increased platelet aggregation and a larger thrombus. Since the primary goal of hemostasis is to minimize blood loss, a focused examination of the profiles is taken between 44 and 46 seconds, where bleeding comes to a complete stop, as shown in Figure 4.11g. Note in Figures 4.11b, 4.11c, 4.11e, 4.11h that an increase in the controlled process output leads to a decrease in the profiles, opposite to what is expected. Note also in Figure 4.11g that a decrease in the output of the controlled process leads to a decrease in the bleeding time. Although this behavior is not expected, it can be explained by the profiles in Figure 4.11h, where the fibrin dimer concentration is increased as a result of the reduced controlled process output, making the thrombus becomes impermeable to blood sooner.

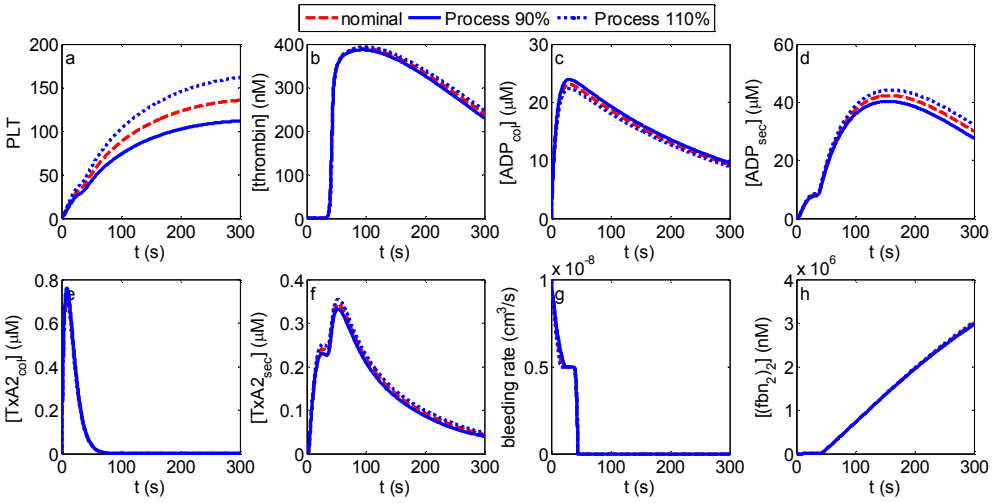

Figure 4.10. Dynamic system responses to ±10% of the controlled process. (a) number of activated platelets, (b) [thrombin], (c) [ADP_{col}], (d) [ADP_{sec}], (e) [$TxA2_{col}$], (f) [$TxA2_{sec}$], (g) bleeding rate, (h) fibrin dimer

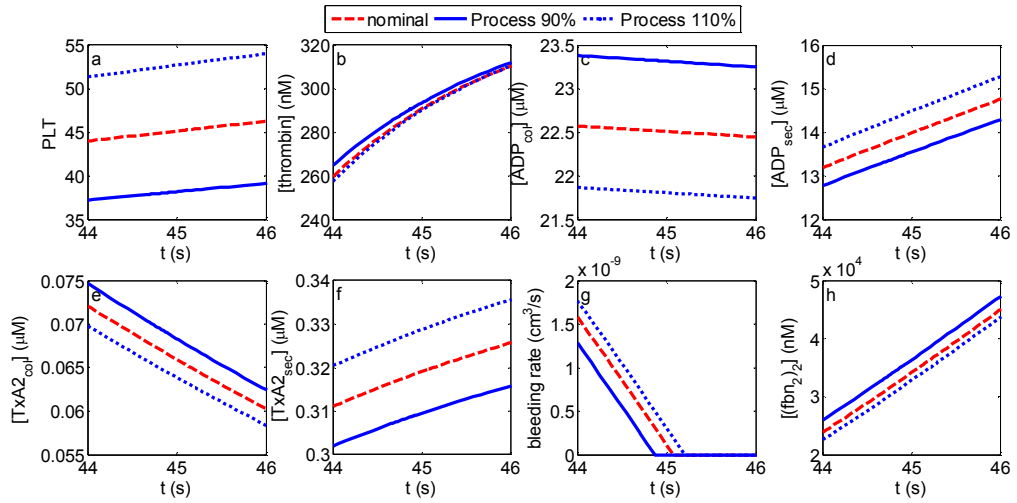

Figure 4.11. Focused dynamic system responses to ±10% of the controlled process. (a) number of activated platelets, (b) [thrombin], (c) [ADP_{col}], (d) [ADP_{sec}], (e) [$TxA2_{col}$], (f) [$TxA2_{sec}$], (g) bleeding rate, (h) fibrin dimer concentration.

4.6.1.2 Primary Hemostasis Sensor

For the primary hemostsasis sensor, the output is the amount of available collagen fibers. A change in the output, as explained in the previous section, could mean a change in the collagen density or a result of additional source of collagen production in the subendothelium. Similar to what is carried out for the controlled process, the output is increased or decreased by 10% and the eight dynamic profiles are examined, as shown in Figures 4.12 and 4.13. The number of activated platelets ADP relseased by secondary platelets are affected the most (Figures 4.12a and 4.12d). On a closer look in Figures 4.13, only Figures 4.13c and 4.13e show a behavior opposite to what is expected, where ADP and TxA2 released by collagen-bound platelet are not increased in response to an increased amount of collagen fibers.

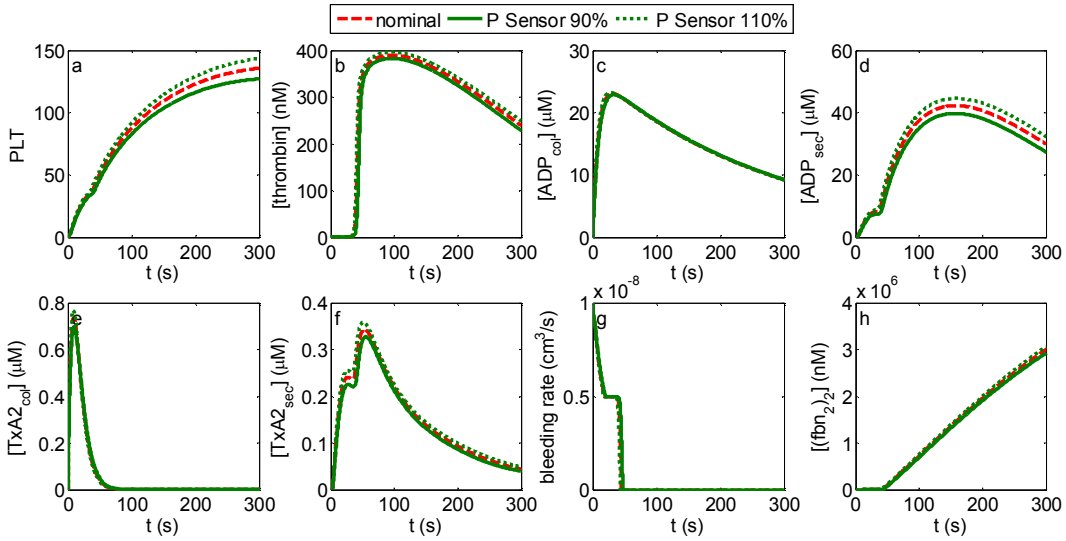

Figure 4.12. Dynamic system responses to ±10% of the primary hemostasis sensor. (a) number of activated platelets, (b) [thrombin], (c) [ADP_{col}], (d) [ADP_{sec}], (e) [$TxA2_{col}$], (f) [$TxA2_{sec}$], (g) bleeding rate, (h) fibrin dimer concentration.

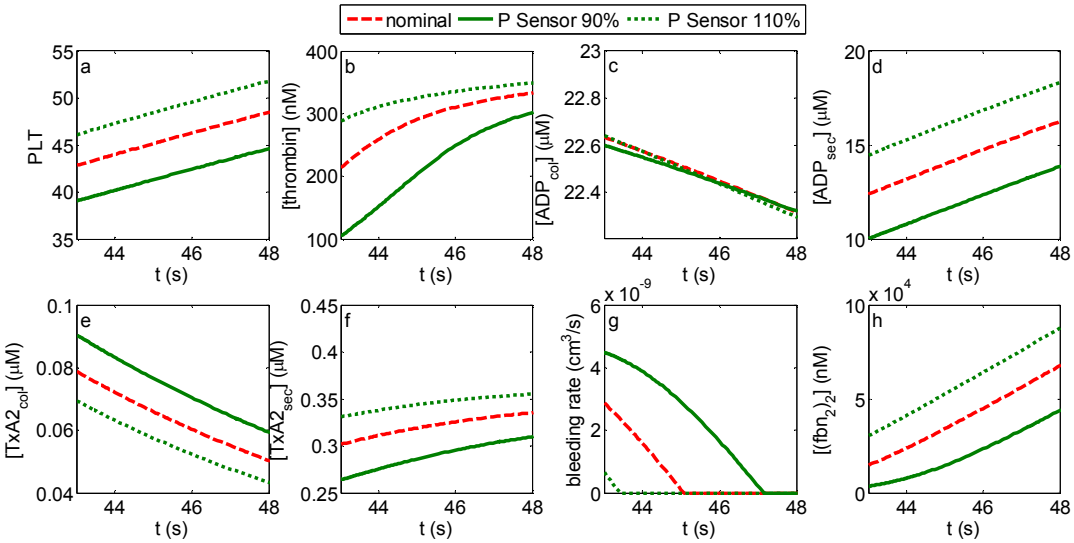

Figure 4.13. Focused dynamic system responses to ±10% of the primary hemostasis sensor. (a) number of activated platelets, (b) [thrombin], (c) [ADP_{col}], (d) [ADP_{sec}], (e) [$TxA2_{col}$], (f) [$TxA2_{sec}$], (g) bleeding rate, (h) fibrin dimer concentration.

4.6.1.3 Primary Hemostasis Controller

There are two outputs in the primary hemostasis controller: (1) ADP and (2) TxA2 released by collagen-bound platelets that will activate and recruit additional secondary platelets. A 10% increase or decrease in the outputs in this case does not have a significant effect on the eight variables of interest, as shown in Figure 4.14. In Figures 4.14c and 4.15e, the profiles are overlapping with the nominal profiles because the profiles are the outputs of the controller before the 10% change is applied. In the other figures, it can be seen that a change in ADP_{col} has a larger effect than a change in $TxA2_{col}$, suggesting a higher sensitivity of the system to ADP_{col}.

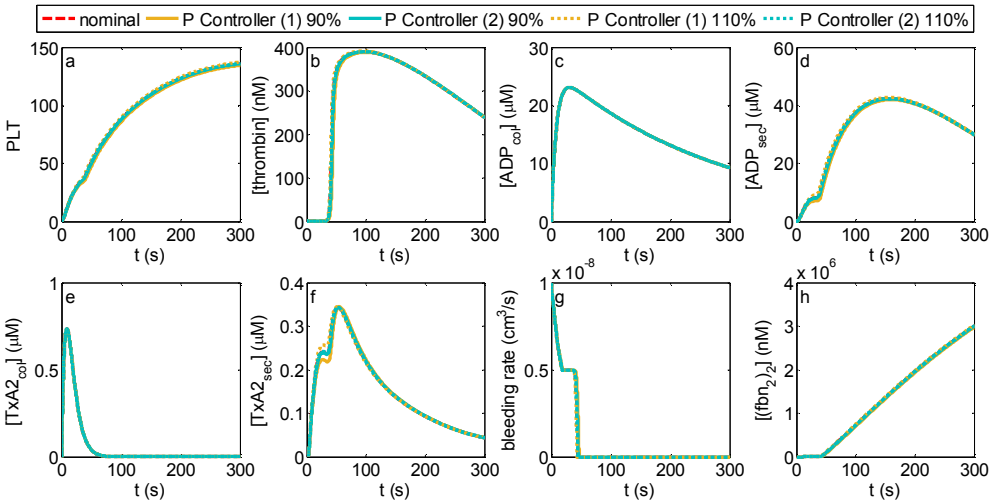

Figure 4.14. Dynamic system responses to ±10% of the primary hemostasis controller output (1) ADP_{col} and output (2) $TxA2_{col}$. (a) number of activated platelets, (b) [thrombin], (c) $[ADP_{col}]$, (d) $[ADP_{sec}]$, (e) $[TxA2_{col}]$, (f) $[TxA2_{sec}]$, (g) bleeding rate, (h) fibrin dimer concentration.

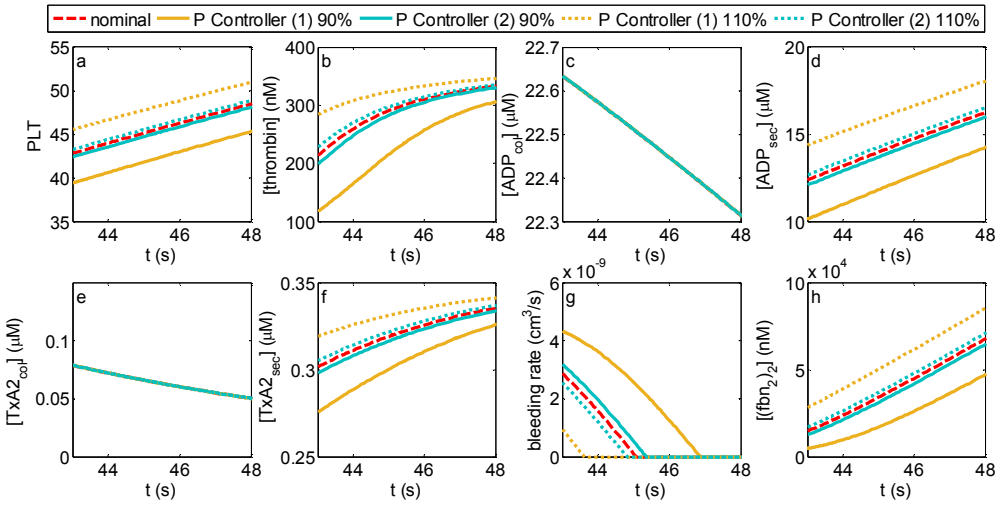

Figure 4.15. Focused dynamic system responses to ±10% of the primary hemostasis controller output (1) ADP_{col} and output (2) $TxA2_{col}$. (a) number of activated platelets, (b) [thrombin], (c) [ADP_{col}], (d) [ADP_{sec}], (e) [$TxA2_{col}$], (f) [$TxA2_{sec}$], (g) bleeding rate, (h) fibrin dimer concentration.

4.6.1.4 Primary Hemostasis Actuator

For the primary hemostasis actuator, the output is the area covered by the platelet aggregate, which is directly proportional to the number of activated platelets. A change in the output of the primary hemostasis actuator could indicate a physiological change in platelet activity. For example, if platelets are hyperactive, as observed in patients with diabetes, platelet aggregation could be increased, resulting in increased thrombotic risk. A 10% increase or decrease in the area covered does not cause any obvious change in the eight profiles investigated (Figure 4.16), even the bleeding time, which is expected to reduce with an increased area covered by the aggregate. Figure 4.17g shows a small effect of the changes on bleeding rate at an early period of simulation. Even though an increased wound coverage with a 10% increase of the primary hemostasis output causes a reduced bleeding rate, without the

help of fibrin (Figures 4.16h and 4.17h) to make the aggregate impermeable to blood, bleeding is not stopped sooner.

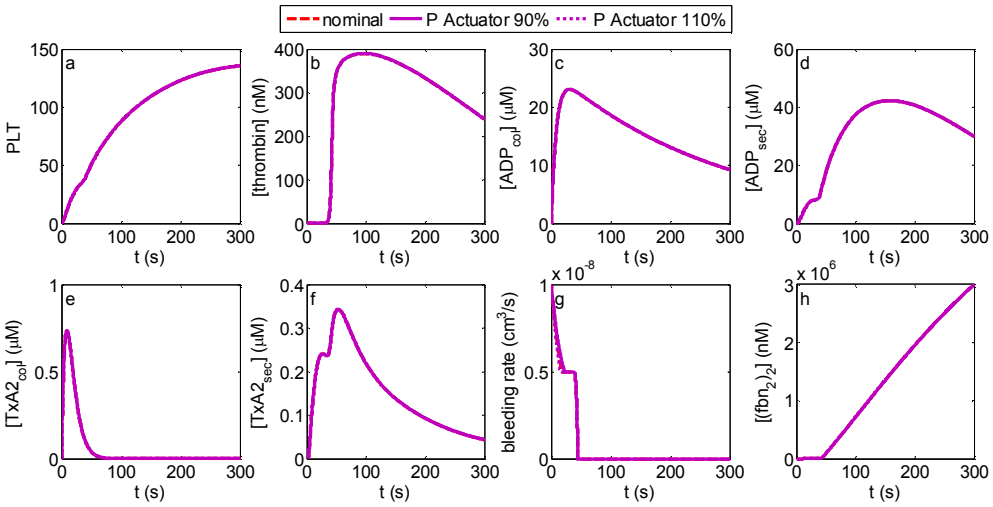

Figure 4.16. Dynamic system responses to ±10% of the primary hemostasis actuator. (a) number of activated platelets, (b) [thrombin], (c) [ADP_{col}], (d) [ADP_{sec}], (e) [$TxA2_{col}$], (f) [$TxA2_{sec}$], (g) bleeding rate, (h) fibrin dimer concentration.

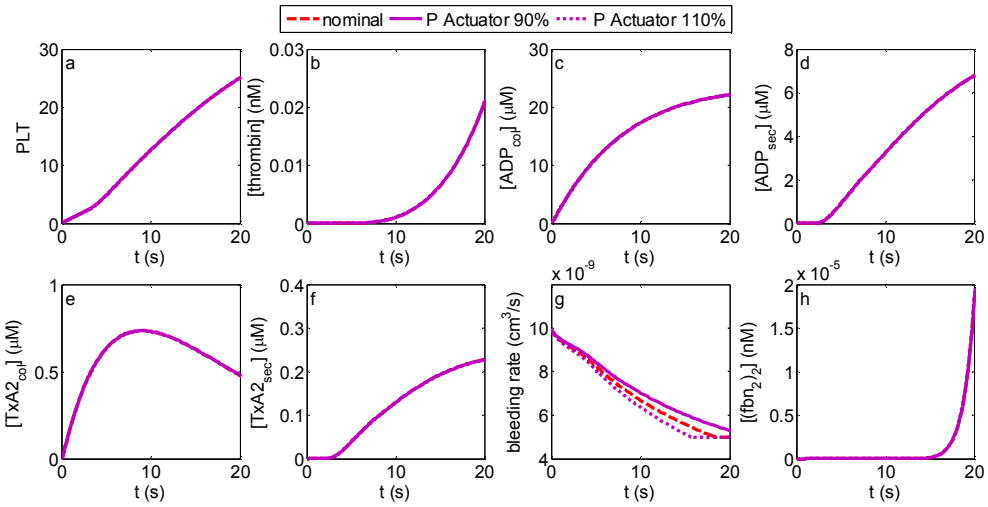

Figure 4.17. Focused dynamic system responses to ±10% of the primary hemostasis actuator. (a) number of activated platelets, (b) [thrombin], (c) [ADP_{col}], (d) [ADP_{sec}], (e) [$TxA2_{col}$], (f) [$TxA2_{sec}$], (g) bleeding rate, (h) fibrin dimer concentration.

4.6.1.5 Secondary Hemostasis Sensor

For the secondary hemostasis sensor, the output is the thickness of the TF-containing layer, which can vary among different sizes of blood vessels. The thickness in the comprehensive model is increased or decreased by 10% and the resulting profiles, shown in Figure 4.18, do not have obvious changes compared to the nominal profiles. The profiles in Figure 4.19 are perplexing. An increase in the TF-containing thickness, which is expected to generate a larger hemostatic response, slightly increases the bleeding time (Figure 4.19g) and reduces the platelet aggregation profile (Figure 4.19a), the thrombin concentration profile (Figure 4.19b), the profiles of ADP and TxA2 released from secondary platelets (Figure 4.19d and Figure 4.19f), and the fibrin dimer concentration profile (Figure 4.19h). This could be a result of a time delay. A thicker TF-containing layer could make the TF take up more coagulation factors, causing slightly diluted concentrations of coagulation factors and leading to a

slightly delayed thrombin production that affects everything affected by thrombin concentration.

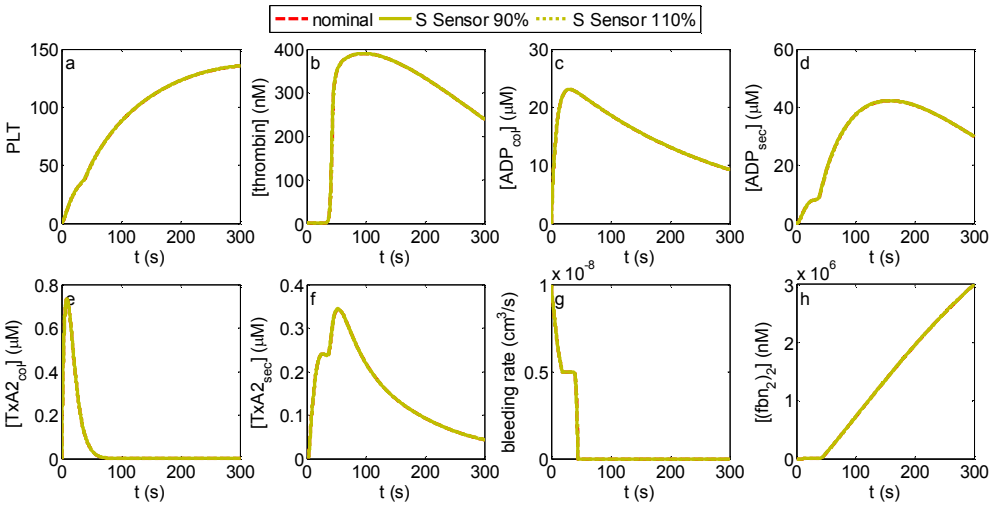

Figure 4.18. Dynamic system responses to ±10% of the secondary hemostasis sensor. (a) number of activated platelets, (b) [thrombin], (c) [ADP_{col}], (d) [ADP_{sec}], (e) [$TxA2_{col}$], (f) [$TxA2_{sec}$], (g) bleeding rate, (h) fibrin dimer concentration.

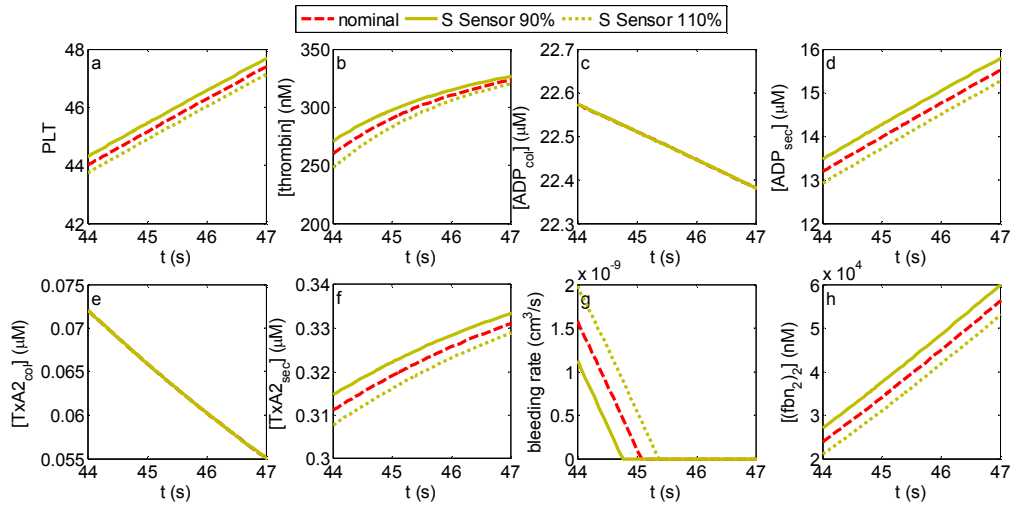

Figure 4.19. Focused dynamic system responses to ±10% of the secondary hemostasis sensor. (a) number of activated platelets, (b) [thrombin], (c) [ADP_{col}], (d) [ADP_{sec}], (e) [$TxA2_{col}$], (f) [$TxA2_{sec}$], (g) bleeding rate, (h) fibrin dimer concentration.

4.6.1.6 Secondary Hemostsasis Controller

The output of the primary hemostasis controller is the TF:FVIIa concentration. Even though a 10% increase or descrease does not lead to apparent effects on the eight variables of interest (Figure 4.20), a closer look on the profiles demonstrate expected trends (Figure 4.21).

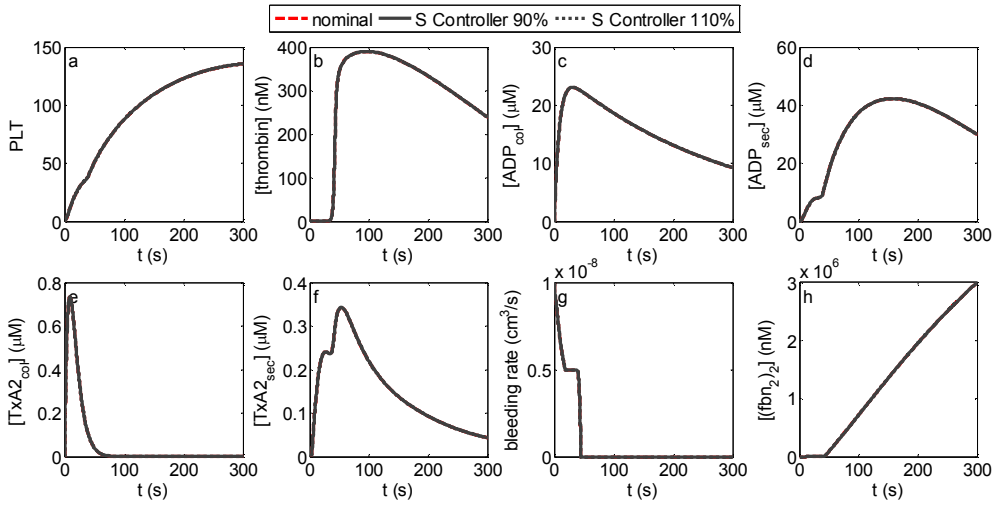

Figure 4.20. Dynamic system responses to ±10% of the secondary hemostasis controller. (a) number of activated platelets, (b) [thrombin], (c) [ADP_{col}], (d) [ADP_{sec}], (e) [$TxA2_{col}$], (f) [$TxA2_{sec}$], (g) bleeding rate, (h) fibrin dimer concentration.

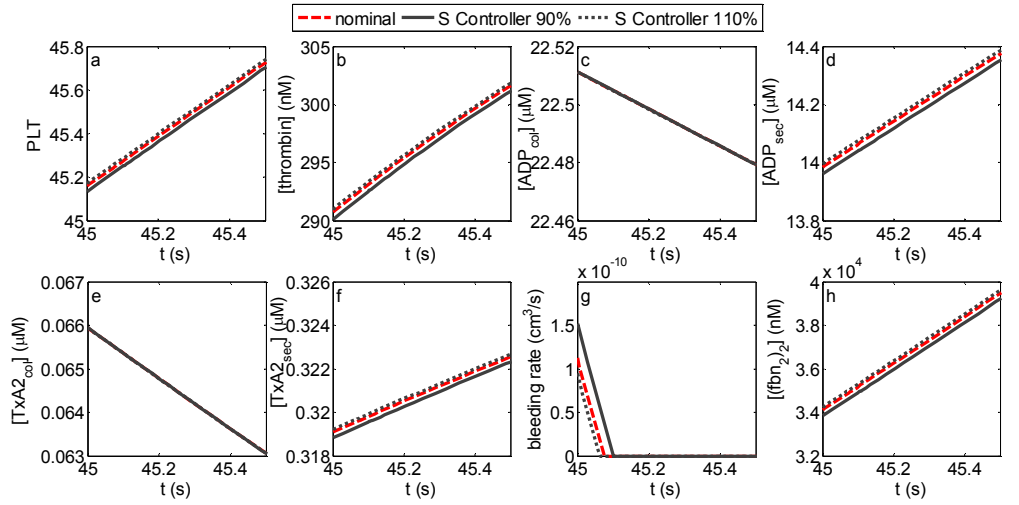

Figure 4.21. Focused dynamic system responses to ±10% of the secondary hemostasis controller. (a) number of activated platelets, (b) [thrombin], (c) [ADP_{col}], (d) [ADP_{sec}], (e) [$TxA2_{col}$], (f) [$TxA2_{sec}$], (g) bleeding rate, (h) fibrin dimer concentration.

4.6.1.7 Secondary Hemostasis Actuator

For the secondary hemostasis actuator, the output is the concentration of the fibrin monomer, which polymerizes and strengthens the platelet aggregate. As expected, a 10% increase in the fibrin monomer concentration leads to an increased fibrin dimer concentration (Figure 4.22h and Figure 4.23h) and a reduced bleeding time (Figure 4.23g).

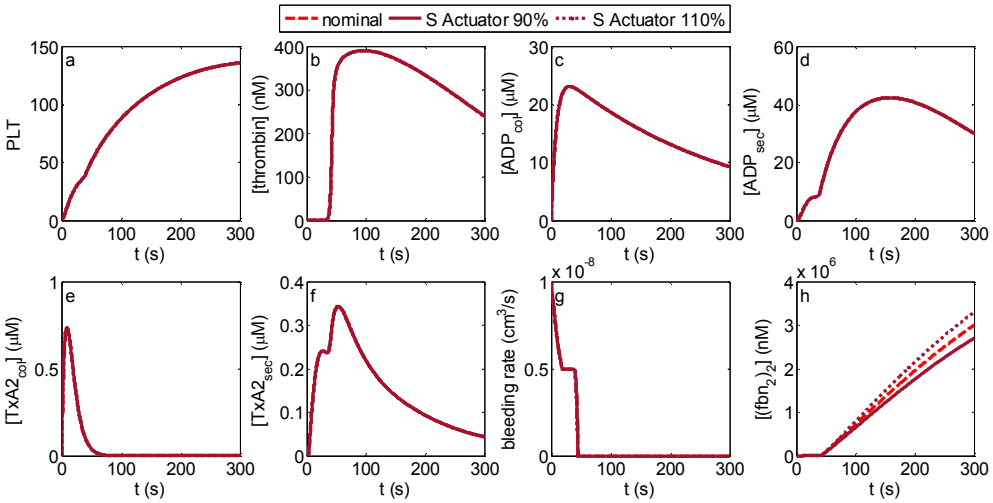

Figure 4.22. Dynamic system responses to ±10% of the secondary hemostasis actuator. (a) number of activated platelets, (b) [thrombin], (c) [ADP_{col}], (d) [ADP_{sec}], (e) [$TxA2_{col}$], (f) [$TxA2_{sec}$], (g) bleeding rate, (h) fibrin dimer concentration.

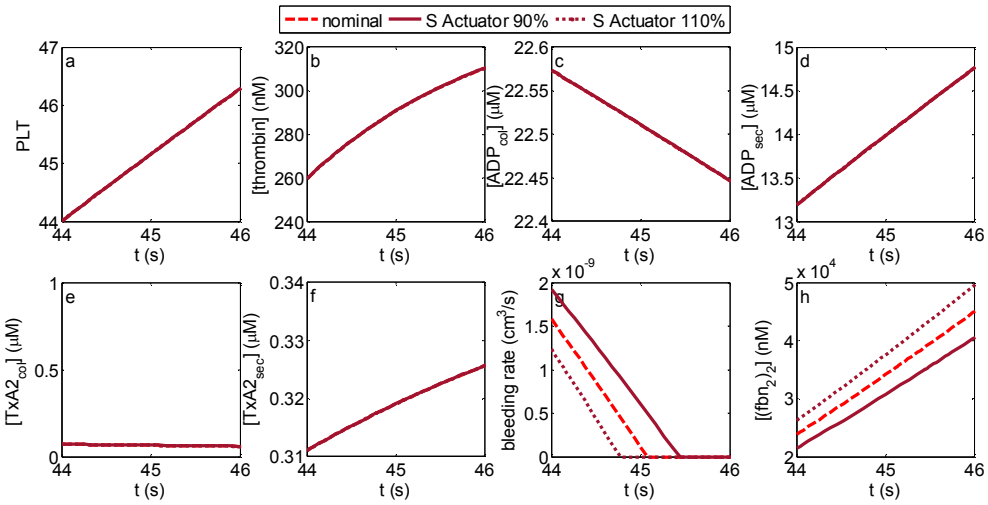

Figure 4.23. Focused dynamic system responses to ±10% of the secondary hemostasis actuator. (a) number of activated platelets, (b) [thrombin], (c) [ADP_{col}], (d) [ADP_{sec}], (e) [$TxA2_{col}$], (f) [$TxA2_{sec}$], (g) bleeding rate, (h) fibrin dimer concentration.

4.6.2 Effect of Interaction Strength between Primary and Secondary Hemostasis

While the modular sensitivity analysis provides us with the information about the importance of each module, the roles of the interactions that form important positive feedback loops are not directly addressed. In this section, we investigate how the interaction strength affects thrombin production. Three major interactions, (i) number of activated platelets, (ii) FV released by platelets, and (iii) thrombin produced from secondary hemostasis, are investigated. As explained in section 4.4.5, a gain block is imposed on each of the three interactions (G_{PLT} for number of activated platelets, G_{FV} for FV released from platelets, G_{e2} for thrombin), and 3 levels (0, 0.5, and 1) are assigned to the gains, leading to a total of 27 combinations. Other than the changes in the gains, the model is run under nominal conditions with a wound size of

100 μm^2 at a shear rate of 400 s^{-1}. Out of the 27 combinations, 5 distinct thrombin profiles are identified.

The first group identified, shown in Figure 4.24, has a high and sustained level of thrombin concentration. The combinations of the three interactions have the same values for G_{PLT} as 1. FV released from platelets does not seem to have any effect on the profile. Thrombin-induced platelet activation do not have an effect once G_{e2} is larger than 0.5. Group 2, shown in Figure 4.25, is complementary to Group 1. The interaction gain for G_{PLT} is again 1, and G_{FV} is again not having an effect on the profile. However, G_{e2} in Group 2 is all zero, meaning that no thrombin is used for inducing more platelet activation. Therefore, the difference in the profiles of Group 1 and Group 2 is caused by thrombin-induced activation, which should activate more platelets for additional membranes that provide sites for thrombin production.

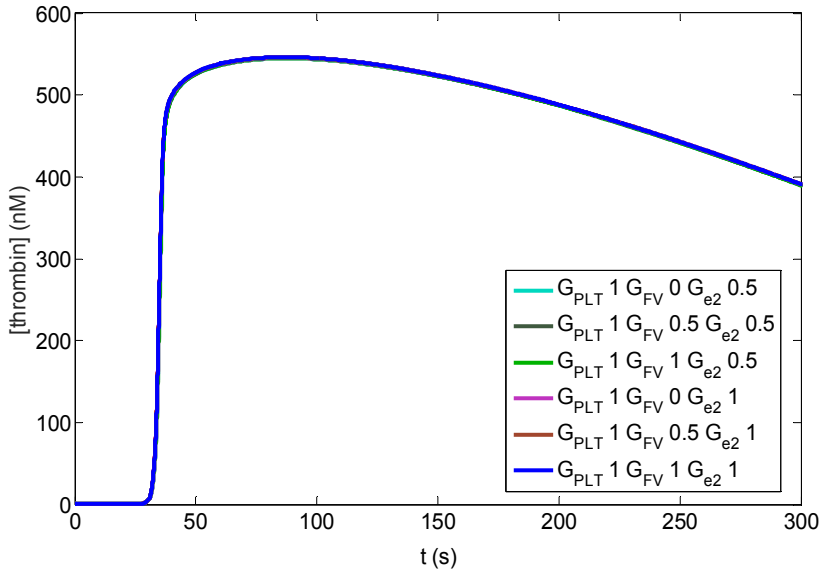

Figure 4.24. Effect of interaction gains on thrombin production. Group 1: high and sustained thrombin concentration.

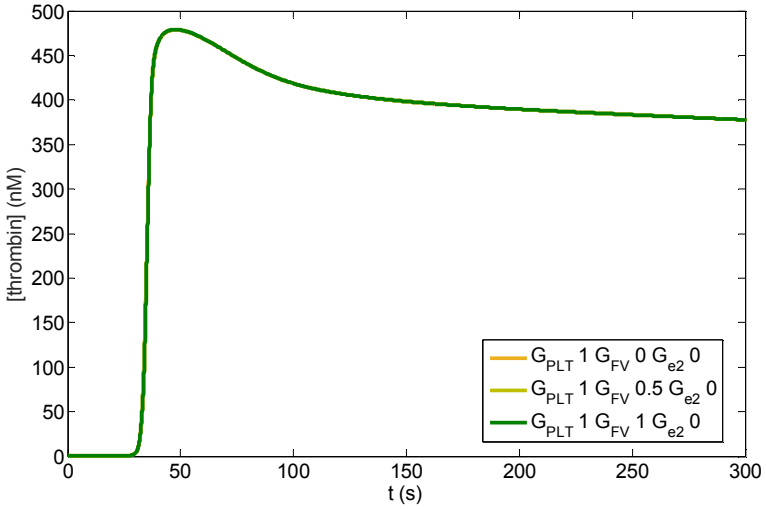

Figure 4.25. Effect of interaction gains on thrombin production. Group 2: high and sustained thrombin concentration with a peak.

The next two groups, Group 3 and Group 4, are also complementary. The interaction gains for number of activated platelets in these two groups are all 0.5. G_{FV} is still not having an effect on thrombin production. The cause of the difference between Group 3 and 4 is again G_{e2}. When G_{e2} is non-zero (Group 3, Figure 4.26), the thrombin profile goes to a slightly higher level and is more sustained. On the other hand, when is G_{e2} zero (Group 4, Figure 4.27), a peak appears and thrombin concentration comes down to a lower level.

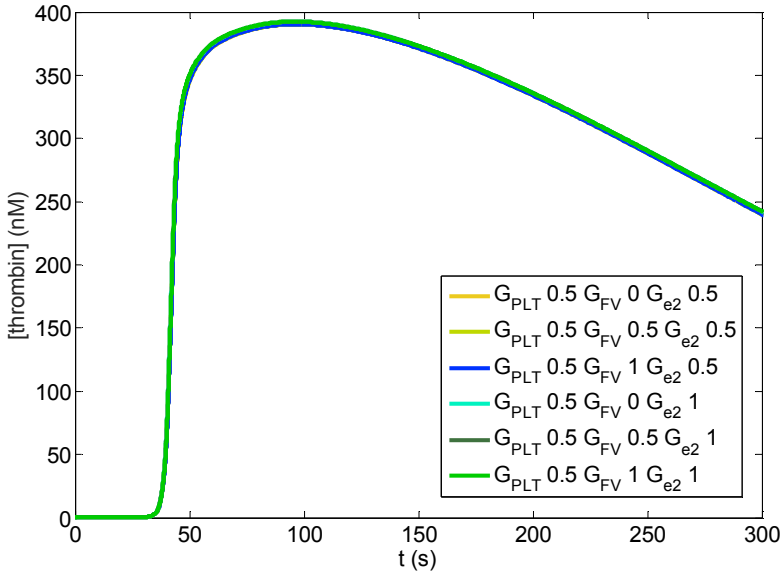

Figure 4.26. Effect of interaction gains on thrombin production. Group 3: medium and sustained thrombin concentration.

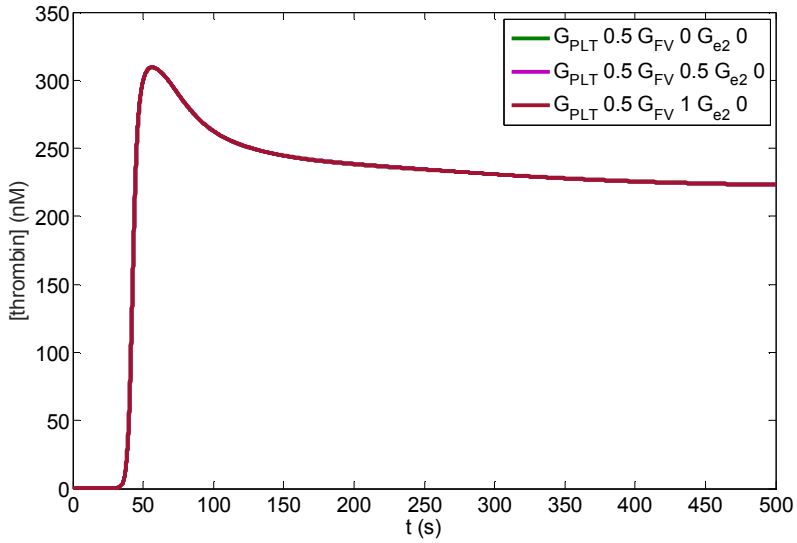

Figure 4.27. Effect of interaction gains on thrombin production. Group 4: medium thrombin concentration with a peak.

The final group, Group 5, show a limited thrombin production with a G_{PLT} of 0 regardless of the values of G_{FV} and G_{e2} (Figure 4.28). The minute amount of thrombin produced in the beginning should be a result of the extrinsic pathway of the coagulation cascade. From these 5 groups identified, it is apparent that the number of activated platelets available to the coagulation cascade is the most significant interactions for thrombin production.

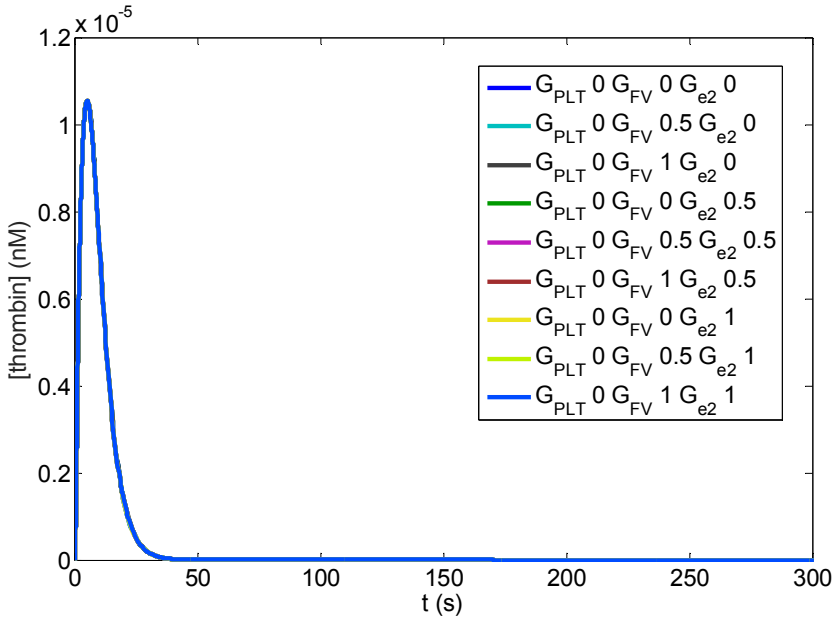

Figure 4.28. Effect of interaction gains on thrombin production. Group 5: minimum thrombin concentration.

4.7 Summary

In this chapter, we combine our primary hemostasis model with an updated secondary hemostasis model that includes up-to-date information on relevant components in secondary hemostasis. Modifications are made to the primary

hemostasis model for the interactions between primary and secondary hemostasis. The combined, comprehensive model demonstrates its capability of simulating various pathological conditions such as hemophilia A and B, and ITP. System-level analyses were performed to obtain insight into the entire hemostatic process. The analysis on the interaction strength between primary and secondary hemostasis identifies platelets as the most significant factor in thrombin production. Modular sensitivity analysis is carried out for investigating the system response with respect to changes in the corresponding control components in hemostasis. Primary hemostasis controller, comprising collagen-bound platelet activation, is shown to be the most significant module for bleeding time.

Chapter 5

RATIONAL IDENTIFICATION OF TREATMENT TARGETS FOR HEMOSTATIC DISORDERS

5.1 Model-based Treatment Target Identification

Now that we have a comprehensive mathematical representation of hemostasis that behaves in many ways in agreement with physiological observations, we use the model for identifying potential treatment strategies for hemostatic disorders. Generally, hemostatic disorders can be characterized as one of the following four categories: hyperactive primary hemostasis, deficient primary hemostasis, hyperactive secondary hemostasis, and deficient secondary hemostasis. Hyperactive primary hemostasis and hyperactive secondary hemostasis constitute the thrombophilic diseases, while deficient primary hemostasis and deficient secondary hemostasis constitute the hemophilic diseases.

In this chapter, we use the comprehensive model to study all four categories. A number of known diseases representative of each category is used as examples of how a comprehensive model of hemostasis can rationally generate potential treatment targets for hemostatic disorders. As the diseases investigated in this section have been studied for a certain period of time and already have existing treatment options, the aim of this chapter is to use the comprehensive to find potential alternative treatment targets that can be tested in the future.

5.2 Methodology

The methods used in identifying potential treatment targets are as follows: (i) create a disease scenario; (ii) choose a metric of interest in order to characterize the hemostatic function and to determine the success of treatment; (iii) calculate the metric of interest for the nominal case and the disease case; (iv) obtain normalized sensitivity coefficients under the disease condition using local parametric sensitivity analysis based on the parameters listed in Table 5.1; (v) select two parameters, with a frequency of being selected proportional to the ratio of the sensitivity coefficient to the sum of sensitivity coefficients of the same sign; (vi) use optimization routine *fminsearch* in MATLAB to drive the comprehensive model to obtain, if possible, a metric of interest that is within a desired range.

Table 5.1. List of parameters in the comprehensive model that are used for parametric sensitivity analysis and for treatment target identification.

Parameter index	Notation	Parameter index	Notation	Parameter index	Notation
1	$k_{1\text{-}1}$	71	k_2^{off}	141	k_{16}^{cat}
2	$n_{1\text{-}1}$	72	k_{2e}^{off}	142	k_{17}^{cat}
3	$a_{1\text{-}1}$	73	k_3^-	143	N_{10}^{pl}
4	$k_{1\text{-}4}$	74	k_3^{cat}	144	N_5^{pl}
5	$k_{1\text{-}2}$	75	k_3^+	145	N_8^{pl}
6	$n_{1\text{-}2}$	76	k_{12}^{cat}	146	N_9^{pl}
7	$a_{1\text{-}2}$	77	k_{12}^-	147	N_2^{pl}
8	$a_{1\text{-}3}$	78	k_{12}^+	148	N_{9*}^{pl}
9	$n_{1\text{-}3}$	79	k_{18}^-	149	k_{10}^+
10	$k_{1\text{-}5}$	80	k_{18}^{cat}	150	k_{10}^-
11	$n_{1\text{-}5}$	81	k_{14}^{cat}	151	k_{10}^{cat}
12	$a_{1\text{-}5}$	82	k_{14}^-	152	k_{11}^+
13	$k_{2\text{-}1}$	83	k_{14}^+	153	k_{11}^-
14	$n_{2\text{-}1}$	84	k_2^{in}	154	Z_2^{out}
15	$a_{2\text{-}1}$	85	k_7^+	155	Z_5^{out}

Table 5.1 continued.

16	$k_{2\text{-}3}$	86	k_7^-	156	Z_7^{out}
17	$n_{2\text{-}2}$	87	k_7^{cat}	157	E_7^{out}
18	$a_{2\text{-}2}$	88	k_{13}^{cat}	158	Z_8^{out}
19	$k_{2\text{-}4}$	89	k_{13}^-	159	Z_9^{out}
20	$n_{2\text{-}4}$	90	k_{13}^+	160	Z_{10}^{out}
21	$a_{2\text{-}4}$	91	k_{15}^{cat}	161	$TFPI^{out}$
22	$k_{3\text{-}1}$	92	k_{15}^-	162	ZPI^{out}
23	$n_{3\text{-}1}$	93	k_{15}^+	163	$ZPI{:}PZ^{out}$
24	$a_{3\text{-}1}$	94	k_5^{on}	164	k_3^b
25	$k_{3\text{-}3}$	95	k_5^{off}	165	k_3^{ub}
26	$a_{3\text{-}2}$	96	k_5^+	166	k_4^{in}
27	$n_{3\text{-}2}$	97	k_5^-	167	k_5^{in}
28	$k_{3\text{-}4}$	98	k_5^{cat}	168	k_6^{in}
29	$n_{3\text{-}4}$	99	k_{pro}^{ub}	169	k_7^{in}
30	$a_{3\text{-}4}$	100	k_{pro}^b	170	k_8^{in}
31	$k_{4\text{-}1}$	101	k_{16}^+	171	k_{11}^{cat}
32	$k_{4\text{-}2}$	102	k_{16}^-	172	k_4^b
33	$k_{5\text{-}1}$	103	k_7^{on}	173	k_4^{ub}
34	$k_{5\text{-}2}$	104	k_7^{off}	174	k_{19}^+
35	$k_{5\text{-}3}$	105	k_1^+	175	k_{19}^-
36	$k_{6\text{-}1}$	106	k_1^-	176	k_{19}^{cat}
37	$k_{6\text{-}2}$	107	k_1^{cat}	177	k_5^b
38	$k_{7\text{-}1}$	108	k_2^+	178	k_5^{ub}
39	$k_{7\text{-}2}$	109	k_2^-	179	k_9^{in}
40	$k_{8\text{-}1}$	110	k_2^{cat}	180	k_{10}^{in}
41	$k_{8\text{-}2}$	111	k_8^-	181	k_{11}^{in}
42	$k_{9\text{-}1}$	112	k_8^{cat}	182	k_2^{scat}
43	$k_{9\text{-}2}$	113	k_8^+	183	k_3^{scat}
44	$k_{9\text{-}3}$	114	k_9^-	184	k_4^{scat}
45	$k_{10\text{-}1}$	115	k_9^{cat}	185	k_5^{scat}
46	$k_{10\text{-}2}$	116	k_9^+	186	k_6^{scat}
47	$n_{10\text{-}1}$	117	k_2^b	187	k_{7z}^{on}
48	$a_{10\text{-}1}$	118	k_2^{ub}	188	k_{20}^+
49	$k_{11\text{-}1}$	119	k_8^{on}	189	k_{20}^-
50	$k_{11\text{-}2}$	120	k_8^{off}	190	k_{20}^{cat}
51	$k_{11\text{-}3}$	121	k_6^+	191	k_1^{scat}

Table 5.1 continued.

52	$k_{12\text{-}1}$	122	k_6^-	192	k_{12}^{in}
53	$k_{12\text{-}2}$	123	k_6^{cat}	193	k_{21}^+
54	$k_{13\text{-}1}$	124	k_{ten}^{ub}	194	k_{21}^-
55	$k_{13\text{-}2}$	125	k_{ten}^{b}	195	k_{21}^{cat}
56	$n_{13\text{-}1}$	126	k_{17}^+	196	N_{11}^{pl}
57	$n_{13\text{-}2}$	127	k_{17}^-	197	k_{11}^{on}
58	k_{14}	128	k_9^{on}	198	k_{11}^{off}
59	ϕ_{ADP}	129	k_9^{off}	199	k_{22}^+
60	k_{15}	130	k_1^{in}	200	k_{22}^-
61	ϕ_{TxA2}	131	k_{10}^{on}	201	k_{22}^{cat}
62	k_{20}	132	k_{10}^{off}	202	k_{23}^+
63	ϕ_{FV}	133	k_1^b	203	k_{23}^-
64	k_{16}	134	k_1^{ub}	204	k_{23}^{cat}
65	a_{16}	135	k_3^{in}	205	k_{11e}^{on}
66	n_{16}	136	k_4^-	206	k_{11e}^{off}
67	k_{17}	137	k_4^+	207	k_{24}^+
68	k_{18}	138	k_4^{cat}	208	k_{24}^-
69	k_{19}	139	k_{18}^+	209	k_{24}^{cat}
70	k_2^{on}	140	k_{APC}		

5.3 Thrombophilic Diseases

5.3.1 Hyperactive Primary Hemostasis: Hyperactive Platelets

Platelet hyperactivity has been observed in patients with diabetes and other diseases [82, 83], leading to increased thrombotic risk. Although many parameters in the single platelet model can be used to represent a state of hyperactive platelets, we work on one particular case of hyperactive Gq activation as an example. The reaction rate constant for Gq activation, $k_{1\text{-}1}$, is increased by 20% (1.2X $k_{nominal}$), 50% (1.5X $k_{nominal}$), and 100% (2X $k_{nominal}$) to represent various degrees of platelet hyperactivity. The resulting profiles of platelet aggregation are shown in Figure 5.1. With a larger

wound size, more platelets are activated to join the aggregate, as expected. Increasing severity of also enhances platelet aggregation, which can be translated into an increased thrombotic risk. The case with a wound size of 100 μm^2 and a 50% increase in the rate constant is used as an example for identifying potential treatment target.

In thrombotic diseases, minimizing the bleeding time is no longer the most urgent concern. The concern is now how to limit thrombus growth. Because the number of activated platelets has a determining effect on the size of a thrombus, the average number of activated platelets over the simulation time is used as the metric for evaluating the function of hemostasis. To identify potential treatment targets, first a local parametric sensitivity analysis is performed under the disease conditions, as explained in section 5.2. The sensitivity coefficients (Figure 5.2) show that the parameters in the primary hemostasis model (parameter 1-69), are significantly more influential in the number of activated platelets, compared to the parameters in the secondary hemostasis model (parameter 70-209). Next, the comprehensive model with the disease condition is used for identifying pairs of parameters that are capable of bringing the average platelet number back to that of the nominal state. Two parameters are changed at a time instead of one to avoid driving the model to extreme conditions. Since bringing the state back to the exact value of the nominal average number of platelets is nearly impossible, a 20% overshoot is allowed. Thus, if the changes in a pair of parameters result in an average number of platelets 80-100% of the nominal condition, the pair is regarded as potential treatment targets.

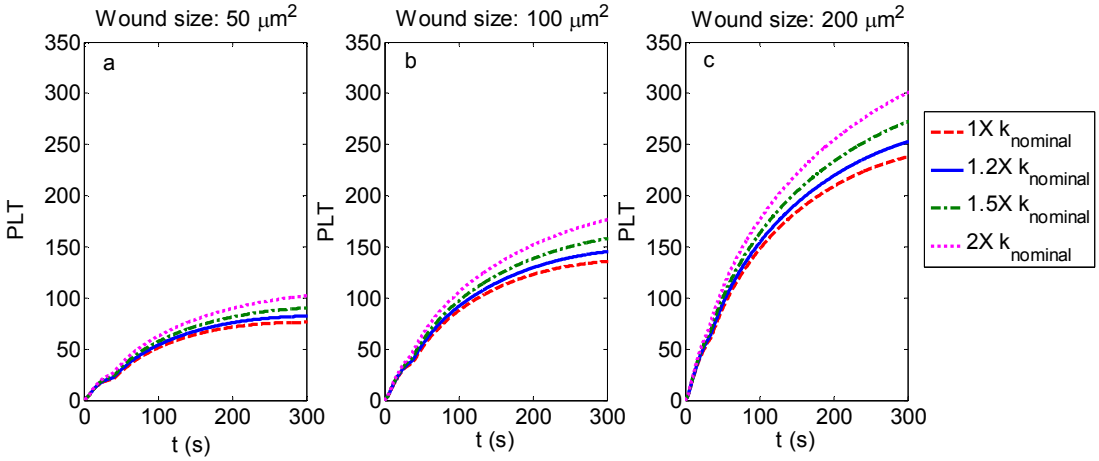

Figure 5.1. Platelet aggregation profiles in response to wound sizes of (a) 50 μm^2, (b) 100 μm^2, and (c) 200 μm^2 with various degrees of hyperactive Gq activation at a shear rate of 400 s^{-1}.

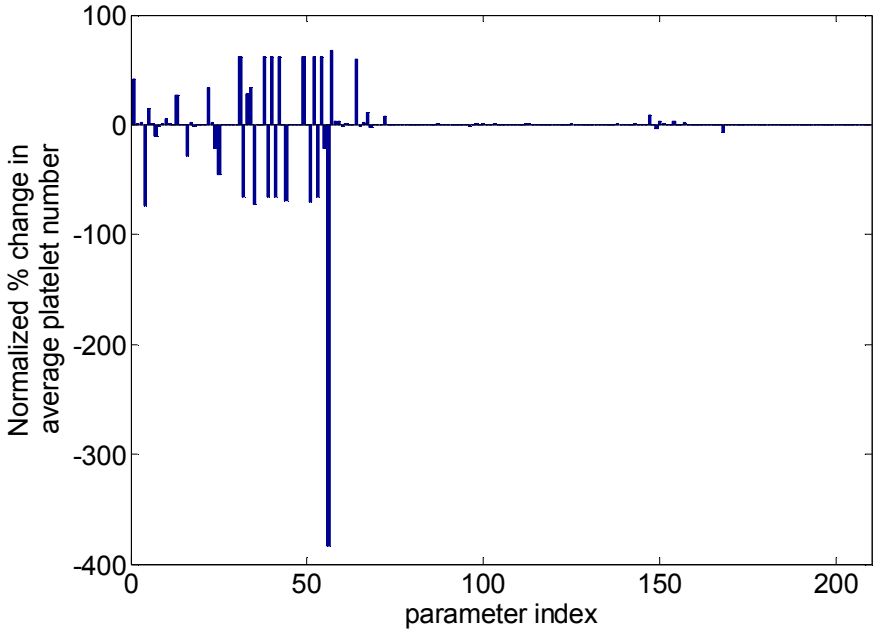

Figure 5.2. Sensitivity coefficients from local sensitivity analysis for the hyperactive Gq activation case with 1.5X $k_{nominal}$, and a wound size of 100 μm^2. A 10% decrease in the parameter values of the disease condition is applied.

Potential treatment targets that have been identified for hyperactive Gq activation are listed in Table 5.2, and the ratios of the parameter values to their original values are schematically shown in Figure 5.3. Interestingly, the list is not predominantly occupied by the parameters in the primary hemostasis model, suggesting possible synergistic effects among the individual processes. The platelet aggregation profiles using the disease condition with the treatments are shown in Figure 5.4. Two distinct groups are identified. The profiles in blue resemble the profiles of the nominal case with different gains, while the profiles in magenta show a delayed second wave of platelet aggregation. The delayed platelet aggregation should be a result of a delayed production of thrombin, as the parameters related to the magenta profiles are all from the secondary hemostasis model.

Table 5.2. List of potential treatment targets for hyperactive Gq activation.

Pair index	Parameter 1	Parameter 2	Pair index	Parameter 1	Parameter 2
a	k_1^b	$k_{3\text{-}1}$	j	k_{10}^{off}	k_{APC}
b	k_{23}^+	$k_{5\text{-}1}$	k	k_6^-	$k_{1\text{-}4}$
c	$a_{1\text{-}3}$	k_5^b	l	k_1^b	$a_{1\text{-}3}$
d	Z_9^{out}	Z_7^{out}	m	Z_2^{out}	k_5^{in}
e	$n_{1\text{-}5}$	$k_{3\text{-}1}$	n	k_6^{scat}	$k_{2\text{-}1}$
f	k_{16}	k_{11}^{off}	o	k_6^-	$k_{2\text{-}3}$
g	k_{16}	k_{11}^{off}	p	$k_{13\text{-}1}$	E_7^{out}
h	$k_{12\text{-}2}$	k_7^{in}	q	k_{20}	$k_{4\text{-}1}$
i	k_5^{off}	k_{22}^{cat}	r	k_4^{in}	k_3^b

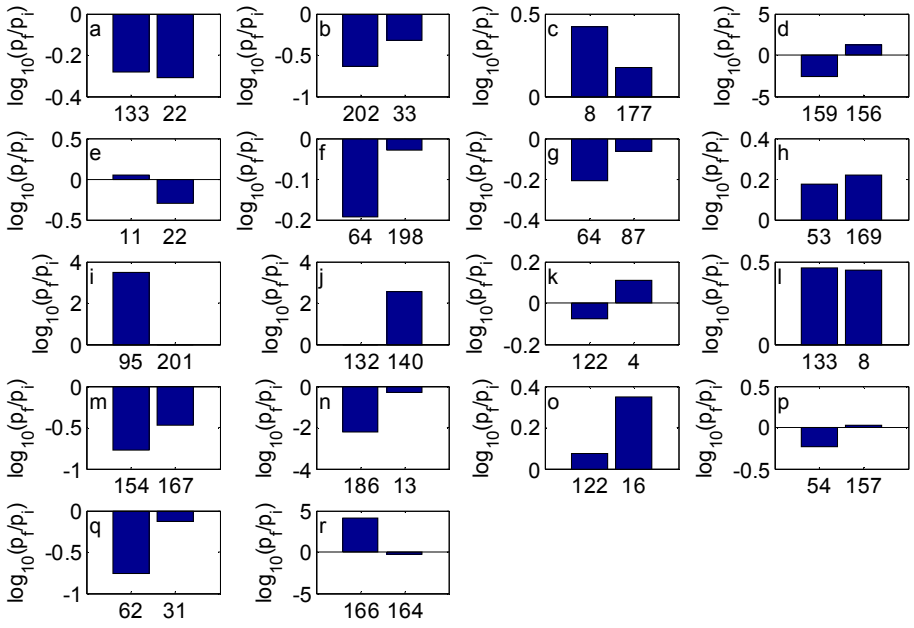

Figure 5.3. Ratio of parameter values used for treating hyperactive Gq activation to corresponding original values. The figure number (a-r) corresponds to the pair index used in Table 5.2 and the number of each bar corresponds to the parameter index in Table 5.1.

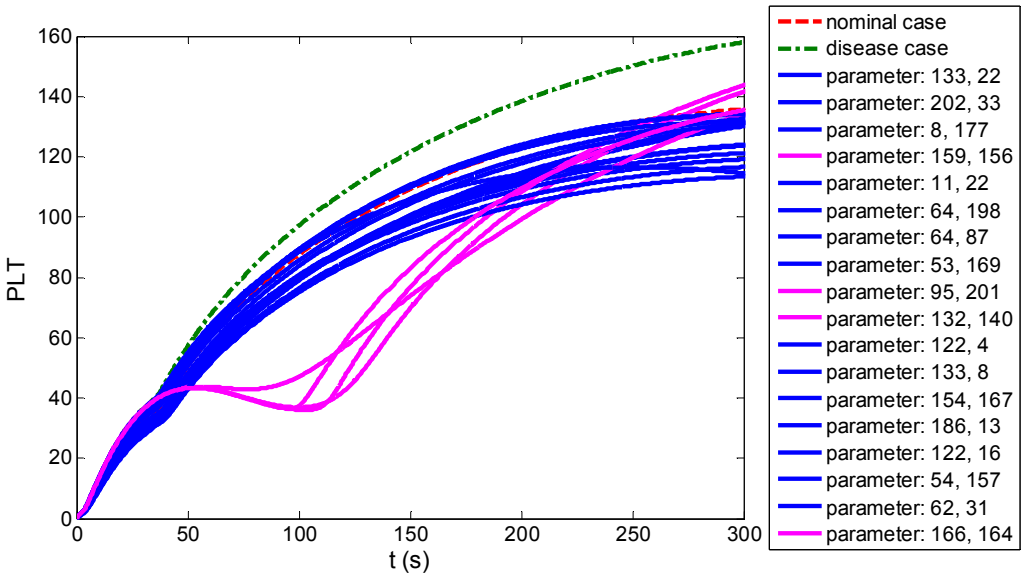

Figure 5.4. Platelet aggregation profiles of the nominal case, the hyperactive Gq activation case, and the treated cases.

5.3.2 Hyperactive Secondary Hemostasis: Antithrombin Deficiency

An increased thombotic risk can also be associated with hyperactivity in secondary hemostasis. Here we investigate the case of antithrombin (ATIII) deficiency, which affects 5 to 17 per 10,000 individuals [84]. The response to various wound sizes with three levels of ATIII deficiency is shown in Figure 5.5. The difference in the aggregation profile is not apparent in the first 300 seconds of simulation, so the simulation time is extended to 500 seconds. The indistinguishable profiles in the first 300 seconds could partially explain why venous thromboembolism (VTE) is usually associated with a hyperactive state in secondary hemostasis. After the primary task of stopping the bleeding is accomplished by hemostasis, the process needs to be regulated to limit the thrombus growth. With a deficiency in a major

regulator, thrombus growth then sustains and could eventually grow to occlude the entire blood vessel.

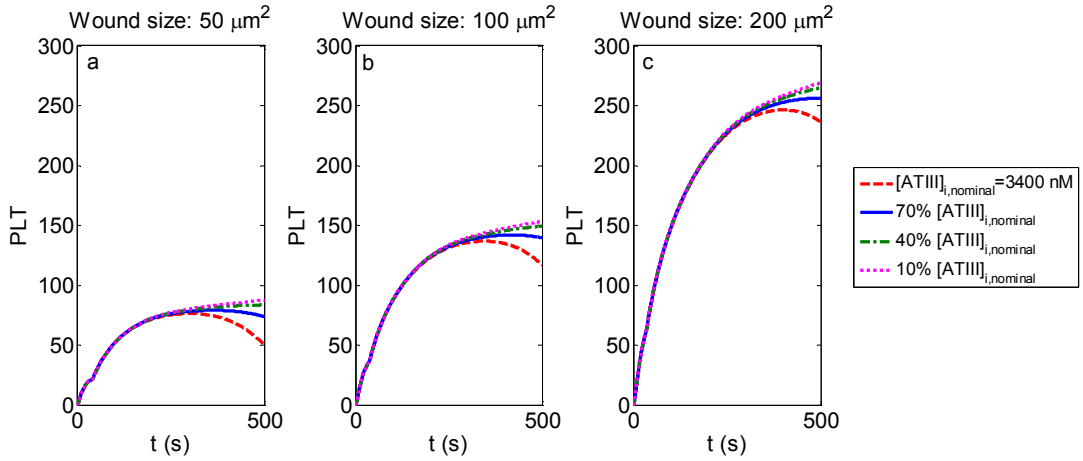

Figure 5.5. Platelet aggregation profiles in response to wound sizes of (a) 50 μm^2, (b) 100 μm^2, and (c) 200 μm^2 with various degrees of ATIII deficiency at a shear rate of 400 s^{-1}.

The disease condition used for identifying potential treatment target is a deficiency level 10% of the nominal ATIII level with a wound size of 100 μm^2 (magenta dotted line in Figure 5.5). A local parametric sensitivity analysis, shown in Figure 5.6, is first carried out. The sensitivity coefficients bear great resemblance to the sensitivity coefficients for hyperactive platelets (Figure 5.2), with the most significant parameters being in the primary hemostasis model. To identify potential treatment targets, the same procedure as that used in hyperactive platelets is applied. The pairs of potential treatment targets are summarized in Table 5.3. Note again that although the sensitivity coefficients under this disease condition take on greater

absolute values for the parameters in primary hemostasis, the identified targets, however, are mostly the parameters in secondary hemostasis (13 out of 18 identified potential targets). It is likely that in such a highly nonlinear system, the local sensitivity coefficients may vary significantly under different conditions. The ratios of the changed values to the original values are schematically shown in Figure 5.7, and the resulting profiles are shown in Figure 5.8. Two distinct types of profiles are also observed in this disease case. The profiles in blue are similar in shape to the profile with ATIII deficiency, while the profile in magenta resembles the nominal profile.

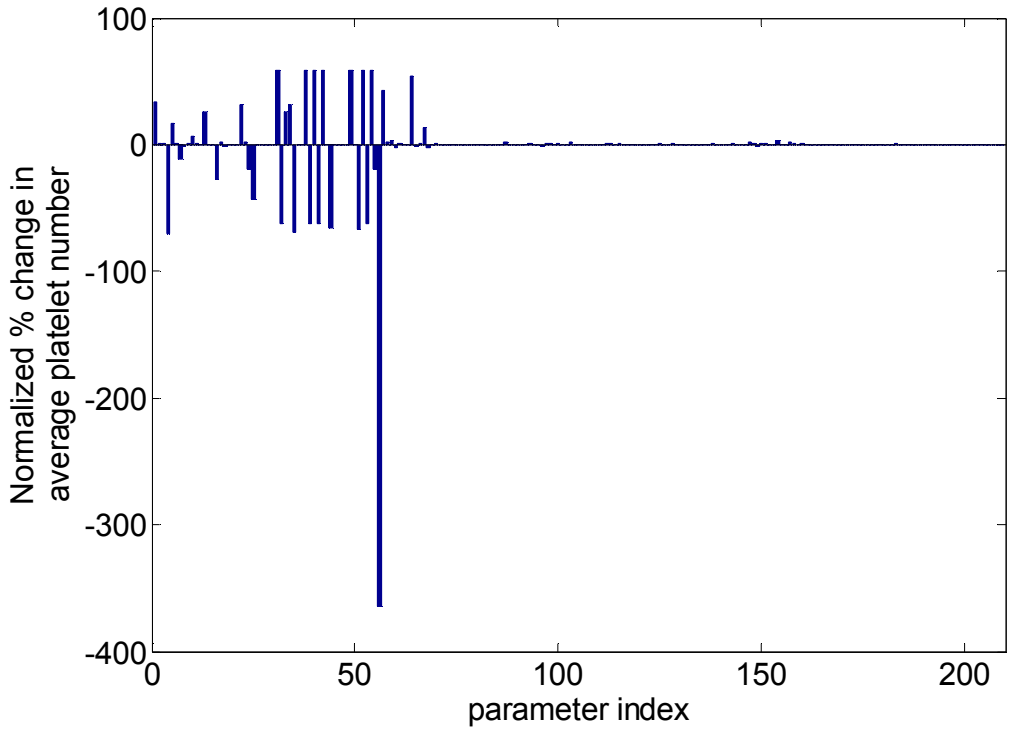

Figure 5.6. Sensitivity coefficients from local sensitivity analysis for ATIII deficiency with an initial ATIII level 10% of the nominal level, and a wound size of 100 μm^2.

Table 5.3. List of potential treatment targets for ATIII deficiency.

Pair index	Parameter 1	Parameter 2
a	k_{22}^{-}	k_{16}^{+}
b	k_{10}^{+}	Z_{8}^{out}
c	$k_{5\text{-}3}$	k_{17}^{-}
d	$a_{3\text{-}1}$	k_{22}^{cat}
e	$k_{12\text{-}1}$	k_{6}^{in}
f	N_{2}^{pl}	k_{10}^{off}
g	k_{10}^{-}	k_{11}^{in}
h	k_{pro}^{b}	$k_{1\text{-}4}$
i	$k_{4\text{-}2}$	k_{3}^{scat}

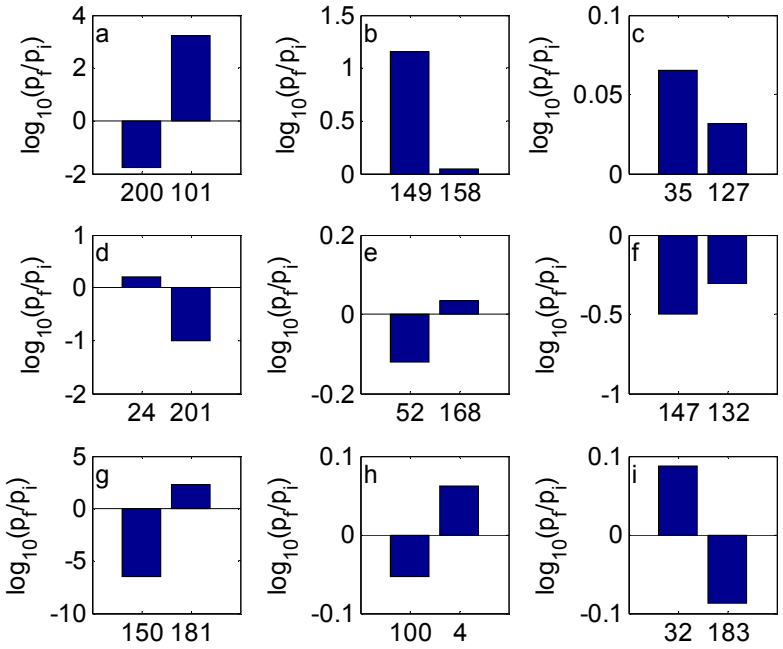

Figure 5.7. Ratio of parameter values used for treating ATIII deficiency to corresponding original values. The figure number (a-i) corresponds to the pair index used in Table 5.3 and the number of each bar corresponds to the parameter index in Table 5.1.

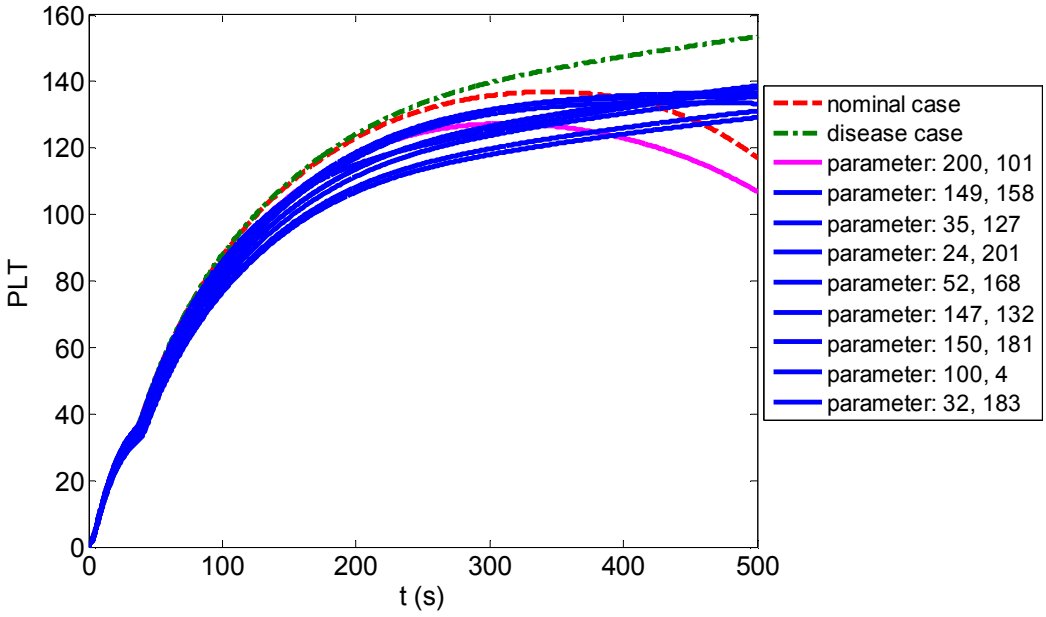

Figure 5.8. Platelet aggregation profiles of the nominal case, the ATIII deficiency case in question, and the treated cases.

5.4 Hemophilic Diseases

The comprehensive model can also be used for studying hemophilic diseases. However, opposite to thrombophilic diseases, where the major concern is to avoid an oversized thrombus, in the case of hemophilic diseases, the most urgent concern is to stop bleeding as soon as possible and minimize blood loss. Hence the bleeding time and total blood loss are the major metrics for evaluating the severity of hemophilic diseases.

5.4.1 Deficient Secondary Hemostasis: Hemophilia A

The first hemophiliic disease in question is hemophilia A, characterized by a deficiency in FVIII. Even though many forms of hemophilia A have been reported in the literature [85], hemophilia A is represented in the model using a reduced plasma

level of FVIII. Profiles of total blood loss in response to various wound sizes with different levels of FVIII are shown in Figure 5.9. The total blood loss profile flattens when bleeding is completely stopped. As expected, with the same wound size, bleeding time increases with increasing severity of hemophilia A, and a larger wound size with the same severity of hemophilia A results in more blood loss. An unexpected characteristic shown in Figure 5.9 is that as wound size increases, the bleeding time is shortened. Such behavior could be attributed to the increased platelet aggregation with a larger wound size. As more platelets are at the wound site, more platelet membranes are available to the coagulation factors, thereby reducing thrombin production initiation time and accelerating thrombin production. With an early onset of thrombin production, the concentration of fibrin dimer will also rise earlier, making the thrombus become impermeable earlier.

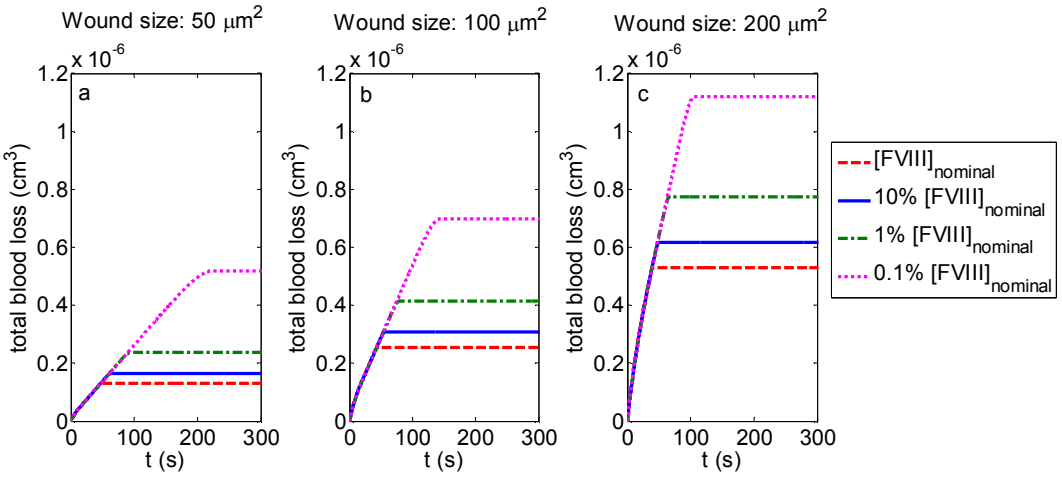

Figure 5.9. Total blood loss in response to wound sizes of (a) 50 μm^2, (b) 100 μm^2, and (c) 200 μm^2 with various degrees of hemophilia A at a shear rate of 400 s^{-1}.

The strategies used for identifying potential treatment targets for hemophilia A are similar to that for thombophilic diseases, except that the metric of interest now becomes the bleeding time. A local parametric sensitivity analysis (Figure 5.10) is performed with a disease condition of 1% nominal FVIII level and a wound size of 200 μm^2 at a shear rate of 400 s^{-1} (green dash-dotted line in Figure 5.9). Although the most significant parameters are still in primary hemostasis (parameters 1-69), many parameters in secondary hemostasis have a higher impact in hemophilia A, compared to the cases of hyperactive platelets and ATIII deficiency (Figures 5.2 and 5.6).

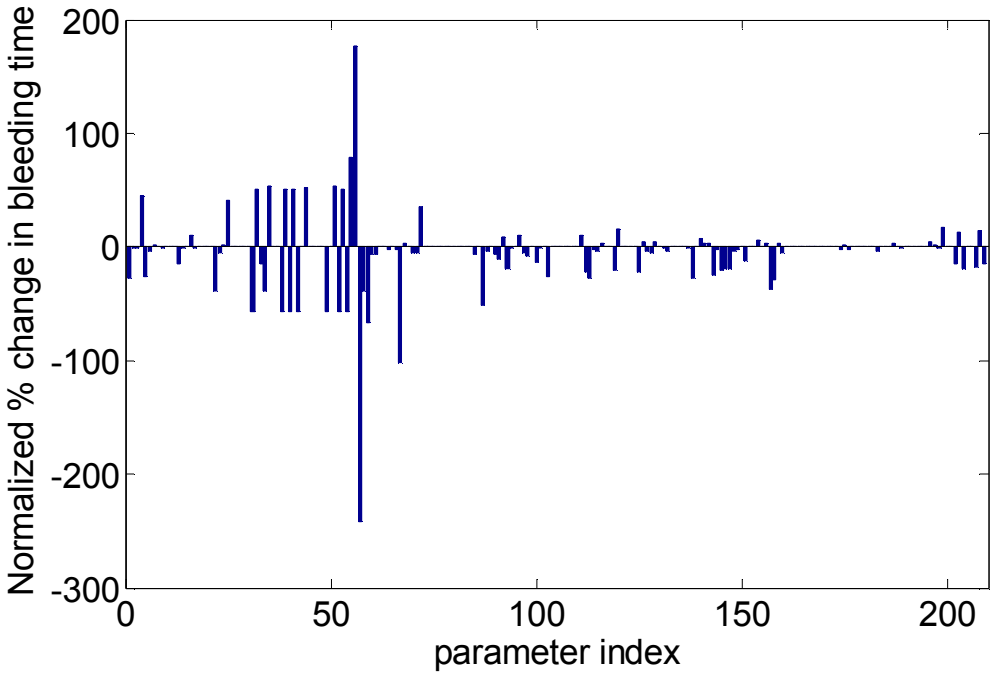

Figure 5.10. Sensitivity coefficients from local sensitivity analysis for hemophilia A with a FVIII level 1% of the nominal case and a wound size of 200 μm^2 at a shear rate of 400 s^{-1}.

Table 5.4 summarizes the potential treatment targets identified using the model and the associated changes in parameter values are shown in Figure 5.11. The bleeding rate profiles of the nominal case, the hemophilia A case, and the treated disease case using the identified treatment targets and associated parameter values are shown in Figure 5.12. Interestingly, many of the potential targets are the processes in primary hemostasis, showing again how a change in primary hemostasis can be relayed to secondary hemostasis through the interactions. One particular treatment pair to note is pair o, where the second parameter is the plasma level of FVIII. Although this is an intuitive and trivial target that has long been in clinical use for hemophilia A patients, the identification of this parameter validates our approach to finding new treatment targets.

Table 5.4. List of potential treatment targets for hemophilia A.

Pair index	Parameter 1	Parameter 2	Pair index	Parameter 1	Parameter 2
a	$k_{1\text{-}1}$	$k_{12\text{-}2}$	i	$k_{11\text{-}3}$	$k_{1\text{-}2}$
b	k_{23}^{cat}	$n_{13\text{-}2}$	j	$k_{12\text{-}2}$	k_{13}^{+}
c	k_{7}^{cat}	k_{8}^{+}	k	ϕ_{ADP}	$k_{4\text{-}1}$
d	$k_{13\text{-}1}$	$n_{13\text{-}1}$	l	$k_{12\text{-}1}$	ϕ_{ADP}
e	$n_{13\text{-}1}$	k_{5}^{+}	m	k_{15}^{cat}	$k_{8\text{-}2}$
f	k_{9}^{+}	$n_{13\text{-}1}$	n	$k_{8\text{-}1}$	N_{10}^{pl}
g	k_{24}^{+}	$n_{13\text{-}2}$	o	$k_{11\text{-}3}$	Z_{8}^{out}
h	$k_{9\text{-}3}$	$n_{13\text{-}1}$			

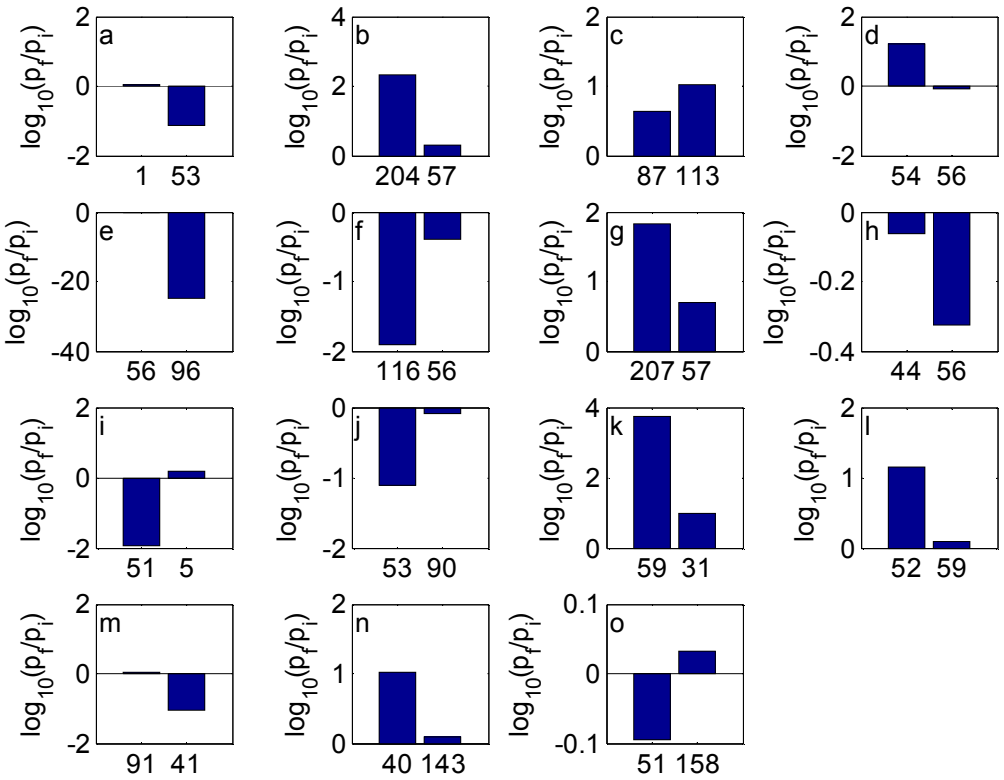

Figure 5.11. Ratio of parameter values used for treating hemophilia A to corresponding original values. The figure number (a-o) corresponds to the pair index used in Table 5.4 and the number of each bar corresponds to the parameter index in Table 5.1.

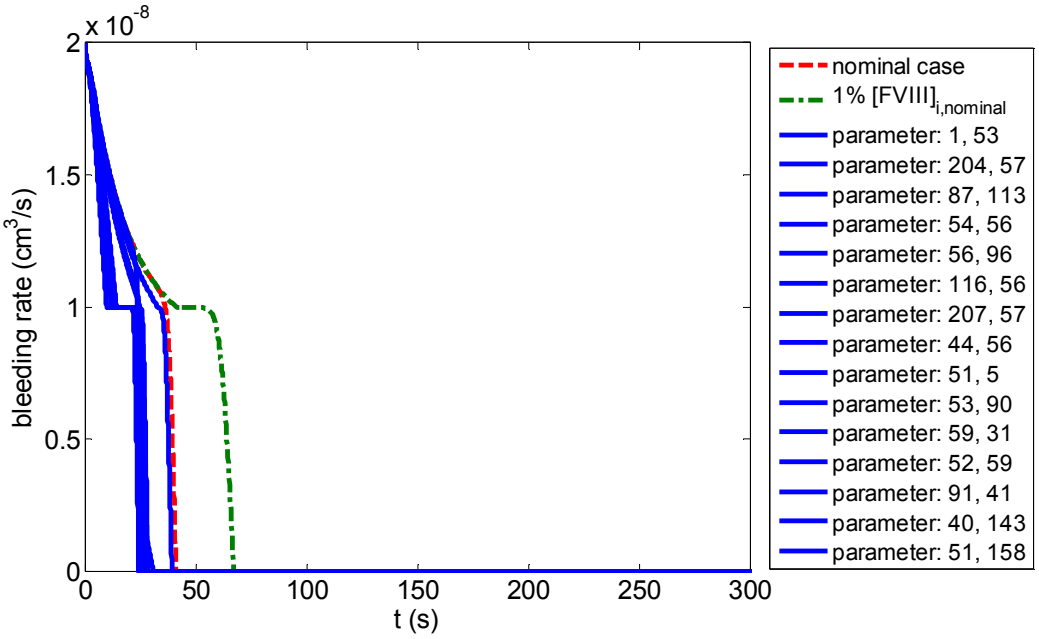

Figure 5.12. Profiles of bleeding rate for the nominal case, the hemophilia A case in question, and the treated cases using the identified targets.

5.4.2 Deficient Secondary Hemostasis: Hemophilia B

In hemophilia B, the bleeding diathesis is caused by a deficiency in FIX. Similar to FVIII, various mutations in the gene coding for FIX have been reported in the literature [86]. However, to simulate the condition of hemophilia B, the disease condition is simply represented as a reduced plasma FIX level in the comprehensive model. The profiles of blood loss in response to various wound sizes with various severities of hemophilia B are shown in Figure 5.13. The profiles are very similar to the profiles with hemophilia A, which is not unexpected since FVIIIa and FIXa comprise tenase and work together. With the same wound size, as the level of FIX decreases, the bleeding time is prolonged and total blood loss increases. An increase in wound size leads to more blood loss with the same FIX level. The bleeding time again

decreases as wound size increases, which can be explained by the abundance of platelet membranes with an increased wound size.

The sensitivity coefficients obtained using a FIX level 1% of the nominal level with a wound size of 200 μm^2 at a shear rate of 400 s^{-1} (condition of the green dash-dotted line in Figure 5.13c) are shown in Figure 5.14. The sensitivity coefficient profile resembles that for hemophilia A (Figure 5.10) but the sensitivity coefficients are generally smaller in magnitude. Potential treatment targets for the same condition identified using the comprehensive model are listed in Table 5.5. The changed values associated with the parameters and the final bleeding rates profiles are shown in Figures 5.15 and 5.16. To once more illustrate how primary and secondary hemsotasis are intertwined, the potential treatment pairs contain parameters from both primary and secondary hemostasis. Note that in treatment pair f, the second parameter is the plasma level of FVIIa. In reality, the injection of recombinant FVIIa is a clinical practice known as the bypass therapy for hemophilia patients who have developed inhibitors or antibodies against FVIII and FIX [87]. Without such prior knowledge used in the treatment target identification process, our model still identifies such potential target. This demonstrates the potential of our comprehensive model in identifying new treatment targets for hemophilic diseases.

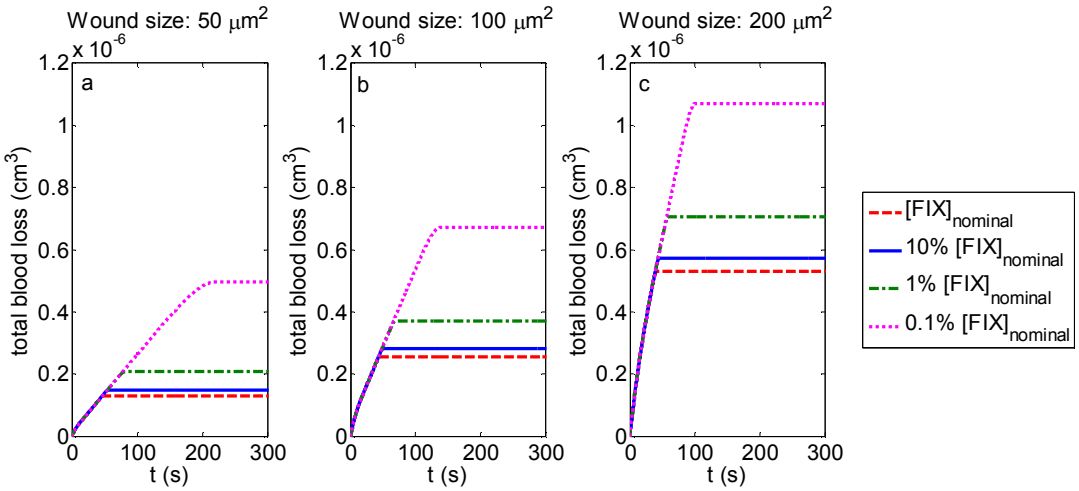

Figure 5.13. Total blood loss in response to wound sizes of (a) 50 μm^2, (b) 100 μm^2, and (c) 200 μm^2 with various degrees of hemophilia B at a shear rate of 400 s^{-1}.

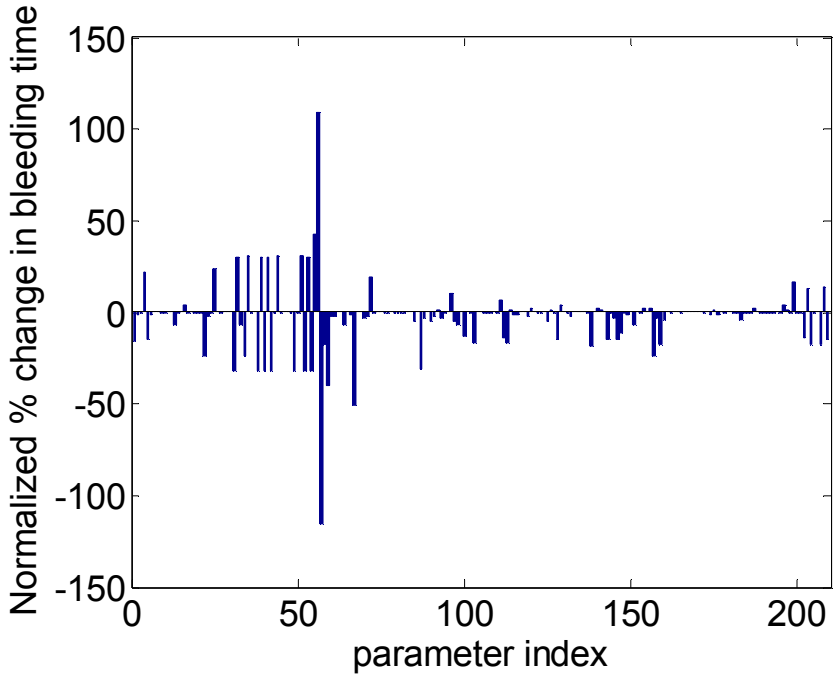

Figure 5.14. Sensitivity coefficients from local sensitivity analysis for hemophilia B with a FIX level 1% of the nominal case and a wound size of 200 μm^2 at a shear rate of 400 s^{-1}.

Table 5.5. List of potential treatment targets for hemophilia B

Pair index	Parameter 1	Parameter 2
a	N_2^{pl}	$n_{13\text{-}2}$
b	ϕ_{ADP}	$n_{13\text{-}1}$
c	$k_{8\text{-}1}$	k_8^{on}
d	$k_{13\text{-}1}$	k_{14}
e	$k_{1\text{-}1}$	$n_{13\text{-}1}$
f	N_{10}^{pl}	E_7^{out}
g	$k_{1\text{-}1}$	$k_{12\text{-}1}$
h	k_{7z}^{on}	$k_{11\text{-}3}$
i	k_7^{cat}	$k_{3\text{-}3}$
j	k_{pro}^{b}	$k_{13\text{-}2}$
k	$n_{13\text{-}2}$	$k_{5\text{-}3}$
l	k_{23}^{cat}	k_{22}^{+}
m	$k_{13\text{-}1}$	$k_{1\text{-}4}$
n	$k_{12\text{-}2}$	k_{2e}^{off}
o	$n_{13\text{-}1}$	$k_{7\text{-}1}$
p	$k_{3\text{-}1}$	k_{13}^{+}
q	$k_{12\text{-}2}$	$n_{13\text{-}2}$
r	$n_{13\text{-}1}$	ϕ_{ADP}
s	$k_{13\text{-}2}$	k_{2e}^{off}
t	k_{17}	$k_{7\text{-}2}$

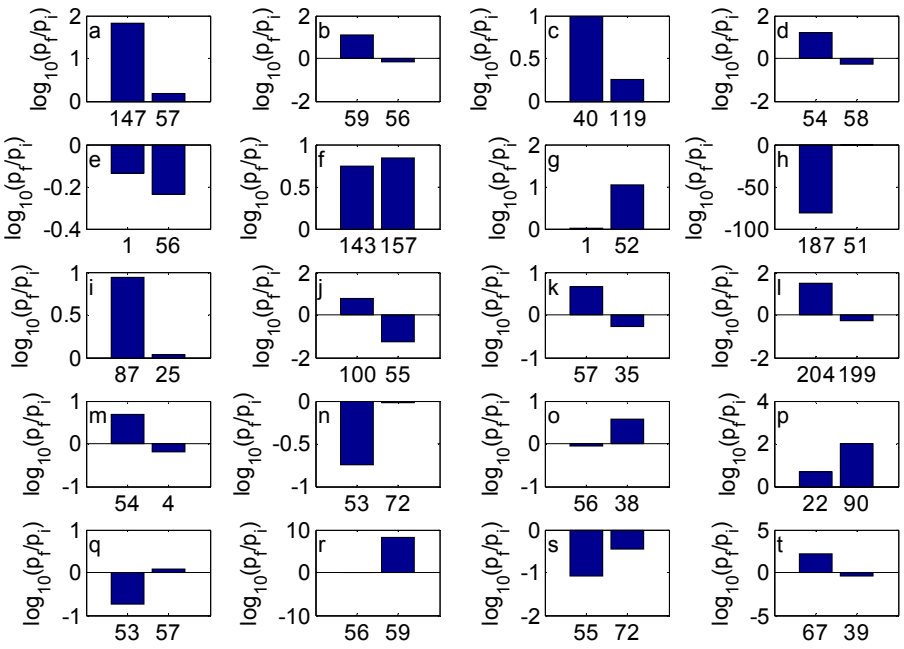

Figure 5.15. Ratio of parameter values used for treating hemophilia B to corresponding original values. The figure number (a-t) corresponds to the pair index used in Table 5.5 and the number of each bar corresponds to the parameter index in Table 5.1.

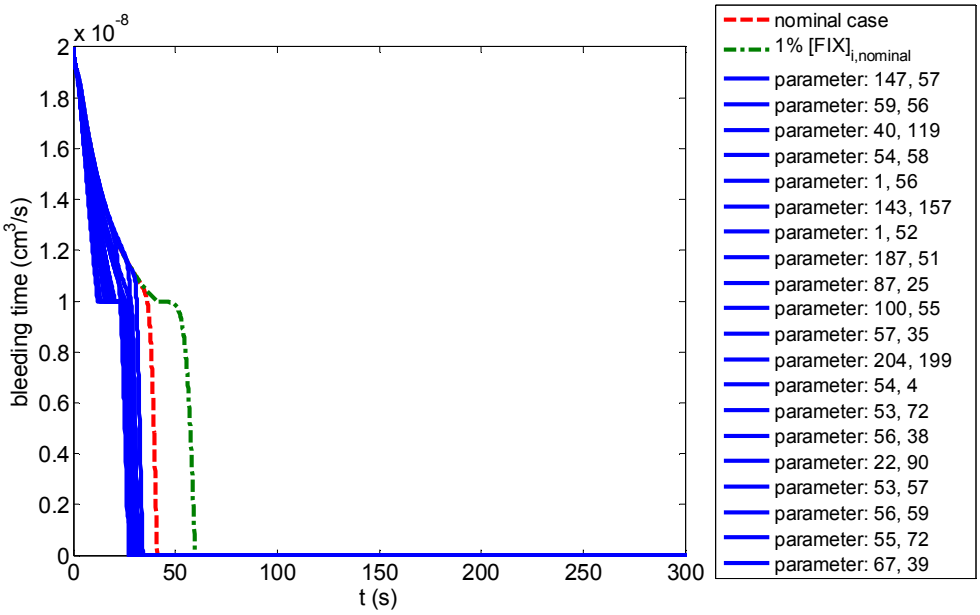

Figure 5.16. Profiles of bleeding rate for the nominal case, the hemophilia B case in question, and the treated cases.

5.4.3 Deficient Primary Hemostasis: Immune Thrombocytopenic Purpura

Immune thrombocytopenic purpura (ITP), as previously mentioned, is a disease with abnormally low platelet count, and thus a disease of deficient primary hemostasis. The profiles of total blood loss in response to various wound sizes with different degrees of ITP are shown in Figure 5.17. With a platelet count of 100×10^9/L (mild ITP, blue lines in Figure 5.17), the blood loss profiles almost overlap with the nominal case. However, as platelet count reduces to 50×10^9/L, hemostasis is not able to stop the bleeding completely for a wound size of 200 μm^2, as shown in the green dash-dotted line in Figure 5.17c. When platelet count is only 10×10^9/L, a severe case of ITP, hemostsais is not able to stop bleeding in all three wound sizes (dotted magenta lines).

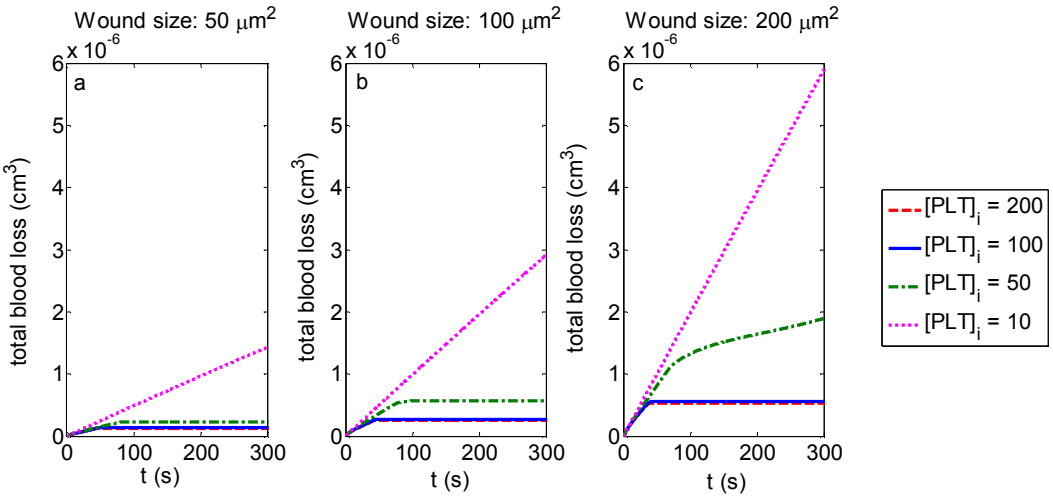

Figure 5.17. Total blood loss in response to wound sizes of (a) 50 μm^2, (b) 100 μm^2, and (c) 200 μm^2 with various degrees of ITP at a shear rate of 400 s^{-1}.

The medium ITP case with a platelet count of 50×10^9/L in response to a wound size of 100 μm^2 (green dash-dotted line in Figure 5.17b) is further used for identifying potential treatment targets. A local parametric sensitivity analysis is first carried out and the sensitivity coefficients are shown in Figure 5.18. In this case, the most influential parameters are again in the primary hemostasis model. However, out of more than 100 pairs tested, no pair of parameters is capable of correcting the disease state.

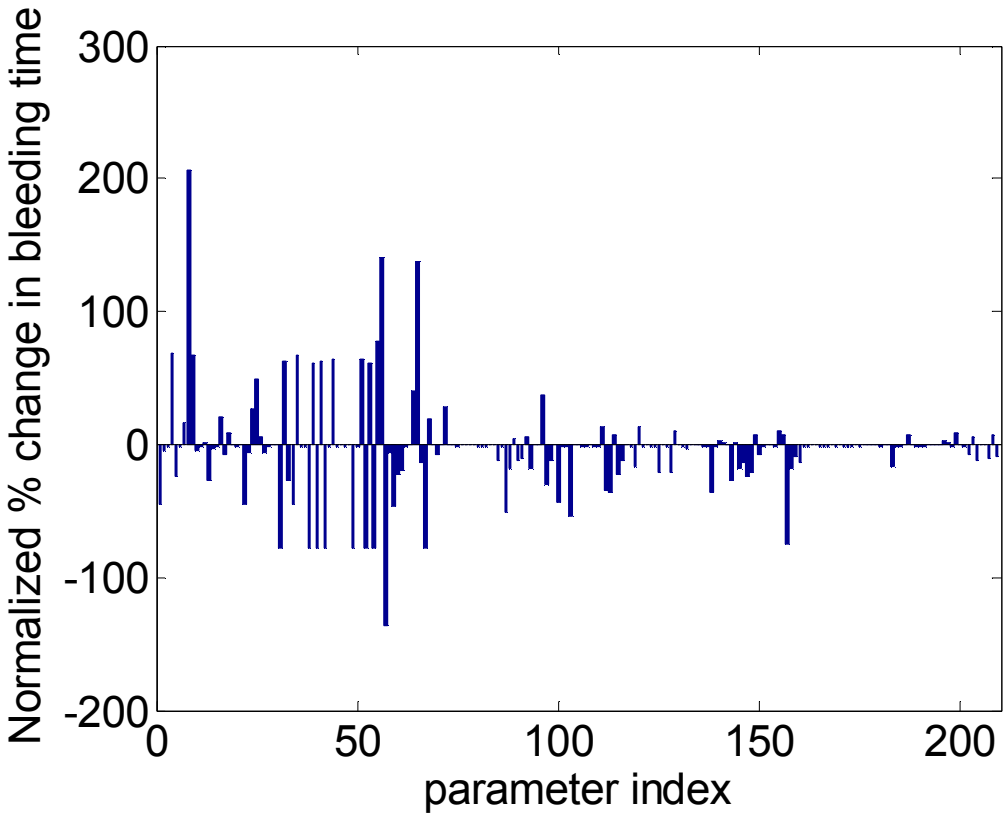

Figure 5.18. Sensitivity coefficients from local sensitivity analysis for ITP with a platelet count of 50×10^9/L and a wound size of 100 μm^2 at a shear rate of 400 s^{-1}.

5.5 Summary

The comprehensive model is later used for identifying potential treatment targets for five thrombophilic and hemophilic diseases that result from a malfunction in either primary or secondary hemostasis. Local parametric sensitivity analyses for various disease states show that the parameters in primary hemostasis usually have a greater influence in the metrics of interest compared to the parameters in secondary hemostasis. With the use of the comprehensive model, potential treatment targets are found for four disease conditions, hyperactive platelets, ATIII deficiency, hemophilia

A, and hemophilia B, while no potential treatment target is found for immune thrombocytopenic purpura.

Chapter 6

PLATELET COUNT CONTROL IN PATIENT WITH IMMUNE THROMBOCYTOPENIC PURPURA

6.1 Introduction

The pro-aggregation and pro-coagulation properties of platelet described in previous chapters make the quantity of platelet, or platelet count, an important indication of the functional state of hemostasis. A high platelet count could indicate a more active hemostatic response, while a low platelet count could generate an underproduced clot that is not capable of covering the entire wound, leading to excessive bleeding. The production process of platelet, thrombopoiesis, thus requires a delicate homeostatic balance where the platelet count in an individual falls within a physiologically safe range, a consensus of which being between 150×10^9/L and 400×10^9/L. Immune thrombocytopenic purpura, or ITP, is a disease generally defined as platelet count below 150×10^9/L, with symptoms varying significantly with different values of platelet count, PLT ($\times10^9$/L), as shown in Table 6.1. Mild cases of ITP, where $30 < PLT < 150$, are frequently untreated because symptoms are often unobservable [88, 89]. However, treatment is required when $PLT < 30$ [90], especially since sustained periods of extremely low PLT (e.g., $PLT < 10$) can lead to serious and sometimes fatal complications [91]. Even though many treatment options exist, the symptoms in an individual might not respond to any of them or might recur frequently as a result of the multiple sources of cause and the complexity of platelet production regulation, leaving 20% of the patients being hospitalized [92]. Therefore, a deeper

understanding of platelet production regulation would provide insight into how to restore hemostasis back to its normal functional state and maintain the platelet count within a safe range.

In this chapter, through the work with a specific ITP patient who was treated with romiplostim, a relatively new drug for treating ITP, we present an example of how to study the platelet production regulation process in an individual and how to develop treatment strategies based on the physiological information obtained. As every individual is unique and various symptoms may manifest among different individuals, especially in the case of ITP, this personalized approach is expected to generate better treatment responses. The majority of the work was published in [93].

Table 6.1. Physiological implications of platelet count

Platelet count, PLT ($\times 10^9$/L)	Description	Symptoms	Treatment suggestion
$150 < PLT < 400$	normal	None	none
$30 < PLT < 150$	mild ITP	might be asymptomatic or symptoms including: excessive bruising, spontaneous nose bleeds, spontaneous bleeding from gums, and prolonged bleeding from cuts	no treatment required
$PLT < 30$	high risk of bleeding	subarachnoid bleeding, gastrointestinal bleeding, and intracranial hemorrhage	treatment usually required; evaluations should be made for the decision of treatment
$PLT < 10$	severe ITP		treatment required

6.2 ITP and Current Treatments

6.2.1 Mechanism of Platelet Production Regulation

Platelet production is regulated according to the following mechanism: The hormone thrombopoietin (TPO) stimulates the proliferation, maturation, and differentiation of platelet precursor cells (megakaryocytes) by binding to c-Mpl, the TPO receptor on the plasma membrane of these platelet precursor cells. Binding of TPO to megakaryocytes activates two pathways: the JAK/STAT5 pathway, which results in cell proliferation, and the MAPK pathway, which promotes megakaryocyte differentiation [94, 95], leading to the production of platelets

TPO is primarily synthesized by hepatocytes at a constant rate in the liver [96] and then secreted into the blood stream. Since c-Mpl is present on the plasma membrane of platelets, TPO can also bind to platelets. This results in an inverse relationship between the circulating concentration of TPO and the platelet count [96, 97]. When platelet count is high, more TPO will bind to platelets, thereby lowering TPO concentration and consequently reducing the availability of TPO for stimulating megakaryocytes. This ultimately lowers the stimulatory effect of TPO on platelet production. Therefore, as more platelets are produced, the effective production rate is reduced automatically by this natural feedback regulatory mechanism whereby the stimulatory TPO is sequestered from megakaryocytes by the produced platelets (Figure 6.1). Conversely, when platelet count is low, more TPO will be available and the increased TPO concentration will thus exert an enhanced stimulatory effect on megakaryocytes, ultimately leading to increased platelet production.

6.2.2 Pathology and Treatment of ITP

Under normal conditions, the intrinsic biological feedback regulatory mechanism described above and illustrated in Figure 6.1 maintains homeostatic production of platelets. In ITP patients, however, complications arise because of the simultaneous incidence of increased platelet destruction and decreased platelet production [98] as a result of any number of conditions including autoimmune responses, reduced TPO production rate due to pathological disorders in the liver, or pathological changes in the c-Mpl receptor or post-receptor signaling events in megakaryocytes [98]. While the root cause of ITP is unknown, an understanding of TPO regulation of platelet production indicates that platelet production can be increased to compensate for inappropriately low production by enhancing TPO levels. Therefore, a logical ITP treatment option is to employ "TPO mimetics", such as romiplostim, that act through the same mechanism as TPO.

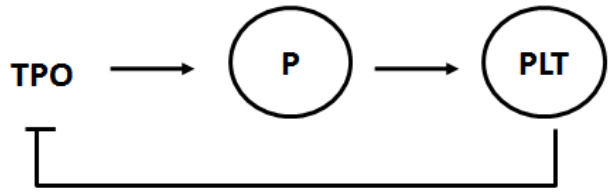

Figure 6.1. Schematic of platelet production regulation. TPO: thrombopoietin; P: precursor (megakaryocyte); PLT: platelet.

Romiplostim, a fusion protein analog of TPO, contains two copies of the human immunoglobulin (IgG_1) Fc domain, each covalently linked at its C-terminus to a peptide chain containing two c-Mpl-binding peptides [100]. It has been approved in

many countries as a treatment for adult patients with chronic ITP [101] and has been shown to increase platelet count (to PLT $\geq$ 50) in the majority of ITP patients [102-104].

However, peak platelet count in response to single romiplostim treatment is highly variable from patient to patient [105]. For example, a platelet count of 130×10^9/L achieved with 1 μg/kg/week in one patient requires 3 μg/kg/week in another [103], possibly due to differences among patients in the extent of decreased platelet production and increased platelet destruction [98].

Furthermore, the time required to reach peak platelet count after romiplostim administration, a delay that reflects the time required for megakaryocyte differentiation, varies significantly from patient to patient, with medians ranging from 10 to 16 days [105, 106]. As a result of the mechanism of romiplostim action, the peak response for each individual patient is generally higher at lower initial platelet counts and attenuated with increasing values of platelet count—a defining characteristic of nonlinear systems. The effect of one romiplostim injection on any particular patient will therefore affect the efficacy of the next, adding another layer of complexity to the problems created by the nonlinear and time delay dynamics. Consequently, maintaining platelet count at a stable value with romiplostim is fundamentally challenging.

The manufacturer recommendation is weekly administration of romiplostim, with the dose depending on the current platelet count. However, as noted above, the time to reach the peak platelet count after romiplostim treatment is more than a week for many patients. Thus it is likely that treatment will be administered while platelet count is still rising, but more importantly, current platelet count measurement will not

adequately reflect the full effect of the immediately preceding treatment. In this case, however, excess romiplostim will simply be sequestered by the platelets, so that its stimulatory effect on platelet production will be muted. The converse is more problematic. If a treatment is administered when platelet count is decreasing, and the dose is determined on the basis of current measurement, platelet count will almost surely continue to decrease and may decrease to an unacceptably low value because it takes a few days for administered romiplostim to take effect. By the time the treatment takes effect, the actual platelet count will not be near the value upon which the treatment dose was based so that the treatment is likely to have been seriously underestimated. To be effective, a treatment strategy must take the complex dynamic characteristics of romiplostim action into consideration.

By now, it has become well established that mathematical modeling is an efficient tool for understanding complex biological systems [107]. In the specific case in question here, pharmacokinetic/pharmacodynamic (PKPD) models of romiplostim have been used effectively to capture the characteristics and mechanisms of romiplostim metabolism in healthy humans [97] and ITP rats [101]. A relatively recent study developed a K-PD model (with the P in PK omitted to indicate the absence of data on drug concentration in the serum) for the effect of romiplostim on platelet production using data from ITP patients, approximating the pharmacokinetic part with a single compartment model [106]. The data reported in the study showed highly variable responses to romiplostim administration in ITP patients, leading the authors to divide the data into two subpopulations each characterized by significantly different parameter estimates. The K-PD model representing the population characteristics of romiplostim-induced platelet production in the patients was subsequently used to

investigate two quantized dosing strategies with the objective of preventing PLT > 400, the conventional upper limit of platelet count in normal individuals. The simulation results showed that from 12 weeks to 42 weeks, PLT can be maintained between 20 and 400 with both dosing strategies in 75% of the subjects, while PLT was predicted to fall below 20 (high bleeding risk) in 20% of the subjects and rise above 400 (increased thrombotic risk) in the remaining 5% of the subjects over the same period.

The question we address here is as follows: given the practical constraint that treatments can only be administered at regular intervals, is a steady platelet count achievable in ITP patients treated with romiplostim (exemplified by the specific patient in question); and if so, what (control) strategy will produce the required dose profile to achieve this objective? Our strategy is to obtain an appropriate mathematical model of romiplostim-mediated platelet production and regulation for the specific ITP patient in question; analyze the model to obtain insight into the important characteristics of the patient; and use the model as the basis of model-based control investigations, framing platelet count regulation as a control problem and utilizing appropriate control theoretic principles to obtain practical solutions. Specifically, this approach is used to determine the theoretical optimum romiplostim profile required to maintain platelet count, PLT ($\times 10^9$/L), at 70, with weekly or bi-weekly subcutaneous injections of various doses of romiplostim over a period of 6 months. Three control strategies were investigated: “fixed dose” open-loop control, “variable dose” proportional-integral (PI) feedback control, and “variable dose” model-based open-loop optimal control. We show that a stable platelet count profile is achievable only with weekly treatment frequency in the specific patient, due to the pharmacological

characteristics of romiplostim. Our results also show that a patient-specific mathematical model and common control strategy combined can yield a better treatment regimen for patients with ITP.

6.3 Development and Validation of Patient-Specific Physiological Model

6.3.1 A Pharmacokinetic-Pharmacodynamic Model of ITP patient

An existing PKPD model of romiplostim [97] (Figure 6.2) was modified, customized for our purposes, and implemented in Simulink/MATLAB. Although the PK data of serum romiplostim concentrations were not available in our dataset, we chose as the initial basis of our investigations, the mechanistic PKPD model developed in [97] over the semi-mechanistic K-PD model used in [106]. As noted earlier, newly produced platelets constitute an additional input (in addition to romiplostim administration) to the PK model, directly affecting the drug concentration, and thereby playing a key role in further regulating platelet production. This crucial intrinsic regulatory feedback mechanism (central to the physiological regulation of platelet production) is missing in the K-PD model in addition to its use of a single simplified compartment to represent the PK portion of the system. Thus the K-PD model is not appropriate for an investigation focused explicitly on designing schemes for effective control of platelet count.

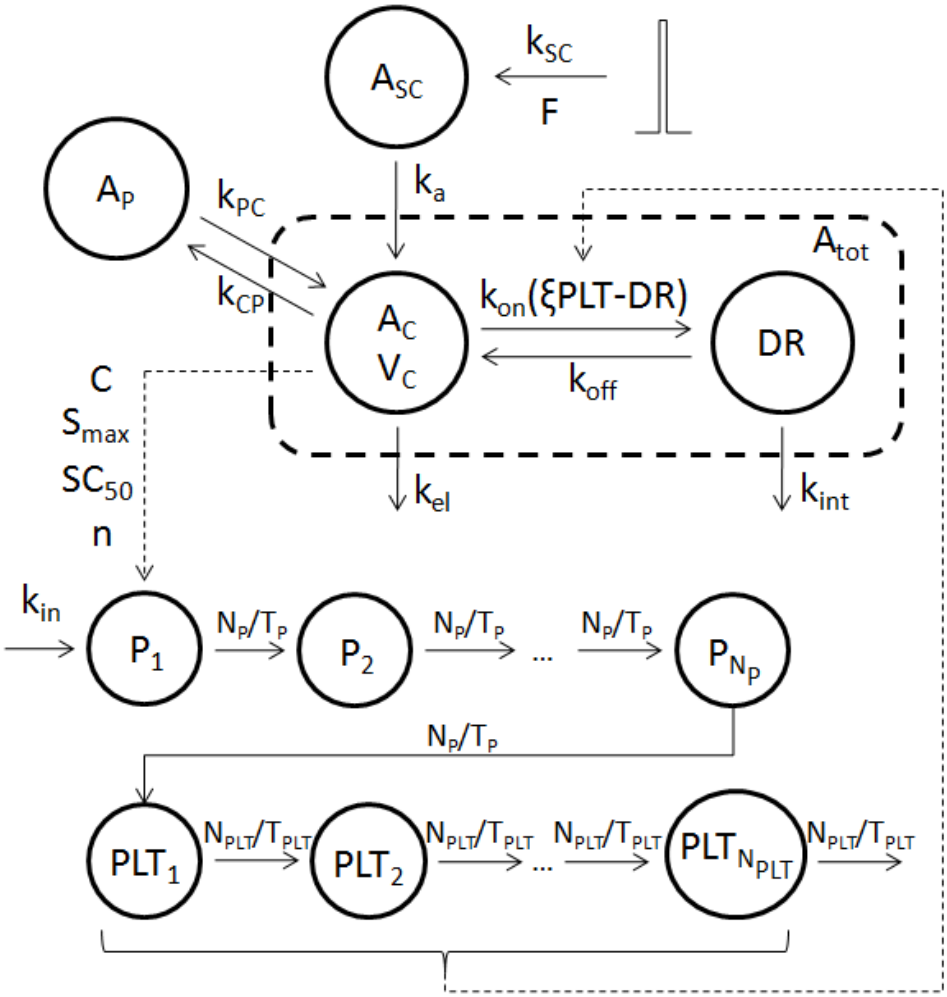
A_{SC}
k_{SC}
F
A_P
k_{PC}
k_a
k_{CP}
A_{tot}
A_C
V_C
$k_{on}(\xi PLT-DR)$
k_{off}
DR
C
S_{max}
SC_{50}
n
k_{el}
k_{int}
k_{in}
P_1
N_P/T_P
P_2
N_P/T_P
...
N_P/T_P
P_{N_P}
N_P/T_P
PLT_1
N_{PLT}/T_{PLT}
PLT_2
N_{PLT}/T_{PLT}
N_{PLT}/T_{PLT}
...
$PLT_{N_{PLT}}$
N_{PLT}/T_{PLT}

Figure 6.2. Schematic representation of the pharmacokinetic/pharmacodynamic (PKPD) model illustrating mechanisms of romiplostim-induced platelet production. Subcutaneous injection of romiplostim is described by rate constant k_{SC} and bioavailability F, with the dose implemented as a rectangular pulse. Romiplostim at the subcutaneous site, whose amount is represented by A_{SC}, is absorbed into the blood stream, represented by rate constant k_a. Free romiplostim is distributed between the serum and the peripheral part with rate constants k_{PC} and k_{CP}. The specific serum volume is denoted as V_c. The amount of romiplostim in the serum and the peripheral part are denoted as A_C and A_P, respectively. Romiplostim can also bind to platelets in the blood stream and form a drug-receptor complex. Formation of such complex, whose amount is represented by DR, is described with rate constant k_{on}. A proportionality constant ξ representing the average number of receptor on each platelet is defined to determine the total amount of receptor on platelets. Dissociation of romiplostim from the drug-receptor complex is described by rate constant k_{off}. Two mechanisms are responsible for romiplostim clearance: receptor internalization, represented by rate constant k_{int}; and metabolic clearance of romiplostim, represented by k_{eli}. The total amount of romiplostim in circulation, A_{tot}, is the summation of Ac and DR. Free romiplostim, with concentration denoted as C, exerts a stimulatory effect on megakaryocyte maturation through a process described by a Hill function, with S_{max} as the maximal effect, SC_{50} as the concentration required to reach half the maximal effect, and n as the Hill coefficient. P_1, P_2, …, P_{NP} are the number of megakaryocytes in different stages, where N_P is the number of stages of megakaryocyte. Similarly, PLT_1, PLT_2, …, P_{NPLT} are the number of platelets in different stages, where N_{PLT} is the number of stages of platelet. Megakaryocytes and platelets move into the next stage at a rate inversely proportional to their respective lifespans, T_P and T_{PLT}. The intrinsic megakaryocyte maturation rate, denoted as k_{in}, maintains the homeostasis of platelet production when romiplostim is absent.

The complete set of model equations is given in Appendix C. Notations and the physiological processes they represent are listed in Table 6.2. Initial conditions for the resulting system of ordinary differential equations (ODEs) are presented in Table C.1. Three modifications were made to the existing model: (1) romiplostim injection was implemented in the PK model as a rectangular pulse function with width of 1/60

hour and magnitude corresponding to the dose; (2) an extra parameter, n, was introduced into the PD model to account for any nonlinear effect of romiplostim on platelet production; (3) the maximal effect of romiplostim on platelet production (S_{max}) was decoupled from the intrinsic megakaryocyte maturation rate (k_{in}) compared to the original model. Decoupling of the intrinsic megakaryocyte maturation rate and the maximal effect of romiplostim provides a more physiologically relevant description of romiplostim-induced platelet production. With the same platelet lifespan, a higher intrinsic megakaryocyte maturation rate indicates a higher initial platelet count, which should reduce the effect of romiplostim, as noted above. A confounded representation for S_{max} and k_{in} would thus be inappropriate. In addition, as k_{in} is representative of the effect of endogenous TPO, the effect of romiplostim, which works through the same mechanism as TPO, should be additive to the entire platelet production process.

Table 6.2. List of parameters in the PKPD model.

Parameter	Unit	Description
PK model		
k_a	h^{-1}	first-order rate constant for the absorption of romiplostim from subcutaneous site to plasma
k_{CP}	h^{-1}	first-order rate constant for romiplostim entering the peripheral part from serum
V_C	L/kg	specific serum volume
k_{PC}	h^{-1}	first-order rate constant for romiplostim entering serum from the peripheral part
k_{el}	h^{-1}	first-order rate constant for romiplostim being eliminated from serum
k_{int}	h^{-1}	first-order rate constant for romiplostim being internalized by platelets
K_D	ng/mL	dissociation equilibrium constant for drug-receptor complex; defined as k_{off}/k_{on}
ξ	fg/platelet	maximum amount of drug-receptor complex per platelet
F	-	bioavailability of romiplostim to patient
PD model		
SC_{50}	ng/mL	drug concentration needed to reach half-maximum response
S_{max}	h^{-1}	maximum platelet production rate achievable with romiplostim
N_p	-	number of stages of precursor cells (megakaryocytes)
N_{PLT}	-	number of stages of platelet
T_P	h	lifespan of precursor cells (megakaryocytes)
T_{PLT}	h	lifespan of platelets
n	-	Hill coefficient for possible nonlinear effect on platelet production by romiplostim

6.3.2 Model Parameter Estimation and Validation

6.3.2.1 Clinical Data Collection

Platelet count data used to determine patient-specific parameters and to validate the PKPD model were based on physician-supervised romiplostim treatment records over a period of 130 days. Each round of treatment involves a complete blood count (CBC) test using a blood sample collected via venipuncture, followed by standard analysis. The physician subsequently determines an appropriate dose of romiplostim, based on the platelet count measurement and supervises its administration. The observed platelet count and the corresponding drug dose are then recorded.

6.3.2.2 Parameter Estimation and Model Validation

Unknown values of parameters in the PKPD model were estimated by optimally matching model predictions to a subset of the patient data (up to day 86, corresponding to the first 7 romiplostim pulses and the open circles in Figure 6.3) via least-squares optimization. The remaining complement of clinical data was used to validate the model. The resulting parameter estimates are presented in Table 6.3.

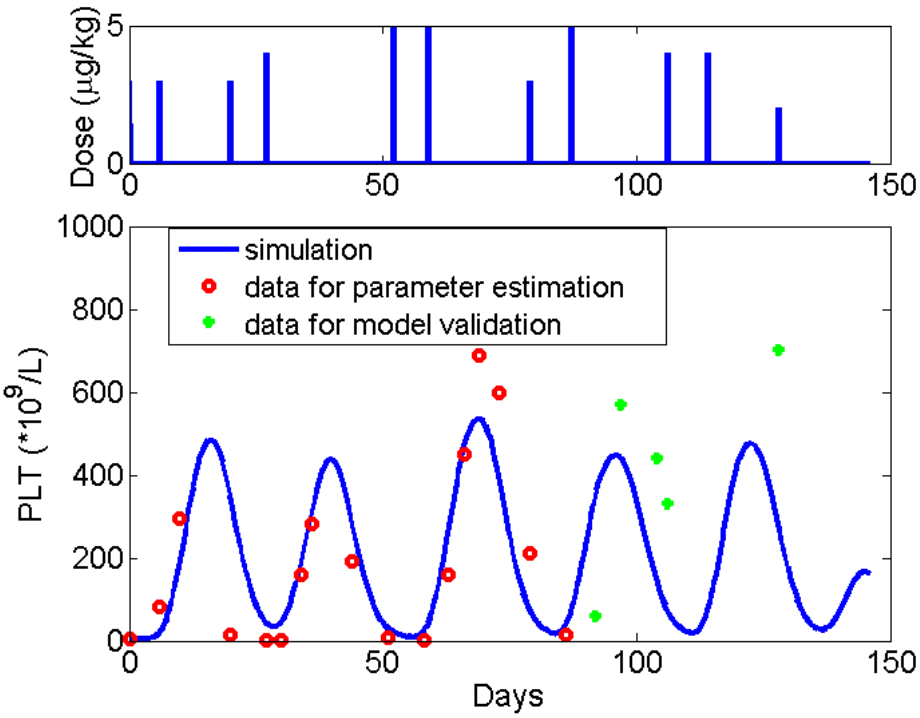

Figure 6.3. Clinical treatment data and platelet count profile with the PKPD model. Upper panel: romiplostim injection profile. Lower panel: platelet count data collected at the clinic and corresponding model prediction. Data in red circles are used to obtain patient-specific parameters for the PKPD model.

Table 6.3. Parameter values for healthy individuals and the ITP patient.

Parameter	healthy subjects value (unit)	ITP patient value (unit)
PK model		
k_a	0.0254 (h^{-1})	0.0124 (h^{-1})
k_{CP}	0.0806 (h^{-1})	0.143 (h^{-1})
V_C	0.0683 (L/kg)	0.0778 (L/kg)
k_{PC}	0.0148 (h^{-1})	0.0098 (h^{-1})
k_{el}	0.0382 (h^{-1})	0.0910 (h^{-1})
k_{int}	0.173 (h^{-1})	0.0248 (h^{-1})
K_D	0.131 (ng/mL)	0.0028 (ng/mL)
ξ	0.0215 (fg/platelet)	0.0190 (fg/platelet)
F	0.499 (-)	0.271 (-)
PD model		
SC_{50}	0.0520 (ng/mL)	0.0560 (ng/mL)
S_{max}	11.07 (h^{-1})	6.00 (h^{-1})
N_p	10 (-)	10 (-)
N_{PLT}	10 (-)	10 (-)
T_P	142 (h)	219 (h)
T_{PLT}	253 (h)	113 (h)
n	1 (-)	0.99 (-)

To validate the model, model-generated predictions of the patient's platelet count response to subsequent treatments, without further adjustment of any of the model parameters, were compared to corresponding data. The model prediction, shown in Figure 6.3 along with the collected data, indicates a generally good fit to the data, with discrepancies at predominantly high platelet counts most likely due to unmodeled effects of platelet destruction and other environmental factors that are not

considered in the model. Note that it was difficult to maintain a steady platelet count in the patient.

6.4 Model Analysis

6.4.1 Parameter Values

The parameter T_{PLT} representing platelet lifespan was estimated to be 4.7 days for the specific patient; for healthy subjects, it is 10.5 days [97]. This indicates that the patient's platelets last only half as long as the platelets in healthy subjects, consistent with commonly observed traits in ITP patients [98, 108]. The value for the newly introduced parameter n is close to 1, indicating that the nonlinear effect of romiplostim on platelet production in the patient is similar to that in healthy subjects. A smaller k_{int} value obtained for the patient suggests a lower than normal clearance rate of romiplostim through receptor internalization and therefore a higher chance of romiplostim being released back to the serum. However, the small K_D value for the patient indicates a high affinity of romiplostim to c-Mpl and therefore less dissociation of romiplostim from the drug-receptor complex. Since romiplostim acts via the same mechanism as endogenous TPO, the observed k_{int} and K_D values, combined with the increased k_{el}, suggest lower availability of TPO to megakaryocytes in the patient, leading to decreased platelet production and a lower platelet count.

6.4.2 Theoretical Dose Responses

One of the benefits of a mathematical model is that it allows one to investigate and analyze, via simulation, system responses to a variety of stimuli quickly and efficiently. Two sets of particularly informative examples are shown here for this specific problem.

Figure 6.4 shows the model response to a single romiplostim injection for a variety of initial platelet count values, PLT_0, ranging from 5×10^9/L to 250×10^9/L. The response to romiplostim treatment is stronger at lower initial platelet counts and is attenuated with increasing initial platelet count values. This result is consistent with known mechanisms of romiplostim action, with a higher initial platelet count providing more opportunity for the excess platelets to bind and sequester the drug, thereby reducing the stimulatory effect of romiplostim. For this specific patient, when PLT_0 is higher than 150, no significant response is observed to a 1 μg/kg romiplostim injection.

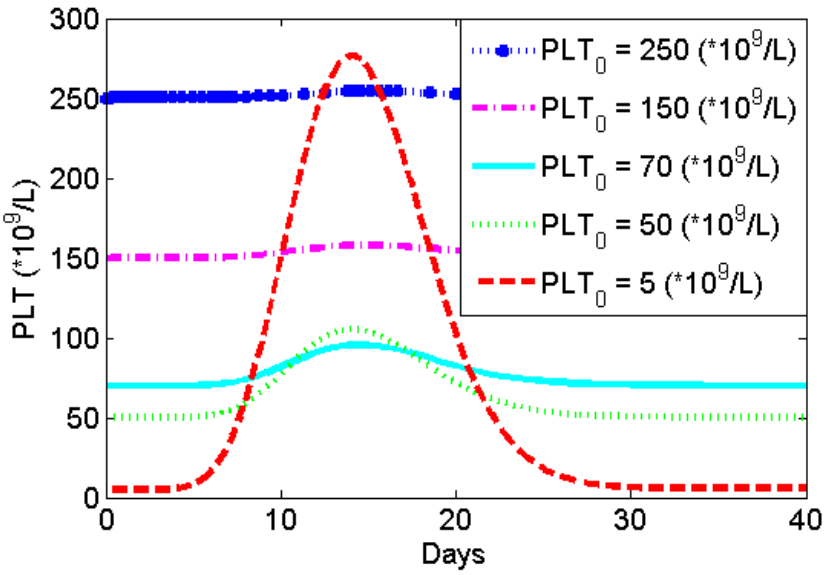

Figure 6.4. Model response to single romiplostim injection of 1 μg/kg for various initial platelet counts. Higher initial platelet count leads to attenuated platelet count response, a result that is consistent with the fundamental mechanism of platelet count regulation.

Figure 6.5 shows the model response to a single injection of various doses ranging from 0.2 µg/kg to 5 µg/kg, starting from a fixed initial platelet count of 5×10^9/L. For this specific patient, the response shows three phases: an initial induction period of approximately 5 days (regardless of dosage) with no noticeable change in platelet count; a gradual increase in platelet count culminating in a peak response at 14-16 days, with the peak occurring progressively later with increasing doses; a final declining phase with platelet count gradually returning to the original starting value after 25-30 days. The magnitude of the peak response is dependent on dosage nonlinearly, as an n-fold increase in the dose does not result in a corresponding n-fold increase in the magnitude of the peak response.

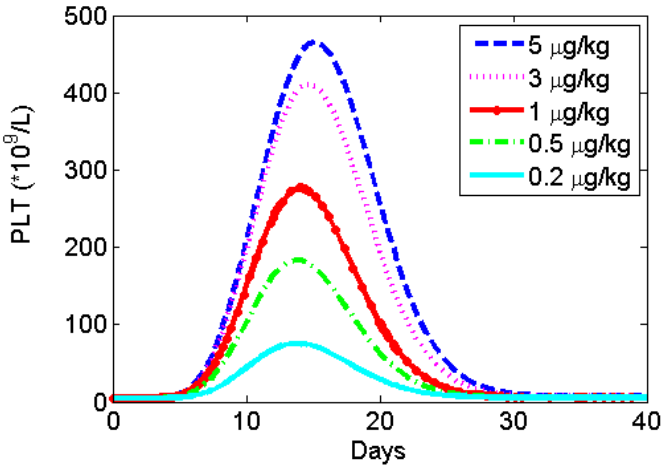

Figure 6.5. Model response to a single romiplostim injection of various doses. Each dose response consists of three phases: an initial induction period of approximately 5 days (regardless of dosage) with no noticeable change in platelet count; a gradual increase in platelet count culminating in a peak response occurring around 14-16 days, with the peak occurring progressively later with increasing doses; a final declining phase with platelet count gradually returning to the original starting value after 25-30 days.

Finally, the response to a single injection is intrinsically periodic, with a period T of approximately 28 days. Consequently, the treatment frequency should take this important characteristic response time into consideration. For example, a treatment regimen restricted to once every 28 days will result in what appear to be perfect sustained oscillations in time with possibly varying amplitude. Similarly, since measurements can be taken only at specific discrete points in time, the sampling period Δt must also be selected carefully to avoid missing critical information about the true state of the patient's platelet count. For instance, measurements taken once every 28 days will provide platelet count information that will completely miss the true nature of the full dynamic response.

6.5 Platelet Count Control in ITP Patient

6.5.1 Motivation of Engineering Control Systems Approach to the Development of Treatment Protocols

Once it was confirmed that the PKPD model provides a reasonable representation of romiplostim-induced platelet production for the patient in question, the model was used to investigate platelet count control strategies. The primary objective was to determine the sequence of romiplostim injections required to maintain a target platelet count, y^* ($\times 10^9$/L), of 70. The injections are represented as $u(k)$, rectangular pulses of magnitude u implemented at discrete time point k (k = 0, 1, 2, …), every Δt time units. Three distinct control techniques—open-loop control, discrete closed-loop PI control, and optimal open-loop control—were used to determine the injection sequence $u(k)$, and the respective performances were evaluated via simulation for two sampling periods: weekly (Δt = 7 days) or bi-weekly (Δt = 14

days). Note that while *u(k)* is allowed to take any value on the real line in this study, in practice romiplostim can be administered only in quantized doses.

6.5.2 Control System Design

6.5.2.1 Open-loop Control

The strategy here is to implement a constant value of *u(k)* regardless of actual platelet count measurements (hence "open-loop"). The primary rationale for such a strategy is its simplicity. The model was used to investigate patient outcome in response to typical injection doses *u(k)* of 2, 1, and 0.5 μg/kg at typical weekly and bi-weekly treatment frequencies in order to determine which of these doses implemented at which of these frequencies, if any, comes close to meeting the stated control objective.

6.5.2.2 Discrete PI Controller without Zero-Order Hold

With this classical feedback control strategy, *u(k)* is determined at each discrete time point *k* on the basis of *ε(k)*, the error between the platelet count measurement and the desired value. The control action *u(k)* is computed as follows:

$$u(k) = K_P \cdot \varepsilon(k) + K_I \cdot \sum_{i=1}^{k} \varepsilon(i), \;\; k = 0, \; 1, \; 2, \; \ldots \tag{6.1}$$

where K_P and K_I are controller parameters. While negative *u(k)* values are mathematically possible from this expression, they are physiologically meaningless; therefore, the implemented control action is constrained to a minimum value of *u(k)* = 0.

For a variety of physiological reasons, the platelet count response profile is very sensitive to u_0, the initial injection dose implemented at $k = 0$. Consequently, this

initial condition is treated as an extra parameter and determined independently. Because romiplostim is implemented as pulses, the PI controller output is implemented without the usual zero-order hold.

Rather than tuning the PI controller using standard tuning rules, the controller parameters were determined via optimization. Specifically, optimal values were determined for u_0, K_P and K_I using the optimization routine *fminsearch* by minimizing the resulting sum-of-squared errors between the set-point and the platelet count, over a prescribed time span of 24 weeks.

6.5.2.3 Model-based Open-Loop Optimal Control

Under this strategy, the dynamic model is used to determine a romiplostim dose sequence $u(k)$ $(k=1, 2, \ldots, N_f)$ that minimizes the sum-of-squared errors, represented mathematically as follows:

$$\min_{u(k)} \Phi(u(k)) = \sum_{i=1}^{N_f} \left(\varepsilon(i)\right)^2 \tag{6.2}$$

where, as with the PI feedback control strategy, $\varepsilon(i)$ is the error between the platelet count measurement and the desired value. The number of time points N_f is chosen arbitrarily as 500 in this study, and the time points at which the errors are calculated are evenly distributed over the simulation time of 24 weeks. The dose sequence $u(k)$ is computed directly using the optimization algorithm *fminsearch* for weekly and bi-weekly treatment frequencies.

6.5.3 Implementation of Control Strategie

6.5.3.1 Open-Loop Control

The performance of the open-loop control strategy shown in Figure 6.6 indicates that this simple and straightforward strategy is unable to maintain a stable platelet count at the desired target value. The obvious oscillatory responses, not unexpected in light of the foregoing model analysis, are the result of a "nonlinear convolution" of the theoretical "basis function" of Figure 6.4. As expected, the peak platelet count values are lower for lower doses, and the "effective period" of the observed oscillations is longer for the bi-weekly treatment regimen.

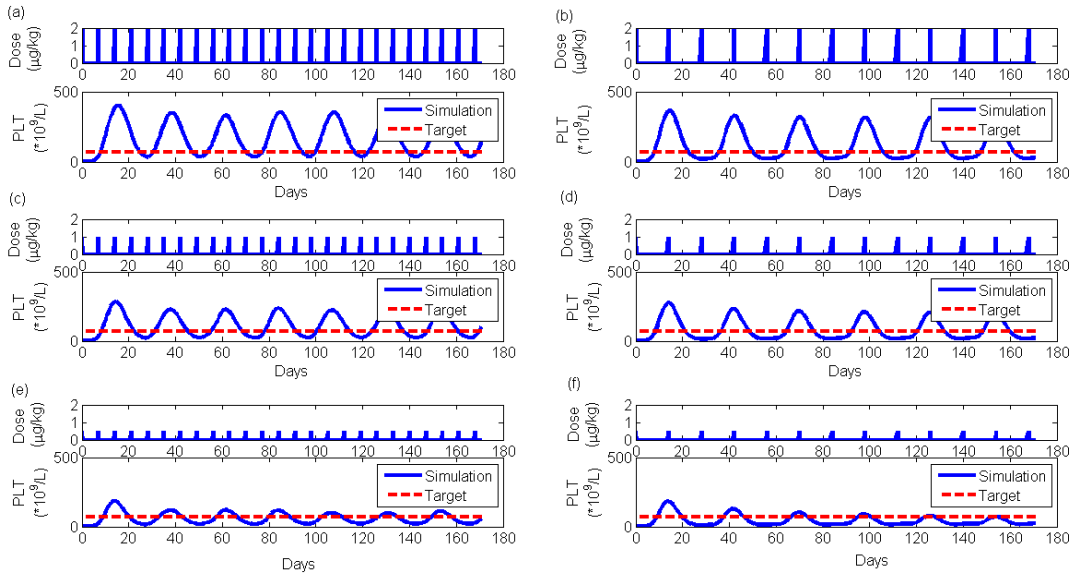

Figure 6.6. Performance under open-loop control. (a) 2 μg/kg every 7 days; (b) 2 μg/kg every 14 days; (c) 1 μg/kg every 7 days; (d) 1 μg/kg every 14 days; (e) 0.5 μg/kg every 7 days; (f) 0.5 μg/kg every 14 days. The results show that the open-loop strategy is ineffective in maintaining a stable platelet count.

6.5.3.2 Discrete PI Controller without Zero-Order Hold

The "optimally tuned" PI controller parameters determined for weekly and bi-weekly injections are shown in Table 6.4. The system performance for weekly injections under this control strategy is shown in Figure 6.7, with the top panel showing the romiplostim doses used to achieve the platelet count trajectory shown in the bottom panel. Note that after about 7 treatments, or 49 days, the platelet count stabilized and remained essentially constant at the desired target value. Thereafter, a steady dose of approximately 1 μg/kg is needed to sustain the platelet count at 70×10^{9}/L.

Table 6.4. Parameter values for optimally tuned discrete PI controller.

Treatment	K_P	K_I	Initial Dose (μg/kg)
Weekly	5.19×10^{-3}	7.59×10^{-5}	0.27
Bi-weekly	4.74×10^{-3}	2.72×10^{-5}	0.16

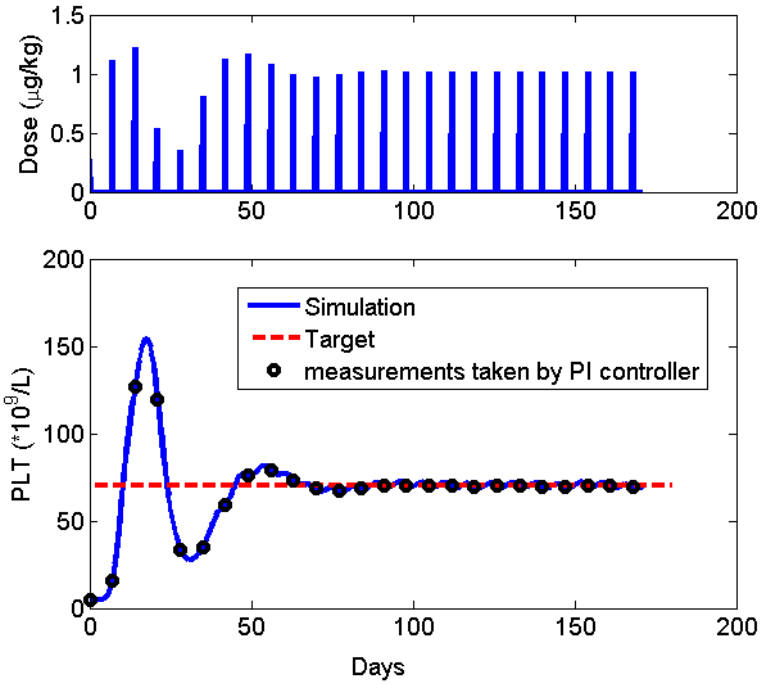

Figure 6.7. Platelet count control: weekly treatments with optimally-tuned discrete PI controller. Stable platelet count is achieved with this control strategy within 50 days, with steady-state romiplostim doses of approximately 1 μg/kg.

The performance under a bi-weekly treatment regimen based on the same control strategy, shown in Figure 6.8, is not as good as the result shown in Figure 6.7 for the weekly treatment regimen. Collectively, the oscillatory response and the discrete measurements used by the controller, indicated by the circles superimposed on the continuous response, give an illusion of reasonable performance. At the discrete time points where the measurements are taken and the control action is implemented, the measured values are indeed somewhat close to the desired target value; however, these infrequently sampled measured values fail to represent the true nature of the full response.

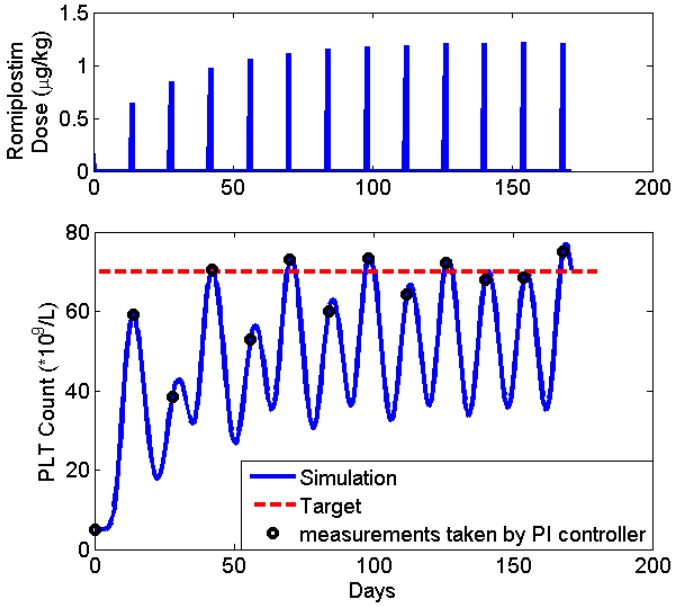

Figure 6.8. Platelet count control: bi-weekly treatments with optimally-tuned discrete PI controller. Platelet count continues to oscillate even after a long period of time has elapsed. Although measurements taken from 70 days onward show values close to the target value, the complete platelet count profile remains mostly, below the target—an indication of the inadequacy of this measurement and treatment frequency

6.5.3.3 Model-based open-loop optimal control

The results under model-based open-loop optimal control, shown in Figure 6.9, are similar to the corresponding results under optimally tuned PI control shown in Figures 6.7 and 6.8. Figure 6.9 shows the results for (a) weekly treatments and (b) bi-weekly treatments, with the top panel in each case showing the corresponding romiplostim doses. As in Figure 6.7, after about 49 days, the platelet count achieved its target in a stable manner, with a steady weekly dose of approximately 1 μg/kg sufficient to maintain the platelet count at target.

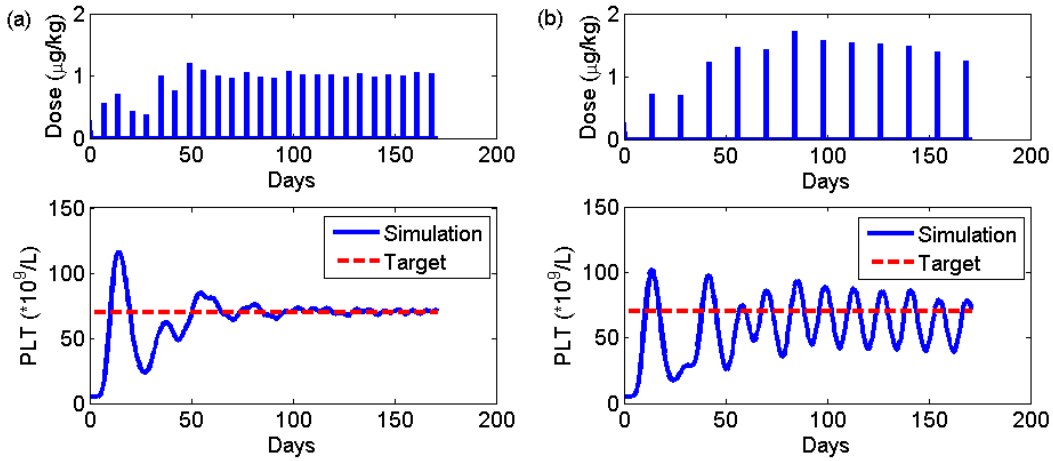

Figure 6.9. Platelet count control: weekly and bi-weekly treatments under optimal open-loop control. (a) With weekly injections, platelet count is stable after approximately 50 days. (b) With bi-weekly injections, beyond 80 days, the platelet count profile shows sustained oscillations with a period of approximately two weeks. This coincides almost perfectly with the natural period of the response to a single injection, with the implication that treatment regimen of single injections administered bi-weekly will always result in sustained oscillations.

As in Figure 6.8, the bi-weekly treatment resulted in a response that, after 75 days, oscillated around the desired target value of 70, with sustained oscillations. The sustained oscillation is a natural consequence of intrinsic romiplostim action as predicted in Figure 6.5 for the ITP patient in question. Observe the natural intrinsically periodic response to a single injection (see also [109] where it is noted that platelet count returns to the baseline level 2 weeks after discontinuing romiplostim treatment).

6.6 Discussion and Conclusions

While the dosages in the dose profile of romiplostim in this study can take on any positive values, current treatment strategy allows only quantized doses. One possible solution is to build a device to deliver romiplostim in smaller quantities,

similar to the insulin pumps used in patients with type I diabetes mellitus. To build a device specifically for ITP patients, two design issues, similar to those associated with the design of the insulin pump, will surface regarding the algorithms incorporated in the device: validation of the model used to determine the control action and specification of desirable characteristics of the platelet count profile [110]. In the case of ITP, the desirable characteristics of the platelet count profile can be simply set at a constant value, as was done in this study. Our results also have shown that employing a validated mathematical model in conjunction with PI feedback control can maintain platelet count in the patient at a stable value given appropriate platelet count measurement frequency. Hence, the major obstacle in building a romiplostim-delivery device will be determining how to take platelet count measurement at an appropriate frequency. Based on our results, a weekly clinic visit should be adequate for obtaining platelet count measurement once a romiplostim-delivery device is available.

In this chapter, a PKPD model was developed for an ITP patient to capture romiplostim-induced platelet production and provide the basis for developing effective treatment strategies for the specific patient. Three different control strategies were investigated. The results show that a stable platelet count can be achieved with weekly injection profiles determined by either "optimally tuned" PI feedback control or by optimal open-loop control. The simple and straightforward open-loop control strategy involving the implementation of a constant dose was completely ineffective. Bi-weekly treatments led to sustained oscillations as a result of the intrinsic pharmacological characteristics of romiplostim. Weekly treatments, on the other hand, produced better results, with platelet count maintained more readily at the target value of 70×10^9/L.

Although response to romiplostim treatment is highly variable from one ITP patient to another, this study has demonstrated that the use of patient-specific mathematical models for making model-based decision could be a promising approach to achieving stable platelet count control. We believe that this personalized treatment approach will benefit individual patients by providing them with the appropriate dose of romiplostim at the right time.

Chapter 7

CONCLUSIONS AND FUTURE DIRECTIONS

7.1 Conclusions

The work presented in this dissertation is aimed at understanding the hemostatic process quantitatively and, more importantly, as a whole. Gaining a system-level understanding of such process in a quantitative way will, as shown in the later part of the dissertation, enable one to rationally identify potential hemostatic disorders. An engineering control system framework proposed in Chapter 1 has allowed us to develop a comprehensive mathematical representation of hemostasis.

Because quantitative studies on primary hemostasis are very limited, compared to the well-characterized secondary hemostasis, primary hemostasis was first investigated. In Chapter 2, a single platelet model in response to ADP-induced signaling was developed to investigate potential approaches to simulating the major signaling pathways induced by ADP and TxA2, and to simulating *in vitro* platelet aggregation and secretion. The resulting model using both mechanistic detailed reaction mechanisms and hypothesized simplified mechanisms was shown to behave in agreement with experimental data in the literature, demonstrating the effectiveness of such hybrid approach.

The primary hemostasis components were represented by a mathematical model of primary hemostasis in Chapter 3. The platelet signaling pathways, from GPCR activation to integrin activation in response to ADP and TxA2, were, for the first time, incorporated into a primary hemostasis model that intended to describe the

platelet aggregation process *in vivo*. The resulting primary hemostasis model has allowed us to provide explanation of why mechanisms in addition to primary hemostasis are required in order to contain blood loss effectively.

In Chapter 4, an existing secondary hemostasis model was first improved by including current understanding of secondary hemostasis. The primary hemostasis model developed in Chapter 3 was modified to incorporate the interactions between primary and secondary hemostasis. Subsequently, the two models were connected to form a comprehensive model of hemostasis, forming, for the first time, a comprehensive model of hemostasis that includes complex platelet signaling events. Various conditions were applied to the comprehensive model and the model appeared to behave in agreement with known physiological conditions. Analysis on the interaction strengths showed that number of activated platelets was the most crucial factor in determining thrombin concentration profile. Modular sensitivity analysis identified the primary hemostasis controller, or collagen-induced platelet activation, as the modst significant module for bleeding time.

Using the comprehensive model, five hemostasis-related diseases, hyperactive platelets, ATIII deficiency, hemophilia A, hemophilia B, and ITP were investigated in Chapter 5 for identifying potential treatment targets. Local parametric sensitivity analysis was first carried out to aid the search. It was found that parameters in primary hemostasis play significant roles in all five disease conditions, but the identified potential treatment targets suggested that a disease caused by a deficiency in one subprocess usually could be corrected by a change in the other subprocess, except for the case of ITP, where the most significant parameter is platelet count. The treatment

targets identified using our rational approach also include current treatment regimens, demonstrating the predictive power of the comprehensive model.

Finally, in Chapter 6, to investigate how a deficient primary hemostasis actuator can be restored to a functional state, we worked with an ITP patient. An existing model PKPD model that simulates romiplostim-induced platelet production was customized for the specific patient and then the model is used to investigate potential control strategies and dosing schedule for maintaining a constant platelet count in the specific patient in question. It was found that a constant platelet count profile is obtainable with weekly romiplostim injections using PI control, while biweekly injections always lead to sustained oscillation as a result of the pharmacological properties of romiplostim in the patient.

7.2 Future Directions

7.2.1 Comprehensive Hemostasis Model

7.2.1.1 Incorporating Effect of Shear Rate

Although in our comprehensive model, the effect of flow is considered, the simulation is all carried out at a shear rate of 400 s^{-1}, which is closer to the venous shear rate. Even though the shear rate can be easily adjusted to a different value in order to simulate hemostasis under different vessel environment, for example, in an arteriole as opposed to the vein, such change should be accompanied by additional necessary changes, as additional biological events might take place under different conditions. The three roles of shear rate currently considered in the model are (i) flow carries away platelet agonists such as ADP, TxA2, and thrombin, as well as active coagulation factors away from the wound site, reducing the concentrations of these

molecules that drives hemostasis further; (ii) flow replenishes the inhibitors such as ATIII, TFPI, ZPI:PZ so that the activity in secondary hemostasis is further limited; (iii) flow replenishes inactive platelets and coagulation factors that have the chance of becoming activated and substantiate the positive feedback loops. Nevertheless, it has been shown that at a higher shear rate, especially in the range of arteriole shear rate, additional mechanism in hemostasis exists to promote more platelet aggregation. Our results using microfluidic devices also confirm that (data shown in Appendix D). The major mediator of such effect is von Willebrand factor, or vWF. Microflidic experiments using human whole blood have shown that at a shear rate of 1000 s^{-1}, platelet aggregation will be significantly increased as a result of the function of vWF. Therefore, if a high shear rate is going to be used in the model, the effect of vWF should not be neglected.

7.2.1.2 Incorporating Additional Proteins of Significance in the Single Platelet Model

As we have explained earlier in chapter 1, more than 5000 proteins are expressed in platelets. In the single platelet model part in the primary hemostasis model, we only considered a very small fraction of the 5000 proteins expressed. Therefore, incorporating additional proteins could make the model more powerful in predicting thrombus growth and also potentially expand the scope of potential treatment targets for diseases. Candidate pathways include: (i) outside-in signaling, the signaling events occurring after integrin activation has significant function in maintaining the platelet activation state; (ii) inhibitory signaling pathways within the platelets, i.e., signaling events downstream of Gz protein, that have also been shown to alter platelet activity significantly.

7.2.1.3 Investigating Effect of Model Structure and Model Parameters in Secondary Hemostasis

Many secondary hemostasis models have been proposed. However, different hypotheses are usually used and the model structure and parameters vary from study to study. Take the reaction of FVIII activation by thrombin for example. The mechanism in the KF model is a two-step process where FVIII first forms a complex with thrombin; then thrombin activates FVIII to FVIIIa and splits with FVIIIa. In this type of construction, three reaction rate constants for the forward reaction, the reverse reaction, and the catalytic reaction are needed. The same process in the model developed by Hockin and colleagues [58] is simplified as a second-order reaction where thrombin directly activates FVIII to FVIIIa. In the work carried out by Balandina et al. [110], the process is represented as:

$$\frac{d[FVIII]}{dt} = -\frac{k_{cat}[FVIII][II_a]}{K_M + [II_a]} \tag{7.1}$$

where k_{cat} is the catalytic reaction rate constant and K_M the Michaelis constant.

In addition to the difference in the model structure, the values of the reaction constants vary as well. Therefore, it is necessary to evaluate the effects of model structure and the associated parameter values on the overall response of the system in order to ensure proper description of a process.

7.2.1.4 Investigating Various Geometries of the Wound

In our comprehensive model of hemostasis, the wound is simulated as a clean punctured wound where a hole is generated and the subendothelium on the side of the hole stimulates hemostasis. However, when a puncturing wound is created, the wound might be left with cell debris mixed with other substances from subendothelium,

providing extra source to initiate hemostasis. In addition, in the case of atherosclerosis, when an atherosclerotic plaque rupture occurs, the surface of the plaque that contains both collagen and TF will serve as a reactive surface to initiate hemostasis. Therefore, the geometries of the wound have to be adjusted for different scenarios in order to obtain physiologically relevant results.

7.2.1.5 Validating the Comprehensive Model

Although it is not currently possible to validate our model intended for simulating *in vivo* hemostasis in humans, as the technology for making artificial organs advances, it is possible that our model can be validated against data obtained using artificial organs, which should be closer to the *in vivo* scenario.

7.2.2 Platelet Count Control in ITP Patients

In Chapter 6, a PKPD model is customized to describe romiplostim-induced platelet production in a specific ITP patient. It was shown that with biweekly administration will lead to sustained oscillation. One recent clinical study, which uses an elaborative biweekly dosing schedule, has also shown it clinically that it is difficult to maintain a target platelet count in a proper range with biweekly treatment regimen. The platelet count in all subjects eventually came down to an undesirable level [111]. Therefore, to address this issue, one solution might be to use variable dosing intervals, where instead of the dose of romiplostim, the injection interval is used as the variable. Even more, both the dose and the injection intervals can be used as variables. With a model at hand, we can even apply different control strategies, such as model predictive control (MPC), which has the capability of anticipating future event and taking actions accordingly.

REFERENCES

[1] B. Jose, P. McCluskey, N. Gilmartin, M. Somers, D. Kenny, A.J. Ricco, N.J. Kent, L. Basabe-Desmonts, Self-powered microfluidic device for rapid assay of antiplatelet Drugs, Langmuir, 32 (2016) 2820-2828.

[2] J.M. Burkhart, M. Vaudel, S. Gambaryan, S. Radau, U. Walter, L. Martens, J. Geiger, A. Sickmann, R.P. Zahedi, The first comprehensive and quantitative analysis of human platelet protein composition allows the comparative analysis of structural and functional pathways, Blood, 120 (2012) E73-E82.

[3] D.U. Silverthorn, Human physiology: an integrated approach, 4th ed., Pearson Education Inc., San Francisco, 2007.

[4] R.J. Westrick, M.E. Winn, D.T. Eitzman, Murine models of vascular thrombosis (Eitzman series), Arteriosclerosis Thrombosis and Vascular Biology, 27 (2007) 2079-2093.

[5] J.E. Purvis, M.S. Chatterjee, L.F. Brass, S.L. Diamond, A molecular signaling model of platelet phosphoinositide and calcium regulation during homeostasis and P2Y(1) activation, Blood, 112 (2008) 4069-4079.

[6] L.L.L. Lenoci, M. Duvernay, S. Satchell, E. DiBenedetto, H.E. Hamm, Mathematical model of PAR1-mediated activation of human platelets, Molecular Biosystems, 7 (2011) 1129-1137.

[7] G.L. Waldo, T.K. Harden, Agonist binding and Gq-stimulating activities of the purified human P2Y(1) receptor, Molecular Pharmacology, 65 (2004) 426-436.

[8] L.R. Lian, Y.F. Wang, J. Draznin, D. Eslin, J.S. Bennett, M. Poncz, D.Q. Wu, C.S. Abrams, The relative role of PLC beta and PI3K gamma in platelet activation, Blood, 106 (2005) 110-117.

[9] M.J. Berridge, R.F. Irvine, Inositol phosphates and cell signaling, Nature, 341 (1989) 197-205.

[10] Z.Y. Li, M.K. Delaney, K.A. O'Brien, X.P. Du, Signaling during platelet adhesion and activation, Arteriosclerosis Thrombosis and Vascular Biology, 30 (2010) 2341-2349.

[11] U.S. Bhalla, R. Iyengar, Emergent properties of networks of biological signaling pathways, Science, 283 (1999) 381-387.

[12] J.R. Crittenden, W. Bergmeier, Y.Y. Zhang, C.L. Piffath, Y.Q. Liang, D.D. Wagner, D.E. Housman, A.M. Graybiel, CalDAG-GEFI integrates signaling for platelet aggregation and thrombus formation, Nature Medicine, 10 (2004) 982-986.

[13] L. Stefanini, R.C. Roden, W. Bergmeier, CalDAG-GEFI is at the nexus of calcium-dependent platelet activation, Blood, 114 (2009) 2506-2514.

[14] P. Lova, S. Paganini, E. Hirsch, L. Barberis, M. Wymann, F. Sinigaglia, C. Balduini, M. Torti, A selective role for phosphatidylinositol 3,4,5-trisphosphate in the G(i)-dependent activation of platelet Rap1B, Journal of Biological Chemistry, 278 (2003) 131-138.

[15] Z.Y. Li, G.Y. Zhang, G.C. Le Breton, X.P. Gao, A.B. Malik, X.P. Du, Two waves of platelet secretion induced by thromboxane A(2) receptor and a critical role for phosphoinositide 3-kinases, Journal of Biological Chemistry, 278 (2003) 30725-30731.

[16] A. Garcia, S. Kim, K. Bhavaraju, S.M. Schoenwaelder, S.P. Kunapuli, Role of phosphoinositide 3-kinase beta in platelet aggregation and thromboxane A(2) generation mediated by G(i) signalling pathways, Biochemical Journal, 429 (2010) 369-377.

[17] A. Smolenski, Novel roles of cAMP/cGMP-dependent signaling in platelets, Journal of Thrombosis and Haemostasis, 10 (2012) 167-176.

[18] R. Opara, D.L. Robbins, V.A. Ziboh, Cyclic-AMP agonists inhibit antiphospholipid/beta(2)-glycoprotein I induced synthesis of human platelet thromboxane A(2) in vitro, Journal of Rheumatology, 30 (2003) 55-59.

[19] S.M. Schoenwaelder, A. Ono, S. Sturgeon, S.M. Chan, P. Mangin, M.J. Maxwell, S. Turnbull, M. Mulchandani, K. Anderson, G. Kauffenstein, G.W. Rewcastle, J. Kendall, C. Gachet, H.H. Salem, S.P. Jackson, Identification of a unique co-operative phosphoinositide 3-kinase signaling mechanism regulating integrin alpha(IIb)beta(3) adhesive function in platelets, Journal of Biological Chemistry, 282 (2007) 28648-28658.

[20] B.B. Dawood, J. Wilde, S.P. Watson, Reference curves for aggregation and ATP secretion to aid diagnose of platelet-based bleeding disorders: Effect of inhibition of ADP and thromboxane A(2) pathways, Platelets, 18 (2007) 329-345.

[21] M. Hamberg, J. Svensson, B. Samuelsson, Thromboxanes - new group of biologically-active compounds derived from prostaglandin endoperoxides, Proceedings of the National Academy of Sciences of the United States of America, 72 (1975) 2994-2998.

[22] G. Hoffmann, B.O. Gobel, U. Harbrecht, H. Vetter, R. Dusing, Platelet cAMP and cGMP in essential-hypertension, American Journal of Hypertension, 5 (1992) 847-850.

[23] M. Hillbom, J. Neiman, Platelet thromboxane formation capacity after ethanol withdrawal in chronic-alcoholics, Haemostasis, 18 (1988) 170-178.

[24] T.C. Detwiler, T.P. McDonald, T.T. Odell, Platelet size, ATP content, and clot retraction in relation to platelet age, American Journal of Physiology, 203 (1962) 107-&.

[25] P. Harrison, B. Wilbourn, N. Debili, W. Vainchenker, J. Bretongorius, A.S. Lawrie, J.M. Masse, G.F. Savidge, E.M. Cramer, Uptake of plasma-fibrinogen into the alpha-granules of human megakaryocytes and platelets, Journal of Clinical Investigation, 84 (1989) 1320-1324.

[26] A.L. Kuharsky, A.L. Fogelson, Surface-mediated control of blood coagulation: The role of binding site densities and platelet deposition, Biophysical Journal, 80 (2001) 1050-1074.

[27] E.N. Sorensen, G.W. Burgreen, W.R. Wagner, J.F. Antaki, Computational simulation of platelet deposition and activation: II. Results for Poiseuille flow over collagen, Annals of Biomedical Engineering, 27 (1999) 449-458.

[28] E.N. Sorensen, G.W. Burgreen, W.R. Wagner, J.F. Antaki, Computational simulation of platelet deposition and activation: I. Model development and properties, Annals of Biomedical Engineering, 27 (1999) 436-448.

[29] F. Storti, T.H.S. van Kempen, F.N. van de Vosse, A continuum model for platelet plug formation and growth, International Journal for Numerical Methods in Biomedical Engineering, 30 (2014) 634-658.

[30] Z.L. Xu, J. Lioi, J. Mu, M.M. Kamocka, X.M. Liu, D.Z. Chen, E.D. Rosen, M. Alber, A multiscale model of venous thrombus formation with surface-mediated control of blood coagulation cascade, Biophysical Journal, 98 (2010) 1723-1732.

[31] Z.L. Xu, N. Chen, M.M. Kamocka, E.D. Rosen, M. Alber, A multiscale model of thrombus development, Journal of the Royal Society Interface, 5 (2008) 705-722.

[32] M.H. Flamm, T.V. Colace, M.S. Chatterjee, H.Y. Jing, S.T. Zhou, D. Jaeger, L.F. Brass, T. Sinno, S.L. Diamond, Multiscale prediction of patient-specific platelet function under flow, Blood, 120 (2012) 190-198.

[33] M.U. Naik, T.J. Stalker, L.F. Brass, U.P. Naik, JAM-A protects from thrombosis by suppressing integrin alpha(IIb)beta(3)-dependent outside-in signaling in platelets, Blood, 119 (2012) 3352-3360.

[34] T.J. Stalker, E.A. Traxler, J. Wu, K.M. Wannemacher, S.L. Cermignano, R. Voronov, S.L. Diamond, L.F. Brass, Hierarchical organization in the hemostatic response and its relationship to the platelet-signaling network, Blood, 121 (2013) 1875-1885.

[35] K.B. Neeves, S.F. Maloney, K.P. Fong, A.A. Schmaier, M.L. Kahn, L.F. Brass, S.L. Diamond, Microfluidic focal thrombosis model for measuring murine platelet deposition and stability: PAR4 signaling enhances shear-resistance of platelet aggregates, Journal of Thrombosis and Haemostasis, 6 (2008) 2193-2201.

[36] H.X. Gong, B. Shen, P. Flevaris, C. Chow, S.C.T. Lam, T.A. Voyno-Yasenetskaya, T. Kozasa, X.P. Du, G Protein Subunit G alpha(13) Binds to Integrin alpha(IIb)beta(3) and Mediates Integrin "Outside-In" Signaling, Science, 327 (2010) 340-343.

[37] J.H. Morrissey, B.G. Macik, P.F. Neuenschwander, P.C. Comp, Quantitation of activated factor-VII levels in plasma using a tissue factor mutant selectively deficient in promoting factor-VII activation, Blood, 81 (1993) 734-744.

[38] K.G. Mann, M.E. Nesheim, W.R. Church, P. Haley, S. Krishnaswamy, Surface-dependent reactions of the vitamin-K-dependent enzyme complexes, Blood, 76 (1990) 1-16.

[39] S. Butenas, K.G. Mann, Kinetics of human factor VII activation, Biochemistry, 35 (1996) 1904-1910.

[40] D.D. Monkovic, P.B. Tracy, Activation of human factor-V by factor-Xa and thrombin, Biochemistry, 29 (1990) 1118-1128.

[41] D.C. Hilleubanks, P. Lollar, Von Willebrand factor is a cofactor for thrombin-catalyzed cleavage of the factor-VIII light chain, Journal of Biological Chemistry, 265 (1990) 17854-17858.

[42] P. Lollar, G.J. Knutson, D.N. Fass, Activation of porcine factor-VIII-C by thrombin and factor Xa, Biochemistry, 24 (1985) 8056-8064.

[43] D. Gailani, G.J. Broze, Factor-XI activation in a revised model of blood coagulation, Science, 253 (1991) 909-912.

[44] J.A. Oliver, D.M. Monroe, H.R. Roberts, M. Hoffman, Thrombin activates factor XI on activated platelets in the absence of factor XII, Arteriosclerosis Thrombosis and Vascular Biology, 19 (1999) 170-177.

[45] E.A. Vogler, C.A. Siedlecki, Contact activation of blood-plasma coagulation, Biomaterials, 30 (2009) 1857-1869.

[46] C.F. Scott, R.W. Colman, Fibrinogen blocks the autoactivation and thrombin-mediated activation of factor-XI on dextran sulfate, Proceedings of the National Academy of Sciences of the United States of America, 89 (1992) 11189-11193.

[47] P.N. Walsh, H. Bradford, D. Sinha, J.R. Piperno, G.P. Tuszynski, Kinetics of the factor XIa catalyzed activation of human-blood coagulation factor-IX, Journal of Clinical Investigation, 73 (1984) 1392-1399.

[48] M.E. Nesheim, J.B. Taswell, K.G. Mann, Contribution of bovine factor-V and factor-Va to the activity of prothrombinase, Journal of Biological Chemistry, 254 (1979) 952-962.

[49] W.A. Wuillemin, E. Eldering, F. Citarella, C.P. deRuig, H. tenCate, C.E. Hack, Modulation of contact system proteases by glycosaminoglycans - Selective enhancement of the inhibition of factor XIa, Journal of Biological Chemistry, 271 (1996) 12913-12918.

[50] N. Brufatto, M.E. Nesheim, The use of prothrombin(S525C) labeled with fluorescein to directly study the inhibition of prothrombinase by antithrombin during prothrombin activation, Journal of Biological Chemistry, 276 (2001) 17663-17671.

[51] I. Takahashi, K. Kato, I. Sugiura, J. Takamatsu, T. Kamiya, H. Saito, Activated factor-IX antithrombin-III complexes in human blood - quantification by an enzyme-linked differential antibody immunoassay and determination of the in vivo half-life, Journal of Laboratory and Clinical Medicine, 118 (1991) 317-325.

[52] J. Jesty, T.C. Wun, A. Lorenz, Kinetics of the inhibition of factor Xa and the tissue factor-factor VIIa complex by the tissue factor pathway inhibitor in the presence and absence of heparin, Biochemistry, 33 (1994) 12686-12694.

[53] X. Huang, R. Swanson, G.J. Broze, S.T. Olson, Kinetic Characterization of the protein Z-dependent protease inhibitor reaction with blood coagulation factor Xa, Journal of Biological Chemistry, 283 (2008) 29770-29783.

[54] X. Huang, Y.H. Yan, Y.Z. Tu, J. Gatti, G.J. Broze, A.W. Zhou, S.T. Olson, Structural basis for catalytic activation of protein Z-dependent protease inhibitor (ZPI) by protein Z, Blood, 120 (2012) 1726-1733.

[55] B. Dahlback, B.O. Villoutreix, The anticoagulant protein C pathway, Febs Letters, 579 (2005) 3310-3316.

[56] P. Blair, R. Flaumenhaft, Platelet alpha-granules: Basic biology and clinical correlates, Blood Reviews, 23 (2009) 177-189.

[57] S. Zhu, R.J. Travers, J.H. Morrissey, S.L. Diamond, FXIa and platelet polyphosphate as therapeutic targets during human blood clotting on collagen/tissue factor surfaces under flow, Blood, 126 (2015) 1494-1502.

[58] M.F. Hockin, K.C. Jones, S.J. Everse, K.G. Mann, A model for the stoichiometric regulation of blood coagulation, Journal of Biological Chemistry, 277 (2002) 18322-18333.

[59] M.S. Chatterjee, W.S. Denney, H.Y. Jing, S.L. Diamond, Systems biology of coagulation initiation: kinetics of thrombin generation in resting and activated human blood, Plos Computational Biology, 6 (2010) 24.

[60] C.M. Danforth, T. Orfeo, S.J. Everse, K.G. Mann, K.E. Brummel-Ziedins, Defining the boundaries of normal thrombin generation: investigations into hemostasis, Plos One, 7 (2012) 12.

[61] M.A. Panteleev, M.V. Ovanesov, D.A. Kireev, A.M. Shibeko, E.I. Sinauridze, N.M. Ananyeva, A.A. Butylin, E.L. Saenko, F.I. Ataullakhanov, Spatial propagation and localization of blood coagulation are regulated by intrinsic and protein C pathways, respectively, Biophysical Journal, 90 (2006) 1489-1500.

[62] M. Anand, K. Rajagopal, K.R. Rajagopal, A model for the formation, growth, and lysis of clots in quiescent plasma. A comparison between the effects of antithrombin III deficiency and protein C deficiency, Journal of Theoretical Biology, 253 (2008) 725-738.

[63] R. Burghaus, K. Coboeken, T. Gaub, L. Kuepfer, A. Sensse, H.U. Siegmund, W. Weiss, W. Mueck, J. Lippert, Evaluation of the efficacy and safety of rivaroxaban using a computer model for blood coagulation, Plos One, 6 (2011) 13.

[64] A.L. Fogelson, N. Tania, Coagulation under flow: the influence of flow-mediated transport on the initiation and inhibition of coagulation, Pathophysiology of Haemostasis and Thrombosis, 34 (2005) 91-108.

[65] A.L. Fogelson, Y.H. Hussain, K. Leiderman, Blood clot formation under flow: the importance of factor XI depends strongly on platelet count, Biophysical Journal, 102 (2012) 10-18.

[66] M.E. Nesheim, R.P. Tracy, K.G. Mann, CLOTSPEED, a mathematical simulation of the functional-properties of prothrombinase, Journal of Biological Chemistry, 259 (1984) 1447-1453.

[67] K.C. Jones, K.G. Mann, A model for the tissue factor pathway to thrombin 2: a mathematical simulation, Journal of Biological Chemistry, 269 (1994) 23367-23373.

[68] M.W. Mosesson, Antithrombin I. Inhibition of thrombin generation in plasma by fibrin formation, Thrombosis and Haemostasis, 89 (2003) 9-12.

[69] X. Han, R. Fiehler, G.J. Broze, Isolation of a protein Z-dependent plasma protease inhibitor, Proceedings of the National Academy of Sciences of the United States of America, 95 (1998) 9250-9255.

[70] R.S. Voronov, T.J. Stalker, L.F. Brass, S.L. Diamond, Simulation of Intrathrombus fluid and solute transport using in vivo clot structures with single platelet resolution, Annals of Biomedical Engineering, 41 (2013) 1297-1307.

[71] E.A. Shavlyugin, L.G. Hanin, M.A. Khanin, Dynamics of pathologic clot formation: a mathematical model, Journal of Theoretical Biology, 340 (2014) 96-104.

[72] J.H. Morrissey, S.H. Choi, S.A. Smith, Polyphosphate: an ancient molecule that links platelets, coagulation, and inflammation, Blood, 119 (2012) 5972-5979.

[73] S.A. Smith, N.J. Mutch, D. Baskar, P. Rohloff, R. Docampo, J.H. Morrissey, Polyphosphate modulates blood coagulation and fibrinolysis, Proceedings of the National Academy of Sciences of the United States of America, 103 (2006) 903-908.

[74] G.M. Willems, M.P. Janssen, I. Salemink, T.C. Wun, T. Lindhout, Transient high affinity binding of tissue factor pathway inhibitor-factor Xa complexes to negatively charged phospholipid membranes, Biochemistry, 37 (1998) 3321-3328.

[75] A. Kramoroff, J.M. Nigretto, In vitro factor XI activation mechanism according to an optimized model of activated partial thromboplastin time test, Blood Coagulation & Fibrinolysis, 12 (2001) 289-299.

[76] T.R. Baird, P.N. Walsh, The interaction of factor XIa with activated platelets but not endothelial cells promotes the activation of factor IX in the consolidation phase of blood coagulation, Journal of Biological Chemistry, 277 (2002) 38462-38467.

[77] L. Bolkun, M. Galar, J. Piszcz, D. Lemancewicz, J. Kloczko, Plasma concentration of protein Z and protein Z-dependent protease inhibitor in patients with haemophilia A, Thrombosis Research, 131 (2013) E110-E113.

[78] M. Makris, Is VIII worse than IX?, Blood, 114 (2009) 750-751.

[79] G. Tagariello, A. Iorio, E. Santagostino, M. Morfini, R. Bisson, M. Innocenti, M.E. Mancuso, M.G. Mazzucconi, G.L. Pasta, P. Radossi, G. Rodorigo, C. Santoro, R. Sartori, A. Scaraggi, L.P. Solimeno, P.M. Mannucci, A. Italian Assoc Hemophilia Ctr, Comparison of the rates of joint arthroplasty in patients with severe factor VIII and IX deficiency: an index of different clinical severity of the 2 coagulation disorders, Blood, 114 (2009) 779-784.

[80] P. Damman, P. Woudstra, W.J. Kuijt, R.J. de Winter, S.K. James, P2Y12 platelet inhibition in clinical practice, Journal of Thrombosis and Thrombolysis, 33 (2012) 143-153.

[81] R.Z. Li, S.L. Diamond, Detection of platelet sensitivity to inhibitors of COX-1, P2Y(1), and P2Y(12) using a whole blood microfluidic flow assay, Thrombosis Research, 133 (2014) 203-210.

[82] A. Natarajan, A.G. Zaman, S.M. Marshall, Platelet hyperactivity in type 2 diabetes: role of antiplatelet agents, Diabetes & Vascular Disease Research, 5 (2008) 138-144.

[83] G.N. Pandey, X.G. Ren, S.C. Pandey, Y. Dwivedi, R. Sharma, P.G. Janicak, Hyperactive phosphoinositide signaling pathway in platelets of depressed patients: effect of desipramine treatment, Psychiatry Research, 105 (2001) 23-32.

[84] I. Martinelli, V. De Stefano, P.M. Mannucci, Inherited risk factors for venous thromboembolism, Nature Reviews Cardiology, 11 (2014) 140-156.

[85] A.B. Payne, C.H. Miller, F.M. Kelly, J.M. Soucie, W.C. Hooper, The CDC Hemophilia A Mutation Project (CHAMP) mutation list: a new online resource, Human Mutation, 34 (2013) E2382-E2391.

[86] T.G. Li, C.H. Miller, J. Driggers, A.B. Payne, D. Ellingsen, W.C. Hooper, Mutation analysis of a cohort of US patients with hemophilia B, American Journal of Hematology, 89 (2014) 375-379.

[87] A.A. Onasoga-Jarvis, K. Leiderman, A.L. Fogelson, M. Wang, M.J. Manco-Johnson, J.A. Di Paola, K.B. Neeves, The effect of factor VIII deficiencies and replacement and bypass therapies on thrombus formation under venous flow conditions in microfluidic and computational models, Plos One, 8 (2013) 12.

[88] L. Kahanov, L. Eberman, S. Grammer, Diagnosis and Treatment of Idiopathic Thrombocytopenic Purpura, International Journal of Athletic Therapy & Training, 17 (2012) 25-28.

[89] R. Stasi, M.L. Evangelista, E. Stipa, F. Buccisano, A. Venditti, S. Amadori, Idiopathic thrombocytopenic purpura: current concepts in pathophysiology and management, Thromb Haemost, 99 (2008) 4-13.

[90] M. Schipperus, R. Fijnheer, New therapeutic options for immune thrombocytopenia, Neth J Med, 69 (2011) 480-485.

[91] R. Stasi, Immune thrombocytopenic purpura: the treatment paradigm, European Journal of Haematology, 82 (2009) 13-19.

[92] J.B. Segal, N.R. Powe, Prevalence of immune thrombocytopenia: analyses of administrative data, Journal of Thrombosis and Haemostasis, 4 (2006) 2377-2383.

[93] C.-H. Tsai, J.B. Bussel, A.A. Imahiyerobo, S.I. Sandler, B.A. Ogunnaike, Platelet count control in immune thrombocytopenic purpura patient: Optimum romiplostim dose profile, Journal of Process Control, 45 (2016) 76-83

[94] S. Jeanpierre, F.E. Nicolini, B. Kaniewski, C. Dumontet, R. Rimokh, A. Puisieux, V. Maguer-Satta, BMP4 regulation of human megakaryocytic differentiation is involved in thrombopoietin signaling, Blood, 112 (2008) 3154-3163.

[95] I. Matsumura, Y. Kanakura, Molecular control of megakaryopoiesis and thrombopoiesis, International Journal of Hematology, 75 (2002) 473-483.

[96] E.M. Wolber, W. Jelkmann, Thrombopoietin: the novel hepatic hormone, News Physiol Sci, 17 (2002) 6-10.

[97] Y.M.C. Wang, W. Krzyzanski, S. Doshi, J.J. Xiao, J.J. Perez-Ruixo, A.T. Chow, Pharmacodynamics-mediated drug disposition (PDMDD) and precursor pool lifespan model for single dose of romiplostim in healthy subjects, AAPS Journal, 12 (2010) 729-740.

[98] D.J. Kuter, T.B. Gernsheimer, Thrombopoietin and platelet production in chronic immune thrombocytopenia, Hematol Oncol Clin North Am, 23 (2009) 1193-1211.

[99] D.J. Kuter, The physiology of platelet production, Stem Cells, 14 Suppl 1 (1996) 88-101.

[100] B. Wang, J.L. Nichol, J.T. Sullivan, Pharmacodynamics and pharmacokinetics of AMG 531, a novel thrombopoietin receptor ligand, Clinical Pharmacology & Therapeutics, 76 (2004) 628-638.

[101] Y.M.C. Wang, B. Sloey, T. Wong, P. Khandelwal, R. Melara, Y.N. Sun, Investigation of the pharmacokinetics of romiplostim in rodents with a focus on the clearance mechanism, Pharmaceutical Research, 28 (2011) 1931-1938.

[102] S. Panzer, New therapeutic options for adult chronic immune thrombocytopenic purpura: a brief review, Vox Sanguinis, 94 (2008) 1-5.

[103] O. Meyer, E. Herzig, A. Salama, Platelet Kinetics in Idiopathic Thrombocytopenic purpura patients treated with thrombopoietin receptor agonists, transfusion medicine and hemotherapy, 39 (2012) 5-8.

[104] F. Palandri, N. Polverelli, F. Lifrieri, L. Catani, M.B. Giannini, M. Baccarani, N. Vianelli, Romiplostim as early treatment of immune thrombocytopenia with severe immunodeficiency, Hematology reports, 4 (2012).

[105] J.B. Bussel, D.J. Kuter, J.N. George, R. McMillan, L.M. Aledort, G.T. Conklin, A.E. Lichtin, R.M. Lyons, J. Nieva, J.S. Wasser, I. Wiznitzer, R. Kelly, C.F. Chen, J.L. Nichol, AMG 531, a thrombopoiesis-stimulating protein, for chronic ITP, New England Journal of Medicine, 355 (2006) 1672-1681.

[106] J.J. Perez-Ruixo, B. Green, S. Doshi, Y.M. Wang, D.R. Mould, Romiplostim dose response in patients with immune thrombocytopenia, Journal of Clinical Pharmacology, 52 (2012) 1540-1551.

[107] F.J. Doyle, J. Stelling, Systems interface biology, Journal of the Royal Society Interface, 3 (2006) 603-616.

[108] L.A. Harker, L.K. Roskos, U.M. Marzec, R.A. Carter, J.K. Cherry, B. Sundell, E.N. Cheung, D. Terry, W. Sheridan, Effects of megakaryocyte growth and development factor on platelet production, platelet life span, and platelet function in healthy human volunteers, Blood, 95 (2000) 2514-2522.

[109] S. Thota, G. Kistangari, H. Daw, T. Spiro, Immune thrombocytopenia in adults: An update, Cleveland Clinic journal of medicine, 79 (2012).

[110] G.M. Steil, A.E. Panteleon, K. Rebrin, Closed-loop insulin delivery - the path to physiological glucose control, Advanced Drug Delivery Reviews, 56 (2004) 125-144.

[111] A.N. Balandina, A.M. Shibeko, D.A. Kireev, A.A. Novikova, Shmirev, II, M.A. Panteleev, F.I. Ataullakhanov, Positive feedback loops for factor V and factor VII activation supply sensitivity to local surface tissue factor density during blood coagulation, Biophysical Journal, 101 (2011) 1816-1824.

[112] S. Park, S.S. Yoon, J.H. Lee, J.S. Park, J.H. Jang, J.W. Lee, Multicenter, prospective study to evaluate the efficacy of biweekly romiplostim administration in patients with immune thrombocytopenia, International Journal of Hematology, 103 (2016) 44-52.

[113] M.S. Chatterjee, J.E. Purvis, L.F. Brass, S.L. Diamond, Pairwise agonist scanning predicts cellular signaling responses to combinatorial stimuli, Nature Biotechnology, 28 (2010) 727-U1737.

[114] D.E. Mager, W. Krzyzanski, Quasi-equilibrium pharmacokinetic model for drugs exhibiting target-mediated drug disposition, Pharmaceutical Research, 22 (2005) 1589-1596.

Appendix A

LIST OF PARAMETERS IN THE SINGLE PLATELET MODEL

Table A.1. List of parameters used for sensitivity analysis of the single platelet model

Parameter index	Related regulatory event	Notation	Description
1	inhibition	$PGI2_i$	initial concentration of PGI2
2	inhibition	NO_i	initial concentration of NO
3	aggregation	PLT	initial platelet concentration
4	aggregation; outside-in signaling	Fg	fibrinogen concentration
5	P2Y1-induced Gq activation	β	rate constant of Gq activation induced by P2Y1
6	P2Y1-induced Gq activation	n	Hill coefficient for Gq activation induced by P2Y1
7	P2Y1-induced Gq activation	a	affinity constant for Gq activation induced by P2Y1
8	P2Y1-induced Gq activation	k	rate constant of degradation of Gq
9	P2Y12-induced Gi activation	β	rate constant of Gq activation induced by P2Y12
10	P2Y12-induced Gi activation	n	Hill coefficient for Gq activation induced by P2Y12
11	P2Y12-induced Gi activation	a	affinity constant for Gq activation induced by P2Y12
12	P2Y12-induced Gi activation	k	rate constant of degradation of Gi
13	TxA2-induced Gq and G13activation	k	rate constant of degradation of G13
14	TxA2-induced Gq and G13activation	β	rate constant of Gq activation induced by TxA2 receptor
15	TxA2-induced Gq and G13activation	n	Hill coefficient for Gq activation induced by TxA2 receptor

Table A.1 continued.

16	TxA2-induced Gq and G13activation	a	affinity constant for Gq activation induced by TxA2 receptor
17	TxA2-induced Gq and G13activation	β	rate constant of G13 activation induced by TxA2 receptor
18	TxA2-induced Gq and G13activation	n	Hill coefficient for G13 activation induced by TxA2 receptor
19	TxA2-induced Gq and G13activation	a	affinity constant for G13 activation induced by TxA2 receptor
20	PGI2-induced Gs activation	k	rate constant of degradation of Gs
21	PLCβ activation	k_1	binding of PLCβ to GqGTP
22	PLCβ activation	k_{-1}	dissociation of PLCβ*GqGTP
23	PLCβ activation	k_{cat}	deactivation of PLCβ*GqGTP
24	PLCβ activation	k_1	dissociation of PLCβGqGDP
25	PLCβ activation	k_{-1}	binding of PLCβ to GqGDP
26	PI3K activation by inside-out signaling	β	rate constant of PI3K activation induced by GiGTP
27	PI3K activation by inside-out signaling	β	rate constant of PI3K activation induced by G13GTP
28	PI3K activation by inside-out signaling	k	rate constant of degradation of PI3K
29	PI3K activation by inside-out signaling	n	Hill coefficient for PI3K activation induced by Gi
30	PI3K activation by inside-out signaling	a	affinity constant for PI3K activation induced by Gi
31	PI3K activation by inside-out signaling	n	Hill coefficient for PI3K activation induced by G13
32	PI3K activation by inside-out signaling	a	affinity constant for PI3K activation induced by G13
33	RhoA activation	β	rate constant of RhoA activation
34	RhoA activation	k	rate constant of degradation of RhoA
35	RhoA activation	n	Hill coefficient for RhoA activation
36	RhoA activation	a	affinity constant for RhoA activation
37	AC regulation	k	activation of AC by GsGTP
38	AC regulation	β	rate constant of AC* deactivation by Gi
39	AC regulation	k	deactivation of AC

Table A.1 continued.

40	AC regulation	n	Hill coefficient for AC* deactivation by Gi
41	AC regulation	a	affinity constant for AC* deactivation by Gi
42	NO-induced cGMP production	k	rate constant of degradation of cGMP
43	DAG production and IP3 formation	k_1	binding of PLCβ* to PI
44	DAG production and IP3 formation	k_{-1}	dissociation of PLCβ*PI
45	DAG production and IP3 formation	k_{cat}	rate constant of production of PIP and DAG
46	DAG production and IP3 formation	k_1	binding of PLCβ* to PIP
47	DAG production and IP3 formation	k_{-1}	dissociation of PLCβ*PIP
48	DAG production and IP3 formation	k_{cat}	rate constant of production of PIP2, IP3, and DAG
49	DAG production and IP3 formation	k_1	binding of PLCβ* to PIP2
50	DAG production and IP3 formation	k_{-1}	dissociation of PLCβ*PIP2
51	DAG production and IP3 formation	k_{cat}	rate constant of production of PIP3 and DAG
52	DAG production and IP3 formation	k_{cat}	rate constant of degradation of DAG by DGK
53	DAG production and IP3 formation	K_M	equilibrium constant of binding DAG and DGK
54	DAG production and IP3 formation	k	rate constant of degradation of IP3
55	DAG production and IP3 formation	k	rate constant of degradation of DAG
56	cAMP regulation	β	rate constant of cAMP production induced by AC
57	cAMP regulation	a	affinity constant for cAMP production induced by AC
58	cAMP regulation	n	Hill coefficient for cAMP production induced by AC
59	cAMP regulation	k	rate constant of cAMP production induced by cGMP

Table A.1 continued.

60	cAMP regulation	k	rate constant of degradation of cAMP
61	calcium release	β	rate constant of calcium increase induced by IP3
62	calcium release	n	Hill coefficient for calcium increase induced by IP3
63	calcium release	a	affinity constant for calcium increase induced by IP3
64	calcium release	k	rate constant of calcium consumption
65	calcium release	k	rate constant of calcium increase induced by cAMP
66	PKC and CalDAGGEF activation	k_1	rate constant of PKC activation induced by Ca2+
67	PKC and CalDAGGEF activation	k_{-1}	rate constant of calcium-related deactivation of PKC*
68	PKC and CalDAGGEF activation	k_1	rate constant of PKC activation induced by Ca2+ and DAG
69	PKC and CalDAGGEF activation	k_{-1}	rate constant of deactivation of PKC* related to calcium and DAG
70	PKC and CalDAGGEF activation	β	rate constant of CalDAGGEF activation
71	PKC and CalDAGGEF activation	k	rate constant of degradation of CalDAGGEF
72	PKC and CalDAGGEF activation	n	Hill coefficient for CalDAGGEF activation
73	PKC and CalDAGGEF activation	a	affinity constant for CalDAGGEF activation
74	dense granule secretion	n	Hill coefficient for the effect of RhoA on dense granule secretion
75	dense granule secretion	a	affinity constant for the effect of RhoA on dense granule secretion
76	dense granule secretion	k	rate constant for the consumption of ATP
77	dense granule secretion	k	rate constant for the release of dense granules
78	Rap1 activation	β	rate constant of Rap1 activation by PI3K
79	Rap1 activation	n	Hill coefficient for Rap1 activation by PI3K

Table A.1 continued.

80	Rap1 activation	a	affinity constant for Rap1 activation by PI3K
81	Rap1 activation	k	rate constant of degradation of Rap1
82	Rap1 activation	k	rate constant of Rap1 activation by PI3K and CalDAGGEF
83	integrin activation	β	rate constant of integrin activation by Rap1 and PKC*
84	integrin activation	n	not considered in the equation
85	integrin activation	a	not considered in the equation
86	integrin activation	k	rate constant of integrin deactivation
87	platelet aggregation	k_1	rate constant of platelet aggregation
88	platelet aggregation	k_{-1}	rate constant of disaggregation
89	outside-in signaling	k	rate constant of activation of outside-in signaling
90	outside-in signaling	k	rate constant of consumption of outside-in signaling
91	PLCγ activation	n	Hill coefficient for PLCγ activation by outside-in signaling
92	PLCγ activation	a	affinity constant for PLCγ activation by outside-in signaling
93	PLCγ activation	β	rate constant of PLCγ activation by outside-in signaling
94	PLCγ activation	k	rate constant of deactivation of PLCγ
95	PI3K activation by outside-in signaling	n	Hill coefficient for PI3K activation by outside-in signaling
96	PI3K activation by outside-in signaling	a	affinity constant for PI3K activation by outside-in signaling
97	PI3K activation by outside-in signaling	β	rate constant of PI3K activation by outside-in signaling
98	PI3K activation by outside-in signaling	k	rate constant of deactivation of PI3K
99	PLA activation	β	rate constant of PLA activation by outside-in signaling
100	PLA activation	n	Hill coefficient for PLA activation by outside-in signaling
101	PLA activation	a	affinity constant for PLA activation by outside-in signaling
102	PLA activation	k	rate constant of deactivation of PLA

Table A.1 continued.

103	TxA2 synthesis	[COX]	concentration of COX, which synthesizes TxA2; the effect is combined with the rate constants β
104	TxA2 synthesis	k	rate constant of consumption of TxA2
105	TxA2 synthesis	β	rate constant of TxA2 production independent of PI3K
106	TxA2 synthesis	n	Hill coefficient for the effect of PLA on TxA2 production
107	TxA2 synthesis	a	affinity constant for the effect of PLA on TxA2 production
108	TxA2 synthesis	β	rate constant of TxA2 production dependent of PI3K
109	TxA2 synthesis	n	Hill coefficient for the effect of cAMP on TxA2 production
110	TxA2 synthesis	a	affinity constant for the effect of cAMP on TxA2 production

Appendix B

EQUATIONS AND PARAMETER VALUES IN THE SECONDARY HEMOSTASIS MODEL

B.1 List of Equations in the Updated Secondary Hemostasis Model.

$$\frac{dz_2}{dt} = -k_2^{on} z_2 P_2 + k_2^{off} z_2^m + k_{flow}^c \left(z_2^{out} - z_2\right) - k_2^{scat} z_2 \left(e_{10} + e_{10}^m\right) \tag{B.1}$$

$$\frac{dP_2}{dt} = \frac{d}{dt}\begin{pmatrix} p_2 - z_2^m - [Z_2^m : PRO] - e_2^m - [Z_5^m : E_2^m] \\ -[Z_8^m : E_2^m] - [Z_{11}^m : E_2^m] - [ATIII : E_2^m] \end{pmatrix} \tag{B.2}$$

$$\begin{aligned} \frac{de_2}{dt} = & -k_2^{on} e_2 P_2 \\ & + k_2^{off} e_2^m + \left(k_3^- + k_3^{cat}\right)[Z_7^m : E_2] - k_3^+ z_7^m e_2 \\ & + \left(k_{12}^- + k_{12}^{cat}\right)[Z_5 : E_2] - k_{12}^+ z_5 e_2 + \left(k_{18}^- + k_{18}^{cat}\right)[Z_7 : E_2] \\ & - k_{18}^+ z_7 e_2 + \left(k_{14}^- + k_{14}^{cat}\right)[Z_8 : E_2] - k_{14}^+ z_8 e_2 \\ & - k_{flow}^c e_2 - k_2^{in} e_2 \\ & - k_{10}^+ [Fg] e_2 + \left(k_{10}^- + k_{10}^{cat}\right)[Fg : E_2] \\ & - k_{11}^+ [Fbn1] e_2 + \left(k_{11}^- + k_{11}^{cat}\right)[Fbn1 : E_2] - k_{19}^+ [(Fbn1)_2] e_2 \\ & + \left(k_{19}^- + k_{19}^{cat}\right)[(Fbn1)_2 : E_2] - k_5^b [Fbn2] e_2 + k_5^{ub} [Fbn2 : E_2] \\ & - k_{20}^+ z_{11} e_2 + (k_{20}^- + k_{20}^{cat})[Z_{11} : E_2] + k_2^{scat} z_2 \left(e_{10} + e_{10}^m\right) \\ & + k_{20}^{cat} [Z_{11} : E_2][polyP] + k_{12}^{cat} [Z_5 : E_2][polyP] \end{aligned} \tag{B.3}$$

$$\frac{dz_2^m}{dt} = k_2^{on} z_2 P_2$$
$$- k_2^{off} z_2^m - k_7^+ z_2^m [PRO] + k_7^- [Z_2^m : PRO]$$
$$- k_2^{scat} z_2^m \left(e_{10} + e_{10}^m \right) - \frac{\frac{dPLT_{disagg}}{dt}}{PLT_{col} + PLT_{sec} + \varepsilon} z_2^m \qquad \text{(B.4)}$$

$$\frac{de_2^m}{dt} = k_2^{on} e_2 P_2$$
$$- k_2^{off} e_2^m + k_7^{cat} [Z_2^m : PRO]$$
$$+ \left(k_{13}^- + k_{13}^{cat} \right) [Z_5^m : E_2^m] - k_{13}^+ z_5^m e_2^m + \left(k_{15}^- + k_{15}^{cat} \right) [Z_8^m : E_2^m] - k_{15}^+ z_8^m e_2^m$$
$$- k_{23}^+ z_{11}^m e_2^m + \left(k_{23}^- + k_{23}^{cat} \right) [Z_{11}^m : E_2^m] \qquad \text{(B.5)}$$
$$- k_6^{in} [ATIII] e_2^m + k_2^{scat} z_2^m \left(e_{10} + e_{10}^m \right)$$
$$+ k_{13}^{cat} [Z_5^m : E_2^m][polyP] + k_{23}^{cat} [Z_{11}^m : E_2^m][polyP]$$
$$- \frac{\frac{dPLT_{disagg}}{dt}}{PLT_{col} + PLT_{sec} + \varepsilon} e_2^m$$

$$\frac{dz_5}{dt} = -k_5^{on} z_5 P_5$$
$$+ k_5^{off} z_5^m - k_{12}^+ z_5 e_2 + k_{12}^- [Z_5 : E_2]$$
$$+ R_{FV,plt} + k_{flow}^c \left(z_5^{out} - z_5 \right) \qquad \text{(B.6)}$$
$$- k_3^{scat} \left(e_{10} + e_{10}^m \right) z_5 - k_3^{scat} \left(e_{10} + e_{10}^m \right) z_5 [polyP]$$

$$\frac{dP_5}{dt} = \frac{d}{dt} \begin{pmatrix} p_5 - z_5^m - [Z_5^m : E_2^m] - [Z_5^m : E_{10}^m] - e_5^m - [E_5^m : APC] - [PRO] \\ - [Z_2^m : PRO] - [ATIII : PRO] - e_5^{m,in} \end{pmatrix} \qquad \text{(B.7)}$$

$$\frac{de_5}{dt} = -k_5^{on} e_5 P_5$$
$$+ k_5^{off} e_5^m + k_{12}^{cat}[Z_5 : E_2] - k_{flow}^c e_5$$
$$+ k_3^{scat}\left(e_{10} + e_{10}^m\right) z_5 + k_{12}^{cat}[Z_5 : E_2][polyP] + k_3^{scat}\left(e_{10} + e_{10}^m\right) z_5[polyP] \quad \text{(B.8)}$$

$$\frac{dz_5^m}{dt} = k_5^{on} z_5 P_5$$
$$- k_5^{off} z_5^m - k_5^+ z_5^m e_{10}^m + k_5^-[Z_5^m : E_{10}^m]$$
$$- k_{13}^+ z_5^m e_2^m + k_{13}^-[Z_5^m : E_2^m] - k_3^{scat} e_{10} z_5^m - \frac{\underline{dPLT_{disagg}}}{PLT_{col} + PLT_{sec} + \varepsilon} z_5^m$$
$$- k_3^{scat} e_{10} z_5^m[polyP] \quad \text{(B.9)}$$

$$\frac{de_5^m}{dt} = k_5^{on} e_5 P_5$$
$$- k_5^{off} e_5^m + k_5^{cat}[Z_5^m : E_{10}^m] + k_{13}^{cat}[Z_5^m : E_2^m] + k_{pro}^{ub}[PRO] - k_{pro}^b e_5^m e_{10}^m$$
$$- k_{16}^+[APC] e_5^m + k_{16}^-[APC : E_5^m] + k_3^{scat} z_5^m e_{10} \quad \text{(B.10)}$$
$$+ k_{13}^{cat}[Z_5^m : E_2^m][polyP] + k_5^{cat}[Z_5^m : E_{10}^m][polyP] + k_3^{scat} z_5^m e_{10}[polyP]$$
$$- \frac{\underline{dPLT_{disagg}}}{PLT_{col} + PLT_{sec} + \varepsilon} e_5^m$$

$$\frac{dz_7}{dt} = -k_{7z}^{on} z_7 \begin{pmatrix} [TF] - z_7^m - [Z_7^m : E_{10}] - [Z_7^m : E_2] - e_7^m \\ -[Z_{10} : E_7^m] - [Z_9 : E_7^m] - [TFPI : E_{10} : E_7^m] \end{pmatrix}$$
$$+ k_7^{off} z_7^m - k_1^+ z_7 e_{10} + k_1^-[Z_7 : E_{10}] \quad \text{(B.11)}$$
$$+ k_{18}^-[Z_7 : E_2] + k_{flow}^c\left(z_7^{out} - z_7\right)$$
$$- k_5^{scat} z_7 e_{10}^m - k_6^{scat} z_7 e_7^m$$

$$\frac{de_7}{dt} = -k_7^{on} e_7 \begin{pmatrix} [TF] - z_7^m - [Z_7^m : E_{10}] - [Z_7^m : E_2] - e_7^m \\ -[Z_{10} : E_7^m] - [Z_9 : E_7^m] - [TFPI : E_{10} : E_7^m] \end{pmatrix}$$
$$+ k_7^{off} e_7^m + k_1^{cat} [Z_7 : E_{10}]$$
$$+ k_{18}^{cat} [Z_7 : E_2] + k_{flow}^c \left(e_7^{out} - e_7 \right) \tag{B.12}$$
$$+ k_5^{scat} z_7 e_{10}^m + k_6^{scat} z_7 e_7^m$$

$$\frac{dz_7^m}{dt} = k_{7z}^{on} z_7 \begin{pmatrix} [TF] - z_7^m - [Z_7^m : E_{10}] - [Z_7^m : E_2] - e_7^m \\ -[Z_{10} : E_7^m] - [Z_9 : E_7^m] - [TFPI : E_{10} : E_7^m] \end{pmatrix}$$
$$- k_7^{off} z_7^m - k_2^+ z_7^m e_{10} + k_2^- [Z_7^m : E_{10}] \tag{B.13}$$
$$- k_3^+ z_7^m e_2 + k_3^- [Z_7^m : E_2] - z_7^m \frac{p'}{1-p}$$

$$\frac{de_7^m}{dt} = k_7^{on} e_7 \begin{pmatrix} [TF] - z_7^m - [Z_7^m : E_{10}] - [Z_7^m : E_2] - e_7^m \\ -[Z_{10} : E_7^m] - [Z_9 : E_7^m] - [TFPI : E_{10} : E_7^m] \end{pmatrix}$$
$$- k_7^{off} e_7^m + k_2^{cat} [Z_7^m : E_{10}] + k_3^{cat} [Z_7^m : E_2]$$
$$+ \left(k_8^- + k_8^{cat} \right) [Z_{10} : E_7^m] - k_8^+ z_{10} e_7^m \tag{B.14}$$
$$+ \left(k_9^- + k_9^{cat} \right) [Z_9 : E_7^m] - k_9^+ z_9 e_7^m$$
$$- k_2^b [TFPI : E_{10}] e_7^m + k_2^{ub} [TFPI : E_{10} : E_7^m] - e_7^m \frac{p'}{1-p}$$

$$\frac{dz_8}{dt} = -k_8^{on} z_8 P_8$$
$$+ k_8^{off} z_8^m - k_{14}^+ z_8 e_2 + k_{14}^- [Z_8 : E_2] + k_{flow}^c \left(z_8^{out} - z_8 \right) \tag{B.15}$$
$$- k_4^{scat} \left(e_{10} + e_{10}^m \right) z_8$$

$$\frac{dz_8}{dt} = -k_8^{on} z_8 P_8 + k_8^{off} z_8^m - k_{14}^{+} z_8 e_2 + k_{14}^{-}[Z_8 : E_2] + k_{flow}^{c}\left(z_8^{out} - z_8\right) - k_4^{scat}\left(e_{10} + e_{10}^m\right) z_8 \tag{B.16}$$

$$\frac{dP_8}{dt} = \frac{d}{dt}\begin{pmatrix} p_8 - z_8^m - [Z_8^m : E_{10}^m] - [Z_8^m : E_2^m] - e_8^m - [TEN] - [TEN^*] \\ -[Z_{10}^m : TEN] - [Z_{10}^m : TEN^*] - [APC : E_8^m] - E_8^{m,in} \end{pmatrix} \tag{B.17}$$

$$\frac{de_8}{dt} = -k_8^{on} e_8 P_8 + k_8^{off} e_8^m + k_{14}^{cat}[Z_8 : E_2] - k_{flow}^{c} e_8 + k_4^{scat}\left(e_{10} + e_{10}^m\right) z_8 \tag{B.18}$$

$$\frac{dz_8^m}{dt} = k_8^{on} z_8 P_8 - k_8^{off} z_8^m - k_6^{+} z_8^m e_{10}^m + k_6^{-}[Z_8^m : E_{10}^m] - k_{15}^{+} z_8^m e_2^m + k_{15}^{-}[Z_8^m : E_2^m] - k_4^{scat} z_8^m e_{10} - \frac{\frac{dPLT_{disagg}}{dt}}{PLT_{col} + PLT_{sec} + \varepsilon} z_8^m \tag{B.19}$$

$$\frac{de_8^m}{dt} = k_8^{on} e_8 P_8 - k_8^{off} e_8^m + k_6^{cat}[Z_8^m : E_{10}^m] + k_{15}^{cat}[Z_8^m : E_2^m] + k_{ten}^{ub}[TEN] - k_{ten}^{b} e_8^m e_9^m - k_{17}^{+}[APC] e_8^m + k_{17}^{-}[APC : E_8^m] - k_{ten}^{+} e_8^m e_9^{m,*} + k_{ten}^{-}[TEN^*] + k_4^{scat} z_8^m e_{10} - \frac{\frac{dPLT_{disagg}}{dt}}{PLT_{col} + PLT_{sec} + \varepsilon} e_8^m \tag{B.20}$$

$$\frac{dz_9}{dt} = -k_9^{on} z_9 P_9 + k_9^{off} z_9^m - k_9^+ z_9 e_7^m + k_9^-[Z_9 : E_7^m] + k_{flow}^c \left(z_9^{out} - z_9 \right) - k_{21}^+ e_{11} z_9 + k_{21}^-[E_{11} : Z_9] \tag{B.21}$$

$$\frac{dP_9}{dt} = \frac{d}{dt}\left(p_9 - z_9^m - e_9^m - [TEN] - [Z_{10}^m : TEN] - [Z_9^m : E_{11}^m] \right) \tag{B.22}$$

$$\frac{de_9}{dt} = -k_9^{on} e_9 P_9 + k_9^{off} e_9^m + k_9^{cat}[Z_9 : E_7^m] - k_9^{in} e_9 [ATIII] - k_{flow}^c e_9 - k_9^{on} e_9 \left(p_9^* - e_9^{m,*} - [TEN^*] - [Z_{10}^m : TEN^*] \right) + k_9^{off} e_9^{m,*} + k_{21}^{cat}[E_{11} : Z_9] \tag{B.23}$$

$$\frac{dz_9^m}{dt} = k_9^{on} z_9 P_9 - k_9^{off} z_9^m - k_{24}^+ z_9^m e_{11}^m + k_{24}^-[Z_9^m : E_{11}^m] - \frac{\frac{dPLT_{disagg}}{dt}}{PLT_{col} + PLT_{sec} + \varepsilon} z_9^m \tag{B.24}$$

$$\frac{de_9^m}{dt} = k_9^{on} e_9 P_9 - k_9^{off} e_9^m + k_{ten}^{ub}[TEN] - k_{ten}^b e_8^m e_9^m + k_{nn11}^{cat}[Z_9^m : E_{11}^m] - \frac{\frac{dPLT_{disagg}}{dt}}{PLT_{col} + PLT_{sec} + \varepsilon} e_9^m \tag{B.25}$$

$$\frac{dz_{10}}{dt} = -k_{10}^{on} z_{10} P_{10} + k_{10}^{off} z_{10}^m - k_8^+ z_{10} e_7^m + k_8^-[Z_{10} : E_7^m] + k_{flow}^c \left(z_{10}^{out} - z_{10} \right) \tag{B.26}$$

$$\frac{dP_{10}}{dt} = \frac{d}{dt}\begin{pmatrix} p_{10} - z_{10}^m - [Z_{10}^m : TEN] - [Z_{10}^m : TEN^*] - e_{10}^m \\ -[Z_5^m : E_{10}^m] - [Z_8^m : E_{10}^m] - [PRO] - [Z_2^m : PRO] \\ -[TFPI : E_{10}^m] - [ATIII : E_{10}^m] - [ATIII : PRO] \\ -[ZPI : E_{10}^m] - [ZPIPZ : E_{10}^m] \end{pmatrix} \tag{B.27}$$

$$\begin{aligned} \frac{de_{10}}{dt} &= -k_{10}^{on} e_{10} P_{10} \\ &+ k_{10}^{off} e_{10}^m - k_1^b [TFPI] e_{10} + k_1^{ub} [TFPI : E_{10}] \\ &+ \left(k_1^- + k_1^{cat}\right)[Z_7 : E_{10}] - k_1^+ z_7 e_{10} + k_8^{cat} [Z_{10} : E_7^m] \\ &+ \left(k_2^- + k_2^{cat}\right)[Z_7^m : E_{10}] - k_2^+ z_7^m e_{10} - k_3^{in} e_{10} - k_{flow}^c e_{10} \end{aligned} \tag{B.28}$$

$$\begin{aligned} \frac{dz_{10}^m}{dt} &= k_{10}^{on} z_{10} P_{10} \\ &- k_{10}^{off} z_{10}^m + k_4^- [Z_{10}^m : TEN] - k_4^+ z_{10}^m [TEN] \\ &- k_4^+ z_{10}^m [TEN^*] + k_4^- [Z_{10}^m : TEN^*] - \frac{\frac{dPLT_{disagg}}{dt}}{PLT_{col} + PLT_{sec} + \varepsilon} z_{10}^m \end{aligned} \tag{B.29}$$

$$\begin{aligned} \frac{de_{10}^m}{dt} &= k_{10}^{on} e_{10} P_{10} \\ &- k_{10}^{off} e_{10}^m + \left(k_5^- + k_5^{cat}\right)[Z_5^m : E_{10}^m] - k_5^+ z_5^m e_{10}^m \\ &+ \left(k_6^- + k_6^{cat}\right)[Z_8^m : E_{10}^m] - k_6^+ z_8^m e_{10}^m + k_{pro}^{ub} [PRO] - k_{pro}^b e_5^m e_{10}^m \\ &+ k_4^{cat} [Z_{10}^m : TEN] + k_4^{cat} [Z_{10}^m : TEN^*] \\ &- k_3^b [TFPI] e_{10}^m + k_3^{ub} [TFPI : E_{10}^m] - k_4^{in} [ATIII] e_{10}^m \\ &- k_7^{in} [ZPI] e_{10}^m - k_8^{in} [ZPI : PZ] e_{10}^m - \frac{\frac{dPLT_{disagg}}{dt}}{PLT_{col} + PLT_{sec} + \varepsilon} e_{10}^m \\ &+ k_5^{cat} [Z_5^m : E_{10}^m][polyP] \end{aligned} \tag{B.30}$$

$$\frac{d[TEN]}{dt} = k_{ten}^{b} e_8^m e_9^m - k_{ten}^{ub}[TEN] + \left(k_4^- + k_4^{cat}\right)[Z_{10}^m : TEN] - k_4^+ z_{10}^m [TEN] - \frac{\frac{dPLT_{disagg}}{dt}}{PLT_{col} + PLT_{sec} + \varepsilon}[TEN] \tag{B.31}$$

$$\frac{d[PRO]}{dt} = k_{pro}^{b} e_5^m e_{10}^m - k_{pro}^{ub}[PRO] + \left(k_7^- + k_7^{cat}\right)[Z_2^m : PRO] - k_7^+ z_2^m [PRO] - k_5^{in}[ATIII][PRO] - \frac{\frac{dPLT_{disagg}}{dt}}{PLT_{col} + PLT_{sec} + \varepsilon}[PRO] \tag{B.32}$$

$$\frac{d[Z_2^m : PRO]}{dt} = k_7^+ z_2^m [PRO] - \left(k_7^- + k_7^{cat}\right)[Z_2^m : PRO] - \frac{\frac{dPLT_{disagg}}{dt}}{PLT_{col} + PLT_{sec} + \varepsilon}[Z_2^m : PRO] \tag{B.33}$$

$$\frac{d[Z_5 : E_2]}{dt} = k_{12}^+ z_5 e_2 - \left(k_{12}^- + k_{12}^{cat}\right)[Z_5 : E_2] - k_{flow}^c [Z_5 : E_2] - k_{12}^{cat}[Z_5 : E_2][polyP] \tag{B.34}$$

$$\frac{d[Z_5^m : E_2^m]}{dt} = k_{13}^+ z_5^m e_2^m - \left(k_{13}^- + k_{13}^{cat}\right)[Z_5^m : E_2^m] - k_{13}^{cat}[Z_5^m : E_2^m][polyP] - \frac{\frac{dPLT_{disagg}}{dt}}{PLT_{col} + PLT_{sec} + \varepsilon}[Z_5^m : E_2^m] \tag{B.35}$$

$$\frac{d[Z_5^m : E_{10}^m]}{dt} = k_5^+ z_5^m e_{10}^m - \left(k_5^- + k_5^{cat}\right)[Z_5^m : E_{10}^m] - k_5^{cat}[Z_5^m : E_{10}^m][polyP] - \frac{\frac{dPLT_{disagg}}{dt}}{PLT_{col} + PLT_{sec} + \varepsilon}[Z_5^m : E_{10}^m] \tag{B.36}$$

$$\frac{d[Z_7^m : E_2]}{dt} = k_3^+ z_7^m e_2 - \left(k_3^- + k_3^{cat}\right)[Z_7^m : E_2] - [Z_7^m : E_2]\frac{p'}{1-p} \tag{B.37}$$

$$\frac{d[Z_7 : E_2]}{dt} = k_{18}^{+} z_7 e_2 - \left(k_{18}^{-} + k_{18}^{cat}\right)[Z_7 : E_2] - k_{flow}^{c}[Z_7 : E_2] \tag{B.38}$$

$$\frac{d[Z_7 : E_{10}]}{dt} = k_{1}^{+} z_7 e_{10} - \left(k_{1}^{-} + k_{1}^{cat}\right)[Z_7 : E_{10}] - k_{flow}^{c}[Z_7 : E_{10}] \tag{B.39}$$

$$\frac{d[Z_7^m : E_{10}]}{dt} = k_{2}^{+} z_7^m e_{10} - \left(k_{2}^{-} + k_{2}^{cat}\right)[Z_7^m : E_{10}] - [Z_7^m : E_{10}]\frac{p'}{1-p} \tag{B.40}$$

$$\frac{d[Z_8 : E_2]}{dt} = k_{14}^{+} z_8 e_2 - \left(k_{14}^{-} + k_{14}^{cat}\right)[Z_8 : E_2] - k_{flow}^{c}[Z_8 : E_2] \tag{B.41}$$

$$\begin{aligned}\frac{d[Z_8^m : E_2^m]}{dt} &= k_{15}^{+} z_8^m e_2^m - \left(k_{15}^{-} + k_{15}^{cat}\right)[Z_8^m : E_2^m] \\ &\quad - \frac{\frac{dPLT_{disagg}}{dt}}{PLT_{col} + PLT_{sec} + \varepsilon}[Z_8^m : E_2^m]\end{aligned} \tag{B.42}$$

$$\begin{aligned}\frac{d[Z_8^m : E_{10}^m]}{dt} &= k_{6}^{+} z_8^m e_{10}^m - \left(k_{6}^{-} + k_{6}^{cat}\right)[Z_8^m : E_{10}^m] \\ &\quad - \frac{\frac{dPLT_{disagg}}{dt}}{PLT_{col} + PLT_{sec} + \varepsilon}[Z_8^m : E_{10}^m]\end{aligned} \tag{B.43}$$

$$\frac{d[Z_9 : E_7^m]}{dt} = k_{9}^{+} z_9 e_7^m - \left(k_{9}^{-} + k_{9}^{cat}\right)[Z_9 : E_7^m] - [Z_9 : E_7^m]\frac{p'}{1-p} \tag{B.44}$$

$$\frac{d[Z_{10} : E_7^m]}{dt} = k_{8}^{+} z_{10} e_7^m - \left(k_{8}^{-} + k_{8}^{cat}\right)[Z_{10} : E_7^m] - [Z_{10} : E_7^m]\frac{p'}{1-p} \tag{B.45}$$

$$\begin{aligned}\frac{d[Z_{10}^m : TEN]}{dt} &= k_{4}^{+} z_{10}^m [TEN] - \left(k_{4}^{-} + k_{4}^{cat}\right)[Z_{10}^m : TEN] \\ &\quad - \frac{\frac{dPLT_{disagg}}{dt}}{PLT_{col} + PLT_{sec} + \varepsilon}[Z_{10}^m : TEN]\end{aligned} \tag{B.46}$$

$$\frac{d[APC]}{dt} = k_{apc}k^{c}_{flow}e_2\left(t - t_{lag}\right) - k^{+}_{16}[APC]e^{m}_{5} + \left(k^{-}_{16} + k^{cat}_{16}\right)[APC:E^{m}_{5}] - k^{+}_{17}[APC]e^{m}_{8} + \left(k^{-}_{17} + k^{cat}_{17}\right)[APC:E^{m}_{8}] - k^{c}_{flow}[APC] \tag{B.47}$$

$$\frac{d[APC:E^{m}_{5}]}{dt} = k^{+}_{16}[APC]e^{m}_{5} - \left(k^{-}_{16} + k^{cat}_{16}\right)[APC:E^{m}_{5}] - \frac{\frac{dPLT_{disagg}}{dt}}{PLT_{col} + PLT_{sec} + \varepsilon}[APC:E^{m}_{5}] \tag{B.48}$$

$$\frac{d[APC:E^{m}_{8}]}{dt} = k^{+}_{17}[APC]e^{m}_{8} - \left(k^{-}_{17} + k^{cat}_{17}\right)[APC:E^{m}_{8}] - \frac{\frac{dPLT_{disagg}}{dt}}{PLT_{col} + PLT_{sec} + \varepsilon}[APC:E^{m}_{8}] \tag{B.49}$$

$$\frac{d[TFPI]}{dt} = -k^{b}_{1}[TFPI]e_{10} + k^{ub}_{1}[TFPI:E_{10}] + k^{c}_{flow}\left([TFPI]^{out} - [TFPI]\right) - k^{b}_{3}[TFPI]e^{m}_{10} + k^{ub}_{3}[TFPI:E^{m}_{10}] \tag{B.50}$$

$$\frac{d[TFPI:E_{10}]}{dt} = k^{b}_{1}[TFPI]e_{10} - k^{ub}_{1}[TFPI:E_{10}] + k^{ub}_{2}[TFPI:E_{10}:E^{m}_{7}] - k^{b}_{2}[TFPI:E_{10}]e^{m}_{7} - k^{c}_{flow}[TFPI:E_{10}] \tag{B.51}$$

$$\frac{d[TFPI:E_{10}:E^{m}_{7}]}{dt} = -k^{ub}_{2}[TFPI:E_{10}:E^{m}_{7}] + k^{b}_{2}[TFPI:E_{10}]e^{m}_{7} - [TFPI:E_{10}:E^{m}_{7}]\frac{p'}{1-p} \tag{B.52}$$

$$\frac{dTF}{dt} = -TF\frac{p'}{1-p} \tag{B.53}$$

$$\frac{dp_{10}}{dt} = N^{pl}_{10}\frac{d\left([PLT_{col}] + [PLT_{sec}]\right)}{dt} \tag{B.54}$$

$$\frac{dp_5}{dt} = N_5^{pl} \frac{d\left([PLT_{col}]+[PLT_{\sec}]\right)}{dt} \tag{B.55}$$

$$\frac{dp_8}{dt} = N_8^{pl} \frac{d\left([PLT_{col}]+[PLT_{\sec}]\right)}{dt} \tag{B.56}$$

$$\frac{dp_9}{dt} = N_9^{pl} \frac{d\left([PLT_{col}]+[PLT_{\sec}]\right)}{dt} \tag{B.57}$$

$$\frac{dp_2}{dt} = N_2^{pl} \frac{d\left([PLT_{col}]+[PLT_{\sec}]\right)}{dt} \tag{B.58}$$

$$\frac{de_9^{m,*}}{dt} = k_9^{on} e_9 P_9^* - k_9^{off} e_9^{m,*} + k_{ten}^{ub}[TEN^*] - k_{ten}^{b} e_8^m e_9^{m,*} - \frac{\frac{dPLT_{disagg}}{dt}}{PLT_{col}+PLT_{\sec}+\varepsilon} e_9^{m,*} \tag{B.59}$$

$$\frac{dP_9^*}{dt} = \frac{d}{dt}\left(p_9^* - e_9^{m,*} - [TEN^*] - [Z_{10}^m : TEN^*]\right) \tag{B.60}$$

$$\begin{aligned}\frac{d[TEN^*]}{dt} &= k_{ten}^{b} e_8^m e_9^{m,*} - k_{ten}^{ub}[TEN^*] + \left(k_4^- + k_4^{cat}\right)[Z_{10}^m : TEN^*] - k_4^+ z_{10}^m [TEN^*] \\ &\quad - \frac{\frac{dPLT_{disagg}}{dt}}{PLT_{col}+PLT_{\sec}+\varepsilon}[TEN^*]\end{aligned} \tag{B.61}$$

$$\begin{aligned}\frac{d[Z_{10}^m : TEN^*]}{dt} &= k_4^+ z_{10}^m [TEN^*] - \left(k_4^- + k_4^{cat}\right)[Z_{10}^m : TEN^*] \\ &\quad - \frac{\frac{dPLT_{disagg}}{dt}}{PLT_{col}+PLT_{\sec}+\varepsilon}[Z_{10}^m : TEN^*]\end{aligned} \tag{B.62}$$

$$\frac{dp_9^*}{dt} = N_9^{pl,*} \frac{d\left([PL_a^s]+[PL_a^v]\right)}{dt} \tag{B.63}$$

$$\frac{d[Fg]}{dt} = -k_{10}^+ [Fg] e_2 + k_{10}^- [Fg : E_2] + k_{flow}^c \left([Fg]^{out} - [Fg]\right) \tag{B.64}$$

$$\frac{d[Fg:E_2]}{dt} = k_{10}^{+}[Fg]e_2 - \left(k_{10}^{-} + k_{10}^{cat}\right)[Fg:E_2] - k_{flow}^{c}[Fg:E_2] \tag{B.65}$$

$$\begin{aligned}\frac{d[Fbn1]}{dt} &= k_{10}^{cat}[Fg:E_2] - k_{11}^{+}[Fbn1]e_2 + k_{11}^{-}[Fbn1:E_2] \\ &\quad - 2k_4^{b}[Fbn1][Fbn1] + 2k_4^{ub}[(Fbn1)_2]\end{aligned} \tag{B.66}$$

$$\frac{d[Fbn1:E_2]}{dt} = k_{11}^{+}[Fbn1]e_2 - \left(k_{11}^{-} + k_{11}^{cat}\right)[Fbn1:E_2] - k_{10}^{in}[Fbn1:E_2][ATIII] \tag{B.67}$$

$$\frac{d[Fbn2]}{dt} = k_{11}^{cat}[Fbn1:E_2] - k_5^{b}[Fbn2]e_2 + k_5^{ub}[Fbn2:E_2] \tag{B.68}$$

$$\frac{d[Fbn2:E_2]}{dt} = k_5^{b}[Fbn2]e_2 - k_5^{ub}[Fbn2:E_2] - k_{11}^{in}[Fbn2:E_2][ATIII] \tag{B.69}$$

$$\begin{aligned}\frac{d[(Fbn1)_2]}{dt} &= k_4^{b}[Fbn1][Fbn1] - k_4^{ub}[(Fbn1)_2] \\ &\quad - k_{19}^{+}[(Fbn1)_2]e_2 + k_{19}^{-}[(Fbn1)_2:E_2]\end{aligned} \tag{B.70}$$

$$\begin{aligned}\frac{d[(Fbn1)_2:E_2]}{dt} &= k_{19}^{+}[(Fbn1)_2]e_2 - \left(k_{19}^{-} + k_{19}^{cat}\right)[(Fbn1)_2:E_2] \\ &\quad - k_9^{in}[(Fbn1)_2:E_2][ATIII]\end{aligned} \tag{B.71}$$

$$\begin{aligned}\frac{d[ATIII]}{dt} &= -k_9^{in}[(Fbn1)_2:E_2][ATIII] - k_{10}^{in}[Fbn1:E_2][ATIII] \\ &\quad - k_{11}^{in}[Fbn2:E_2][ATIII] \\ &\quad + k_{flow}^{c}\left([ATIII]^{out} - [ATIII]\right) - k_{12}^{in}e_{11}[ATIII] \\ &\quad - k_1^{in}e_9[ATIII] - k_2^{in}e_2[ATIII] - k_3^{in}e_{10}[ATIII] \\ &\quad - k_4^{in}e_{10}^{m}[ATIII] - k_5^{in}[PRO][ATIII] - k_6^{in}e_2^{m}[ATIII]\end{aligned} \tag{B.72}$$

$$\frac{d[(Fbn2)_2]}{dt} = k_{19}^{cat}[(Fbn1)_2 : E_2] \tag{B.73}$$

$$\frac{d[TFPI : E_{10}^m]}{dt} = k_3^b[TFPI]e_{10}^m - k_3^{ub}[TFPI : E_{10}^m] - \frac{\frac{dPLT_{disagg}}{dt}}{PLT_{col} + PLT_{sec} + \varepsilon}[TFPI : E_{10}^m] \tag{B.74}$$

$$\frac{d[ZPI]}{dt} = -k_7^{in}[ZPI]e_{10}^m + k_{flow}^c\left([ZPI]^{out} - [ZPI]\right) \tag{B.75}$$

$$\frac{d[ZPI : PZ]}{dt} = -k_8^{in}[ZPI : PZ]e_{10}^m + k_{flow}^c\left([ZPI : PZ]^{out} - [ZPI : PZ]\right) \tag{B.76}$$

$$\frac{d[ZPI : E_{10}^m]}{dt} = +k_7^{in}[ZPI]e_{10}^m - \frac{\frac{dPLT_{disagg}}{dt}}{PLT_{col} + PLT_{sec} + \varepsilon}[ZPI : E_{10}^m] \tag{B.77}$$

$$\frac{d[ZPI : PZ : E_{10}^m]}{dt} = +k_8^{in}[ZPI : PZ]e_{10}^m - \frac{\frac{dPLT_{disagg}}{dt}}{PLT_{col} + PLT_{sec} + \varepsilon}[ZPI : PZ : E_{10}^m] \tag{B.78}$$

$$\frac{dz_{11}}{dt} = -k_{20}^{+}z_{11}e_2 + k_{20}^{-}[Z_{11} : E_2] - k_1^{scat}z_{11}e_{11} + k_{flow}^c\left(z_{11}^{out} - z_{11}\right) - k_{11z}^{on}z_{11}P_{11} + k_{11z}^{off}z_{11}^m \tag{B.79}$$

$$\frac{d[Z_{11} : E_2]}{dt} = k_{20}^{+}z_{11}e_2 - (k_{20}^{-} + k_{20}^{cat})[Z_{11} : E_2] - k_{flow}^c[Z_{11} : E_2] - k_{20}^{cat}[Z_{11} : E_2][polyP] \tag{B.80}$$

$$\frac{de_{11}}{dt} = k_{20}^{cat}[Z_{11} : E_2] + k_1^{scat} z_{11} e_{11} - k_{12}^{in} e_{11}[ATIII] - k_{21}^{+} e_{11} z_9 + \left(k_{21}^{-} + k_{21}^{cat}\right)[Z_9 : E_{11}] - k_{flow}^{c} e_{11} - k_{11e}^{on} e_{11} P_{11} + k_{11e}^{off} e_{11}^{m} + k_{20}^{cat}[Z_{11} : E_2][polyP] \tag{B.81}$$

$$\frac{d[E_{11} : ATIII]}{dt} = k_{12}^{in} e_{11}[ATIII] - k_{flow}^{c}[E_{11} : ATIII] \tag{B.82}$$

$$\frac{d[E_{11} : Z_9]}{dt} = k_{21}^{+} e_{11} z_9 - (k_{21}^{-} + k_{21}^{cat})[E_{11} : Z_9] - k_{flow}^{c}[E_{11} : Z_9] \tag{B.83}$$

$$\frac{dp_{11}}{dt} = N_{11}^{pl} \frac{d\left([PLT_{col}] + [PL_{\sec}]\right)}{dt} \tag{B.84}$$

$$\frac{dz_{11}^{m}}{dt} = k_{11z}^{on} z_{11} P_{11} - k_{11z}^{off} z_{11}^{m} - k_{22}^{+} z_{11}^{m} e_{11}^{m} + k_{22}^{-}[Z_{11}^{m} : E_{11}^{m}] - k_{23}^{+} z_{11}^{m} e_2^{m} + k_{23}^{-}[Z_{11}^{m} : E_2^{m}] - \frac{\frac{dPLT_{disagg}}{dt}}{PLT_{col} + PLT_{\sec} + \varepsilon} z_{11}^{m} \tag{B.85}$$

$$\frac{dP_{11}}{dt} = \frac{d}{dt}\left(p_{11} - z_{11}^{m} - e_{11}^{m} - 2[Z_{11}^{m} : E_{11}^{m}] - [Z_{11}^{m} : E_2^{m}] - [Z_9^{m} : E_{11}^{m}]\right) \tag{B.86}$$

$$\frac{de_{11}^{m}}{dt} = k_{11e}^{on} e_{11} P_{11} - k_{11e}^{off} e_{11}^{m} - k_{22}^{+} z_{11}^{m} e_{11}^{m} + \left(k_{22}^{-} + 2k_{22}^{cat}\right)[Z_{11}^{m} : E_{11}^{m}] - k_{24}^{+} z_9^{m} e_{11}^{m} + \left(k_{24}^{-} + k_{24}^{cat}\right)[Z_9^{m} : E_{11}^{m}] + k_{23}^{cat}[Z_{11}^{m} : E_2^{m}] + k_{23}^{cat}[Z_{11}^{m} : E_2^{m}][polyP] - \frac{\frac{dPLT_{disagg}}{dt}}{PLT_{col} + PLT_{\sec} + \varepsilon} e_{11}^{m} \tag{B.87}$$

$$\frac{d[Z_{11}^{m} : E_{11}^{m}]}{dt} = +k_{22}^{+} z_{11}^{m} e_{11}^{m} - \left(k_{22}^{-} + k_{22}^{cat}\right)[Z_{11}^{m} : E_{11}^{m}] - \frac{\frac{dPLT_{disagg}}{dt}}{PLT_{col} + PLT_{\sec} + \varepsilon}[Z_{11}^{m} : E_{11}^{m}] \tag{B.88}$$

$$\frac{d[Z_{11}^m : E_2^m]}{dt} = k_{23}^+ z_{11}^m e_2^m - \left(k_{23}^- + k_{23}^{cat}\right)[Z_{11}^m : E_2^m] - k_{23}^{cat}[Z_{11}^m : E_2^m][polyP] - \frac{\frac{dPLT_{disagg}}{dt}}{PLT_{col} + PLT_{sec} + \varepsilon}[Z_{11}^m : E_2^m] \quad \text{(B.89)}$$

$$\frac{d[Z_9^m : E_{11}^m]}{dt} = k_{24}^+ z_9^m e_{11}^m - \left(k_{24}^- + k_{24}^{cat}\right)[Z_9^m : E_{11}^m] - \frac{\frac{dPLT_{disagg}}{dt}}{PLT_{col} + PLT_{sec} + \varepsilon}[Z_9^m : E_{11}^m] \quad \text{(B.90)}$$

$$\frac{d[ATIII : E_2^m]}{dt} = +k_6^{in} e_2^m [ATIII] - \frac{\frac{dPLT_{disagg}}{dt}}{PLT_{col} + PLT_{sec} + \varepsilon}[ATIII : E_2^m] \quad \text{(B.91)}$$

$$\frac{d[ATIII : PRO]}{dt} = +k_5^{in}[PRO][ATIII] - \frac{\frac{dPLT_{disagg}}{dt}}{PLT_{col} + PLT_{sec} + \varepsilon}[ATIII : PRO] \quad \text{(B.92)}$$

$$\frac{d[ATIII : E_{10}^m]}{dt} = +k_4^{in} e_{10}^m [ATIII] - \frac{\frac{dPLT_{disagg}}{dt}}{PLT_{col} + PLT_{sec} + \varepsilon}[ATIII : E_{10}^m] \quad \text{(B.93)}$$

$$\frac{de_5^{m,in}}{dt} = +k_{16}^{cat}[APC : E_5^m] - \frac{\frac{dPLT_{disagg}}{dt}}{PLT_{col} + PLT_{sec} + \varepsilon} e_5^{m,in} \quad \text{(B.94)}$$

$$\frac{de_8^{m,in}}{dt} = +k_{17}^{cat}[APC : E_8^m] - \frac{\frac{dPLT_{disagg}}{dt}}{PLT_{col} + PLT_{sec} + \varepsilon} e_8^{m,in} \quad \text{(B.95)}$$

B.2 Parameter Values Used in the Secondary Hemostasis Model

Table B.1. Parameter values of the rate constants used in the updated secondary hemostasis model

Rxn	Model Expressions	k_1 ($nM^{-1}s^{-1}$)	k_{-1} (s^{-1})	k_{cat} (s^{-1})	k_{scat} ($nM^{-1}s^{-1}$)	Ref.
1	$Z_7 + TF \leftrightarrow Z_7^m$	3.2×10^{-3}	5×10^{-3}			[26, 58]
2	$E_7 + TF \leftrightarrow E_7^m$	5×10^{-2}	5×10^{-3}			[26]
3	$Z_7^m + E_{10} \leftrightarrow Z_7^m{:}\,E_{10} \rightarrow E_7^m + E_{10}$	5×10^{-3}	1	1		[26]
4	$Z_7^m + E_2 \leftrightarrow Z_7^m{:}\,E_2 \rightarrow E_7^m + E_2$	3.92×10^{-4}	1	6.1×10^{-2}		[26]
5	$Z_{10} + E_7^m \leftrightarrow Z_{10}{:}E_7^m \rightarrow E_7^m + E_{10}$	4.78×10^{-3}	1	1.15		[26, 38]
6	$Z_9 + E_7^m \leftrightarrow Z_9{:}E_7^m \rightarrow E_7^m + E_9$	5.19×10^{-3}	1	2.6×10^{-1}		[26, 38]
7	$Z_7 + E_{10} \leftrightarrow Z_7 : E_{10} \rightarrow E_7 + E_{10}$	5×10^{-3}	1	5		[26]
8	$Z_7 + E_2 \leftrightarrow Z_7 : E_2 \rightarrow E_7 + E_2$	3.92×10^{-4}	1	6.1×10^{-2}		[26]
9	$Z_5 + E_2 \leftrightarrow Z_5 : E_2 \rightarrow E_5 + E_2$	1.72×10^{-2}	1	2.3×10^{-1}		[26]
10	$Z_8 + E_2 \leftrightarrow Z_8 : E_2 \rightarrow E_8 + E_2$	9.5×10^{-3}	1	9×10^{-1}		[26]
11	$Z_9 + P_9 \leftrightarrow Z_9^m$	1×10^{-2}	2.5×10^{-2}			[26]
12	$E_9 + P_9 \leftrightarrow E_9^m$	1×10^{-2}	2.5×10^{-2}			[26]
13	$E_9 + P_9^* \leftrightarrow E_9^{m*}$	1×10^{-2}	2.5×10^{-2}			[26]
14	$Z_{10} + P_{10} \leftrightarrow Z_{10}^m$	1×10^{-2}	2.5×10^{-2}			[26]
15	$E_{10} + P_{10} \leftrightarrow E_{10}^m$	1×10^{-2}	2.5×10^{-2}			[26]
16	$Z_5 + P_5 \leftrightarrow Z_5^m$	5.7×10^{-2}	1.7×10^{-1}			[26]
17	$E_5 + P_5 \leftrightarrow E_5^m$	5.7×10^{-2}	1.7×10^{-1}			[26]
18	$Z_8 + P_8 \leftrightarrow Z_8^m$	5×10^{-2}	1.7×10^{-1}			[26]
19	$E_8 + P_8 \leftrightarrow E_8^m$	5×10^{-2}	1.7×10^{-1}			[26]
20	$Z_2 + P_2 \leftrightarrow Z_2^m$	1×10^{-2}	5.9			[26]
21	$E_2 + P_2 \leftrightarrow E_2^m$	1×10^{-2}	5.9			[26]
22	$Z_5^m + E_{10}^m \leftrightarrow Z_5^m{:}\,E_{10}^m \rightarrow E_5^m + E_{10}^m$	1×10^{-1}	1	4.6×10^{-2}		[26]
23	$Z_5^m + E_2^m \leftrightarrow Z_5^m{:}\,E_2^m \rightarrow E_5^m + E_2^m$	1.72×10^{-2}	1	2.3×10^{-1}		[26]

Table B.1 continued.

24	$Z_8^m + E_{10}^m \leftrightarrow Z_8^m{:}\, E_{10}^m \rightarrow E_8^m + E_{10}^m$	5.1×10^{-2}	1	2.3×10^{-2}		[26]
25	$Z_8^m + E_2^m \leftrightarrow Z_8^m{:}\, E_2^m \rightarrow E_8^m + E_2^m$	9.5×10^{-3}	1	0.9		[26, 41, 42]
26	$E_8^m + E_9^m \leftrightarrow$ TEN	1×10^{-1}	1×10^{-2}			[26]
27	$E_8^m + E_9^{m*} \leftrightarrow$ TEN*	1×10^{-1}	1×10^{-2}			[26]
28	$E_5^m + E_{10}^m \leftrightarrow$ PRO	1×10^{-1}	1×10^{-2}			[26]
29	Z_{10}^m + TEN $\leftrightarrow Z_{10}^m$:TEN $\rightarrow E_{10}^m$ + TEN	1.31×10^{-1}	1	20		[26]
30	Z_{10}^m + TEN* $\leftrightarrow Z_{10}^m$:TEN* $\rightarrow E_{10}^m$ + TEN*	1.31×10^{-1}	1	20		[26]
31	Z_2^m + PRO $\leftrightarrow Z_2^m$:PRO $\rightarrow E_2^m$ + PRO	1.03×10^{-1}	1	30		[26]
32	APC + $E_8^m \leftrightarrow$ APC: $E_8^m \rightarrow E_8^{m,in}$	1.2×10^{-1}	1	0.5		[26]
33	APC + $E_5^m \leftrightarrow$ APC: $E_5^m \rightarrow E_5^{m,in}$	1.2×10^{-1}	1	0.5		[26]
34	TFPI + $E_{10} \leftrightarrow$ TFPI: E_{10}	1.6×10^{-2}	3.3×10^{-4}			[26]
35	TFPI: E_{10} + $E_7^{\mathrm{m}} \leftrightarrow$ TFPI: E_{10}:E_7^{m}	1×10^{-2}	1.1×10^{-3}			[26]
36	ATIII + $E_9 \rightarrow E_9^{in}$				2.94×10^{-5}	[26]
37	ATIII + $E_{10} \rightarrow E_{10}^{in}$				5.88×10^{-5}	[26]
38	ATIII + $E_2 \rightarrow E_2^{in}$				2.94×10^{-5}	[26]
39	Fg + $E_2 \leftrightarrow$ Fg: $E_2 \rightarrow Fbn_1 + E_2$ + FPA	1×10^{-1}	636	84		[59]
40	$Fbn_1 + E_2 \leftrightarrow Fbn_1 : E_2 \rightarrow Fbn_2 + E_2$ + FPB	1×10^{-1}	742.6	7.4		[59]
41	2 $Fbn_1 \leftrightarrow (Fbn_1)_2$	1×10^{-3}	6.4×10^{-2}			[59]
42	$(Fbn_1)_2 + E_2 \leftrightarrow (Fbn_1)_2{:}\, E_2 \rightarrow (Fbn_2)_2 + E_2$ + 2 FPB	1×10^{-1}	701	49		[59]
43	Fbn2 + $E_2 \leftrightarrow$ Fbn2: E_2	1×10^{-1}	1×10^{3}			[59]
44	$(Fbn_1)_2{:}\, E_2$ + ATIII $\rightarrow (Fbn_1)_2$2:E2:ATIII				1.6×10^{-5}	[59]
45	$Fbn_1 : E_2$ + ATIII $\rightarrow Fbn_1 : E_2$:ATIII				1.6×10^{-5}	[59]
46	$Fbn_2 : E_2$ + ATIII $\rightarrow Fbn_2 : E_2$:ATIII				1×10^{-5}	[59]
47	TFPI + E10m $\leftrightarrow$ TFPI:E10m	1.6×10^{-2}	8×10^{-2}			[74]
48	PRO + ATIII $\rightarrow$ PRO:ATIII				1.55×10^{-6}	[50]
49	E_2^m + ATIII $\rightarrow E_2^m$:ATIII				3.44×10^{-6}	[50]

Table B.1 continued.

50	E_{10}^{m} + ATIII → E_{10}^{m}:ATIII				3.23×10^{-6}	[50]
51	ZPI + E_{10}^{m} ↔ ZPI: E_{10}^{m}				1×10^{-6}	[54]
52	ZPI:PZ + E_{10}^{m} ↔ ZPI:PZ: E_{10}^{m}				3.1×10^{-3}	[54]
53	Z_2 + E_{10} → E_2 + E_{10}				7.5×10^{-6}	[63]
54	Z_2 + E_{10}^{m} → E_2 + E_{10}^{m}				7.5×10^{-6}	[63]
55	Z_2^{m} + E_{10} → E_2^{m} E_{10}+				7.5×10^{-6}	[63]
56	Z_2^{m} + E_{10}^{m} → E_2^{m} + E_{10}^{m}				7.5×10^{-6}	[63]
57	Z_5 + E_{10} → E_5 + E_{10}				4.1×10^{-3}	[63]
58	Z_5 + E_{10}^{m} → E_5 + E_{10}^{m}				4.1×10^{-3}	[63]
59	Z_5^{m} + E_{10} → E_5^{m} + E_{10}				4.1×10^{-3}	[63]
60	Z_8 + E_{10} →E_8 + E_{10}				1.15×10^{-3}	[63]
61	Z_8 + E_{10}^{m} → E_8 + E_{10}^{m}				1.15×10^{-3}	[63]
62	Z_8^{m} + E_{10} → E_8^{m} + E_{10}				1.15×10^{-3}	[63]
63	Z_7 + E_{10}^{m} → E_7 + E_{10}^{m}				1.3×10^{-2}	[63]
64	Z_7 + E_7^{m} → E_7 + E_7^{m}				1.3×10^{-2}	[63]
65	Z_{11} + P_{11} ↔ Z_{11}^{m}	1×10^{-2}	1×10^{-1}			[63]
66	E_{11} + P_{11} ↔E_{11}^{m}	1×10^{-2}	1.7×10^{-2}			[63]
67	Z_{11} + E_2 ↔ Z_{11}: E_2 → E11 + E_2	1×10^{-1}	5	1.3×10^{-4}		[59]
68	Z_{11} + E_{11} ↔ Z_{11}: E_{11} → 2 E_{11}				3.19×10^{-3}	[59]
69	E_{11} + ATIII → E11:ATIII				3.2×10^{-7}	[59]
70	Z_9 + E_{11} ↔ Z_9 : E_{11} → E_9 + E_{11}	1×10^{-1}	41	7.7		[59]
71	Z_{11}^{m} + E_{11}^{m} ↔ Z_{11}^{m}: E_{11}^{m} → 2 E_{11}^{m}	1×10^{-1}	1.2×10^{-3}	1×10^{-5}		[59, 75]
72	Z_9^{m} + E_{11}^{m} ↔ Z_9^{m}: E_{11}^{m} → E_9^{m} + E_{11}^{m}	1×10^{-1}	41	7.7		[59]
73	Z_{11}^{m} + E_2^{m} ↔ Z_{11}^{m}: E_2^{m} → E_{11} +E_2^{m}	1×10^{-1}	5	1.3×10^{-4}		[59]
74	Z_{11}^{m}: E_2^{m} + polyP → E_{11} + E_2^{m} + polyP			1.3×10^{-4}		[59, 72]
75	Z_{11}: E_2 + polyp → E_{11} + E_2 + polyP			1.3×10^{-4}		[72, 112]
76	Z_5 : E_2 + polyP → E_5 + E_2 + polyP			2.3×10^{-1}		[26, 72]
77	Z_5^{m}: E_2^{m} + polyP → E_5^{m} + E_2^{m} + polyP			2.3×10^{-1}		[26, 72]
78	Z_5^{m}: E_{10}^{m} + polyP → E_5^{m} + E_{10}^{m} + polyP			4.6×10^{-2}		[26, 72]

Table B.1 continued.

79	$Z_5^m + E_{10} + \text{polyP} \rightarrow E_5^m + E_{10} + \text{polyP}$	4.1×10^{-3}	[63, 72]
80	$Z_5 + E_{10} + \text{polyP} \rightarrow E_5 + E_{10} + \text{polyP}$	4.1×10^{-3}	[63, 72]
81	$Z_5 + E_{10}^m + \text{polyP} \rightarrow E_5 + E_{10}^m + \text{polyP}$	4.1×10^{-3}	[63, 72]
82	$E_2 + \text{PC} \rightarrow \text{APC}$	1	[26]

Appendix C

A PHARMACOKINETIC–PHARMACODYNAMIC MODEL OF ROMIPLOSTIM-INDUCED PLATELET PRODUCTION

C.1 Equations for the Pharmacokinetic/Pharmacodynamic (PKPD) Model

The PKPD model introduced in this section is based on the model proposed by [97], with the modifications described in section 6.3.1.

C.1.1 The Pharmacokinetic Model

The PK model, a pharmacodynamics-mediated drug disposition (PDMDD) subtype, consists of 4 segments that represent the locations of romiplostim in the body: the subcutaneous site, the serum in circulation, the peripheral part, and the drug-receptor complex. Romiplostim injection is implemented as a rectangular pulse function with width of 1/60 hour and magnitude corresponding to the dose. The sequence *u(k)* denotes pulses of romiplostim of magnitude *u* implemented at discrete time point *k (k = 0, 1, 2, 3, ...)*. The injection process is represented with the first-order rate constant k_{SC} pre-determined to be 60 h^{-1}. The absolute bioavailability of romiplostim to the specific patient, *F,* is a parameter to be estimated from data. Romiplostim absorption is represented as a first-order process with rate constant k_a. The amount of romiplostim at the subcutaneous site (A_{SC}) is then described by the following differential equation:

$$\frac{dA_{SC}}{dt} = k_{SC} \cdot F \cdot u(k) - k_a \cdot A_{SC} \tag{C.1}$$

After absorption, romiplostim is distributed between the serum and the peripheral part according to first-order distribution processes with rate constants k_{CP} and k_{PC}. In the circulatory system, free romiplostim binds to c-Mpl on platelets and forms a drug-receptor complex (DR) according to a second-order process with rate constant k_{on}. Receptor binding, limited by the total number of c-Mpl (R_{tot}), is assumed to be directly proportional to the platelet count (PLT) with a proportionality constant ξ which represents the theoretical total amount of c-Mpl per platelet. Although romiplostim has four c-Mpl binding sites, the stoichiometry is assumed to be 1:1 due to steric hindrance. The resulting drug-receptor complex either dissociates according to a first-order mechanism with rate constant k_{off} and generates free romiplostim and receptor, or internalizes into the cell according to a first-order process with rate constant k_{int}. Free romiplostim is eliminated from the serum according to a first-order process with rate constant k_{el}. These mechanistic details lead to the following equations:

$$\frac{dA_C}{dt} = k_a \cdot A_{SC} + k_{PC} \cdot A_P + k_{off} \cdot DR - \left(k_{el} + k_{CP} + \frac{k_{on}}{V_c} \cdot \left(\xi \cdot PLT - DR \right) \right) \cdot A_C \tag{C.2}$$

$$\frac{dA_P}{dt} = k_{CP} \cdot A_C - k_{PC} \cdot A_P \tag{C.3}$$

$$\frac{dDR}{dt} = \frac{k_{on}}{V_c} \cdot \left(\xi \cdot PLT - DR \right) \cdot A_C - k_{off} \cdot DR - k_{\text{int}} \cdot DR \tag{C.4}$$

$$R_{tot} = \xi \cdot PLT \tag{C.5}$$

where A_P and A_C represent the amount of free romiplostim in the peripheral part and in serum, respectively.

To avoid estimating k_{on} and k_{off} separately, a quasi-equilibrium state for the drug-receptor complex is assumed and the dissociation equilibrium constant K_D, defined as k_{off}/k_{on}, is estimated instead [113]. The quasi-equilibrium assumption allows us to combine A_C and DR as A_{tot}, which is the total amount of romiplostim in circulation, with the corresponding differential equation obtained by combining Eqs. (C.2) and (C.4) to yield:

$$\frac{dA_{tot}}{dt} = k_a \cdot A_{SC} - \left(k_{el} + k_{CP}\right) \cdot C \cdot V_C + k_{PC} \cdot A_P - k_{\text{int}} \cdot DR \tag{C.6}$$

where A_C is expressed as the product of C, serum concentration of free romiplostim, and V_C, the specific serum volume. The serum concentration of free romiplostim and the amount of the drug-receptor complex are calculated from the quasi-equilibrium equation according to:

$$C = 0.5 \cdot \left(\frac{A_{tot}}{V_C} - R_{tot} - K_D + \sqrt{\left(\frac{A_{tot}}{V_C} - R_{tot} - K_D \right)^2 + 4 \cdot K_D \cdot \frac{A_{tot}}{V_C}} \right) \tag{C.7}$$

$$DR = \frac{R_{tot} \cdot C}{K_D + C} V_C \tag{C.8}$$

C.1.2 The Pharmacodynamic Model

The PD model is based on the maturation-structured cytokinetic concept which accounts for the maturation process of platelet precursor cells in the bone marrow and the aging process of platelets in circulation. Ten stages are used for the precursors (number represented by N_P), as well as platelets (number represented by N_{PLT}). In addition to the intrinsic maturation rate of the precursors k_{in}, the concentration of free romiplostim in serum C also exerts a stimulatory effect on the maturation of

precursors. The stimulatory effect is described by a Hill function, with S_{max} as the maximal effect, SC_{50} as the romiplostim concentration required for obtaining half the maximal effect, and n, as the customary Hill coefficient. Note that there is a difference in the equation used here compared to [96]. The maximal romiplostim effect on platelet production S_{max} is not confounded with k_{in}. This provides a more physiologically-relevant description of romiplostim-induced platelet production. With the same platelet lifespan, a faster intrinsic platelet production rate indicates a higher initial platelet count, which should reduce the effect of romiplostim as explained in Figure 5.1 in the main text. A confounded representation will thus be inappropriate. In addition, as k_{in} is representative of the effect of endogenous TPO, the effect of romiplostim, which works through the same mechanisms as TPO, should be additive to the whole platelet production process.

The model assumes that all precursors and platelets mature into the next stage without being cleared from the body. The lifespans of precursors and platelets, denoted respectively by T_P and T_{PLT} (indicative of how fast a cell moves from one stage to the next in the maturation or aging process), are introduced as parameters. The intrinsic maturation rate is then determined by the initial platelet count and the lifespan of platelet. The resulting model equations used are:

$$\frac{dP_1}{dt} = k_{in} + S_{\max}\frac{C^n}{SC_{50}{}^n + C^n} - \frac{N_P}{T_P}P_1 \tag{C.9}$$

$$\frac{dP_i}{dt} = \frac{N_P}{T_P}\left(P_{i-1} - P_i\right), \quad i = 2,3,...,N_P \tag{C.10}$$

$$\frac{dPLT_1}{dt} = \frac{N_P}{T_P}P_{N_P} - \frac{N_{PLT}}{T_{PLT}}PLT_1 \tag{C.11}$$

$$\frac{dPLT_i}{dt} = \frac{N_{PLT}}{T_{PLT}}\left(PLT_{i-1} - PLT_i\right), \quad i = 2,3,...,N_{PLT} \tag{C.12}$$

P_i represents the number of precursor cells in the i-th stage while PLT_i is the number of platelets in the i-th stage. Initial conditions for both the PK and PD models are summarized in Table C.1.

C.2 Initial Conditions and Original Clinical Data for Parameter Estimation

Table C.1. Initial conditions of the PKPD model.

Variable	Value (unit)	Variable	Value (unit)
$A_{SC}(0)$	0 (μg/kg)	$P_i(0)$	$\frac{T_P \cdot PLT_0}{N_P \cdot T_{PLT}}$ ($\times 10^9$/L)
$A_P(0)$	0 (μg/kg)	k_{in}	$\frac{PLT_0}{T_{PLT}}$ ($\times 10^9$/L-h)
$A_{tot}(0)$	0 (μg/kg)	$PLT_i(0)$	$\frac{PLT_0}{N_{PLT}}$ ($\times 10^9$/L)
PLT_0	5 ($\times 10^9$/L)		

Table C.2. Original data of romiplostim dose and platelet count.

Days	Romiplostim dose (μg/kg)	Platelet count ($\times 10^9$/L)
0	3	5
6	3	81
10		296
20	3	15
27	4	3
30		2
34		160
36		283
44		192
51		8
52	5	
58		3
59	5	
63		159
66		449
69		688
73		600
79	3	212
86		15
87	5	
92		59
97		570
104		440
106	4	332
114	4	
128	2	703

Appendix D

EFFECT OF SHEAR RATE ON PLATELET ADHESION AND AGGREGATION

Microfluidic experiments introduced in section 3.4.1 were carried out to study the effect of shear rate on platelet adhesion and aggregation. The representative pictures of the effect of shear rate are shown in Figure D.1. Two metrics were quantified from the resulting figures: (i) surface coverage that measures how much of the collagen-coated area is covered by platelets and (ii) fluorescence intensity that indicates the number of platelets in the platelet aggregate. Quantification of the figures from three blood donors is shown in Figures D.2 and D.3. It can be seen that platelet aggregation is significantly promoted with increased shear rate. This is consistent with the data reported in the literature.

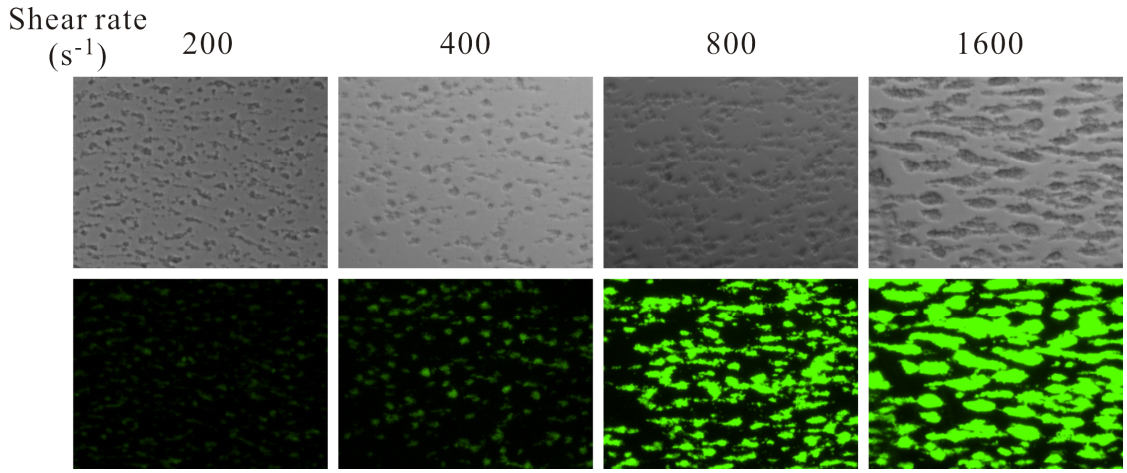

Figure D.1. Representative pictures of the effect of shear rate on platelet adhesion and aggregation over collagen-coated surface. Upper panel: phase contrast images. Lower panel: fluorescence images. Anti-coagulated human blood was perfused through collagen-coated channel for 3 minutes at designated shear rate.

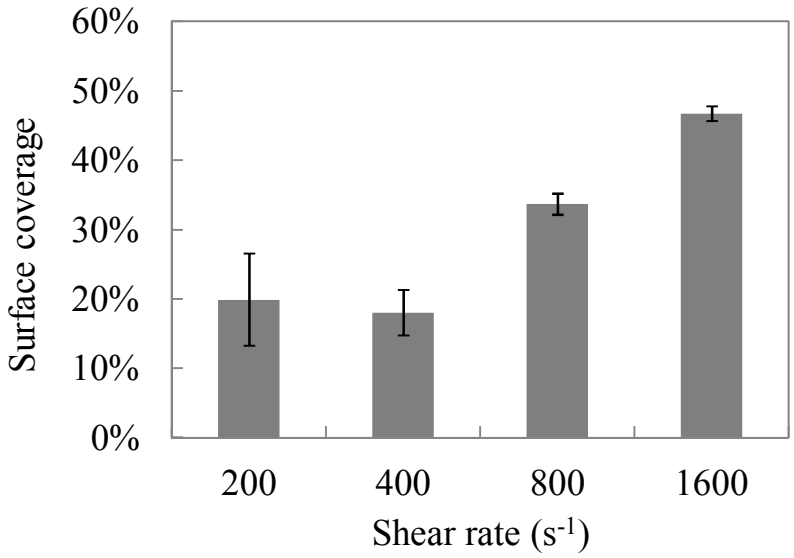

Figure D.2. Surface coverage in microfluidic experiments of collagen-induced platelet adhesion and aggregation under various shear rates. Error bar indicates standard error of the mean.

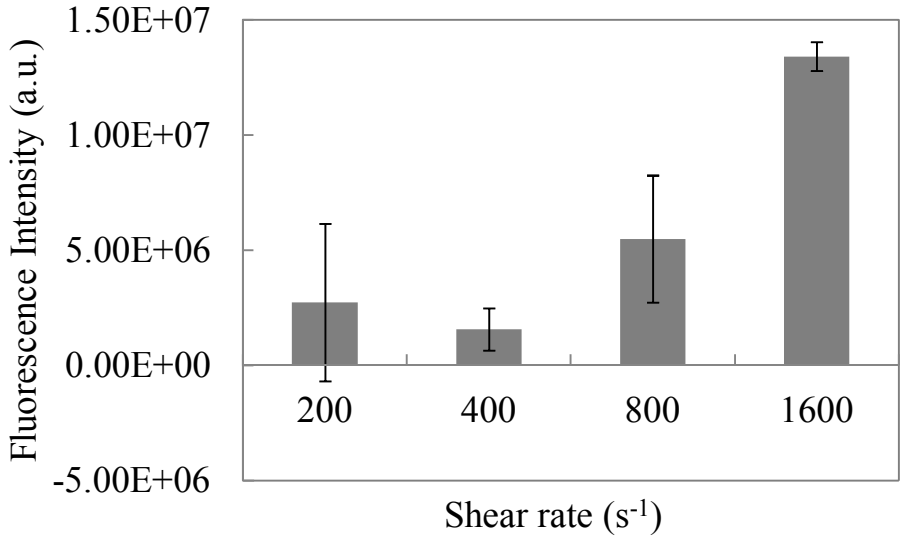

Figure D.3. Fluorescence intensity in microfluidic experiments of collagen-induced platelet adhesion and aggregation under various shear rates. Fluorescence intensity is proportional to number of activated platelets. Error bar indicates standard error of the mean.